APRIL 1961 VOLUME 10 (1961) No. 4

GREGG M. SINCLAIR LIBRARY
UNIVERSITY OF HAWAII
8-7-63

NUCLEAR INSTRUMENTS & METHODS

A JOURNAL ON ACCELERATORS, INSTRUMENTATION AND TECHNIQUES IN NUCLEAR PHYSICS

EDITOR: K. SIEGBAHN - UPPSALA

CONTENTS

D. E. CARO and J. L. ROUSE, The Melbourne university variable energy cyclotron 249
G. V. H. WILSON, Phase changes near the cyclotron centre 259
G. G. KELLEY, N. H. LAZAR and O. B. MORGAN, A source for the production of large DC ion currents 263
D. J. CAIRNS, T. C. GRIFFITH, G. J. LUSH, A. J. METHERINGHAM and R. H. THOMAS, The use of a counter controlled high pressure cloud chamber for experiments with charged particles 272
I. T. MYERS and H. V. LARSON, Precision instrumentation for an electron accelerator . . . 281
K. BLINOWSKI and J. SOSNOWSKI, Parasitic reflections of neutrons in crystal monochromators 289
K. FELBINGER, H. KULENKAMPFF, M. SCHEER und E. SCHRÜFER, Ein magnetisches Compton-Spektrometer zur Untersuchung hochenergetischer Röntgen-Bremsstrahlung . . 295
E. KEIL und E. ZEITLER, Eine Theorie magnetischer Compton-Spektrometer 301
H. VERWEIJ, A fast transistorized discriminator 308
P. THIEBERGER and I. BERGSTRÖM, Use of cathode ray tubes in pulse-height spectroscopy 315
E. ARBMAN and B. JUNG, Improved automatic operation of a double focusing iron-yoke β-spectrometer 322
J. A. BIGGERSTAFF, R. L. BECKER and M. T. MCELLISTREM, Charged particle discrimination in a CsI(Tl) detector 327
H. NEU und H. WERNER, Analytisches Näherungsverfahren zur Berechnung azimuthal periodischer Magnetfelder in Kreisbeschleunigern 333
HANS ACKERMANN and HELMUT FAISSNER, Fading in nuclear emulsions induced by acid agents 339
R. N. GLOVER, K. H. PURSER and E. WEIGOLD, A counter telescope system for fast neutron studies 343
LAWRENCE W. JONES and MARTIN L. PERL, An image intensifier-scintillator device for determination of profiles and images of weak beams of ionizing particles or X-rays 348
H. GRÄSSLER and K. TESCH, Detection efficiency of a plastic scintillator for neutrons in the energy range of 1 to 14 MeV 353

Book Reviews 356
Author Index 357
Subject Index 359

This last Number of Volume 10 will be followed by a Master Index of the Volumes 1-10

NORTH-HOLLAND PUBLISHING COMPANY — AMSTERDAM

NUCLEAR INSTRUMENTS AND METHODS

A journal on accelerators, instrumentation and techniques in nuclear physics

EDITOR: K. SIEGBAHN, UPPSALA

EDITORIAL BOARD:

J. B. ADAMS (CERN)
F. A. ALSINA (Buenos Aires)
E. AMALDI (Rome)
H. L. ANDERSON (Chicago)
K. T. BAINBRIDGE (Cambridge, Mass.)
P. R. BELL (Oak Ridge)
R. E. BELL (Montreal)
A. BERTHELOT (Saclay)
H. BRINKMAN (Groningen)
E. H. COOKE-YARBOROUGH (Harwell)
S. DE BENEDETTI (Pittsburgh)
M. DE HEMPTINNE (Louvain)
A. DE-SHALIT (Rehovoth)
M. DEUTSCH (Cambridge, Mass.)
S. DU TOIT (Pretoria)
B. S. DŽELEPOV (Leningrad)
W. GENTNER (Heidelberg)
P. C. GUGELOT (Amsterdam)
H. HALBAN (Paris)
O. HAXEL (Heidelberg)
P. HUBER (Basel)
S. KIKUCHI (Tokyo)
J. KOCH (Copenhagen)
M. S. KOZODAEV (Moscow)
S. LIVINGSTON (Cambridge, Mass.)
E. M. MCMILLAN (Berkeley)
M. G. MEŠČERJAKOW (Moscow)
P. B. MOON (Birmingham)
M. L. OLIPHANT (Canberra)
W. PAUL (Bonn)
A. S. RAO (Bombay)
G. SALVINI (Rome)
P. SAVIĆ (Belgrade)
P. SCHERRER (Zürich)
CH. SCHMELZER (CERN)
R. TANGEN (Oslo)
D. TAYLOR (Northampton)
V. I. VEKSLER (Moscow)
G. VON DARDEL (CERN)
O. WERNHOLM (Stockholm)
R. R. WILSON (Cornell)
S. D. WINTER (Saclay)

INSTRUCTIONS FOR CONTRIBUTORS

Contributions may be sent to the Editor, Professor K. Siegbahn, Institute of Physics, University of Uppsala, Sweden, either directly or through the intermediation of one of the members of the Editorial Board. Contributions may be written in English, French or German but should always, except for very short papers, be supplied with a brief abstract in English. Figures should be inked original drawings or glossy prints and they should be sufficiently large. Contributors should make sure that important details in drawings and photographs will show up clearly in the diminished copy used by the publisher.

Books for review should be sent to Professor Siegbahn.

Objective and descriptive material on endeavours and product developments from the industry for the section "Spotlight on Industry" should be sent directly to the publishers, North-Holland Publishing Company, P.O. Box 103, Amsterdam.

Nuclear Instruments and Methods is published monthly. The subscription price of a volume of about 360 pages is $ 17.00 (130 s), postage free.

Subscriptions should be sent to the publishers, North-Holland Publishing Company, P.O. Box 103, Amsterdam, or to any subscription-agent.

No part of this issue may be reproduced in any form, by print, photoprint, microfilm or any other means without written permission from the publisher.

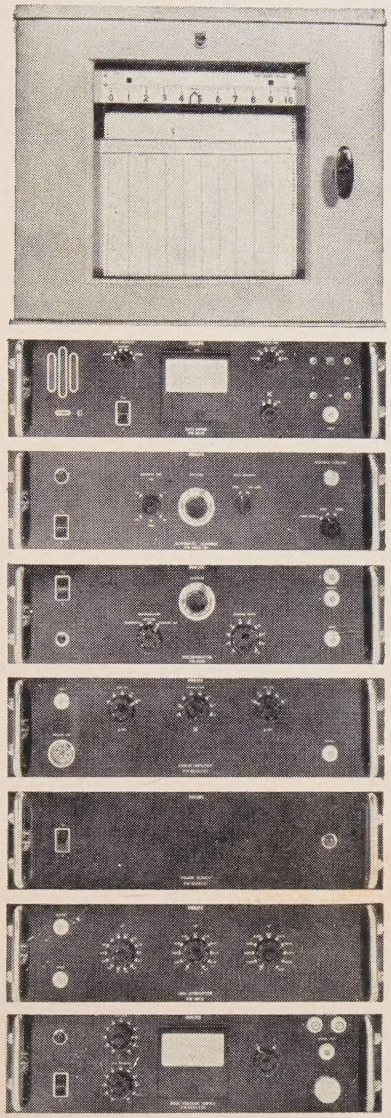

Automatic Single-Channel Gamma Spectrometer

for the qualitative analysis of radiation patterns produced by separate radio-active isotopes or by isotope mixtures. The instrument is also used for quantitative measurements of radiation, for the determination of the purity of isotopes, to study scattering and absorption effects.
The instrument is equipped to produce differential as well as integral spectra.
Both manual and automatic operation provided.
Four scanning times; chart speed adjustable to obtain uniform curve length.

HALF-VALUE WIDTH guaranteed better than 9½% (for the 662 KeV photopeak of Cs 137) with scintillation detector PW 4119 and preamplifier PW 4071 - **HIGH VOLTAGE RANGE** 300-2500 V in steps of 22 V - **REGULATION AND DRIFT** H.V. variations less than 0.005% per 1% mains fluctuation. Drift less than 0.05% in 24 hours - **LOG. ATTENUATION** 1-660 x, in steps of $10^{0.002}$ - **AMPLIFIER RESOLUTION** 1 μsec (5 μsec for 100 x overload) - **CHANNEL HEIGHT** 4-100 V (10-turn helical potentiometer) - **CHANNEL WIDTH** 1-2-4-8-12-16-20-24-28-32 V - **SCANNING TIMES** 3.5-14-24-100 min - **MEASURING RANGES** 300-1000-3000-10 000-30 000 c.p.m. - **TIME CONSTANT** 0.1-1-3-10-30-100 sec.

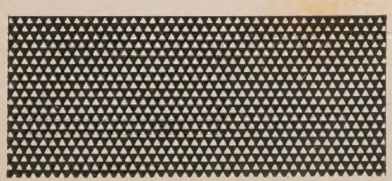

PHILIPS

nuclear equipment

N.V. PHILIPS' GLOEILAMPENFABRIEKEN - EINDHOVEN - HOLLAND

Particle accelerators - Reactor control instrumentation - Health protection and monitoring equipment - Radiation measuring and detection equipment - Geiger-Müller counters - Photomultipliers - Radio-active isotopes.

Interested in tritium counting efficiencies up to 40% with a single photomultiplier spectrometer system at room temperatures?

The Nuclear Enterprises NE 8301 assembly for small-volume internal-sample liquid scintillation counting offers:

* Room temperature counting efficiencies up to 35% for H3 in water, up to 40% for H3 in organic compounds, and up to 90% for C14, using single selected 1″ diameter photomultiplier. For H3 in water the background is 10 cps at 35%, 2 cps at 20%, and 1 cps at 10%, at room temperature.

* New shielded Scintillation Head Unit, NE 5503 (see Bulletin 19), with special rotary and translational light locking device, permitting daylight operation and main water temperature stabilisation.

* Specially coated quartz counting cells.

* New liquid scintillators NE 213 (xylene based) and NE 220 (dioxane based) for maximum light output, minimum quenching, and minimum chemiluminescence.

* Silicone oil reservoir with complete intimate coupling of counting cell and photomultiplier.

* Non-overloading linear pulse amplifier NE 5202 with high gain (50,000), high stability, and absence of blocking.

* Broad gate pulse height selector NE 5102 to optimise signal to background ratio for particular problems.

* E.H.T. supply NE 5302 with long term stability of 100 parts per million.

Write for detailed specifications in Bulletins 19 & 20

The NE 8301 obsoletes all coincidence systems and is adaptable to a wide range of problems.

Nuclear Enterprises (G.B.) Ltd.

BANKHEAD MEDWAY, SIGHTHILL, EDINBURGH 11, SCOTLAND. (TEL. CRA 5262)

Associate Company: Nuclear Enterprises Ltd., 550, Berry Street, Winnipeg 12, Canada. (nuh) 6116

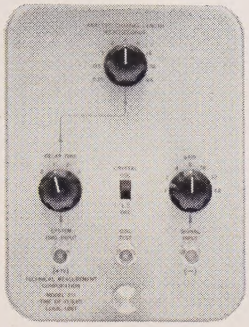

MODEL 211 TIME-OF-FLIGHT UNIT— Channel lengths from 0.25 to 64 μsec.

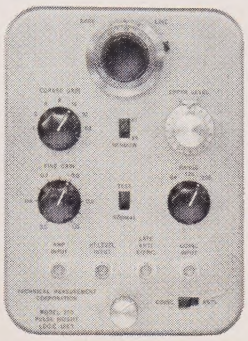

MODEL 210 PULSE HEIGHT UNIT—10+0.25 N μsec. dead time, built-in linear amplifier

NOW—

7 PLUG-IN LOGIC CIRCUITS

...for the TMC 256-channel Pulse Analyzer

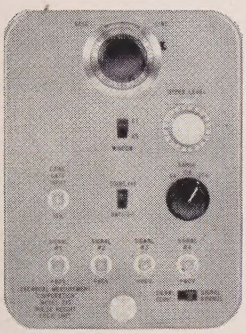

MODEL 213 PULSE HEIGHT UNIT—4 simultaneous inputs, 4 methods of storage, 10+0.25N μsec. dead time

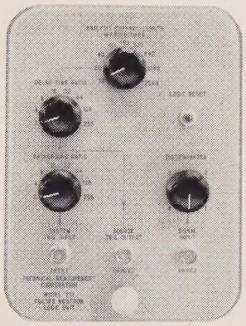

MODEL 212 PULSED NEUTRON UNIT—Used for exponential and critical experiments

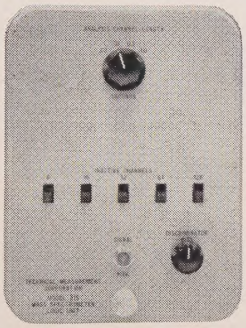

MODEL 215 MASS SPECTROMETER UNIT — Accepts ion counts in each channel for a preset time

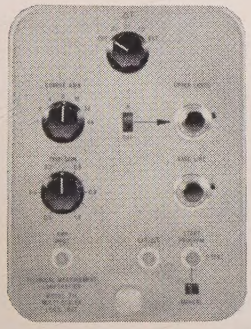

MODEL 214 MULTISCALER UNIT—Allows consecutive channel scaling for preset times

MODEL 216 COINCIDENCE PAIR UNIT—2-dimensional (16 x 16 channels) nuclear analyses

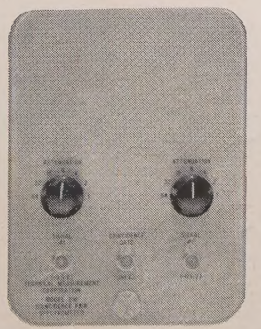

The 7 standard plug-in logic circuits now available make this 256-channel pulse analyzer the most useful system you can own.

By loosening one thumbscrew, you can remove one logic circuit — replace it with another — and have a completely different system in operation in a few seconds. The 7 units shown are standard but, TMC can build custom units to your exact requirements.

The basic transistorized 256-channel computer provides all memory circuits and data output selection circuits. Add the plug-in of your choice — have the exact system for your application.

Data handling is accomplished through an accessory, the Model 220 data handling unit. Strip chart and X-Y recorders, paper tape printers and punches may be used for readout.

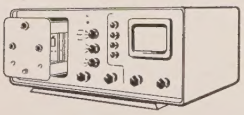

Complete literature on request.

TMC

TECHNICAL MEASUREMENT CORPORATION

441 WASHINGTON AVE., NORTH HAVEN, CONN., U.S.A.

-how to sell your nuclear products internationally-

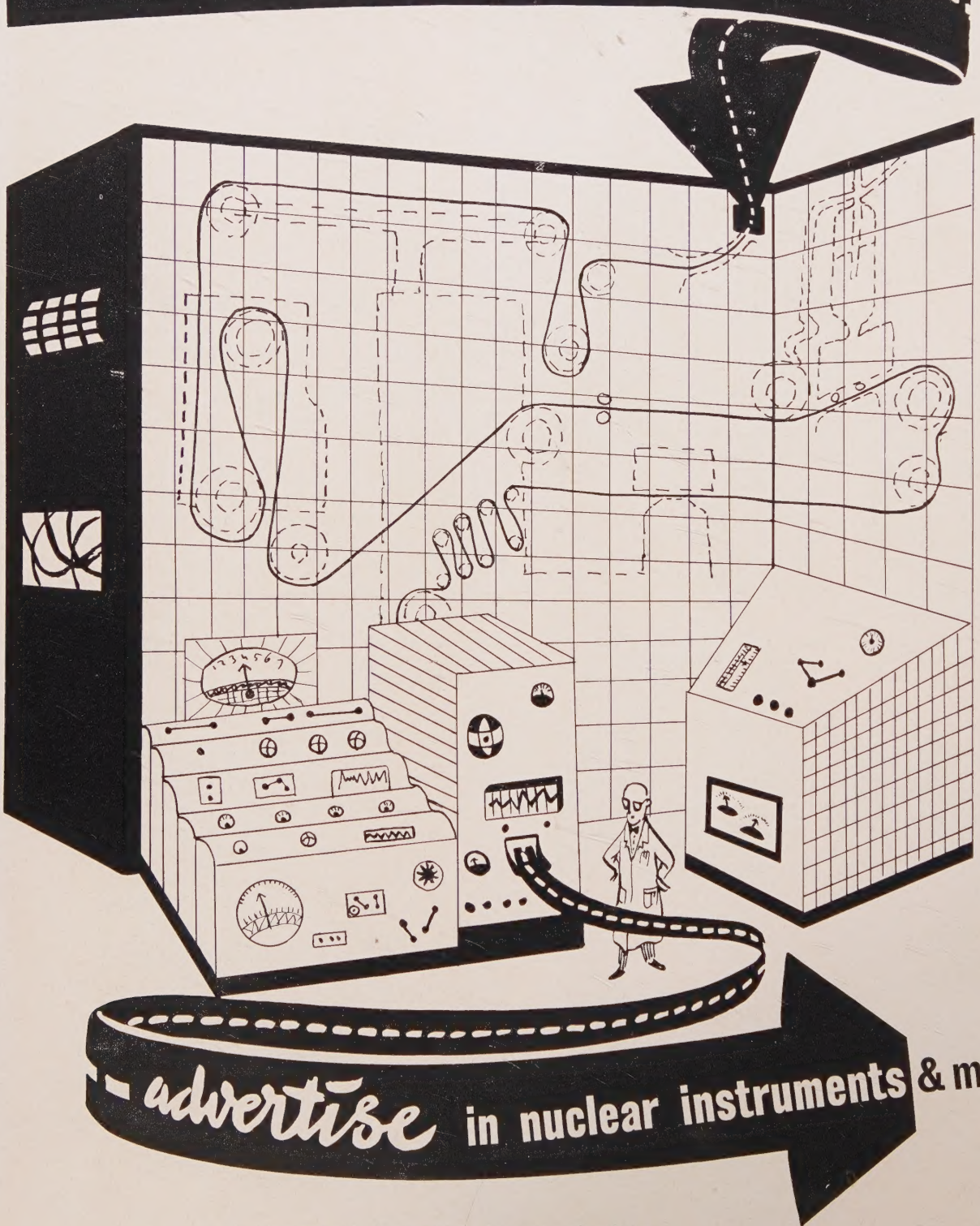

-advertise in nuclear instruments & methods

Go International with your Sales Program today-Write

William F. Baars-Advertising Manager, North-Holland Publishing Company

P.O. Box 103, Amsterdam, The Netherlands

Turn this page and step into the future of Automatic Sample Counting . . .

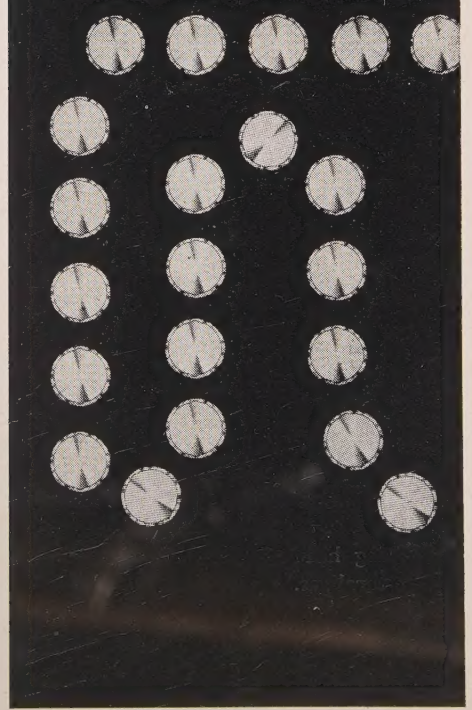

Now you can do ALL your Sample Counting Automatically ...with the New Tracerlab *multi/matic* Sample Changer

Fifty sample capacity . . . any size up to two inch . . . any type of detector (Scintillation, Flow Counters, GM Tube) . . . simple one-knob operation . . . these exclusive advantages plus low initial cost and low operating costs . . . are all yours in the outstanding new Tracerlab MULTI/MATIC Sample Counting System.

Only from Tracerlab — the world's largest and *first* manufacturer of Sample Changers could you expect — and get — such a revolutionary new system.

The New SC-100 MULTI/MATIC Sample Changer provides positive, accurate positioning of samples. Samples are readily accessible because they are loaded and driven on a horizontal plane (in contrast to tower or stack types). Automatic recycling of a single sample, automatic by-pass of empty sample positions, automatic recycling to the starting position plus the ability to operate with all types of detectors are other features of this most versatile new Tracerlab development.

The New Tracerlab FD-1 and FD-2 Flow Counters feature the ultra-thin Tracerlab Mono/mol window (less than 125μg/cm^2). These low cost units, available in 1″ or 2″ window diameters plug in to a common shield and feature low background . . . excellent plateau characteristics . . . very low gas consumption and will operate with a wide variety of counting gases including helium-isobutane, argon-methane, methane or natural gas.

The New Tracerlab SH-1 Shield operates with either the automatic changer or the SC-101 Manual Changer pictured. It accommodates both the 1″ and 2″ FI Series Flow Counters, windowless flow counters, P-20I Scintillation Detectors or standard GM detectors. Convenient handles make it easy to insert or remove from any changer, shield thickness of 2 inches of lead provides low reproducible backgrounds.

The Tracerlab MULTI/MATIC Sample Counting System when combined with other Tracer/matic components . . . scalers, time and count printers, or time count and CPM printers . . . provides more specific sample information than any other system.

For complete specifications on the new low cost, economical-to-operate Tracerlab MULTI/MATIC Sample Changer write for Bulletin M.

Tracerlab Tracerlab Kelvet

1601 Trapelo Road, Waltham 54, Massachusetts
2030 Wright Avenue, Richmond 3, California
European Office: TRACERLAB (Holland)
N.V. 119 Singel, Amsterdam, Netherlands

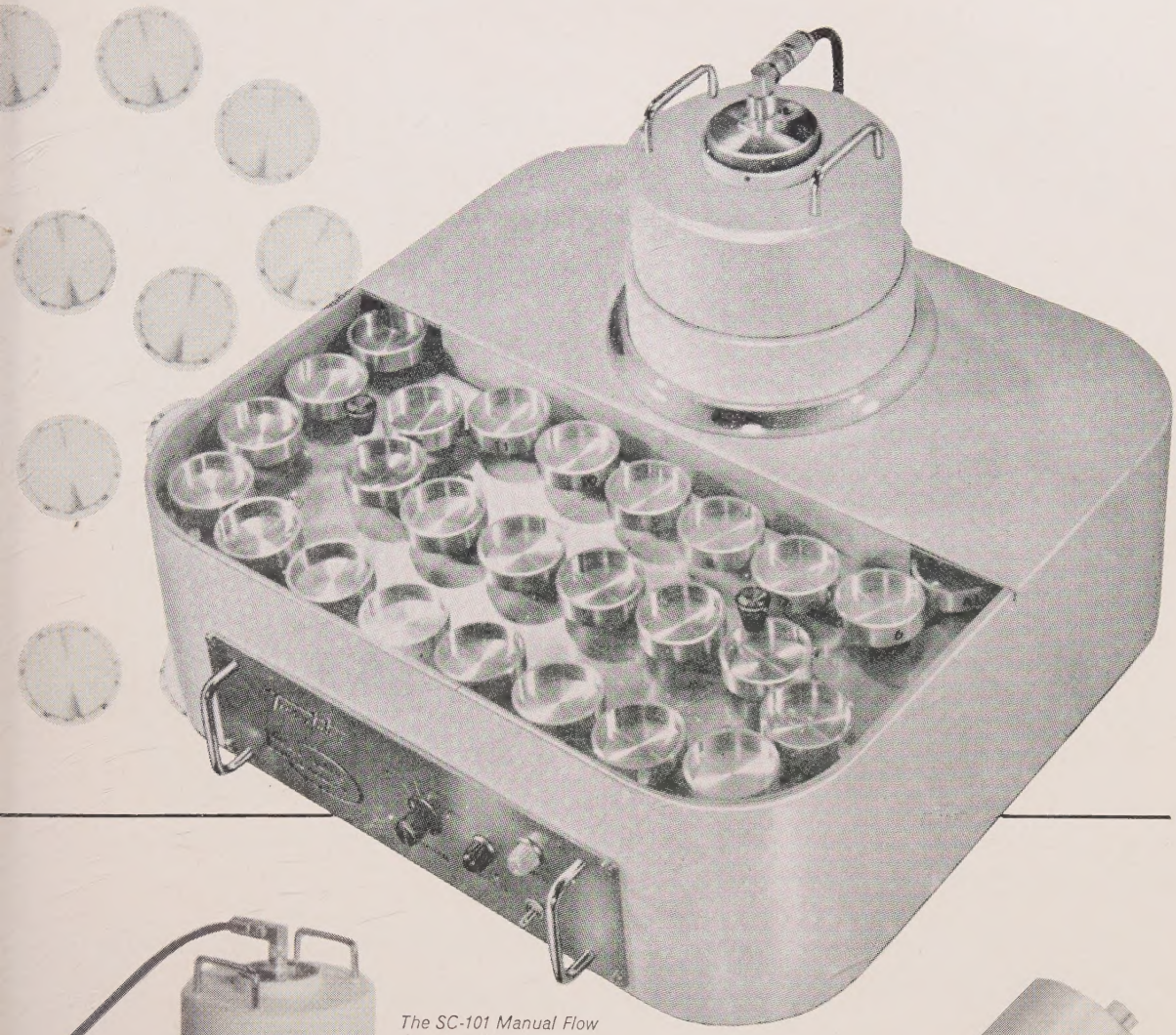

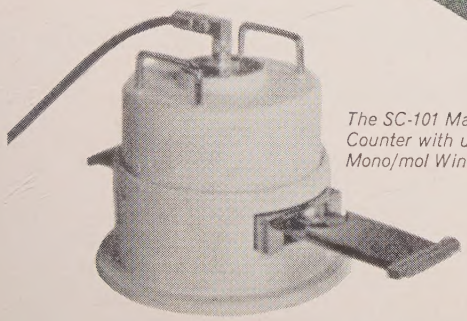

The SC-101 Manual Flow Counter with ultra-thin Mono/mol Window Detector.

New FD Series Flow Counter with the ultra-thin Mono/mol Window features plug-in assembly.

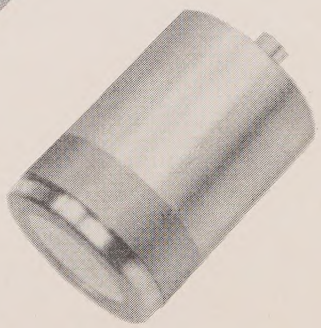

The New Tracerlab MULTI/MATIC Sample Changer combined with the Tracerlab Compu/Matic Scaler and Auto/Computer provides more useful, recorded data than any other system on the market.

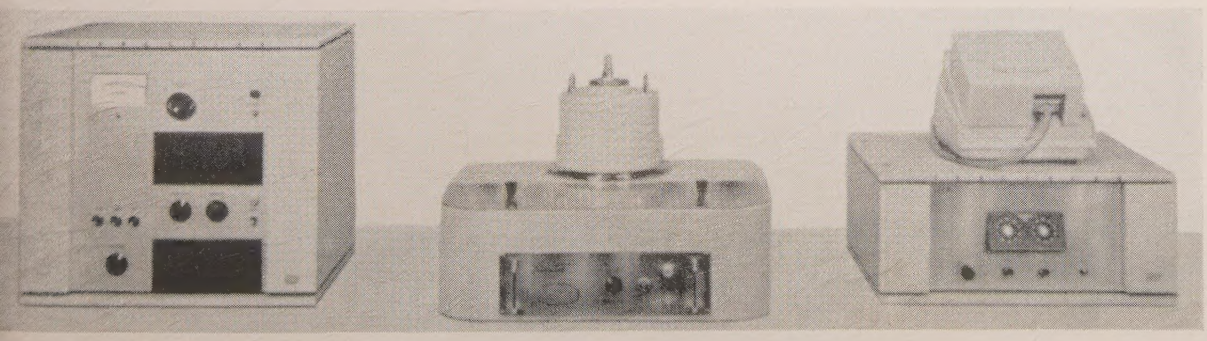

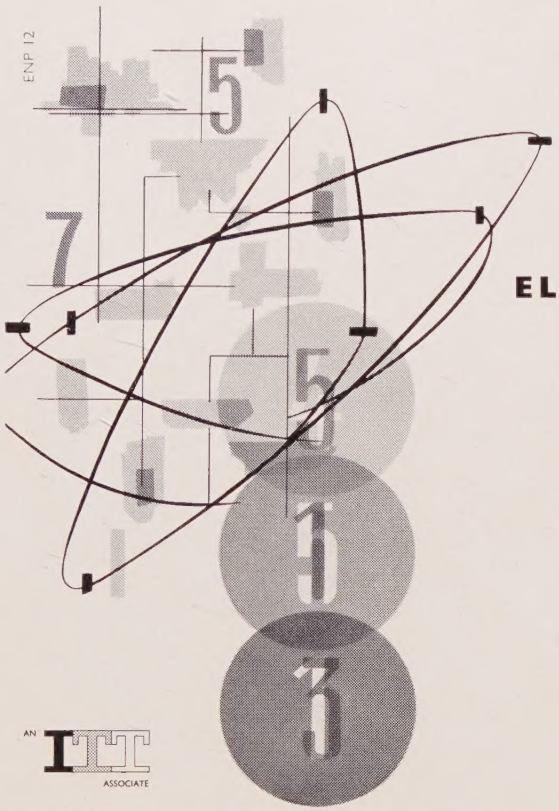

ELECTRONICS FOR NUCLEONICS

SCALER CHRONOSCOPE

Bell Telephone scaler chronoscope gives you top quality reproduction of automatic counting and printing.
It is so constructed that from a small stock of basic modules a wide scope of performances can be covered. This type normally supplied in a metal case is also available for rack mounting

- preset time
- preset count
- result printing facilities
- interchangeable modules
- in line read out
- fully transistorized

Our staff is always available to answer your inquiries.

Bell Telephone Mfg Co

"Nuclear Energy division"
33, Berkenrodelei
HOBOKEN-Antwerp-BELGIUM

NANOSECOND PULSES? - MICROSECOND PULSES?

MODEL 414

CALIBRATION PULSER

Decay Times	*Ranges*
0.003 microseconds	0 - 1 millivolts
0.01 microseconds	0 - 5 millivolts
0.03 microseconds	0 - 10 millivolts
0.1 microseconds	0 - 50 millivolts
0.3 microseconds	0 - 100 millivolts
1. microseconds	0 - 500 millivolts
3. microseconds	0 - 5 Volts
10. microseconds	0 - 10 Volts
100. microseconds	0 - 50 Volts
	0 - 100 Volts

Dual purpose- manual or motor driven slider.
Dual 50 ohm output permits coincidence circuit applications.
Internal standard cell calibration.
Polarity switch for positive or negative pulses.
0.1% helical potentiometer.
High pressure hermetically sealed mercury relay.

Write for details

$ 785 f.o.b. factory

RADIATION INSTRUMENT CO.

P.O. BOX 733

SILVER SPRING, MARYLAND, U.S.A.

NORTH-HOLLAND BOOKS

Plasma Physics

by

J.G. Linhart

CERN, Geneva

"The author of the present work, who is well known for his contributions in the C.T.R. field, has given in his book an interesting presentation of the complementary approaches of (1) individual particle motion, and (2) a fluid description of a plasma in relation to the study of high temperature discharges.
This book can be highly recommended."

Institute of Physics Bulletin

6×9″ 290 pp. 125 figs. Gld. 25.00 (50 s.)

NORTH-HOLLAND PUBLISHING COMPANY
AMSTERDAM

Sole distributor U.S.A.: Interscience Publishers Inc. New York

High accuracy
Maximum flexibility

FEATURED BY

200-Channel Pulse Height Analyzer - mod. C31 - CISE

- spectrum storage in 200 channels; 16 bits per channel ferrite memory
- independent spectrum storage in two sets of 100 channels (100′ and 100″)
- spectrum storage of the input pulses in either undelayed or delayed coincidence with other external pulses
- simultaneous storage of two independent spectra, one in the first and the other in the second 100 channel set, by using optional mixer
- spectrum storage in the first 100 channel set with automatic transfer in the second 100 channel set of the pulses coincident with other external driving pulses
- three dimensional-coincident energy spectra with 10 × 20 channel memory subgrouping
- optional possibility to store ten spectra of 20 channels each, shifting from one spectrum to the following in a time sequence triggered by an external programmer
- optional possibility to connect, in place of the normal pulse height to time input Converter, a time-of-flight unit for neutron spectrography
- optional possibility to obtain the automatic programming of device's operation by using an external programmer
- 0.5% linearity through 60 V range
- 1/3 channel per day maximum drift
- Dead Time:
variable:
$20 + 0.5\,N + T\,\mu$ sec, where:
N = channel number
T = rise time protection (μ sec);
fixed: $120 + T\,\mu$ sec
- simultaneous oscilloscope display
- optional strip-chart recorder
- printing performed by a modified « Olivetti Lexicon » electrical typewriter

BEFORE YOU DECIDE contact our technical staff

LABEN Laboratori Elettronici e Nucleari S. r. l.
MILANO - VIA AMADEO 41 - TELEFONO 712494/95

CDC's PROVEN PERFORMANCE

100-CHANNEL PULSE HEIGHT ANALYZER

CHALK RIVER KICKSORTER

Manufactured by Computing Devices of Canada, Limited, from specifications prepared by Atomic Energy of Canada, Limited.

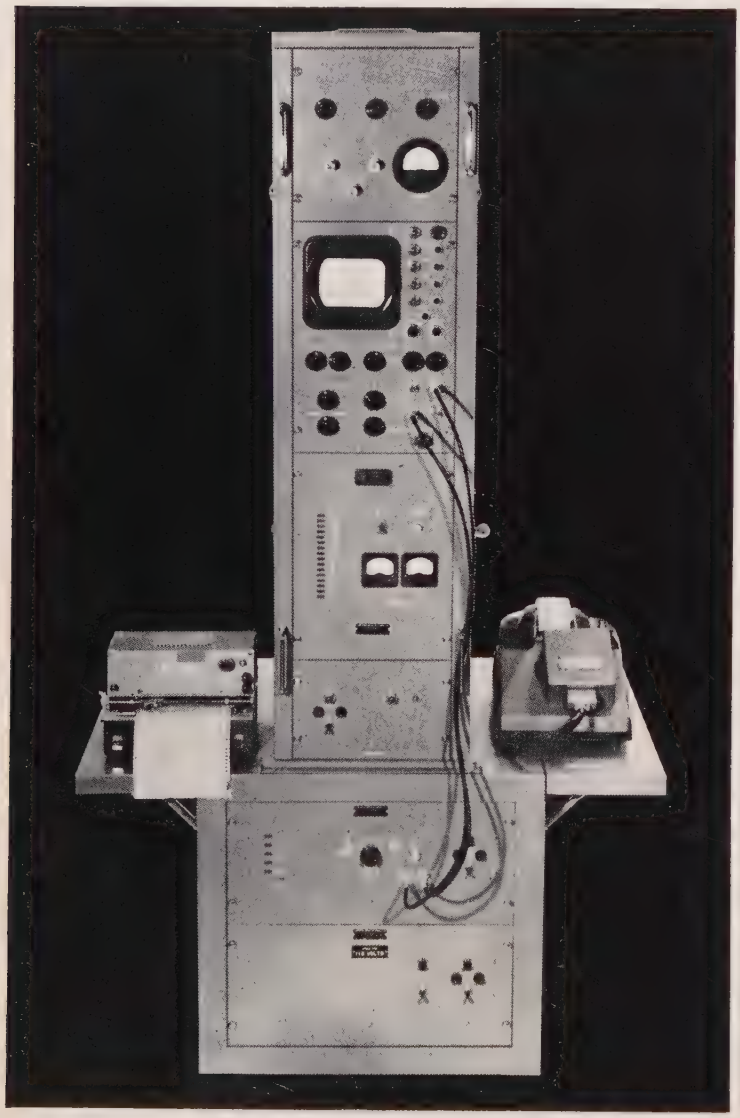

The convenience and speed of automatic printout can be obtained by add ng a Decimal Scaler, a Print Control Unit, and an Electric Printer as accessories, shown with the Kicksorter. Provision is also made in the circuitry for the addition of a Pen Recorder for more accurate analog output.

88% TRANSISTORIZED

- Printed Circuitry
- Low Maintenance—High Reliability
- Low Power Consumption—120 Watts
- No Ventilation or Cooling Problems

VERSATILE DATA PRESENTATION

- Oscilloscope Display
- Binary Manual count readout allows the count on any channel to be displayed in digital form.
- Magnetic Core Memory—65,535 counts can be stored per channel.
- Permanent Count Storage—sixteen magnetic cores for each of the 100 channels.
- Highly Versatile—can be modified to accommodate most applications which require additional features.

The Chalk River "Kicksorter" is designed to span random pulses of various amplitudes and shapes, sort them according to amplitude into 100 channels, and store a record of the counted pulses in a magnetic core memory. This computer, with its magnetic core memory and versatile data display system, makes it possible to observe the pulse amplitude spectrum as it accumulates or after it has accumulated.

In addition to its wide use in gamma spectroscopy, the "kicksorter" has many applications in medical research, neutron time-of-flight studies, radioactive fallout studies, shielding studies, oil well and uranium logging, neutron activation analyses, measuring of radioactivity in humans, and other areas.

The analyzer is designed so that information accumulated may be displayed or read out in various ways. Data may be observed on the oscilloscope, or information already accumulated in the memory core may be displayed on the screen, plotted on a strip chart recorder, or printed out in decimal form on an automatic printer.

For additional information, wire or write to:

Bendix International

DIVISION OF THE BENDIX CORPORATION
205 East 42nd Street
New York 17, N. Y., U.S.A.
Cable Address: "Bendixint"

Sales Representative for Great Britain

NUCLEAR ENTERPRISES (G.B.) LTD.

BANKHEAD MEDWAY, SIGHTHILL,
EDINBURGH 11, SCOTLAND

SALES AND SERVICE AVAILABLE THROUGHOUT THE WORLD

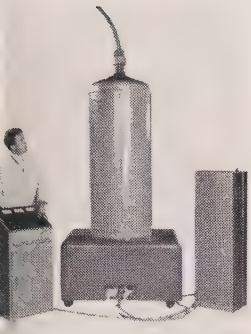

600 kV Generator

Research Centres and Industry alike find the modern, polished solution to the problem of continued high voltage in the

SAMES ELECTROSTATIC GENERATOR

Electrostatic Painting with the STATRON

HIGH VOLTAGE GENERATORS

- 50 kV to 600 kV
- 20W to 3 kW
- Positive or negative polarity
- Medium or high stability

for

- Electrostatic precipitation
- Electrical testing
- Electronic optics
- X-rays
- Nuclear Physics, etc.

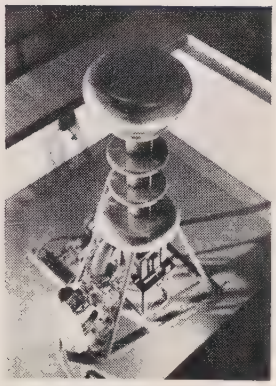

Vertical 600 kV
Accelerator at the Centre d'Etudes Nucléaires de Grenoble

ELECTROSTATIC PAINTING

The STATRON is a portable equipment for electrostatic painting, featuring

* 90 kV voltage
* Complete safety, owing to use of electrostatic generator.
* Paint output: 15 litres/hour
* Supply: 110 or 220 V, single phase.
* Consumption: 110 Watts

PARTICLE ACCELERATORS

Type	Acceleration Voltage	Particles Accelerated	Application
J	150 kV	ions	Neutron Generator by D/T or D/D reaction
L	300 kV	ions	
S	600 kV	ions or electrons	All applications

SOCIETE ANONYME DE MACHINES ELECTROSTATIQUES

21, RUE JEAN MACÉ, P.O. BOX 150, TEL: 44.77.64 GRENOBLE, FRANCE

REPRESENTATIVES

GENERATORS AND ACCELERATORS

Austria: AUSTRONIK, Salzburg – Belgium: CENTRONICS, Brussels – Chinese People's Republic: Cie OLIVIER, Paris – Denmark: DANSK SCIENTA, Copenhagen – Great Britain: MILES HIVOLT LTD., Shoreham by Sea – Italy: SECI, Milan – Netherlands: PROJECTO, Amsterdam – Norway: LEHMKUHL, Oslo – Portugal: A.G.M.E., Lisbon – Spain: CRESA, Barcelona – Sweden: SCIENTA SCANDIA, Gothenburg – Switzerland: OMNIRAY, Zurich – Western Germany: DR. NAMUR, Darmstadt – Bulgaria, Czechoslovakia, Eastern Germany, Hungary, Poland, Rumania, U.S.S.R.: CIFAL, Paris.

ELECTROSTATIC PAINTING EQUIPMENT

Algeria: FAMPA, Algiers – Austria: PETER PETERSEN, Vienna – Belgium: DURMECO, Brussels – Chinese People's Republic: Cie OLIVIER, Paris – Denmark: DANSK SCIENTA, Copenhagen – Eire: HODGES & SONS, Dublin – Great Britain: AEROSTYLE LTD., London – Italy: TRASMETAL, Milan – Netherlands: STUURMAN, Wormerveer – Norway: LEHMKUHL, Oslo – Portugal, RAMADA, Ovar – Spain: INSTITUTO ELECTROQUIMICO, Barcelona – Sweden: SCIENTA SCANDIA, Gothenburg – Switzerland: REGSA, Lausanne – Western Germany: A. WIRTH, Reutlingen – Bulgaria, Czechoslovakia, Eastern Germany, Hungary, Poland, Rumania, U.S.S.R.: CIFAL, Paris.

Van de Graaff®
Accelerators
0.4 to 15 Mev Energy
Electrons:
up to 1 ma at 3 Mev
Positive Ions:
up to 400 μa at 3 Mev
Neutrons:
up to 10^{12} n per sec

For Research
In Nuclear Physics
Biology & Medicine
Solid State Physics
Radiation Chemistry
Reactor Kinetics

For Application
In Polymerization
Sterilization — Therapy
High Energy Radiography
Catalysis
Nuclear Engineering
and Teaching

LINACS
Microwave Linear Electron Accelerators
4 to 150+ Mev Energy
Peak Pulse Current:
up to 1 ampere
in 0.3 μsec pulses
Neutrons:
up to 10^{16} n per sec
during pulse

160 cm
Electromagnetic Isotope Separator
10 μa of most abundant isotope in mass range 1 to 400
(Resolving Power: 400)
Ion Sources
Duoplasmatron—200 ma protons
Neutral and Negative Ion Sources

Cockcroft-Walton Accelerators
40 to 800 kev Energy
Beam Current:
up to 2 ma
Neutrons:
up to 10^{11} n per sec

Electromagnetic Accelerator
100 to 600 kev Energy
Current Capacity:
up to 8 ma

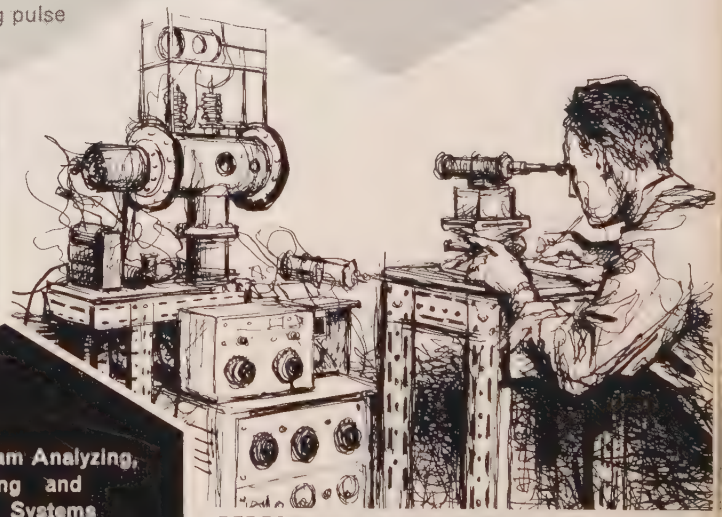

Beam Pulsing Equipment
Van de Graaff:
1.0 millimicrosecond
up to millisecond
Linacs:
0.1 to 30 μsec pulses

Magnetic Beam Analyzing, Stabilizing and Switching Systems
Ion Lens Systems
Electron Scanners
5" to 30"

PERFORMANCE SPECIFICATIONS ALWAYS GUARANTEED
More than 275 particle accelerators by High Voltage Engineering Corporation and Applied Radiation Corporation are now installed world-wide

Mass Spectrograph/ Spectrometers
for energy analysis of protons, deutrons, alpha particles
(Resolving Power: 10^{-3})

HVEC

HIGH VOLTAGE ENGINEERING CORPORATION
BURLINGTON, MASSACHUSETTS • U.S.A.
APPLIED RADIATION CORPORATION
WALNUT CREEK, CALIFORNIA, U. S. A.
HIGH VOLTAGE ENGINEERING (EUROPA)
AMERSFOORT, THE NETHERLANDS

NUCLEAR INSTRUMENTS AND METHODS 10 (1961) 249–258; NORTH-HOLLAND PUBLISHING CO.

THE MELBOURNE UNIVERSITY VARIABLE ENERGY CYCLOTRON

D. E. CARO and J. L. ROUSE

Physics Department, University of Melbourne

Received 12 January 1961

A description is given of a variable energy cyclotron designed primarily to produce protons with an energy in the range 2 to 12 MeV, and with an energy resolution of 0.1 %.

1. Introduction

For the study of the structure and behaviour of atomic nuclei, machines are required which can accelerate protons or other atomic particles to high energies. For many years it has been possible to obtain electrostatic accelerators capable of producing beams with good energy definition up to four or five MeV. Cyclotrons have given good service at higher energies but their utility has been somewhat limited by the restriction that only one output energy was generally possible.

For some years workers in the nuclear physics field have felt the need for a machine capable of accelerating particles to any energy up to 10 MeV or more. Recently, this has become possible with electrostatic accelerators using the tandem principle. In these machines, negative ions are accelerated towards a positive electrode within which they are stripped of their electrons. The resulting positive ions are then further accelerated through the same potential difference. Machines using this principle are now working satisfactorily in a number of laboratories. The energy definition is good, the energy is easily controlled and beam currents are sufficient for most experiments.

In June 1953, it was decided to tackle the problem of a variable energy accelerator in a different way, and a design study was made of a variable energy cyclotron. Such a machine appeared feasible and construction was started in 1954. Some preliminary design features of the cyclotron were reported by Caro, Martin and Rouse (1955)[1]). Since then the cyclotron has been brought into operation, many difficulties have been overcome and the original design has been modified in a number of ways.

The Melbourne University Variable Energy Cyclotron (MUVEC) is designed to have a performance comparable with that of the most advanced electrostatic tandem accelerators although its cost is very much less. The primary specification of MUVEC is the production of protons with an energy in the range 2 to 12 MeV although other positively charged particles can be accelerated. At present the machine is being used exclusively as a proton accelerator. The specifications also include the extraction of the beam from the cyclotron so that, after focussing and analysing, a beam with an energy spread of $\pm 0.1\%$ can be put on to an external target which is well away from the cyclotron itself.

2. Energy Relations in a Variable Energy Cyclotron

In a cyclotron, the energy of the beam at a radius R metre in a field of induction B weber metre^{-2} is

$$E = \frac{Z^2 e R^2 B^2}{2 A M_p} \text{ electron volt} \qquad (1)$$

where Z is the atomic number and A the mass number of the particle undergoing acceleration, e is the charge on the electron in coulomb and M_p the proton mass in kilogram. The relation is of course approximate, no allowance having been made for the relativistic increase in mass with energy. The

[1]) D. E. Caro, L. H. Martin and J. L. Rouse, Australian J. of Phys. 8 (1955) 306.

angular frequency ω of the R.F. system is related to the magnetic field by

$$\omega = \frac{ZeB}{AM_p} \text{ radian per second.} \quad (2)$$

In a variable energy cyclotron, the magnetic field and the frequency of the R.F. voltage applied to the accelerating electrode must both be variable. For MUVEC they are adjustable over a range of 2.5 to 1. The ranges chosen are as follows:

Central magnetic field: 0.55 to 1.4 weber metre^{-2},

Radio frequency: 8.6 to 21.5 Mc/s.

The maximum energy to which a particle can be accelerated is determined by the maximum magnetic field attainable while the minimum energy is determined by the lowest radio frequency which can be produced. For MUVEC, the proton energy range is 2–12 MeV. In terms of the proton energy limits $E_{p\,max}$ and $E_{p\,min}$ the energies which can be achieved with other particles are

$$E_{max} = \frac{Z^2}{A} E_{p\,max} \quad (3)$$

and

$$E_{min} = AE_{p\,min}. \quad (4)$$

If E_{min} is greater than E_{max} the particle cannot be accelerated in the normal mode.

There remains the possibility of acceleration in the third harmonic mode where ω has three times the value given by eq. (2). In this mode, the maximum energy is determined by the maximum radio frequency while the minimum energy is determined by the lowest useable magnetic field. This gives the energy relations for third harmonic acceleration,

$$E_{3\,max} = \frac{A}{9} E_{p\,max} \quad (5)$$

and

$$E_{3\,min} = \frac{Z^2}{A} E_{p\,min} \quad (6)$$

where $E_{p\,max}$ and $E_{p\,min}$ are the proton energy limits for first harmonic acceleration. The table below inidicates the energy ranges to be expected from MUVEC for a number of particles which it may be attractive to accelerate.

Particle	Fundamental Mode (MeV)	Third Harmonic Mode (MeV)
proton	2–12	—
deuteron	4–6	1–2.7
alpha	8–12	2–5.3
He^3	6–16	2.7–4

3. Description of MUVEC

While most machine parameters need adjustment with energy in a variable energy cyclotron, the magnetic field and the frequency of the R.F. voltage applied to the accelerating electrode present the main problems.

3.1. THE MAGNET

The design and performance of the cyclotron magnet have been described previously (Caro *et al.* 1955, ref.[1]). Since 1955,the width of the shim gaps has been increased from $\frac{5}{16}$ inch to $\frac{7}{16}$ inch. Each of these two gaps now contains seven sets of coils

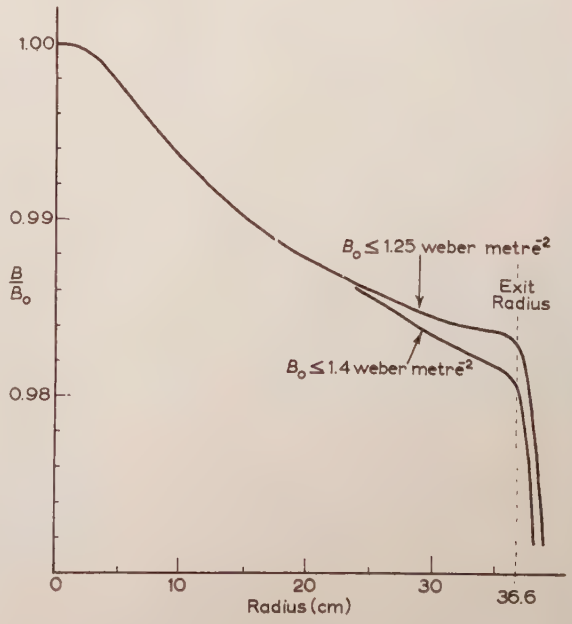

Fig. 1. Magnetic field profile of cyclotron magnet.

concentric with the magnet axis and excited from the magnet supply. By adjusting the magnitude and direction of the current in these coils small

variations may be obtained in the magnetic field profile and the position of the median plane. Steel shims may also be inserted for field correction, but their use is limited because of the difficulty associated with positioning or removing them. The electric and steel shimming has been used primarily to raise the magnetic median plane which was found to be low over the operating range of magnetic fields. The measured magnetic field profile for central fields from 0.55 to 1.25 weber metre^{-2} and for 1.4 weber metre^{-2} is shown in fig. 1. The small change in profile at large fields is due to saturation of the steel at the edge of the pole tips.

A nuclear resonance set is used to stabilize the magnetic field in conjunction with a voltage stabilizer. Initial tests with the nuclear resonance head mounted in a shim gap were unsatisfactory due to the inhomogeneity of the magnetic field there. The head is now mounted in the main gap. Nuclear resonance stabilization provides both high stability and reproducibility. The stability is important when extracting a beam and the good field reproducibility allows the machine to be set up at any energy in the minimum time.

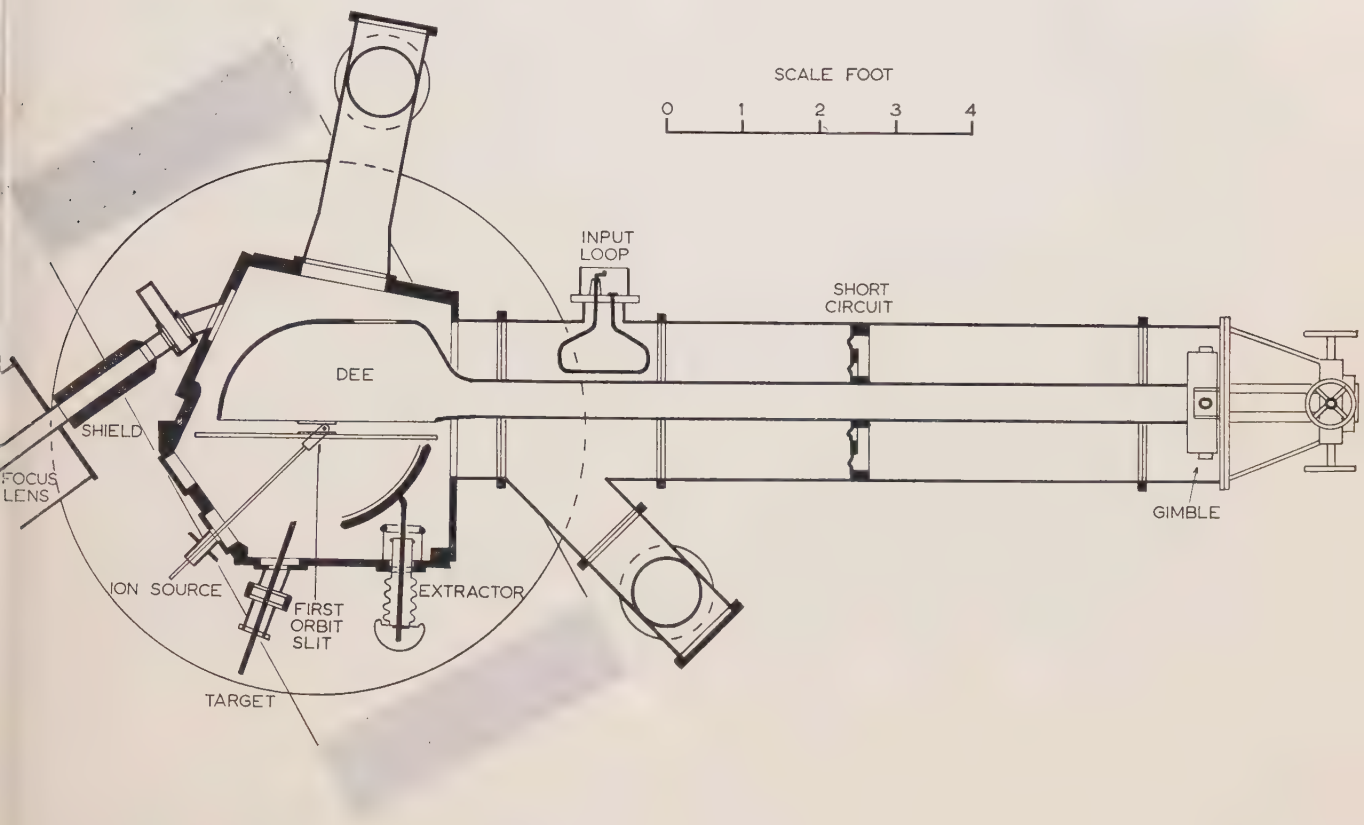

Fig. 2. Layout of dee and dee line resonator.

3.2. THE RADIO-FREQUENCY SYSTEM

To cover the full machine energy range and to allow the acceleration of ions heavier than protons the radio-frequency system is tunable over the range 8.6 to 21.5 Mc/s. The power output required depends on frequency and reaches a maximum of about 30 kW at the highest frequency. A frequency stability of one part in 10^4 and a dee voltage stability approaching one part in 10^3 are necessary if the cyclotron is to perform efficiently.

MUVEC has a single active dee mounted on a coaxial line resonator. This system is simpler to tune than the more conventional twin dee arrangement. Since the whole accelerating potential appears between dee and ground, high voltage gradients in the direction of the magnetic field

result. At the maximum machine energy of 12 MeV, voltages in excess of 120 kV are applied to the dee and flashover sets a limit to the performance of the cyclotron.

Fig. 2 shows the layout of the dee and dee-resonator. The internal height of the water-cooled dee is 2 inch and this is reduced to 1.75 inch by graphite blocks located so as to prevent any beam from hitting the copper dee. The dee is supported on a steel stem sheated with a water-cooled copper tube 6 inch in diameter. The R.F. joint to the dee is made using aluminium bolts which pull down tightly on undercut copper washers. These provide a series of contact edges round the stem and carry the maximum circulating current of 2500 ampere RMS without overheating.

The gimble mounting and adjusting screws at the rear end of the dee stem allow movement of the dee up to $\frac{1}{4}$ inch in any direction. The dee resonator outer conductor is a 24 inch diameter copper cylinder of length 9 foot, and this is coupled to the vacuum box through a short cast dural transition section. The vacuum box is also of cast dural lined with copper plates in the region occupied by the R.F. field. Three tuning arrangements are provided, (i) a moveable short-circuit in the coaxial line, (ii) moveable liners to vary the dee to ground capacity and (iii) a rotating short-circuited loop. Above 14 Mc/s (approximately 5 MeV for protons), the moveable liners are set for maximum dee to liner spacing ($1\frac{9}{16}$ inch). The dee to ground capacitance is then about 200 pF and the resonator has a Q of about 8000. For the lower frequencies required for proton energies less than 5 MeV, and for the acceleration of particles heavier than a proton, the dee to liner spacing is reduced. The increased dee to ground capacity results in greater circuit losses but since lower dee voltages are required this is not important. In both cases, coarse tuning is achieved by movement of the short-circuit and fine tuning over a range of $\pm$ 0.5% is achieved by rotating the short-circuited tuning loop. Both the variable liners and the moveable short-circuit can be adjusted through vacuum seals. The former are designed to be used only for range setting and take half an hour to reset. The latter can be moved to any position in a few minutes.

The design of a short-circuit which is capable of carrying an R.F. current of 2500 ampere RMS, which can be moved without opening the vacuum system, and which at the same time provides no constraint on the inner conductor, posed serious problems. Several designs were tried before the present one was adopted. Fig. 3 shows the principle

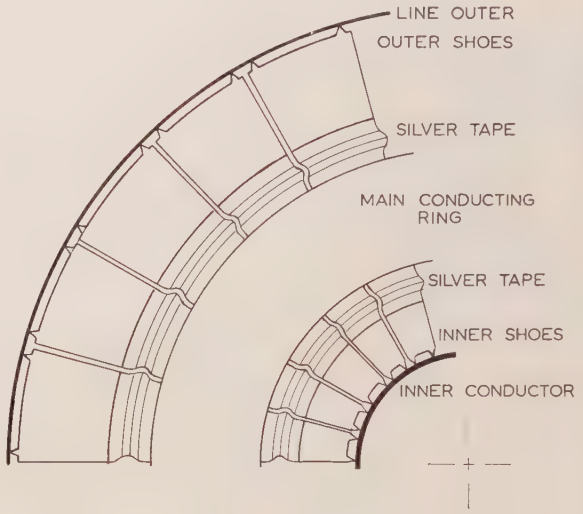

Fig. 3.
Principle used in the construction of the dee line short circuit.

used in the existing short-circuit which has now given trouble free service for two years. Fig. 4 shows the short-circuit, excitation loop and tuning loop assembled within the dee line resonator. R.F. currents are conducted from the line outer conductor through about 30 contact shoes each carrying two wedge shaped conductor bars 2 inch long in the axial direction. These contact shoes are water-cooled and form a ring which is expanded by a neoprene bicycle tube to press the contact bars firmly against the outer conductor. The outer shoe ring runs on a trolley which is carried on the outer conductor. Current flows from these shoes through silver tapes 0.006 inch thick, $1\frac{1}{4}$ inch wide and $1\frac{1}{2}$ inch long to the main conductor ring. A similar arrangement carries current from this ring to the coaxial line inner conductor, the inner shoe ring being carried by a trolley running on the inner conductor. The two rings are loosely linked together and when the shoes are retracted by evacuating the pneumatic tubes the assembly can

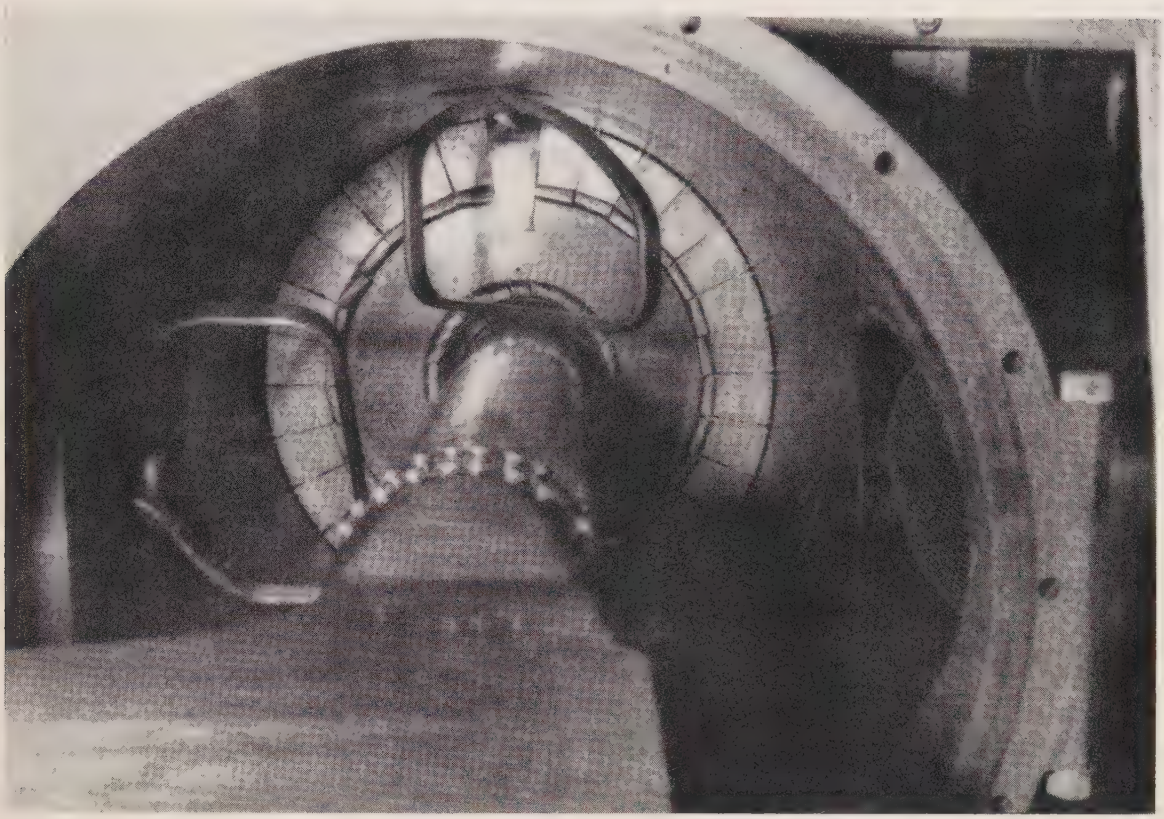

Fig. 4. Photograph showing the short circuit, excitation loop and tuning loop assembled within the dee line resonator.

be driven along the coaxial line by a 20 turn per inch screw. The position of the short-circuit is recorded on a revolution counter. The longitudinal contact bars touch the line conductors at two or three points only, but with 30 lb/sq. inch pressure in the pneumatic tubes, the resulting R.F. contact is entirely satisfactory.

Radio-frequency power to the dee resonator is supplied by an oscillator-power amplifier system, loop coupled to the dee line. Fig. 5 shows a block diagram of the arrangement. A stable variable frequency oscillator with a range of 2 to 4 Mc/s provides the necessary frequency accuracy and stability for satisfactory machine operation. The oscillator signal is amplified and multiplied in frequency by four or eight through the buffer amplifier stages of the exciter. The exciter power amplifier, using four 813 tetrodes provides the necessary grid power for the push-pull driver using water cooled tetrodes type QBW5/3000. This unit is capable of a power output of 4 kW or more and it provides ample grid drive for the final amplifier.

A simplified circuit of the final amplifier is shown in fig. 6. A single grounded cathode stage is employed, the valve being a water cooled triode (S.T.C. Type 3Q/261E) with a plate dissipation rating of 20 kW. This circuit is capable of generating 50 kW of radio frequency power but like the

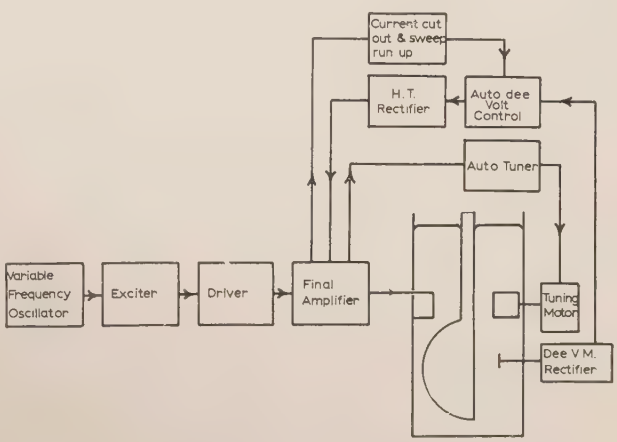

Fig. 5. Block diagram of radio frequency system.

driver it is generously rated and its power output rarely exceeds 25 kW. Drive is applied to the valve grid through the π-network C_1, L_1, C_2. L_1 and C_1 are adjustable to provide a match for the coaxial

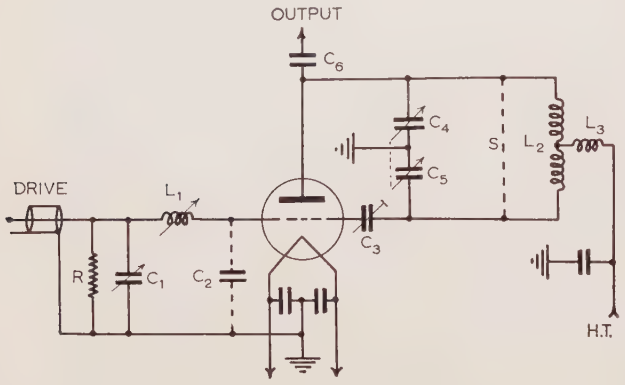

Fig. 6. Simplified final amplifier circuit.

transmission line from the driver. C_2 is provided by the valve input capacitance. The plate circuit is neutralised by the balanced tank circuit C_4, C_5 and L_2 and the neutralising condenser C_3. C_3, C_4 and C_5 are variable vacuum condensers. The full tuning range is achieved in two steps. From 8.5 to 13.5 Mc/s the full plate tank circuit is employed, while from 13.5 to 21.5 Mc/s a shorting strap S is placed across L_2. The connecting tubes from L_2 to the valve form a resonant twin line for the high frequency range. Power is fed to the cyclotron dee line through the D.C. blocking condenser C_6 and an adjustable coupling loop in the dee line.

The amplifier is neutralised with the load disconnected and the tuning condensers C_4, C_5 are adjusted for minimum plate current. The cyclotron dee line is then connected and tuned for an approximate plate current minimum. The amplifier does not require reneutralising unless a large change in frequency is made, or the valve is changed. C_4 and C_5 need be tuned only when the frequency is altered but the cyclotron dee line needs to be retuned every few minutes, particularly during the "warm up" period.

The amplifier high tension is provided by a six phase grid controlled rectifier. Two methods of voltage adjustment are used. A manual control adjusts the phasing of the firing pulses sent to the thyratron grids and sets the rectifier to the correct operating voltage for the power required from the final amplifier. The rectifier output is also adjusted automatically by an electronic phase delay system. A fraction of the dee voltage, measured by capacitor probes above and below the dee, is subtracted from a fixed reference voltage and applied to the rectifier electronic control system (see fig. 5). This circuit provides dee voltage stabilisation. The circuit also incorporates a fast electronic recycling cut-out which protects the valve and rectifier when dee flashes occur.

To maintain the dee line on tune, an automatic tuner is provided. The amplifier is adjusted to operate slightly off plate dip so that small tuning changes produce a monotonic variation of plate current. A servo-system operates the dee line fine tuner loop to maintain the selected plate current. This very simple system copes with all tuning drifts which occur after the first minutes of operation. The tuning changes immediately after turning on are too rapid for the servo-system. With the auto-tuner and dee voltage stabilizer in operation, the R.F. system runs without attention for periods of several hours.

All controls for the radio frequency system are located in the control room except for those used to set the position of the dee line short circuit and the moveable liners in the vacuum box. An experienced operator can set the system to any frequency from 8.6 to 13.5 Mc/s or from 13.5 to 21.5 Mc/s within 10 minutes. Changing from one range to another takes about half an hour.

While the oscillator-power amplifier system is more complicated than the more usual power oscillator arrangement, it has two important advantages for a variable energy machine. The first is the frequency stability achieved. Since this is governed entirely by the stability of a low power oscillator, tuning changes due to heating of the dee line structure have no effect. It is therefore relatively easy to maintain the frequency to about 1 in 10^4. This, combined with nuclear resonance stabilisation of the magnet, results in the accurate maintenance of the cyclotron resonance condition without continual adjustments. The second advantage of a power amplifier is the reduction of multipactoring troubles. Oscillators are notoriously difficult to

start under multipactoring conditions. The power amplifier on the other hand can be started at zero power and slowly wound up to full power. Multipactor troubles are greatly reduced and the system usually runs up to the desired voltage without difficulty.

An unexpected trouble occurs with the power amplifier system at low frequencies when the moveable liners are close to the dee. In this state the liners are only supported at their edge and it is found that power is fed into the liners so that they vibrate like a drum skin at about their natural resonance frequency. This results in the dee voltage being modulated. It has been established that the feedback can be removed by having a non-reactive low impedance output from the high tension supply for the final amplifier. It is planned to include a series control valve in this supply to overcome this effect. The improved rectifier will also reduce dee voltage ripple which impairs extraction efficiency. It is considered desirable to maintain the dee voltage constant within 0.1%.

3.3. THE ION SOURCE

The ion source is a conventional enclosed arc type source (see fig. 7). The filament chamber is made of ELKONITE and water-cooled. The hood or arc chamber is made from graphite and screws into the filament chamber. The filament is $\frac{1}{8}''$ diameter tungsten and has a life of 100 to 150 hours. Beneath the filament there is a tungsten shield electrically connected to the filament to prevent the arc striking downwards. The filament assembly can be removed from the system in order to replace the filament without breaking the vacuum. Hydrogen gas is fed into the arc chamber via the tube containing the filament and its leads. The hydrogen is generated in an automatic electrolytic cell and dried with concentrated sulphuric acid. Under normal operating conditions the filament current is about 350 ampere, arc potential 60 to 120 volt and arc current 0.4 to 2 ampere.

Protons are drawn out from the arc chamber through a slot $\frac{1}{16}''$ wide by $\frac{1}{2}''$ high and then pass through a $\frac{1}{4}''$ wide slit mounted as part of the dee

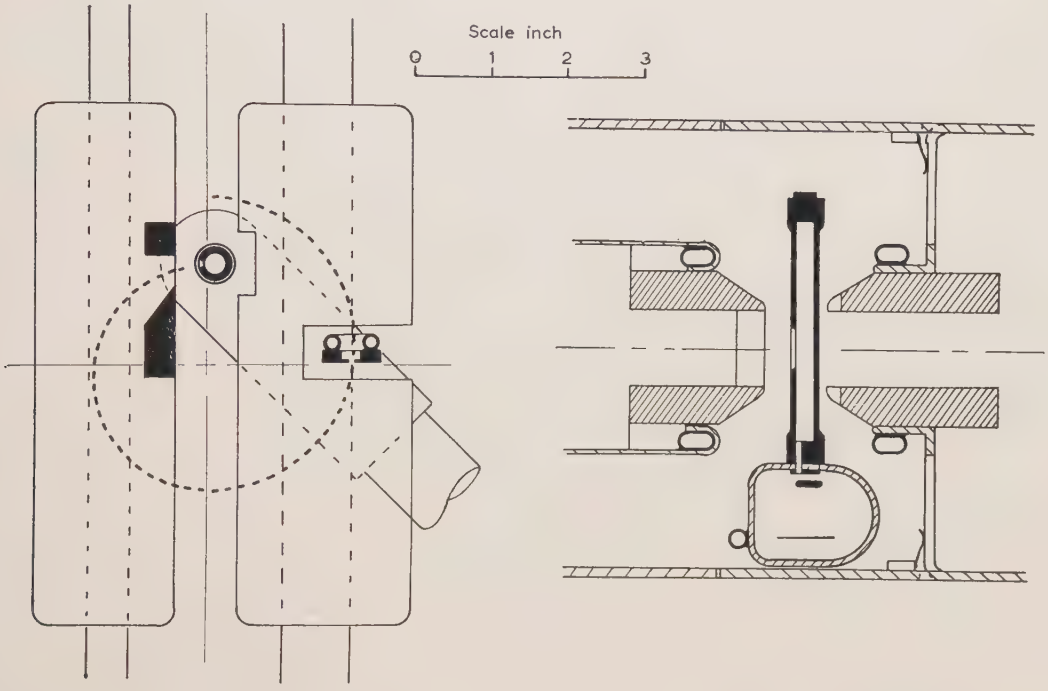

Fig. 7. Sections showing ion source and dee feelers in horizontal and vertical planes.

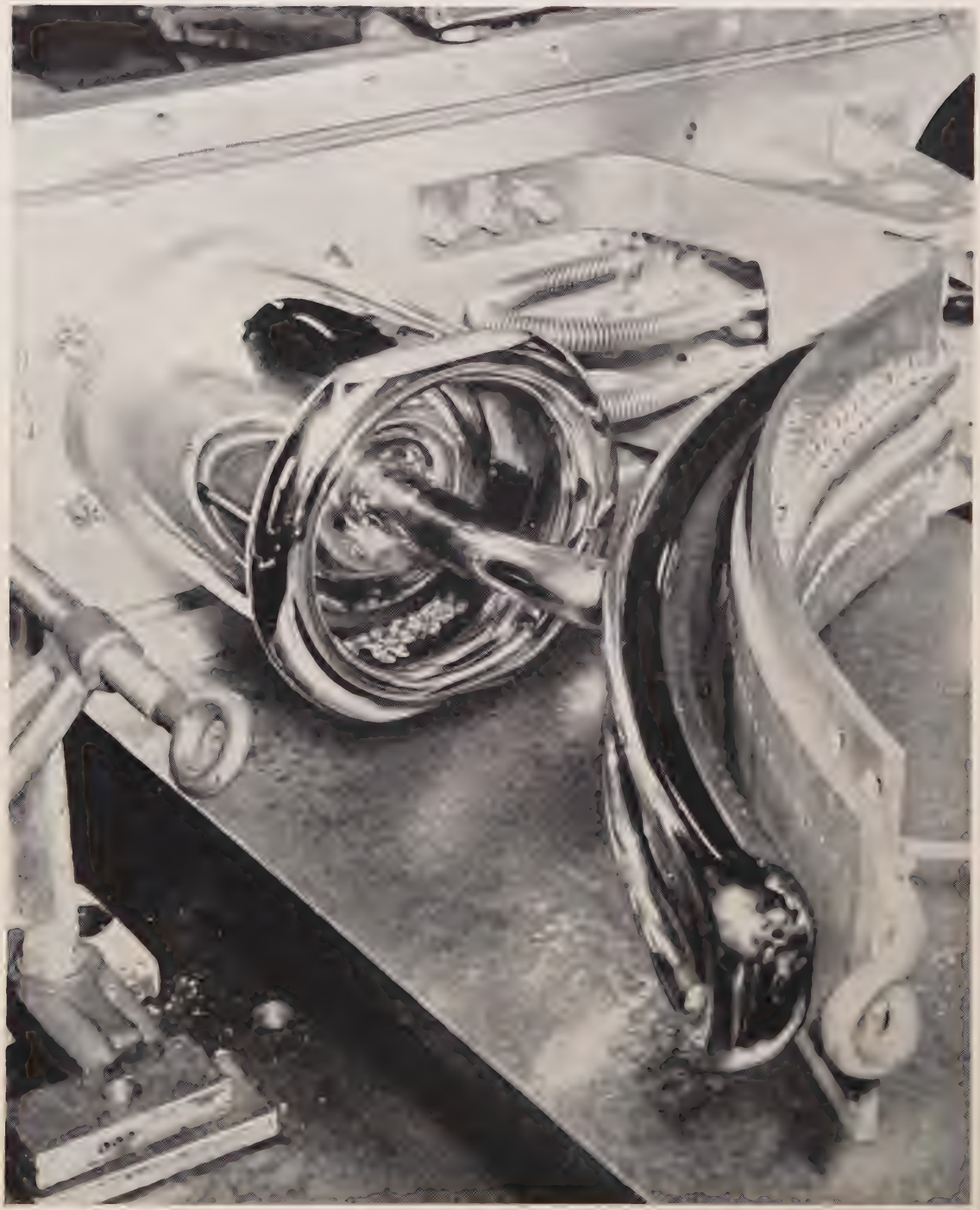

Fig. 8. Photograph of extractor viewed from exit end. On the left is the shield surrounding the deflector feed through insulator.

feelers. Provision is made to adjust the horizontal position of the ion source. The optimum position of the arc column depends upon the dee potential used and lies on a line through the cyclotron centre parallel to the dee edge at a point about 1.3 inch from the centre. Using D.C. extraction proton currents greater than 10 mA have been obtained from the source, and currents up to 1 mA have been

accelerated to the exit radius of the cyclotron.

A small slit located in the first beam orbit restricts the range of initial phase angles of the accelerated ions (Morton and Smith, 1959, ref.[2])). This increases the extraction efficiency and leads to less erosion of the splitter.

3.4. THE EXTRACTOR

The extractor is D.C. energised and is mounted inside the dummy dee with its entrance 36.6 cm from the cyclotron centre. The splitter is made from 45 graphite strips, each $\frac{3}{8}''$ wide, mounted on a water-cooled copper frame. The leading edge of the splitter is 0.5 mm thick and beam erosion produces a V. The oil cooled deflector is shaped like a banana, its surface being well rounded to reduce flash-over. It is machined from copper and plated with chromium. The deflector feed-through insulation is shielded inside the vacuum box to prevent oil or carbon contaminating its surface. The separation of the splitter from the deflector is 5 mm at the entrance to the extractor and about 7 mm at the exit. The splitter can be rotated a few degrees about a vertical axis through its leading edge, while the deflector is effectively fixed. The maximum deflector potential used is 58 kV and a $\frac{3}{4}$ Megohm resistor is in series with the power supply to limit the energy in a flash between deflector and the liners. The splitter is insulated from earth so that the beam current striking the splitter can be measured. An adjustable target reduces the beam striking the deflector. Fig. 8 shows a photograph of the extractor viewed from the exit end.

About 30% of the beam which is accelerated to just inside the splitter radius passes through the extractor, and of this up to 25% can be focussed through a 1 mm wide 2 cm high slit placed about 10 foot from the cyclotron centre.

4. The External Beam Facilities

Fig. 9 shows the layout of the external beam and experimental facilities. After leaving the vacuum box of the cyclotron, the extracted beam enters a tubular magnetic shield. The position of this shield is adjustable along the axis of the beam and this, together with the correct setting of deflector voltage, ensures that the beam passes straight through the centre of the tube. After leaving the shield, the beam enters a two element magnetic quadrupole lens F_1 which produces a vertical line focus on a one mm slit S_1. This forms the object for the singly focussing 60° analyser magnet which produces an image at the second 1 mm slit S_2. The focus lens produces the first focus in the vertical plane at this point. With the 60° analyser turned off and S_1 opened, the beam can be focussed onto the target T_1 at the end of the tube which passes through the yoke of the 60° magnet.

At present, the straight through target position is in use for activation experiments and a scattering chamber is in use just past the second slit S_2. This latter arrangement is temporary and it is intended to install a second focus lens F_2 and a bending magnet to allow the beam to be sent about another 30 feet to target stations T_2–T_5. A 180° double focussing analyser capable of handling reaction particles with energies up to 20 MeV is being installed at T_5. The scattering chamber will be located at T_3 while the intermediate positions T_2 and T_4 will become available for any experiments not requiring these facilities.

Both the 60° beam analyser and the 180° analyser are designed to give a resolution of 0.1% in energy. The 60° analyser has been tested using alpha particles from a thin polonium source and the resolution at 5.3 MeV is better than 0.1%.

The shield walls of the cyclotron are made of brick and sand 30 inch thick with 18 inch of water on the inside. Where the beam leaves the cyclotron room the wall is made of concrete blocks to provide flexibility. This shielding together with a shield around slit S_2 is sufficient to keep the background radiation in the control room below tolerance and the background in the experimental room reasonably low.

5. Performance

At present MUVEC is only accelerating protons. The machine only operates in the range 5 to 12 MeV due to liner vibration at low proton energies. For bombardments where the internal beam can be used, currents up to 0.5 mA are available. On the

[2]) A. H. Morton and W. I. B. Smith, Nucl. Instr. and Meth. **4** (1959) 36.

straight through target T_1 a beam of up to 10 μA of protons is available with an energy spread of $\pm$ 0.3%. The beam in the principal output just past the second slit S_2 has an energy spread of $\pm$ 0.1% and beam currents up to 0.5 μA can be obtained. It is expected that equipment to prevent dee and liner vibration will be installed early in 1961 and the full design range of the machine will then be achieved.

The cyclotron is at present in scheduled operation for fifty hours a week, with a half day maintenance period each week. It is hoped to raise the operating period to eighty hours per week when more operating crews have been trained.

Acknowledgements

The development of this machine would not have been possible without the financial assistance of a large number of organizations outside the University. We are particularly grateful for the support given by the Australian Atomic Energy Commission; The Anti-Cancer Council of Victoria; and The Thomas Baker (Kodak), Alice Baker, and Eleanor Shaw benefactions.

The authors wish to thank Sir Leslie Martin, C.B.E., F.R.S., who, as Professor of Physics, was, the instigator of the variable energy accelerator programme. Throughout the sometimes painful years of development prior to his resignation, he offered helpful advice and support.

This machine has been built very largely by the research students and the workshop staff of the department. During the development years, too many were involved to allow individual acknowledgement, but the authors would like to thank collectively all those whose work has contributed to the ultimate success of this machine.

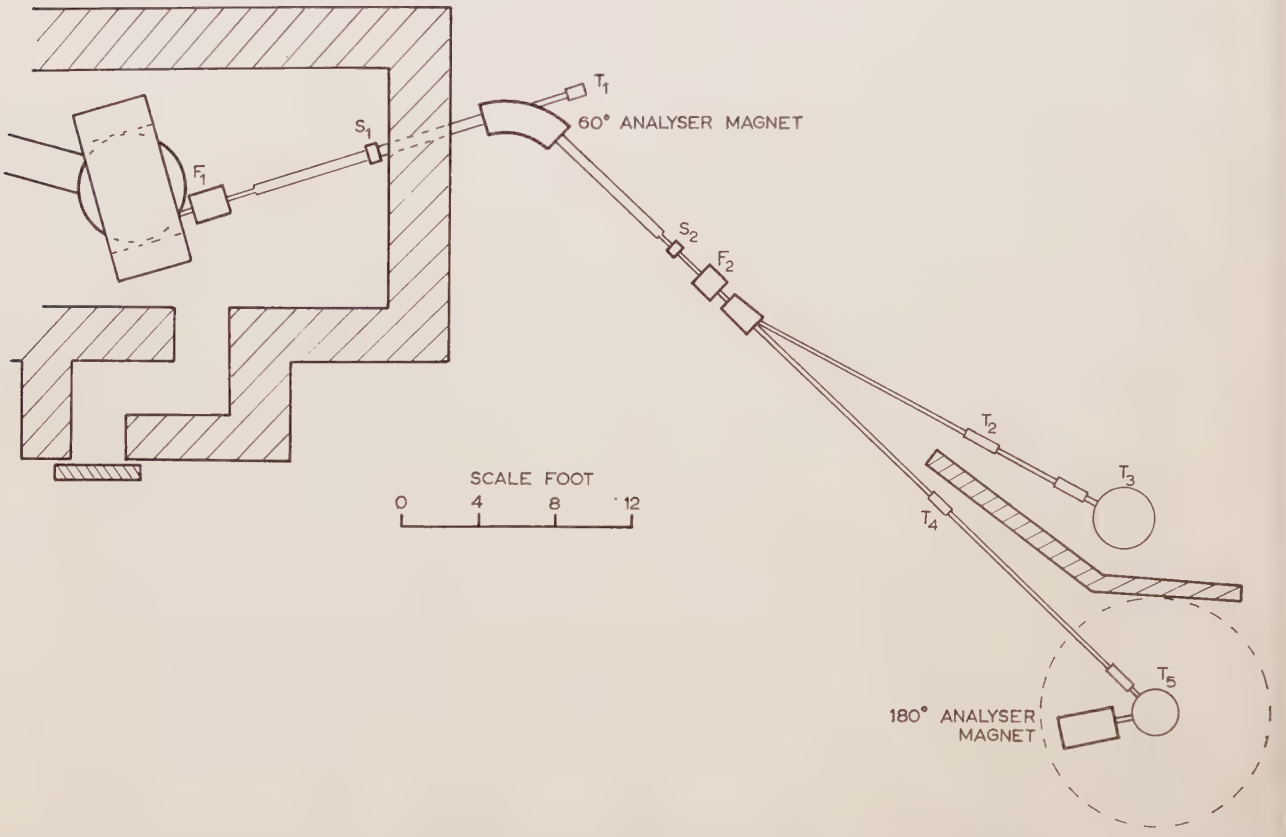

Fig. 9. External beam layout and experimental facilities of MUVEC.

NUCLEAR INSTRUMENTS AND METHODS **10** (1961) 259–262; NORTH-HOLLAND PUBLISHING CO.

PHASE CHANGES NEAR THE CYCLOTRON CENTRE

G. V. H. WILSON †

Physics Department, University of Melbourne

Received 12 January 1961

Orbits were calculated for the first three turns of ions in the Melbourne University Variable Energy Cyclotron for a number of initial phases and several peak dee voltages for an electric field distribution which was determined from electrolytic tank measurements. The phase motion has some interesting features. These are explained by a simple qualitative theory which also explains the dependence of the phase changes upon electrode geometry.

1. Introduction

The aim of this project was a study of electrode design near the cyclotron centre. In previous investigations of the initial motion of ions in a cyclotron, a uniform electric field has been assumed. The effective dee gap width for the uniform field has been obtained from considerations of electric field profiles determined from electrolytic tank measurements[1]) or by calculation[2,3]).

Orbits were first calculated for the Melbourne cyclotron assuming a uniform electric field. Phase changes were found to be largely dependent upon the assumed gap width. This dependence, which has been recently studied by Federov[4]), means that, to investigate phase motion, it is necessary to allow for the non-uniform electric field near the ion source. Orbits were then calculated using electric field profiles from electrolytic tank measurements.

Geometry near the cyclotron centre is shown in fig. 1. The origin of the coordinate system is chosen at the ion source slit with the x axis perpendicular to the dee edge. x and y are given in inches. It is assumed that y and z components of the electric field may be neglected. The electric field is a function of x and time:

$$E = V_0 \phi (x) \cos (\omega_e t + \theta_0)$$

where ω_e is the angular frequency of the electric field, and V_0 the peak dee potential. Let $t = 0$ when an ion leaves the ion source. Then θ_0 is the initial phase of the ion.

† Now at Physics Department, Monash University, Clayton, Victoria.

$\phi (x)$ is the static electric field distribution normalised such that

$$\int \phi (x) \, dx = 1 \, . \qquad (1)$$

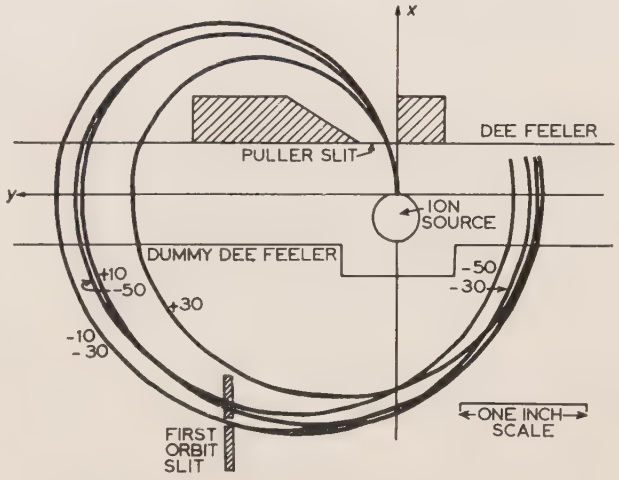

Fig. 1. Electrode geometry and typical beam orbits near the cyclotron centre.

Electric field distributions for the ion source to puller gap (ϕ_1) and for the feeler gap away from the ion source (ϕ_2) were obtained from electrolytic tank measurements and are shown in fig. 2.

The differential equations of motion of an ion in the dee gap are:

$$\ddot{x} = \frac{q}{m(1-\varepsilon)^2} \left(\frac{V_0}{\omega^2}\right) \phi (x) \cos (T + \theta_0) - (1-\varepsilon)^{-2} x$$
$$\dot{y} = \frac{x}{(1-\varepsilon)} \qquad (2)$$

[1]) R. R. Wilson, Phys. Rev. **53** (1938) 410.
[2]) M. E. Rose, Phys. Rev. **53** (1938) 392.
[3]) R. L. Murray and L. T. Ratner, J. App. Phys. **11** (1940) 781.
[4]) N. D. Federov, Nuc. Energy **6** (1957–58) 255.

where $T = \omega_e t$ and the dashes represent differentiation with respect to T. $(1 - \varepsilon)$ is the mean ratio of ω_e to ω, the resonant angular frequency of the ions in the magnetic field, during the first three turns.

Eq. (2) were solved for the first five gap crossings for the initial conditions $\dot{x} = \dot{y} = x = y = 0$ at $t = 0$. Motion between gap crossings is circular. The calculations were carried out for θ_0 between $-50°$ and $+30°$ for five values of (V_0/ω^2) using the CSIRAC digital computer.

$\phi_1(x)$ was tabulated in the computer memory and $\phi_2(x)$ was represented by the Gaussian function:

$$\phi_2(x) = 0.7933\, e^{-(1.272\,x)^2} - 0.0333\,. \qquad (3)$$

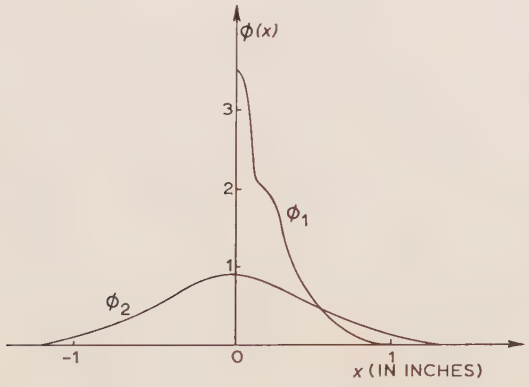

Fig. 2. Electric field distributions
$\phi_1(x)$: ion source to puller gap
$\phi_2(x)$: feeler gap away from ion source.

2. Phase Motion

The phase motion is shown in fig. 3. After several gap crossings the variation of phase with the number of half turns, ν is almost linear with a slope of $-2.63°$ per half turn. For the assumed value (0.9854) of $(1 - \varepsilon)$ this is given exactly by:

$$\left(\frac{d\theta}{d\nu}\right)_a \quad -\varepsilon\,\pi \qquad (4)$$

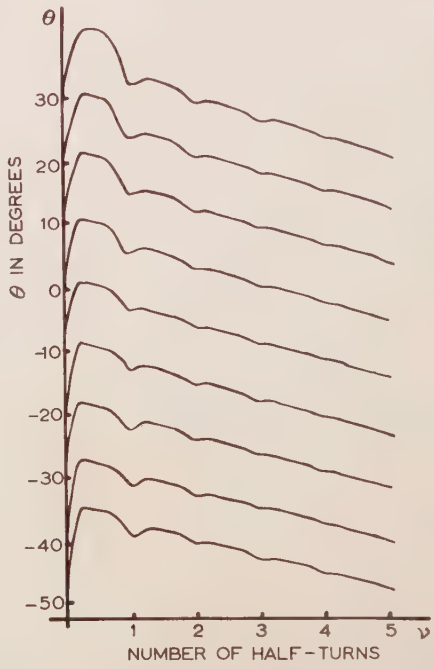

Fig. 3. Phase motion during the first three turns.

Strong grouping of orbit centres to within ± 1 mm was found for ions with initial phases in the range $-50°$ to $0°$. This is in agreement with the results of Morton and Smith[5]) who showed that the strong grouping of orbit centres and radii of ions of negative phases may outweight their disadvantages of electric vertical defocussing and the higher dee potentials required. After three turns ions with initial phases in the range $-25°$ to $+15°$ have radii bunched to within ± 1 mm. A 1.5 mm wide first orbit slit placed as in fig. 1 will select ions with initial phases in the range $-35°$ to $0°$. The disadvantages of ions of negative phases may be largely overcome by designing electrodes near the cyclotron centre to produce large positive phase changes during the first few gap crossings[6]).

which is Cohen's[7]) equation for phase changes due to the difference between ω_e and ω (type (a) phase changes).

Fig. 3 shows that ions of all phases undergo a positive phase change during the first gap crossing. During all other gap crossings there is a negative followed by a positive phase change. These geometry dependent changes are due to differences between ω and the actual angular frequency of the motion of the ions. They were termed "type (b)" phase changes by Cohen. Cohen[7]) obtained expressions for these phase changes for the case in which the

[5]) A. H. Morton and W. I. B. Smith, Nucl. Instr. and Meth. **4** (1959) 36.
[6]) W. I. B. Smith, Preprint.
[7]) B. L. Cohen, Rev. Sci. Instr. **24** (1953) 589.

ons make at least one revolution inside the dee gap.

In most cyclotrons the use of feelers means that the gap width is smaller than the radius of the first orbit and type (b) phase changes occur only during the small portions of the motion when an ion is inside the dee gap. To understand these phase changes and their dependence upon electrode geometry we must consider separately the effects of each gap crossing.

Provided the motion is non-relativistic the angular frequency of an ion in a uniform magnetic field is independent of speed. Now consider a hypothetical case in which an ion receives a packet of energy, $V_0 \cos\theta_0$, at time $t = 0$. If this were the only energy received during the first half-turn, all ions would cross the y-axis at a time $t = \pi/\omega$ and there would be no type (b) phase changes. Consider the case of a uniform electric field and an ion source to puller gap width smaller than the radius of the first orbit. The variation of electric field with time as "seen" by an ion during the first gap crossing is shown in figs. 4(a) and 4(b). An ion with negative initial phase receives most of its energy at a time considerably later than $t = 0$ and hence will again cross the y-axis after $t = \pi/\omega$. Hence the ion suffers a positive phase change which fig. 4(b) shows could be quite large. An ion of positive phase receives its energy after $t = 0$ but the lag is less than that of an ion of equal but negative phase. Hence during the first gap crossing all ions undergo phase bunching about $\theta_0 = 0$ together with a positive phase change. Actually the electric field is position dependent and falls off more rapidly than is shown.

If the field falls off more rapidly, or the gap width is decreased, then smaller positive phase changes will result. However, if the ions make at least one turn inside the dee gap, and the field is made to fall off more rapidly, then larger positive phase changes will result.

For a given ω, if the peak dee voltage, V_0, is

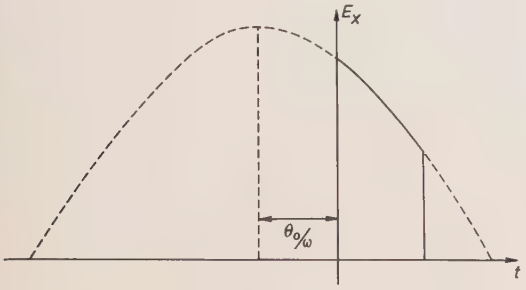

Fig. 4(a) First gap crossing, $\theta_0 > 0$

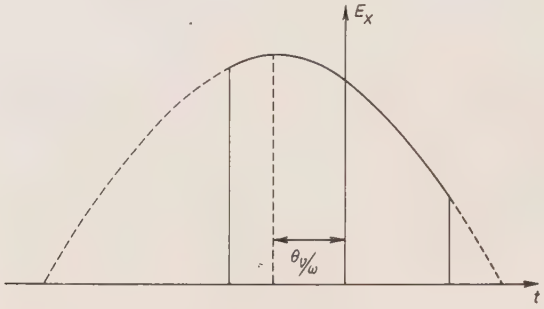

Fig. 4(c) $(\nu + 1)^{\text{th}}$ gap crossing, $\theta_\nu > 0$

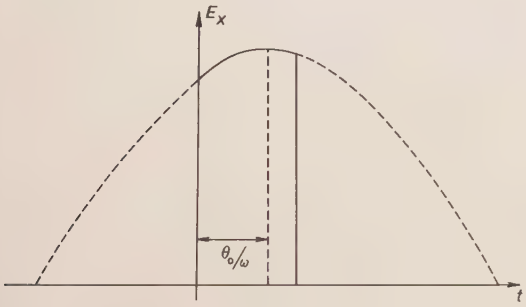

Fig. 4(b) First gap crossing, $\theta_0 < 0$

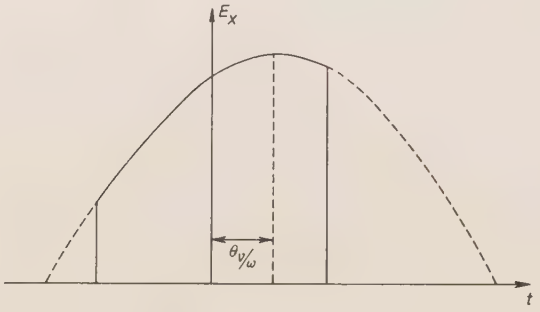

Fig. 4(d) $(\nu + 1)^{\text{th}}$ gap crossing, $\theta_\nu < 0$.

Fig. 4. Variation of electric field with time. The continuous portions of the curves correspond to the time spent by an ion inside the gap.

lowered we would expect larger positive phase changes since the gap transit time would increase. This is shown in fig. 5.

For gap crossings other than the first the electric field distribution is symmetrical about the y-axis. Energy received before crossing the y-axis will produce a negative phase change. The later acceleration will cause a positive phase change. Which of the two is the greater will depend on the sign of the phase, θ_ν, after the previous gap crossing. This is shown in figs. 4(c) and 4(d) for the case of a uniform electric field. The total phase change due

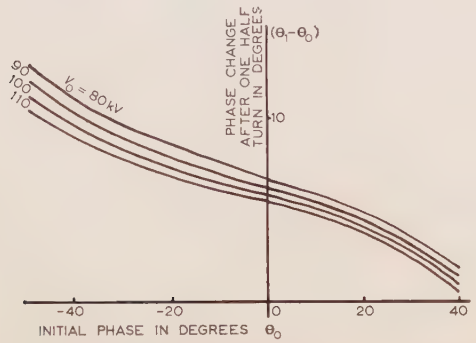

Fig. 5. Dependence upon peak dee voltage of the phase change during the first half turn.

to gap crossings other than the first is of opposite sign to the phase and the main effect is bunching about $\theta_0 = 0°$. These phase changes decrease with increasing radius since the fractional change in energy per gap crossing and the gap transit time both decrease. The effect of the variation of the static electric field with position is to reduce these phase changes.

Fig. 6 illustrates the variation with θ_0 of the first positive phase shift, the negative shift during the first half of the second gap crossing, and the small phase bunching produced by later gap crossings. For a small gap width, the positive phase shift due to the first gap crossing is larger than the other phase shifts. Since all phase shifts of type (b) will increase if the gap width is increased the net result would be an increased positive shift. This would be especially so if only the effective gap width near the ion source were increased. However if the gap width exceeds a certain value, ions of positive phase will be retarded before moving through 90°. This late retardation is equivalent to a negative phase change. Ions of positive phase therefore have a maximum phase after one half turn if they leave the gap when the electric field changes sign. This critical gap width is smaller for larger θ_0. This is in agreement with the uniform field calculations of Federov[4]).

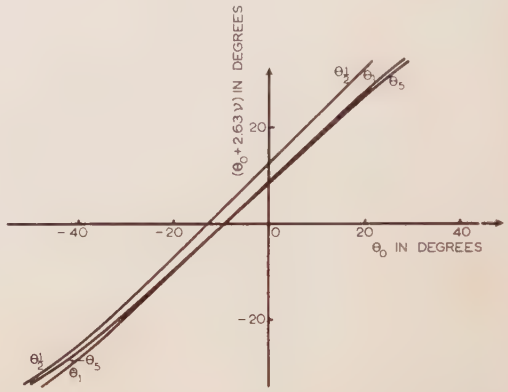

Fig. 6. Dependence of $(\theta_\nu + 2.63\,\nu)$ upon the initial phase θ_0. $(\theta_\nu + 2.63\,\nu)$ is the phase after ν half-turns if there were no type (a) phase changes.

Morton and Smith[5]) pointed out that the use of a large gap width to give more phase bunching would result in too large a spread in orbit centres and radii. An offset ion source[6]) should give a large positive phase shift and have little effect on bunching of orbit centres and radii if the electrodes are designed to give only a small-y-component of electric field near the ion source.

Acknowledgements

The author would like to thank Dr. D. E. Caro for his encouragement of the project and Dr. J. L. Rouse for his helpful advice and discussions. The invaluable work and advice of Dr. F. Hirst and the staff of the Computation Laboratory is most gratefully acknowledged. Financial assistance was received by the author in the form of a University Research Grant.

NUCLEAR INSTRUMENTS AND METHODS 10 (1961) 263–271; NORTH-HOLLAND PUBLISHING CO.

A SOURCE FOR THE PRODUCTION OF LARGE DC ION CURRENTS

G. G. KELLEY, N. H. LAZAR and O. B. MORGAN

Oak Ridge National Laboratory†, Oak Ridge, Tennessee

Received 10 December 1960

A source for the production of large ion currents has been developed based on the "duo-plasmatron" principle suggested by M. von Ardenne[1]). Constant hydrogen ion currents in excess of 300 mA have been obtained with accelerating voltages up to 80 kV. The mass ratios of hydrogen ions have been analyzed magnetically with currents up to 100 mA. In this range, up to 70 per cent of the total current could be made H_2^+. The operating characteristics of the source were determined as the various parameters were independently varied.

1. Introduction

The approach at ORNL to the attainment of a sustained thermonuclear reaction involves the injection of a high energy beam of molecular ions into a magnetic volume. By one of several processes, the molecular ions may be dissociated into protons inside the volume and will then be trapped. One of the critical problems is the production of large currents (perhaps up to an ampere) of high energy (in the DCX experiments, 600 keV) molecular hydrogen or deuterium ions. It is necessary to have high gas efficiency as well, because of the tremendous pumping speeds required otherwise, and in addition, it would be desirable to have a very high molecular ion to atomic ion ratio in order to avoid the problem of disposing of unwanted beam fractions.

The ion source developed originally by M. von Ardenne and coworkers[1,2]), called by them a "duo-plasmatron", seemed to fit the requirement of high current and high efficiency and has been adapted as described below, into a practical and satisfactory ion source for use in DCX experiments[3]). A development of the principle for low current applications is described by Moak *et al.*[4]). It is felt that sufficient experience with various geometries has now been obtained so that the behavior of the source is predictable over certain ranges. Thus extrapolation to many other applications can be made readily from the data to be presented.

† Operated by Union Carbide Corporation for the U.S. Atomic Energy Commission.

2. Description of Source

In this type of source (fig. 1), a plasma is generated by electrons from a heated filament which are accelerated in a gas at pressures from $\sim$ 50–500 μ. The total potential drop to the anode is of the order of 100–300 volts. The discharge is constricted near the anode. Such a constriction results in an intensification of the discharge. The mechanism for intensification has been described by G. Francis[5]) and results when an insufficient number of electrons is able to diffuse through the constriction to produce the required current. Under these conditions a potential drop results, accelerating electrons into the constriction. The electrons then gain sufficient energy to produce additional ionization in this region. The discharge is further intensified at the anode by means of an inhomogeneous magnetic field (fig. 1). The resulting density at the anode aperture is $\sim 10^{13}$–10^{14} ions/cc[1]). The electrons passing through this aperture have been found to have a mean axial velocity corresponding to an energy of 30–100 eV, depending on the magnetic

[1]) M. von Ardenne *et al.*, Tabellen der Elektronenphysik, Ionenphysik and Übermikroskopie, M. von Ardenne, VEB Deutscher Verlag der Wissenschaften, Berlin (1956).

[2]) H. Fröhlich, Nukleonik **1** (1959) 183.

[3]) See, for example, Thermonuclear Project Semiannual Report ending January 1959, p. 54. ORNL 2693. Later discussions of the uses and development of these sources may be found in other Thermonuclear Division Progress Reports.

[4]) Moak, Banta, Thurston, Johnson and King, Rev. Sci. Inst. **30** (1959) 694.

[5]) G. Francis, Handbuch der Physik, ed. by S. Flügge, Vol. **22** (Springer-Verlag, Berlin, 1956) p. 147.

field. The aperture size is determined empirically to permit passage of the required number of ions per second for the particular source application.

Approximate charge neutrality is maintained through the anode aperture into the cup region below (see insert, fig. 1). The ions which have energy and a suitably shaped accelerating electrode. The current density, j (amps/cm^2), under these conditions is given by

$$j = \frac{5.44 \times 10^{-8} \phi^{\frac{3}{2}}}{M^{\frac{1}{2}} z^2} \tag{1}$$

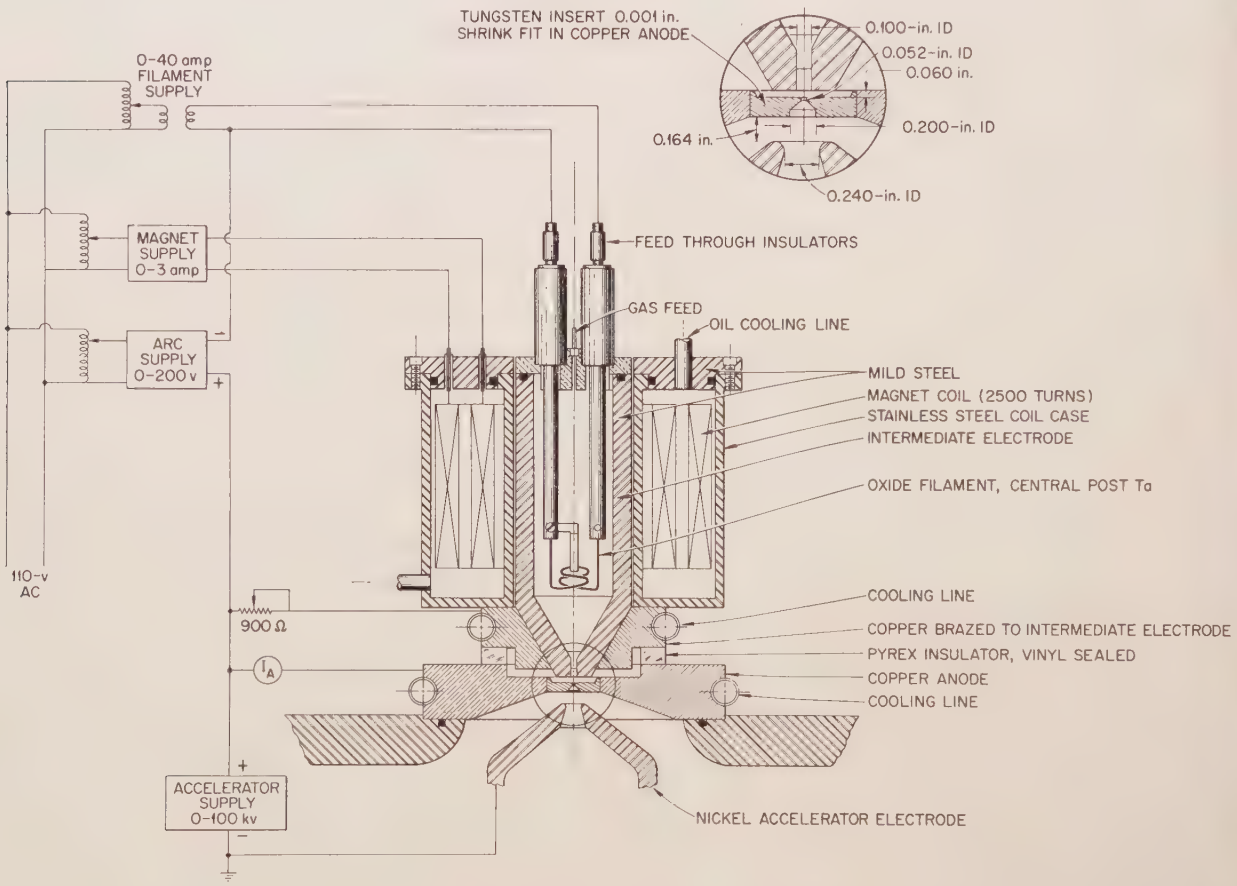

Fig. 1. Cross-sectional view of ion source. Insert shows an expanded view of the anode region.

diffused through the aperture are then accelerated. Even with small accelerating fields below the cup, all the ions which have drifted through the aperture may, in principle, be collected on an accelerator plate of sufficient diameter. However, it is generally necessary to produce an ion beam of small diameter which passes through an aperture in the accelerator electrode into the region beyond. Because of the forces produced in the beam by space charge, the current density in the beam is limited by the applied fields.

Pierce[6]) has shown that it is possible to maintain a parallel beam between a plane disc source at zero

where ϕ is the applied potential difference in volts, M is the ionic mass number and z is the effective spacing between electrodes. With this source the current density as a result of ions diffusing through the anode aperture may exceed 21 amps/cm^2. For the maximum practical potential gradients of 85 kV in 0.4 cm, the current density in a parallel beam is only 2 amps/cm^2. Thus, in most cases, to obtain a parallel beam, the plasma must be permitted to expand to sufficient diameter to reduce its density. In the source shown in fig. 1, this

[6]) J. R. Pierce, Theory and Design of Electron Beams, 2nd Edition (D. Van Nostrand, Co., New York, 1954).

expansion takes place in the cup below the anode aperture. The shape of the cup provides electrostatic shielding of the plasma to insure acceleration only of those ions which leave the bottom surface. It should be emphasized that the total current is determined by the rate of flow of ions through the anode aperture and space charge limitation is always obtained by automatic adjustment of the plasma surface.

Other factors must be considered in the description of the beam phenomena in the accelerating gap. The hole in the accelerating aperture results in curvature of the field lines in the gap. This deviation from "Pierce" geometry results in a divergence of the emerging beam. Furthermore, the surface of the plasma is, in general, not a planar disc, but assumes a concave or convex shape depending on whether the plasma density in the anode cup (fig. 1) is less than or greater than that necessary to match the current density in the beam at a plane surface. The resulting electric field when the plasma surface is concave gives an inward acceleration to the beam. In addition, throughout the accelerating region there is a tendency toward adjustment of the beam diameter, and therefore the space charge fields, in such a direction as to balance the inward and outward radial forces. Because of the dependence of the space charge forces on the beam trajectory, the electrode configuration is not as sensitive a factor as might otherwise be supposed. Indeed, the current density limit (eq. (1)) might be expected to apply over a wide range of electrode configurations. On this basis, a modification of the electrode configuration to permit greater fields in the accelerating gap is desirable. For example, the geometry shown in fig. 2, has been used with 80 kV applied potential. Also shown is the theoretical "Pierce" geometry with the same minimum spacing.

The supposed insensitivity of maximum current on electrode configuration has been borne out experimentally. For an accelerator gap geometry as shown in fig. 2, 300 mA of hydrogen ions at 75 kV were observed on a plate biased to prevent secondary electrons from leaving it. These figures were also checked calorimetrically. Using eq. (1), for the spacing indicated, and assuming all the ions are H_2^+, one would expect 308 mA to pass through the accelerator aperture in a parallel beam. In fact, in all other situations, the current predicted by eq. (1) has been the practical limit obtainable. Upon increasing the plasma density at the source aperture, the beam diverges in the gap region and ions strike the accelerator tip, producing electrons and a discharge usually is initiated between the anode and accelerator.

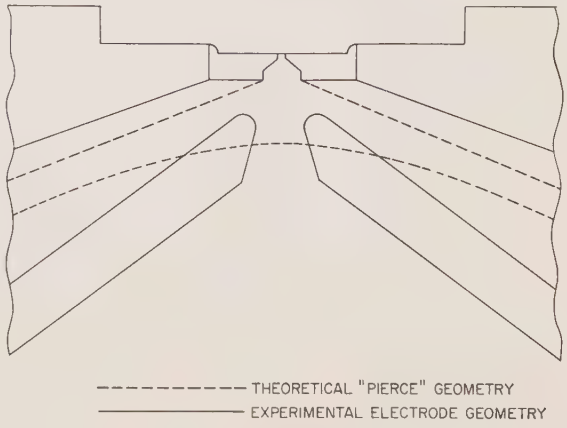

Fig. 2. Comparison of electrode shapes in the acceleration region with the theoretical "Pierce" shapes.

3. Source Construction

The filaments are spirals wound in such a way as to leave a hole through the axis as may be seen in fig. 3, to permit the insertion of a tantalum post in that position. The post was found necessary to stop electrons which are accelerated back through the gap region and focussed by the magnetic field. Fast electrons occur during intermittent sparking in the initial cleanup phase and during operation. The cathode itself is then dipped into a solution of barium-strontium carbonate suspended in amyl acetate, and dried[4]).

The life expectancy of these cathodes is remarkably long, even upon operation with up to 10 amperes discharge current. They are normally run with a power dissipation of 75 watts, although once a discharge is struck they will continue to run with the power to the filament turned off. Fig. 4 shows another view of the source components.

The construction of the discharge volume is shown in fig. 1. The intermediate electrode is made of mild steel and is cooled near the tip as shown. It

Fig. 3. Photograph of disassembled source, view looking from anode end.

is insulated from the anode by the glass ring and the entire assembly is aligned mechanically with a jig. Vinyl acetate is then used to make the vacuum seal. The tungsten anode button is press-fitted into the perimeter cooled copper anode. This type of construction permits continuous operation with discharge currents in excess of 10 amperes. An all copper anode with a 0.052 inch aperture has also been used successfully with these discharge currents.

The magnetic field is produced by a coil wound with approximately 2500 turns of No. 24 formvar coated wire. The coil case slips loosely over the intermediate electrode assembly and is entirely outside the vacuum system. Oil cooling is provided separately for the coil. The magnetic field produced below the tip of the intermediate electrode with $\sim$ 1120 amp-turns is 4 kilogauss.

The gas inlet is generally in the filament assembly as shown, although this position is a matter of convenience. Gas feeds in other regions seem to make little difference in source operation and no observable difference in performance. Since these sources have been used exclusively with hydrogen, a palladium leak has been used to insure purity of the incoming gas.

Fig. 4. Photograph of disassembled source, view looking from cathode end.

The alignment of the accelerator electrode is extremely critical, particularly as one attemps to reach the "Pierce" limit (eq. (1)) in extracted current density. In the design of the test assemblies, the tolerances are limited in the parts critical for alignment so that the total misalignment cannot exceed 0.005 inch. The accelerator is shown in fig. 1, and as indicated, is made of nickel. With the copper anodes generally in use the accelerator should be ferromagnetic. The accelerator electrode need not be cooled since essentially all of the ions pass through the accelerator aperture.

4. Experimental Results

The mass ratios of $H_1^+ : H_2^+ : H_3^+$ ions from the source shown in fig. 1 have been determined by magnetic analysis for currents up to $\sim$ 100 mA at $\phi = 60$ kV under various source operating conditions. The maximum current was limited by the einzel lens used to focus the diverging beam from the accelerator. The resolution was sufficient that the three mass species could be clearly separated on three targets placed suitably in the magnetic field as shown in fig. 5. Because of the combination of space charge forces and beam divergence, for

currents exceeding ~ 100 mA, parts of the beam strike the center section of the einzel lens.

Since the mass ratio is mildly dependent on so many independent parameters, a consistent method of organizing the data is difficult. However, the main parameter which affects the ratios is the source pressure. Table 1 shows the mass fractions in the beam for 70 mA total output current as a function of pressure. The discharge current I_A was varied to maintain constant output. Similar data were obtained with constant I_A which shows essentially the same trend. From observations obtained with various source geometries, the mass ratios seemed to be somewhat sensitive to magnitude of I_A. However, because of the current limit set by the einzel lens, it was impossible to obtain data over a sufficient range of I_A to establish a significant trend. A magnetic lens is being constructed which will permit analysis of larger currents.

Several geometry changes were made in an

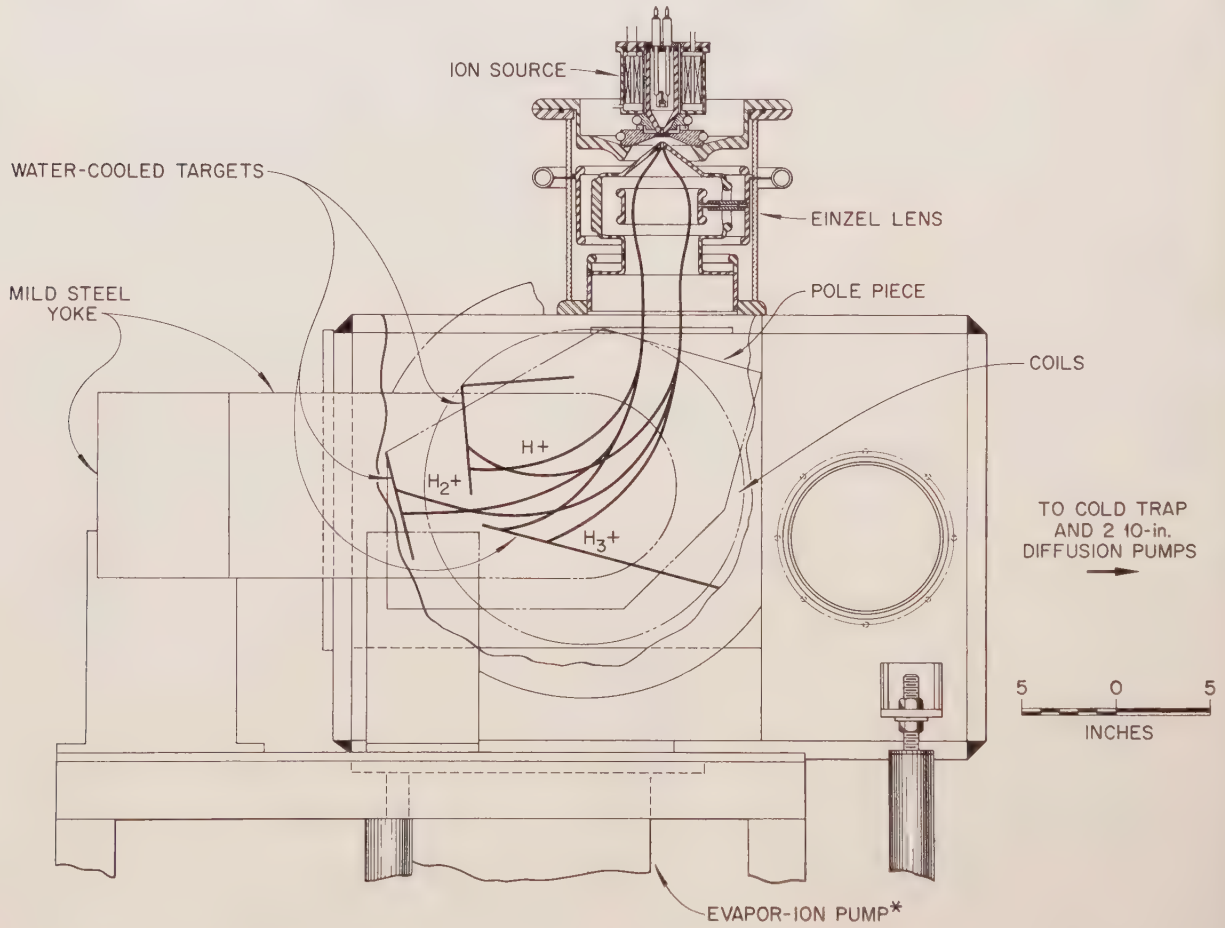

Fig. 5. Elevation view of system for high current analysis showing beam trajectories.

* Consolidated Electrodynamics Corporation, Rochester, New York.

TABLE 1.

Relative ratios of the mass species as a function of indicated gas pressure in the source with 70 mA total output of H_2^+

(μ)	H^+ (%)	H_2^+ (%)	H_3^+ (%)
77	24	71	5
180	27	66	7
320	38	47	15
480	42	37	21

Pressure values are uncorrected thermocouple readings.

attempt to increase the relative H_2^+ fraction. Both heated and cooled surfaces were placed in the intermediate electrode canal, and the surface area available for recombination of H^+ produced in the upper discharge chamber was increased by inserting platinum gauze in that region. These changes had no effect on the output mass ratios. However, changing the length of the gap between the intermediate electrode and the anode did change the mass ratios. Table 2 gives the mass fractions from the source at constant gas feed and the same output with three spacings between the intermediate electrode and anode.

TABLE 2.

Mass fractions as a function of intermediate electrode to anode spacing for constant gas feed and at constant output (70 mA)

spacing (inch)	H^+ (%)	H_2^+ (%)	H_3^+ (%)
0.060	24	71	5
0.110	35	50	15
0.210	41	41	18

Unanalyzed output currents were determined as functions of the various source parameters; viz. arc discharge current, magnetic coil current, acceleration voltage, intermediate electrode potential, gas flow rate (or source pressure), etc. The results of some of these experiments are shown in fig. 6 to 9. In each figure, the output beam current to a biased plate is plotted as a function of source discharge current, I_A, for various magnet current values. The data for each figure were taken with a constant gas flow through the source. The pressure shown correspond to the uncorrected thermocouple

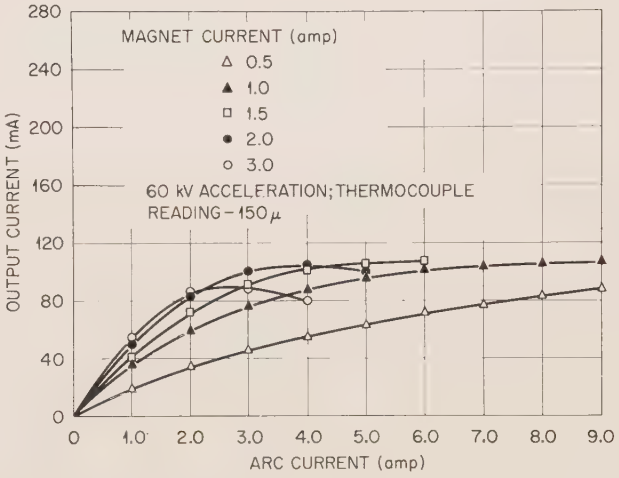

Fig. 7. Source output current as a function of arc current, I_A, at at 150 μ indicated pressure.

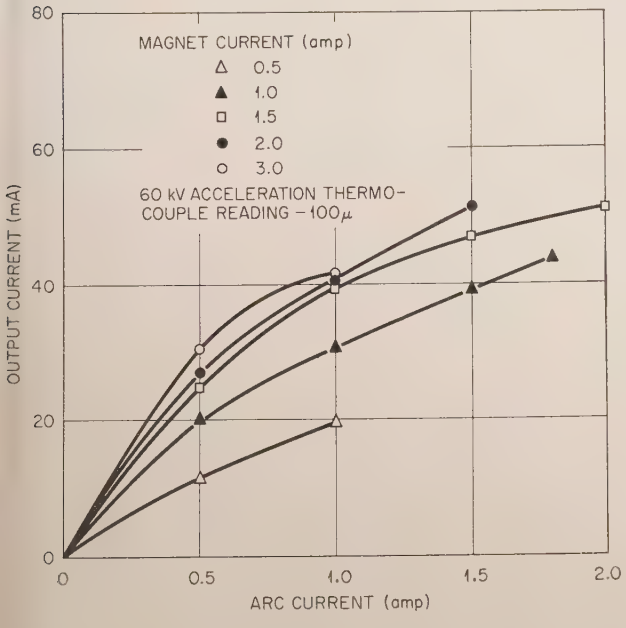

Fig. 6. Source output current as a function of arc current, I_A, at 100 μ indicated pressure.

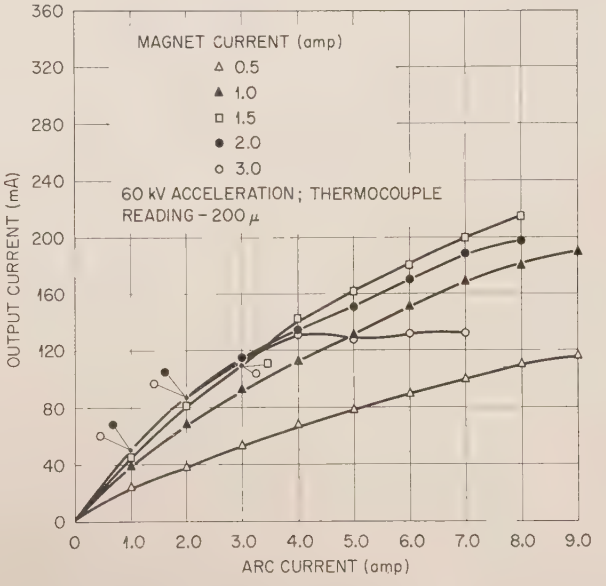

Fig. 8. Source output current as a function of arc current, I_A, at 200 μ indicated pressure.

gauge reading before the discharge is struck.

The gas flow was controlled by a variable fine control valve. Commercial high purity hydrogen gas without further purification was used. A mass analysis showed less than 1 per cent impurities. The

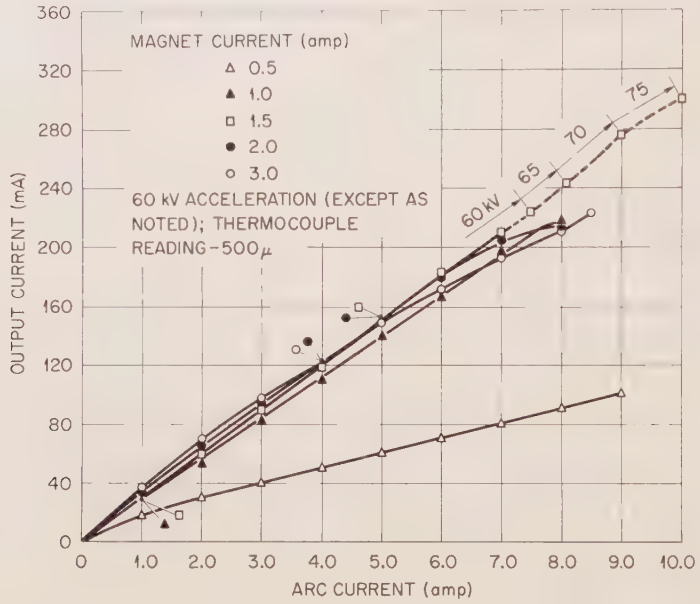

Fig. 9. Source output current as a function of arc current I_A, at 500 μ indicated pressure.

valve was unchanged during a set of runs at a given source pressure and the thermocouple reading was checked before and after the data were taken. It should be pointed out that the thermocouple gauge readings cannot be taken as a reliable indication of pressure from one run to another. Variations of approximately 10 per cent can be expected with constant flow rates. Even greater variations in readings have been obtained when the gauge was affected by voltage transients during sparking. It was found necessary to shield electrostatically the port leading to the thermocouple element to prevent burnout of the gauge during these transients. Within these limitations, however, results consistent with the data shown were also obtained with gas flows controlled by a palladium leak. The gas flow rate as a function of indicated pressure is shown in fig. 10.

The ratio of charged particles per second in the beam to gas flow in particles per second is a measure of the gas efficiency. This ratio may be determined if one knows the molecular mass ratio in the beam at the various pressures. Unfortunately, this is as yet not known for these high outputs. On the assumption that the average mass of the emitted ions is two, a gas efficiency of 92 per cent was obtained at 200 μ source pressure and 215 mA total beam current through a 0.052 inch diameter aperture. The efficiency at lower pressure was considerably less with this aperture—e.g. 43 per cent at 100 μ and 64 per cent at 150 μ; however, an efficiency of 81 per cent was measured at 75 mA output current and 75 μ pressure with an anode aperture of 0.046 inches.

It may be noticed that at high magnetic fields, even at high pressure, the output does not increase as the discharge current increases beyond a critical point. A possible explanation is that at higher magnetic fields the arc diameter is constricted to such an extent that insufficient gas can diffuse into it to provide the necessary ions.

The points at 8, 9 and 10 amps discharge current in fig. 9 show the dependence on $\phi^{\frac{3}{2}}$ as given in eq. (1). All the other data were taken at 60 kV accelerating potential, but for $I > 7.5$ amps (beam current equal to 220 mA as given by eq. (1)) the ratio of power supply current to collected current

rose abruptly as did the X-ray flux, indicating a flow of ions to the accelerator electrode. However, by raising the voltage the discharge current once again could be raised, and the output increased.

Variations of the intermediate potential were made in the same manner as reported by Fröhlich[2]). It was found that the anode current, I_A, was unaffected by these variations except for values very close to anode potential. Further, it was found that all other aspects of source performance were unaffected. When, however, the current to the cathode was considered as the control parameter as was done in ref. [2]), characteristics similar to those reported by Fröhlich were found. For this reason, it is apparent that the current which circulates between filament and intermediate electrode does not affect the discharge in the vicinity of the anode. The arguments presented in ref.[2]) concerning the magnitude of the potential hill just below the intermediate electrode, therefore, cannot be valid.

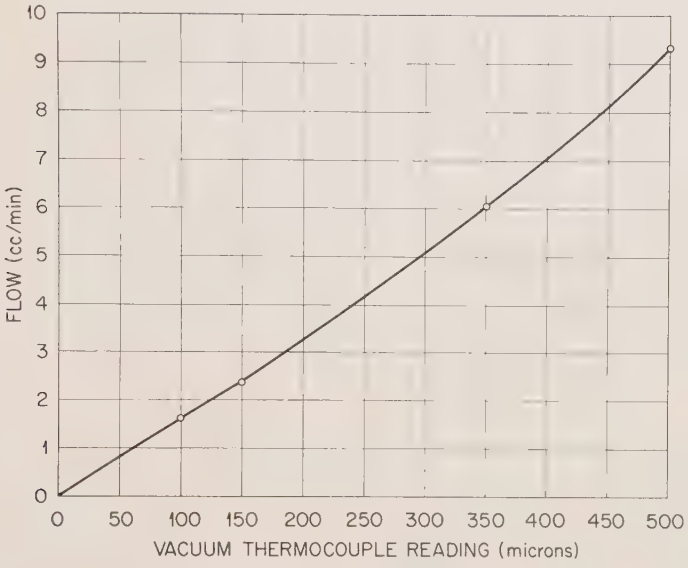

Fig. 10. Gas flow rate as a function of indicated source pressure.

Acknowledgements

The authors gratefully acknowledge the assistance of and early discussions with C. D. Moak, H. E. Banta, R. F. King, and J. H. Neiler. We would also like to express thanks to E. D. Klema and James L. Kassner, Jr. for their contribution as summer participants. The assistance of R. F. Stratton, R. C. Davis, E. C. Moore, and R. R. Hall is gratefully acknowledged. We wish also to express our appreciation to P. R. Bell for his encouragement and support.

NUCLEAR INSTRUMENTS AND METHODS 10 (1961) 272–280; NORTH-HOLLAND PUBLISHING CO.

THE USE OF A COUNTER CONTROLLED HIGH PRESSURE CLOUD CHAMBER FOR EXPERIMENTS WITH CHARGED PARTICLES

D. J. CAIRNS†, T. C. GRIFFITH, G. J. LUSH, A. J. METHERINGHAM and R. H. THOMAS††

Physics Department, University College London

Received 28 November 1960

An account is given of the use of an expansion cloud chamber operated at pressures up to 70 atmospheres with a beam of protons from the Harwell synchrocyclotron. The usefulness of the cloud chamber for experiments with charged particles has been much enhanced by the control system of scintillation counters employed to trigger the expansion only when specific interactions occur in the gas. This arrangement allows events to be photographed at the rate of 30 per hour.

1. Introduction

In recent years the development of new visual techniques, such as the diffusion chamber and bubble chamber, for experiments with accelerators has received much more attention than improvements to expansion cloud chamber techniques. Many improvements are in fact possible and for some experiments expansion cloud chambers, operated both at high and low pressures, can still compete with the modern techniques. In particular, one attribute of the high pressure chamber is that the gas has a stopping power intermediate between the same gas at atmospheric pressure and in the liquid state; this feature has advantages in experiments involving low energy secondary particles. Other features, which for some experiments argue in favour of the high pressure chamber, are its long sensitive time and the ease with which it can be operated with many different gases, both light and heavy.

The present work has been concerned with making efficient use of a pressure chamber (without a magnetic field) in experiments involving the interactions of protons in helium and deuterium. Since the events of interest contained particles stopping in the chamber a magnetic field would not significantly aid the interpretation of the data. The cloud chamber is similar to the one used by Evans and Williams (1940)[1]) and is described by Burhop (1954)[2]) and Evans (1955)[3]). In its original form the cycling time of the chamber was 15–20 minutes between expansions; this, as shown by Duff and Morris (1955)[4]) is determined by the magnitude of the temperature gradient established in the gas during the cycle. As a result of the difficulties experienced by Banford *et al.* (1955)[5]), in finding suitable operating conditions with the 150 MeV proton beam from the Harwell synchrocyclotron, several modifications were essential before the chamber could be used economically in work of this nature. Such modifications, involving facilities for either fast recompression or overcompression (Gaettner and Yeater (1949)[6]) and Barford (1955)[7]) of the gas after each expansion, have been carried out by Tomlinson *et al.* (1961)[8]). The cycling time was thereby reduced to one minute but this

† Present address: Enfield Technical College, Middlesex.

†† Present address: Rutherford Laboratory, Harwell, Berks.

[1]) E. J. Williams and G. R. Evans, Nature **145** (1940) 818.

[2]) E. H. S. Burhop, Suppl. Nuovo Cim. **2** (1954) 343.

[3]) G. R. Evans, Proceedings of Conference on Recent Developments in Cloud Chamber and Associated Techniques (University College London, 1955) 67.

[4]) M. J. B. Duff and N. Morris, Proceedings of Conference on Recent Developments in Cloud Chamber and Associated Techniques (University College London, 1955) 78.

[5]) A. P. Banford, W. E. Duncanson, T. C. Griffith and W. S. C. Williams, Proceedings of Conference on Recent Developments in Cloud Chamber and Associated Techniques (University College London, 1955) 104.

[6]) E. R. Gaettner and M. L. Yeater, Rev. Sci. Instr. **20** (1949) 588.

[7]) N. C. Barford, Proceedings of Conference on Recent Developments in Cloud Chamber and Associated Techniques (University College London, 1955) 137.

[8]) H. S. Tomlinson, M. J. B. Duff and N. Morris, (in press).

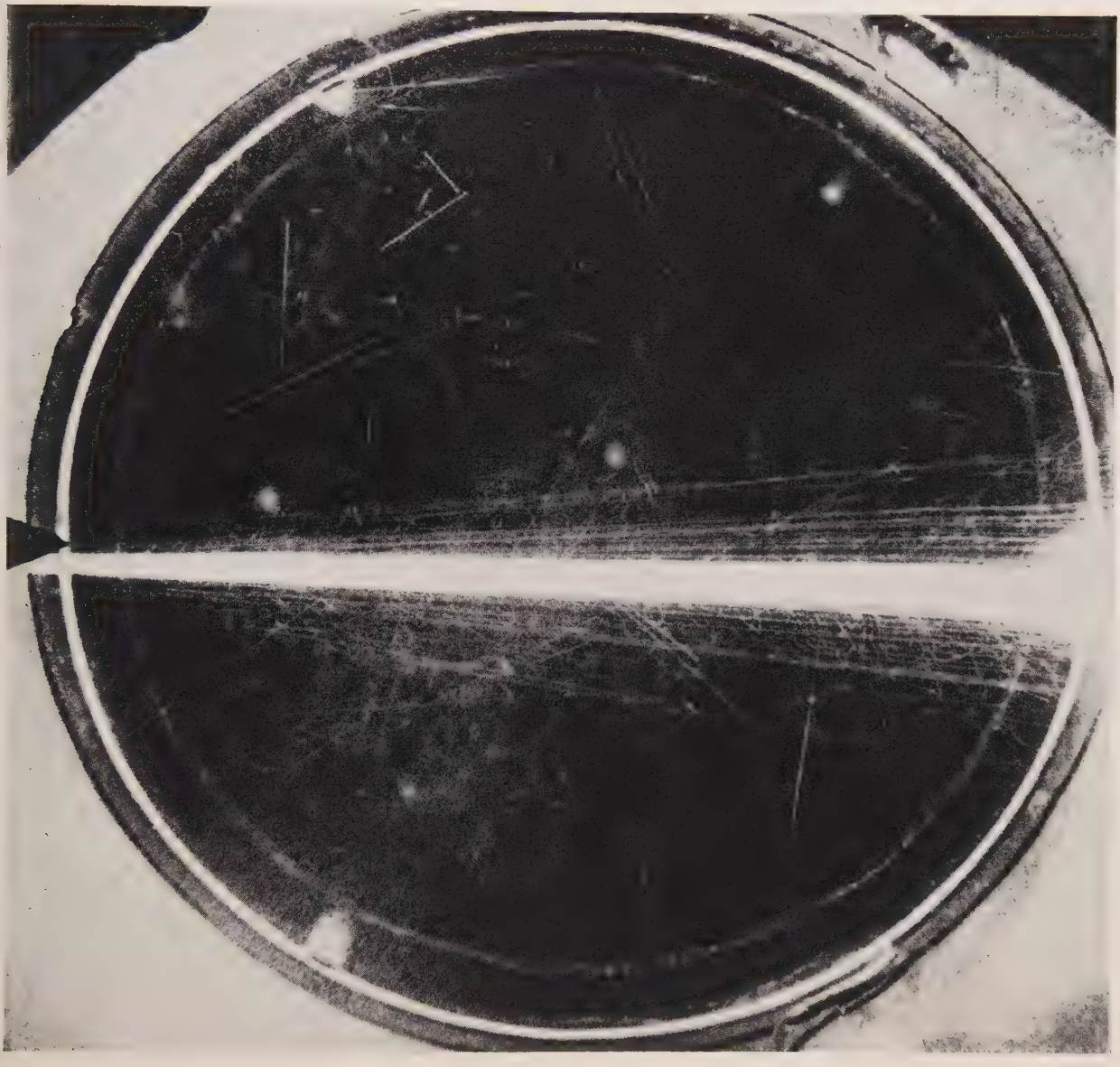

Fig. 1. Photograph of about 300 protons entering the chamber after expansion through a collimator 0.2 cm diameter.

improvement alone was not sufficient to allow efficient use of the available proton beam. Satisfactory efficiency could only be attained by using a selection system of scintillation counters to control the expansion of the chamber. The expansion is only triggered when an interaction has occurred in the gas and in this way up to 30 useful events per hour have been photographed. Without the selection system, assuming that no more than 10 protons per expansion could be admitted into the chamber it is estimated that, for 150 MeV protons in deuterium at 50 atmospheres pressure, only 2 events per hour would be photographed. Using a narrow collimated beam of 100–200 protons per expansion the number of events photographed would be comparable with that achieved with the selection system. As found by Banford *et al.* (1955)[5], it is difficult to produce such a narrow beam because the scattering at the edges of the collimator produces so much divergence (fig. 1) that the majority of the collisions involving low energy secondaries are completely obscured.

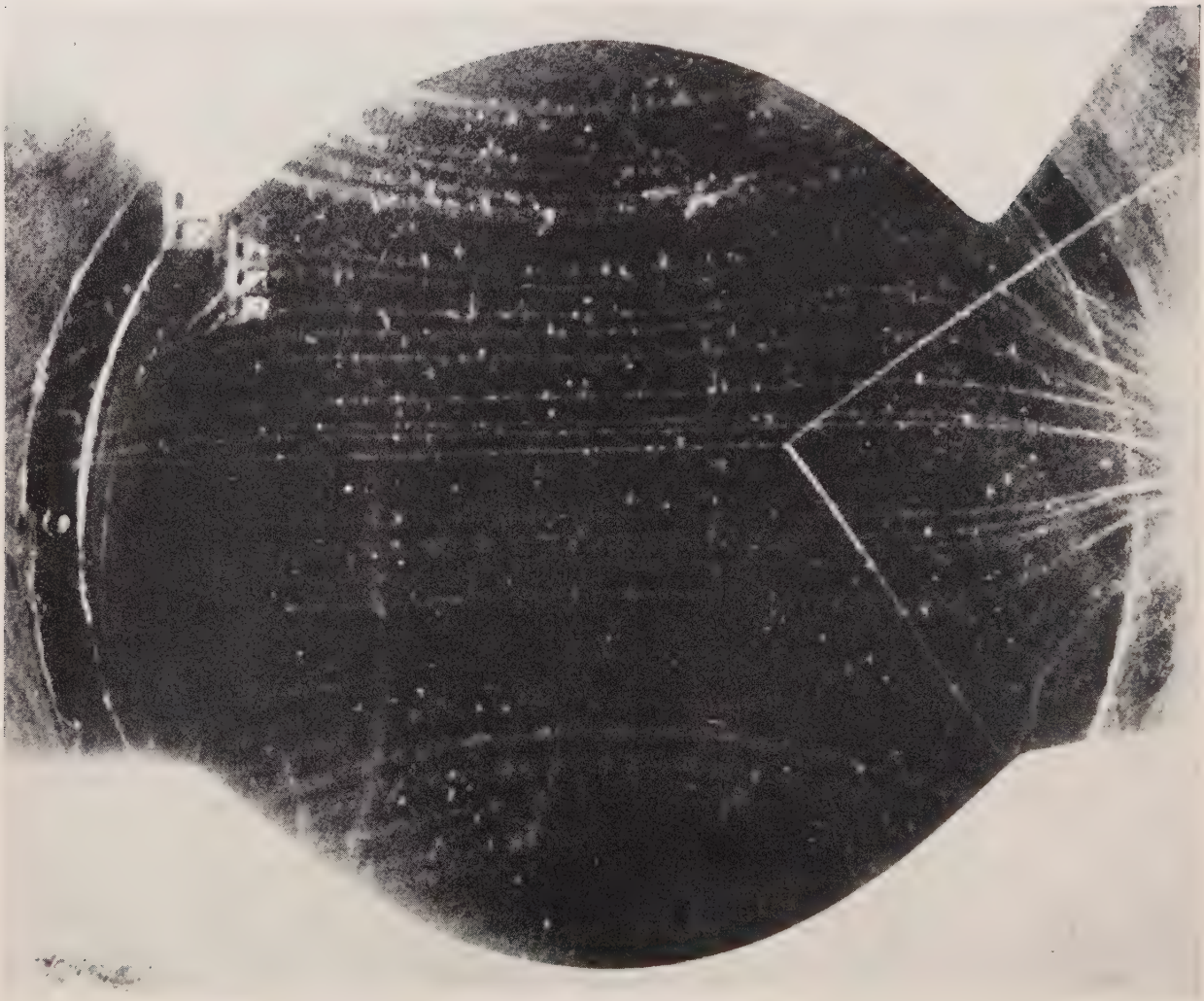

Fig. 2. Counter controlled photograph of a proton-deuteron collision at 136 MeV. The distorted tracks are field separated tracks due to earlier protons.

In operating the chamber with the selection system a continuous beam of 5 to 10 protons per second is admitted into the chamber and the ions along the paths of the unscattered protons crossing the chamber are swept away by an electrostatic clearing field. When an event is detected by the counter system both the clearing field and the cyclotron are rapidly turned off so that the resulting photograph shows the required event, unobscured by other tracks (fig. 2), on the axis along which the protons enter the chamber. Under these conditions there is no loss of events during the scanning of the photographs and all the tracks are visible and measurable. Geometrical corrections to allow for the bias of the selection system are relatively easy to calculate. Particles scattered at angles within $\pm$ 8° of the forward direction cannot be photographed with the selection system. Such collisions (mostly elastic coulomb scatters) were not of direct interest in the present work and are best investigated using other techniques.

2. Operation of the Cloud Chamber

The chamber is cylindrical in shape with internal diameter 22.5 cm, external diameter 42.5 cm, and is operated with its axis horizontal. The expansion is accomplished by means of a hydraulically operated duralumin piston which has a maximum

stroke of 3.8 cm. The sensitive depth of the chamber is 26.0 cm of which 16.0 cm is illuminated. Three armour plate glass windows (fig. 4) of thickness 2.5 cm, and effective diameter 4.0 cm placed symmetrically in the median plane, are used for illumination. The photographs are taken through an armour plate glass window of diameter 16.5 cm and thickness 4.4 cm in the front of the chamber. A port through which the protons are admitted into the chamber lies diametrically opposite one of the windows used for illumination.

Although facilities for both overcompression and fast recompression are available the simpler process of fast recompression is found to be completely satisfactory for light gases. The valves controlling the expansion and recompression have been described by Tomlinson (1955)[9]), and details of the mechanical and hydraulic systems are given by Tomlinson *et al.* (1961)[8]). A trace of the position of the piston as a function of time, showing the expansion-recompression cycle, is reproduced in fig. 3; this is a pen recording of the voltage from a

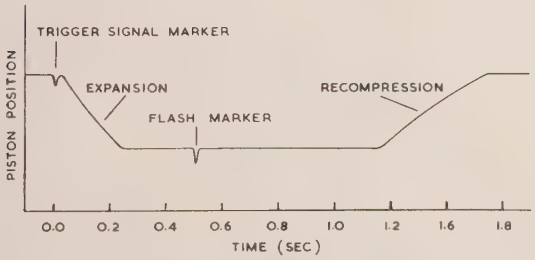

Fig. 3. Pen recorder trace of the expansion-recompression cycle.

strip potentiometer coupled to the piston shaft. The minimum possible value of the expansion time, t, at 50 atmospheres pressure, is 0.12 seconds. When t is short the mechanical parts of the system are subjected to large forces and the chamber is thus normally operated with $t = 0.25$ seconds, in which time the tracks of 150 MeV protons acquire a width of 0.05 cm due to diffusion. The interval, T, between expansion and recompression is adjustable and is normally set at 0.9 seconds. Tomlinson *et al.* (1960)[8]) have shown that, when operating on a one minute cycle with $T = 0.9$ seconds, the temperature difference of the gas at the top and bottom of the chamber is maintained at about 0.2°C. The change in supersaturation due to this temperature difference does not lead to a significant variation of track quality between the top and bottom. A time T shorter than 0.9 seconds, although decreasing the temperature gradient, would not maintain a low level of background in the chamber; this is because the time allowed for the cleansing action of the fall out of the condensed ethyl alcohol droplets is reduced.

During the operation of the chamber the expansion ratio is monitored by a device which samples the voltage on the slider of the strip potentiometer on the piston shaft for a short period while the chamber is in the expanded state. A capacitor is charged to this voltage and feeds a valve voltmeter with very high input impedance thus allowing the expansion ratio to be read from a meter. The chamber can be cycled for long periods without applying any cleaning expansions or altering the expansion ratio, except to compensate for slow variations in the ambient temperature. It appears that in the first few expansions the number of background "re-evaporation nuclei" in the chamber attains an equilibrium which is determined by the efficiency with which ions have been removed by the clearing field before expansion, by the level of ionisation existing in the chamber when it expands and by the amount of condensed alcohol which falls out during the interval T. The performance of the chamber under conditions of high ionisation, viz. many particles per expansion, has not been systematically investigated. In practice the level of ionisation is determined by the requirement that events should not be obscured by the field-separated tracks of other incident protons; under these conditions problems relating to the cleanliness of the chamber are not serious.

An efficient clearing field electrode system is vital to the operation of the chamber with the selection system. The rapid removal of "old" ions from the gas at high pressure needs high clearing field voltages which, if there are sharp points on the electrode system, tend to produce columns of ions in the gas on which the alcohol condenses. This

[9]) H. S. Tomlinson, Proceedings of Conference on Recent Developments in Cloud Chamber and Associated Techniques (University College, London, 1955) p. 74.

effect is avoided by using glass electrodes, E, with smooth rounded edges and coating the glass with a thin, transparent, conducting layer using the technique described by Gomer (1953)[10]). The electrodes are supported 2.5 cm from the chamber wall by insulators of Teflon (P.T.F.E.) which has very low surface leakage even when used in a region supersaturated with alcohol. The two electrodes are maintained at + 3000 volts and — 3000 volts respectively and the voltages are reduced to zero to pass through the electrodes and, as a result of scattering from the conducting layer, they appear black on the photographs. Details of the illumination through W3 are given in § 3. The flash tubes are triggered 0.25 seconds after the end of the expansion; for visual observation of tracks in the chamber the tubes are triggered repetitively at 50 c.p.s. and an energy of 1 joule per tube. Both the piston and the inside cylindrical surface of the chamber are covered with black velvet which

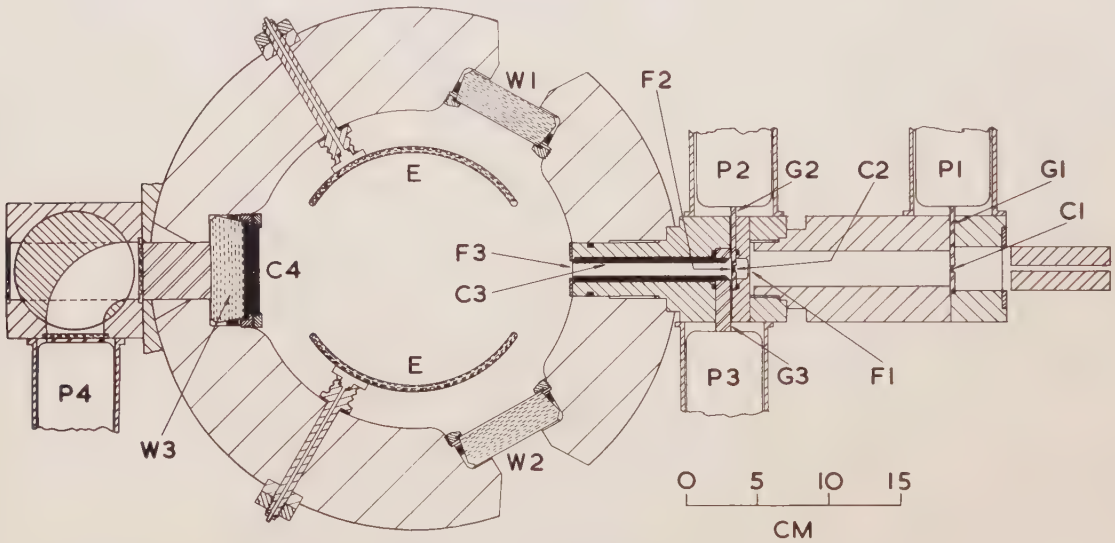

Fig. 4. Section through the median plane of the cloud chamber and the counter system.

within 10 micro-seconds of receiving the triggering pulse from the counters by shorting the outputs of the power supply with thyratrons provided with suitable backing-off voltages. In helium at 55 atmospheres the ions are swept from the centre of the chamber to the electrodes in 0.3 seconds and in 10 micro-seconds the broadening of the counter controlled tracks is less than 2% of their width.

Three Mazda FA 2S flash tubes, each operated at 300 joules, provide the illumination of the chamber for photography. A metal tube with polished inside surface is used as a light guide between the windows W1 and W2 (fig. 4) and the flash tubes; a system of blackened collimating vanes in contact with the windows prevents light from entering the camera lenses directly or falling on the piston. The light entering the chamber through W1 and W2 has provides a suitable background against which the tracks are photographed. The velvet also assists the re-evaporation and diffusion of the alcohol which falls out during the expansions. The photographs are taken on 5G 91, 35 mm, film with a two lens stereo-camera, stereo angle 15°, magnification $\frac{1}{10}$th (approx.) and an aperture of $f/16$.

3. The Counter Selection System

The design of the selection system was determined by the beam port of the chamber being situated opposite the illumination window W3; the line joining the centre of W3 and the beam port defines the axis of the system. Four plastic scintillators are assembled and aligned on this axis: C1 and C2 are coincidence counters, C3 is an anti-coincidence counter and C4 is used both as a coincidence and an anti-coincidence counter.

[10]) R. Gomer, Rev. Sci. Inst. **24** (1953) 993.

Pulses from the four counters are fed into two channels. Channel 1 records 1, 2, $\bar{3}$, $\bar{4}$ coincidences and triggers the expansion of the chamber when an incident particle is scattered in the gas between C3 and C4. Channel 2 records 1, 2, $\bar{3}$, 4 coincidences and monitors the total number of particles crossing the chamber so that absolute cross-sections can be determined.

The beam monitored by the selection system is defined by the diameters and separation of C1 and C2. The region between the main pressure holding window F1 and the differential pressure holding window F3 is filled with gas at the same pressure as that in the cloud chamber. The hollow cylindrical counter C3 functions as a clearing collimator which enables the selection system to ignore any particles from the incident beam which are scattered in F1 and C2 through angles between 4° and 70°. An incident particle interacting in the gas inside C3 is also ignored if one of its charged secondaries enters C3. The diameters of C4 and of the chamber determine the minimum angle through which a particle must be scattered in the cloud chamber gas to trigger the expansion; this angle is 8.3° for a particle scattered just inside the chamber.

Counters C1, C2 and C3 are assembled in a rigid metal structure (fig. 4) which screws into and locates itself in the beam port of the chamber. Both C1 and C2 have a diameter of 0.4 cm, thickness 0.076 cm, and are inserted in circular holes in the polystyrene light guides G1 and G2. These light guides are of rectangular section, thickness 0.32 cm, and are accurately located into slots in the beam port assembly with one end protruding onto the photomultipliers P1 and P2. C1 and C2 are 14.0 cm apart and the pressure holding duralumin window F1, which is 0.12 cm thick and 1.0 cm diameter, is situated 1.0 cm in front of C2. Counter C3 has a length of 10.0 cm, internal diameter 1.0 cm and external diameter 1.6 cm. It is enclosed in a polished aluminium tube up to the light guide G3. The end of C3 is coned inwards at 45° to increase the amount of light reflected into G3, which is 0.80 cm thick. A thin sheet of rubber between the adjacent faces of G2 and G3 and 0-rings on their outer faces are used as pressure seals. Light coupling between C2 and C3 is prevented by an aluminium foil, F2, of thickness 0.0025 cm between the two counters. The protons enter the chamber through the window F3 made of aluminised Melinex foil of thickness 0.013 cm. This window prevents gas from rushing into the chamber from C3 during the expansion and is sufficiently strong to withstand the change in pressure. C4 has a diameter of 6.0 cm, thickness 0.95 cm and is clamped to the window W3 by a metal ring which screws into the wall of the chamber.

A solenoid operated device enables the illumination window W3 to be used for two purposes. In the normal position a curved light pipe filled with xylene transmits light from C4 to P4. The triggering pulse which initiates the expansion also energises the solenoid and provides a direct path for light from the flash tube to enter the chamber, at the same time sealing the photomultiplier P4 from the flash. The photomultipliers P3 and P4 are further protected from the flash by turning off the E.H.T. when the solenoid is energised.

The proton beam from the cyclotron is focussed by two quadrupole magnets and collimated by two brass cylinders of length 7.5 cm with axial holes of diameter 0.4 cm placed at distances of 3.0 cm and 100 cm respectively from C1. The collimator holes and the axis of the selection system (including the chamber) are optically aligned to the proton beam, the final alignment being checked with X-ray films. Lead blocks around the collimators are used to shield the chamber and counters from particles which are not travelling along the axis.

Light from each of the four counters is received E.M.I. type 6097 B photomultipliers followed by a pentode pulse forming circuit which give limited output pulses of amplitude 1 volt. The pulses from the coincidence counters are negative and clipped to 2×10^{-8} seconds duration whilst those from the anticoincidence counters are positive and clipped to 4×10^{-8} secs. Counter C4, which operates both in coincidence and anticoincidence, has a double head amplifier giving pulses of opposite polarity. Each channel in the coincidence unit consists of a number of pentodes with a common low impedance anode load. The output pulses from the pulse forming circuits, applied to the grids of the appropriate pentodes, produce a pulse across the

the common anode load which is proportional to the algebraic sum of the coincidence and anti-coincidence pulses; this pulse is fed to a diode discriminator giving an output signal which, when amplified and stretched, goes to the scalers. The application of a suitable negative bias to the discriminator allows examination of single, double or triple coincidences as desired. A block diagram of the counting electronics is given in fig. 5.

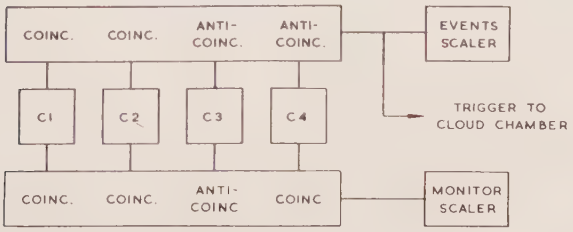

Fig. 5. Block diagram of the electronics.

The pulse used to trigger the chamber is obtained from a cathode follower coupled to the output side of the discriminator of the scaler in the 1, 2, $\bar{3}$, $\bar{4}$ coincidence channel. This pulse initiates a detailed sequence of operations involving expansion, photography, recompression and resetting the oil pressures in the hydraulic system so that the chamber is ready to receive the next pulse. The trigger pulse also rapidly terminates the acceleration of protons in the synchrocyclotron by turning off the R.F. supply to the dees.

4. Performance of the Selection System

The preliminary results from two experiments performed with the cloud chamber have been reported by Cairns *et al.* (1960)[11]) and Esten *et al.* (1960)[12]). Altogether 1500 p–α collisions at 53 MeV and 1100 p–d collisions at 136 MeV have been photographed. The performance of the selection system is best assessed from an analysis of the photographs, although valuable supplementary information has also been acquired from a counting experiment using carbon absorbers of various thicknesses between C3 and C4. The photographs from three different runs, classified in table 1, show how the efficiency of the selection system varies with the experimental conditions.

The photographs are divided into two main categories:

(A) Photographs showing clear evidence of the cause of the expansion.
Three groups can be distinguished, showing:
(i) Collisions in the chamber gas;
(ii) Incident protons stopping in the chamber;
(iii) Interactions in the Melinex window F3 and in the gas on either side of it (events in the chamber gas within 1 cm. of F3 cannot be distinguished from events in F3);

(B) Photographs without events which fall into two groups showing:
(1) Proton tracks, not visibly separated by the clearing field, crossing the chamber into C4.
(2) Random background tracks and field-separated tracks due to earlier protons.

The overall efficiency, ε, of the selection system is determined by all the events in group A whilst the

[11]) D. J. Cairns, T. C. Griffith, G. J. Lush, A. J. Metheringham and R. H. Thomas, London Conference on Nuclear Forces and the Few-Nucleon Problem (Pergamon Press Ltd., 1960). p. 269.

[12]) M. J. Esten, T. C. Griffith, G. J. Lush, A. J. Metheringham and C. P. van Zyl, London Conference on Nuclear Forces and the Few-Nucleon Problem (Pergamon Press Ltd., 1960). p. 277.

Table 1

	Gas filling	Beam energy (MeV)	Pressure of the gas (atmoshperes)	Total no. of photographs	Percentage of the total number of photographs				
					A. 1 E (%)	A. 2 (%)	A. 3 (%)	B (%)	ε (%)
					Interactions in the gas	Incident protons stopping in the gas	Interactions in or near F3	No visible interactions	(A1 + A2 + A3)
Run I	Helium	53	55	1458	48.4 ± 1.8	4.3 ± 0.5	16.5 ± 1.1	30.9 ± 1.5	69.1 ± 2.2
Run II	Deuterium	136	67	461	67.9 ± 3.8	—	13.0 ± 1.7	19.1 ± 2.0	80.9 ± 4.2
Run III	Deuterium	135	46	1393	54.8 ± 2.0	—	12.6 ± 0.9	32.6 ± 1.3	67.4 ± 2.2

useful efficiency, E, is that for the events in group A.1. Photographs of stopping protons, A2, were only obtained in the helium run where an aluminium absorber was employed to reduce the energy of the incident protons from 150 to 53 MeV. In runs II and III the observed number of events in group A3 is in reasonable agreement with the number expected from 0.0125 cm of Melinex and 1.0 cm of gas on either side of F3.

The photographs in B arise from various sources of inefficiency in the system, the significant ones being:

a. Dead time in the C4 anticoincidence pulse forming circuit;

b. Dead time in the C3 pulse forming circuit;

c. Chance coincidences between C1 and C2;

d. Incident protons stopping in C2 or in the gas inside C3;

e. Interactions of protons between F1 and F3 which give 1,2 coincidences but do not produce protons of sufficient energy to enter C3 or the cloud chamber;

f. Inefficient light collection from C3.

The estimated magnitude of these sources of inefficiency, together with the contribution of photographs in groups A2 and A3, are given in table 2.

In run III the coincidence circuit was gated so that only protons in a 25 μsec portion of the cyclotron RF pulse were examined by the counters. This led to an appreciable improvement in the energy spectrum of the gated protons but, since the ratio of gated and ungated protons entering the chamber was 1:4, a five fold increase in the beam intensity was necessary to obtain the required 1, 2, $\bar{3}$, 4 counting rate. The effects (a) and (b), which are directly proportional to the beam intensity, were therefore appreciable in this run. The contribution due to (a) was obtained from the number of photographs in group B1, allowance being made for those photographs with protons entering the chamber in the short interval between the triggering pulse and the complete turn off the cyclotron. These post trigger protons cause photographs of type B2 to appear in group B1 and the number of such photographs was deduced by counting the photographs with events on them (group A1) which also showed tracks crossing the chamber.

The contribution from (b) was investigated by measuring the ratio of the 1, 2, $\bar{3}$, $\bar{4}$ and 1, 2, $\bar{3}$, 4 counting rates as a function of beam intensity. Changes in this ratio are due to both (a) and (b) and the contribution of (b) alone was found by subtraction of the measured value of (a). In run I the ratio of the number of photographs in (b) to those in (a) is larger because 20% of the incident protons are scattered into C3 at 53 MeV compared with 5% at 136 MeV.

The contribution due to (e) has to be estimated by calculation and allowance made for the energy of the incident protons and for the nature and pressure of the gas in the chamber. As a result of the assumptions involved in these calculations the values given in table 2 are only approximate.

In runs II and III the sum of the contributions (a) to (e) is in good agreement with the observed inefficiency. Such agreement, for run I however, is only possible by assigning about 10% to (f), the inefficiency of light collection from C3. Only a small fraction of the light produced by protons entering C3 at the end nearest the chamber is collected by

Table 2
Inefficiencies in the selection system.

	Photographs in group A (% of the total)		Estimated number of photographs in group B (% of the total)						Sum of A + B	Observed percentage inefficiency
	A2	A3	(a)	(b)	(c)	(d)	(e)	(f)		
Run I	4.3	16.5	1.0	1.0	—	3.0	15	10	51	51.6
Run II	—	13.0	4.0	1.0	0.4	—	12	—	30	32.1
Run III	—	12.6	14.0	3.0	1.0	—	15	—	46	45.2

the light guide G3. An inefficiency of 8% due to (f) could arise in run I if only 0.5% of the protons entering C3 escaped detection and were also so scattered as to miss C4. The resulting photographs would appear either in groups B2 or A3. In run I an increase in the number of photogrpahs in group A3 is in fact observed and the 10% assigned to (f) is not unreasonable. In the higher energy runs this effect is not significant because only 5% of the incident protons enter C3; moreover the higher energy implies less scattering and although some of the protons escape detection in C3 they may still reach C4, where they are rejected. There are no reasons for believing that there is any significant inefficiency of light collection from C4.

The above analysis of the sources of inefficiency suggests that improved electronics with shorter dead time will improve the overall efficiency of the selection system; new circuits have been designed and will be used in future experiments. Some means of improving the efficiency of light collection from C3 is desirable but with the existing cloud chamber body this is a difficult problem. The thicknesses of F1, C2 and F3 cannot be less than their present values thus implying that the maximum values of ε and E will not be much greater than 85% and 75% respectively, even if all the other sources of inefficiency are removed. These values have almost been achieved in Run II but similar performance at low gas pressure, low incident proton energy and higher beam intensity is also desirable.

In conclusion it is worth pointing out that when the selection system is used with a cloud chamber having a cycling time T_c which is comparable with the average waiting time τ for a trigger pulse from the counters, the overall efficiency, E_0, in using the accelerator is appreciably higher than that of the selection sytem alone. If n is the number of events photographed with a selection system of efficiency E and N the number photographed with a selection system which is 100% efficient than

$$E_0 = \frac{n}{N} = \frac{E\,\tau_c + \tau}{\tau_c + \tau}.$$

In the present work $T_c = 1$ min. and $\tau \sim 1$ min. Hence with $E = 0.6$, 0.7 and 0.8, E_0 has values of 0.8, 0.85 and 0.90 respectively.

Acknowledgements

The authors gratefully acknowledge the encouragement and the interest shown by Professor Sir Harrie Massey. We have also had the benefit of many invaluable discussions with Mr. H. S. Tomlinson at University College and with Dr. G. H. Stafford, Mr. J. M. Dickson, Mr. B. Rose and Mr. A. E. Taylor at Harwell.

We thank the Director of the Atomic Energy Research Establishment, Harwell for the facilities given to us at Harwell and are most grateful to the cyclotron operators for their kind co-operation at all times. Our thanks are also due to the University of London, Central Research Fund for part of the financial support for this work.

Three of us (D.J.C.; G.J.L. and R.H.T.) wish to thank the Department of Scientific and Industrial Research for the award of Studentships.

NUCLEAR INSTRUMENTS AND METHODS **10** (1961) 281–288; NORTH-HOLLAND PUBLISHING CO.

PRECISION INSTRUMENTATION FOR AN ELECTRON ACCELERATOR†

I. T. MYERS and H. V. LARSON

Hanford Laboratories Operation, General Electric Company, Richland, Washington, U.S.A.

Received 29 November 1960

The supporting instrumentation necessary for an electron Van de Graaff accelerator is described. This includes a beam current integrator, a capacitor divider voltmeter, and an electron beam calorimeter, all with a precision of approximately ± 0.05 %; plus a cavity ion chamber for X-ray measurements, an extrapolation chamber for electron absorbed dose measurements, and an automated gold target.

1. Introduction

The precision of energy control, and flexibility of operation, plus the high absorbed dose rates possible in a medium power electron beam makes the Van de Graaff electron accelerator an exceedingly versatile machine. In order to make full and proper use of its capabilities, however, considerable additional measuring equipment, not normally furnished with the machine, is necessary. Also, adequate facilities for shielding personnel, storing equipment and performing experiments are needed.

The Hanford Laboratories electron Van de Graaff accelerator is horizontally mounted in a concrete shielded room 14.5 feet by 47 feet (fig. 1). The shielding on the end of the building is 30 inches of reinforced concrete; the shield between the control room and accelerator room is likewise 30 inches thick. Side-wall shielding is about 18 inches of concrete. The large shielded area gives desired flexibility to experimental work, as equipment not actually being exposed to the electron beam may be wheeled or pushed to one side, while other work is in progress. An auxiliary shield of lead bricks, which can be varied to suit individual experimental needs, surrounds the target area.

The vacuum pumps for evacuating the accelerator column and drift tube are the standard pumps furnished with the machine by the High Voltage Engineering Corporation. In order to minimize the time spent taking care of vacuum system cold traps, however, a trap refrigeration system†† was added to eliminate the need for dry ice. Not only has this refrigerator system reduced the cost of servicing the traps but it has also substantially improved machine performance by improving the system vacuum. The main trap operates at a temperature below 170°K.

2. Description of Supporting Equipment

The wide variety of experimental work done requires a wide variety of supporting instrumentation. Although it is often necessary to develop special instrumentation to accomodate a specific measurement, a few basic instruments are used in many different experiments. These basic instruments are:

1. Beam current integrator
2. Capacitor divider voltmeter
3. Calorimeter
4. Cavity ion chamber
5. Extrapolation chamber
6. Automatic gold target control.

The stability and reproducibility requirements on the integrator, voltmeter and calorimeter were stringent (± 0.1 %) due to the requirements of the stopping power work.

2.1. BEAM CURRENT INTEGRATOR

Current integration in the microampere region is important in several fields of research. It is a

† General Electric Company, Richland, Washington. Work performed under Contract No. AT(45–1)–1350 for the U.S. Atomic Energy Commission.

†† Harris Refrigeration Company.

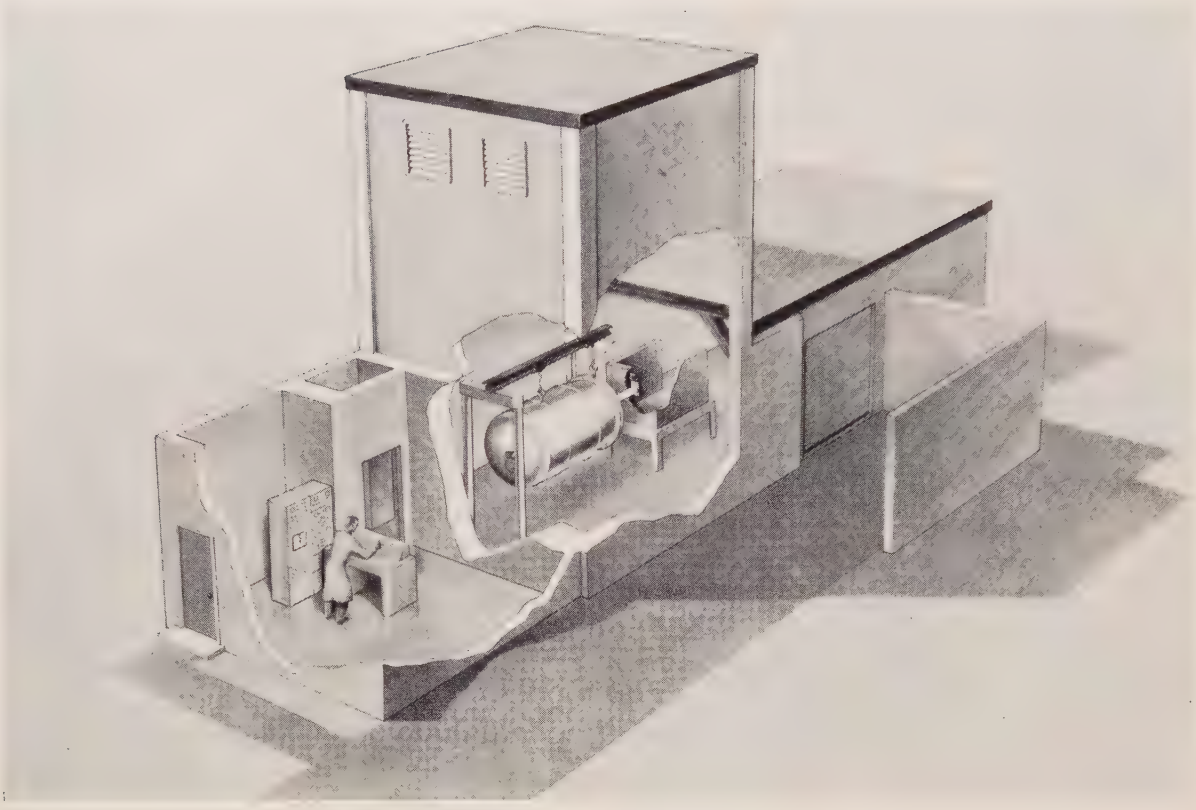

Fig. 1.

problem on which considerable development work has been done[1,2,3]).

The integrator described below[4]) was developed with the idea of making an instrument that would be suitable for use with a Van de Graaff accelerator, be highly stable, and have both a reproducibility and an accuracy of $\pm$ 0.05%. It takes advantage of the highly stable and accurate power supplies now available in the 1–300 volt range, as well as the low leakage polystyrene dielectric capacitors which are now available.

A block diagram is shown in fig. 2. The current to be integrated charges the integrating condenser C. The changing voltage on C produces an unbalance voltage at the amplifier input, which causes a 2-phase motor to drive the helipot until the amplifier input is again zero. The circuit diagram, including limit and range switches, is shown in fig. 3. Not shown is the precision voltage supply which supplies the balance voltage to the 25-turn helipot.

The effects of mechanical wear or creep were minimized by mounting the microswitch tripping mechanism on a 25-turn lead screw. The effect of a slight change in position of the starting and stopping (upper and lower) limit microswitch is

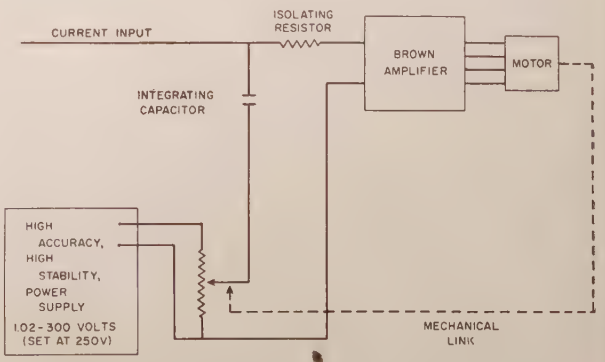

Fig. 2. Block diagram of the beam current integrator.

[1]) W. A. Higinbotham and S. Rankowitz, Rev. Sci. Inst. **22** (1951) 688.

[2]) R. Littauer, Rev. Sci. Inst. **25** (1954) 148.

[3]) R. J. Helmer and A. Hemmendinger, Rev. Sci. Inst. **28** (1957) 649.

[4]) I. T. Myers and G. T. Orton, HW-65802 (1960).

therefore effectively divided by 25 when compared to a comparable single turn or linear arrangement. In fact, it is estimated that the variation in microswitch closing position corresponds to an error of about 1 part in 100000. Similarly, the effect of amplifier gain changes were negligible. The gain of the amplifier could be changed by a factor of 2 with no noticeable change (less than 0.1 of one small

The integrator was calibrated by introducing a known current. The value of capacitance could also be measured using this same known current in the relation

$$i = \frac{dQ}{dt} = \frac{C\,dV}{dt}.$$

The average measured value of the input capacity over a range of input currents was measured on

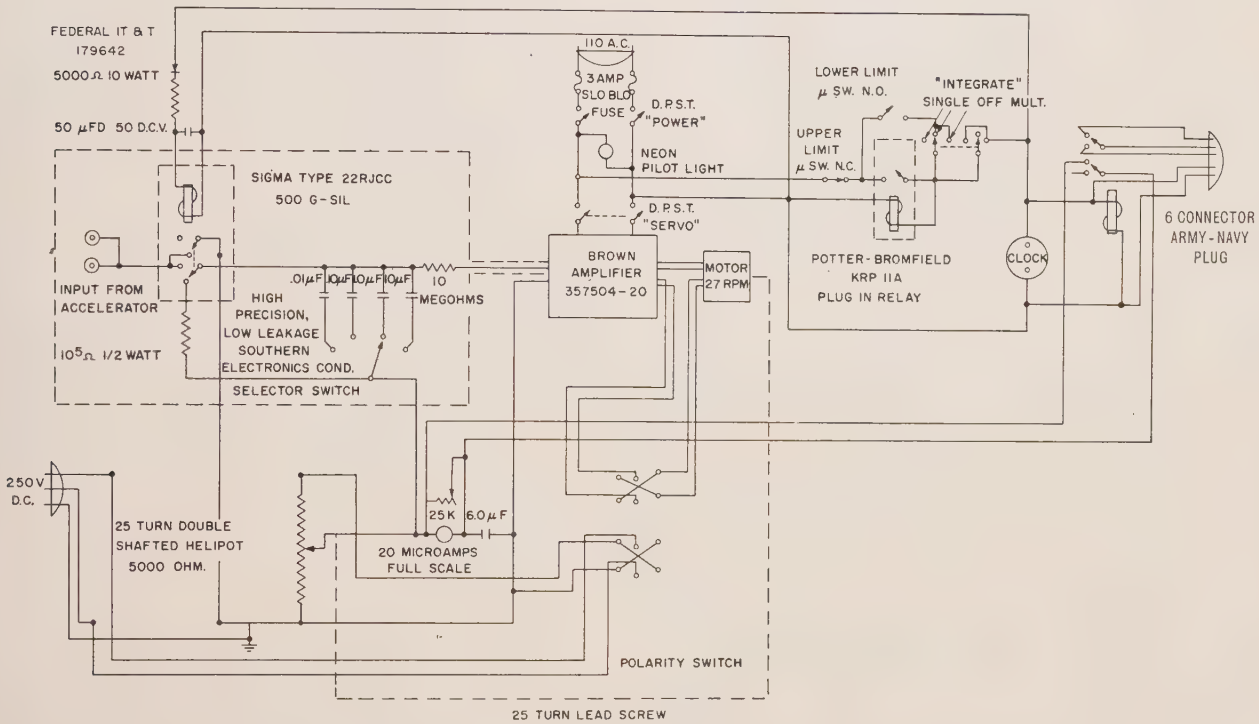

Fig. 3. Beam current integrator wiring diagram.

scale division) in output. This corresponds to an error of less than 1 part in 25000; it is possibly less, because 1 part in 25000 is as close as the integrated current can be read. In order to eliminate mechanical and electrical system oscillation, it was necessary to use an isolating resistance between the integrating capacitor and the amplifier. The deadband with a 2.5 megohm isolating resistor was, conservatively, about $\frac{1}{4}$ small scale division on the potentiometer readout dial, or about 0.01% of full scale. Deadband is defined here as the amount of error signal required before the amplifier-motor system would respond positively.

the 2500 and 250 microcoulomb scales. The measured values of the integrating capacity were 10.034 μF. To make the instrument direct reading on the 250 and 2500 microcoulomb ranges, the power supply voltage was decreased from 250 volts to 250/1.0034 or 249.15 volts.

About a week after the first calibration of the integrator, a test of reproducibility and stability was made by integrating a known current, using the same equipment as in the earlier calibration. The accuracy (reproducibility) with regard to the standard current was always within 0.05%, and was often considerably better.

2.2. CAPACITOR DIVIDER VOLTMETER

A capacitor divider method[5,6]) for measuring high voltages was developed for use with the electron accelerator. (See fig. 4.) The dc amplifier,

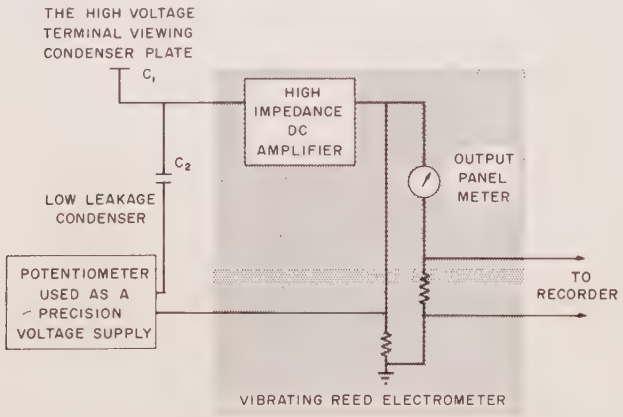

Fig. 4. Diagram of the condenser divider voltmeter.

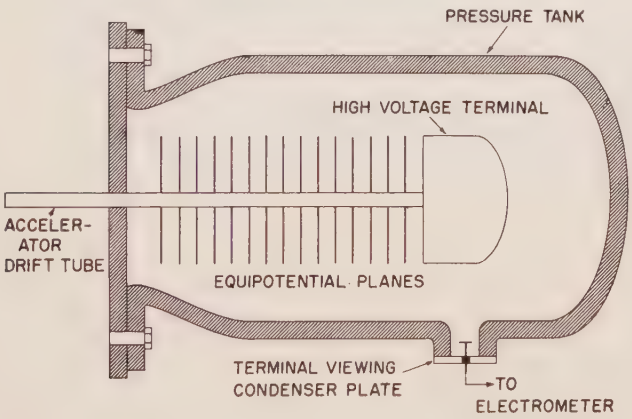

Fig. 5.
Relative position of the terminal viewing condenser plate.

panel meter, and resistances shown are the components of a vibrating reed electrometer. After presetting the potentiometer to the desired value, the accelerator voltage is adjusted until the vibrating-reed electrometer reads zero. Deviations from this preset value, which correspond to variations in the terminal voltage, can then be read on the recorder. High precision is obtained through the high resolution and accuracy of the potentiometer. Condenser C_1 is the capacity between a small insulated plate bolted into the accelerator pressure tank, and the high-voltage terminal. (See fig. 5.) The size of C_1 was about 0.1 $\mu\mu$F. Condenser C_2 is a high quality condenser with low leakage characteristics. For operation at 1 MeV, the voltage across C_2 was about 0.1 V.

The reproducibility of these voltage measurements is about $\pm$ 0.05%. This is the standard deviation of the mean of a series of eight measurements. The absolute error on the voltmeter readings is determined by the method of calibrating this instrument. Our present method of calibration is by use of the Be(γ, n) threshold reaction. Lack of more accurate knowledge of this threshold limits the accuracy of the absolute calibration to $\pm$ 0.1%.

2.3. TOTAL BEAM CALORIMETER

Besides its specific use in stopping power measurements the total beam calorimeter may be used wherever total energy absorption measurements are needed by inserting the absorber into the calorimeter so that it effectively becomes a part of it. The general arrangement of components is shown in fig. 6. The entire calorimeter is mounted inside a

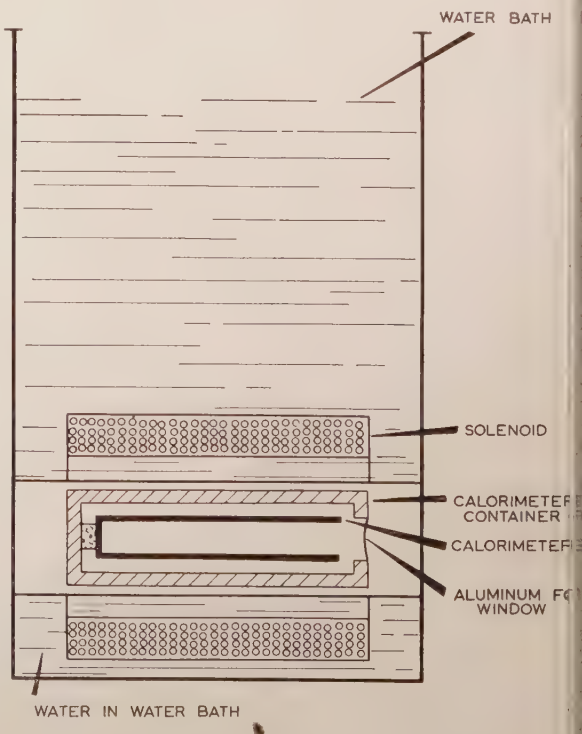

Fig. 6. Electron beam calorimeter and water bath.

[5]) H. V. Larson and I. T. Myers, Rev. Sci. Inst. **30** (1959) 1022.

[6]) I. T. Myers and H. V. Larson, HW-66042 (1960).

tube in a water bath. The water bath may be operated either isothermally or adiabatically. Bath control is achieved with a thermistor mounted in a long glass tube dipping well beneath the bath surface. The thermistor is part of a Wheatstone bridge circuit using a 100-microvolt potentiometric type recorder as a detector. (See fig. 7.) The recorder serves both as a controller and as a bath heat source at different points in the calorimeter. It was found that a period of about 10 minutes was required for heat equilibrium to be established after a few thousand joules of heat were added to the system. Since the time constant of the system is considerably longer than this, for adiabatic operation, the amount of heat lost could be made small.

The electrical heater in the calorimeter was

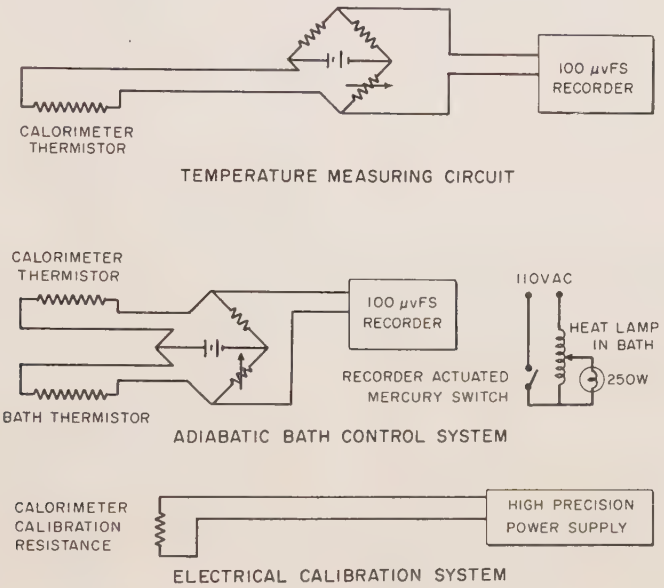

Fig. 7. Calorimeter measurement and control systems.

monitor. When isothermal operation is desired the calorimeter thermistor is replaced by a fixed resistor. One of the remaining legs is variable and can be adjusted to take differences in absolute magnitude of the thermistors into account. No particular attempt was made to match temperature coefficients of the two thermistors, since electrical calibration of the calorimeter was used, and calibration data and measurements were taken over the same region of resistance changes. The calorimeter was constructed for stability rather than for sensitivity, in order to make difference measurements possible. The walls of the calorimeter are thick enough to absorb all the electrons, and the calorimeter is long enough to retain all but a negligibly small fraction of the electrons entering. Thermistors (100000 ohms at room temperature) were mounted in both the end and the side of the calorimeter in order to detect the effect of having a constructed by winding manganin wire on the outside of the calorimeter body in suitable grooves. The heater resistance was 2717.7 ohms, with a total lead resistance of 2.2 ohms. The lead resistance was small enough (0.08%) to be neglected for many measurements; and, also, it could be corrected for easily. The advantages of using a power supply in the 0–300 volt region is that a relatively high resistance heating coil may be used, which makes the lead resistance small compared to the heating coil resistance. Also, the convenience of operation is greatly improved, since only one setting of the calibrating voltage is necessary. Both accuracy and stability are built into the power supply, whose accuracy and stability are claimed to be $\pm$ 0.02% by the manufacturer. Therefore, no readjustment of heating current is necessary during measurements, freeing the investigator for other work. The "heat capacity" was measured to be 0.7004 $\pm$ 0.0020

joules per ohm change in the calorimeter thermistor. This is approximately 1750 joules/°C.

The calorimeter was made of aluminum. Provisions were made for using other materials at the point where the electron beam was stopped in order to minimize radiation losses. The entire calorimeter was mounted on a polystyrene heat and electrical insulator inside a vacuum jacket. The beam entered through a 3 mil aluminum window which could be removed if desired, allowing the calorimeter to be connected directly to the vacuum system of the accelerator through a bellows.

2.4. ELECTRON BEAM SWEEP

An ever present problem in electron irradiation research is non-uniform sample irradiation due to the non uniformity of the electron beam. Scattering foils may be used to give a more uniform, broader beam. They, however, have the disadvantage of introducing non uniformities into the energy of the electrons. Defocusing of the electron beam with a solenoid is another possibility; it is difficult, however, to attain good uniformity. For these reasons, an electrostatically deflected beam is used for experimental work where a high degree of uniformity is required. (See fig. 8.) A 60000 volt power supply is used to energize an RC sawtooth producing network, with the sawtooth in the horizontal direction having a frequency of 1000/sec and in the vertical direction of 20/sec. Hydrogen thyratrons are used for the cutoff tubes. It is possible to generate a beam pattern up to 1 inch square, or a rectangle with the long dimension either horizontal or vertical.

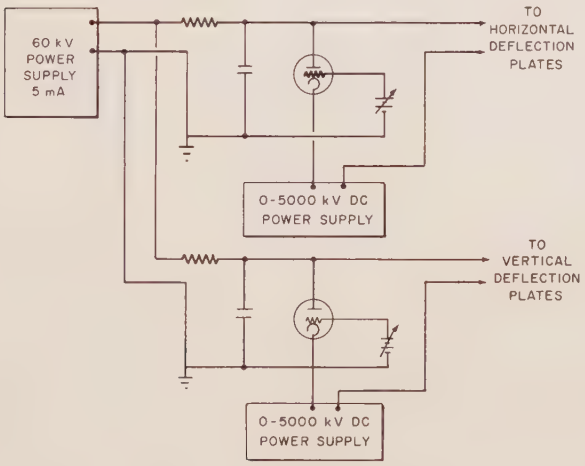

Fig. 8. Beam sweep control.

2.5. DOSE MEASURING EQUIPMENT

Absorbed dose due to electrons may be determined at this laboratory by an extrapolation chamber, by the total beam calorimeter, or by calculation (in thin specimens) from a knowledge of the beam current, beam area and stopping power. The extrapolation chamber[7]) is shown in fig. 9. This chamber consists of a thick electrode that simultates a slab of tissue that is thick enough to stop the most energetic electrons present, a second electrode that is thick enough to simulate the depth at which the dose must be determined, and a screw to vary the electrode spacing. A guard ring is used to accurately define the chamber volume. In practice the chamber volume is varied by changing the electrode separation and the ionization current per unit volume is plotted as a function of volume. For small spacings the current per unit volume becomes independent of the volume, and equal to the absorbed dose in the second electrode divided by SW. W is the energy required to produce an ion pair in the chamber gas, and S is the stopping power of the electrode material relative to the gas.

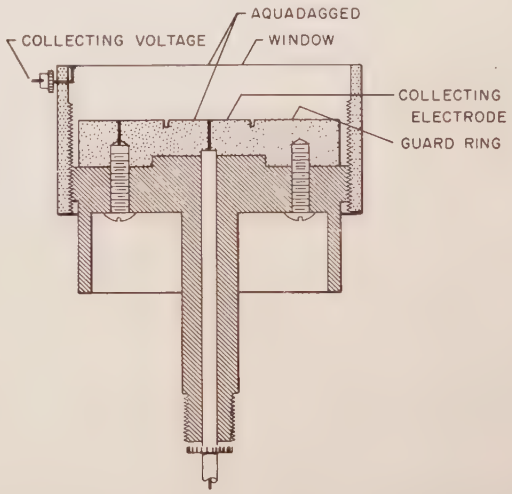

Fig. 9. Extrapolation chamber for surface dose measurements.

[7]) W. C. Roesch and E. E. Donaldson, Proceedings of the International Conference in the Peaceful Uses of Atomic Energy 14 (1956) 172.

The tissue dose may then be calculated using known values of S and W, and a measured value of current per unit volume.

The average dose that a specimen received may be calculated from a knowledge of the integrated beam current, the beam area and either the stopping power for thin specimens or the range and energy for thick specimens. The beam sweep equipment makes this calculation much more accurate.

is controlled from the console. Lights on the console indicate whether the target is in the electron irradiation position (gold target out of the beam) or in the X-ray position (gold target stopping the beam). The target control is valuable in electron exposures, since the beam current can be set by measuring the current to the gold target, and then the target lifted to make the exposure. The excellent current stability of the accelerator, when operated

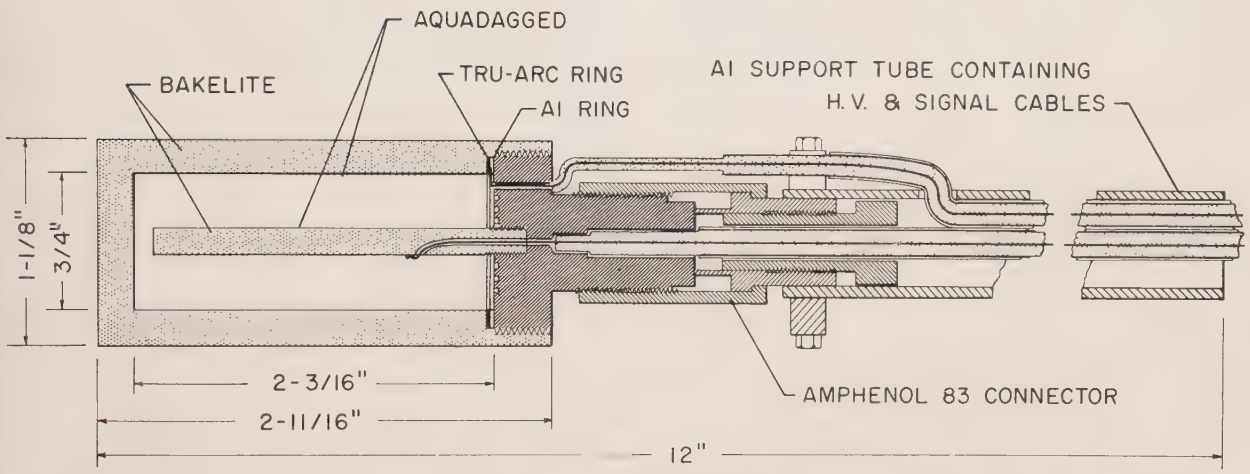

Fig. 10. Ionization chamber for gamma ray exposure dose rate measurements.

Not only does it produce a uniform irradiation over a given area but it also defines that area.

A cavity ionization chamber (see fig. 10) is used to measure X-ray dose rates according to standard ionization chamber techniques. This chamber is calibrated with a standard radium source. A chamber voltage of 600 volts produces voltage saturation up to a dose rate of at least 50000 r/hr which is the maximum dose rate produced by the accelerator. The sensitivity of the chamber is 8.7×10^{11} r/hr ampere.

2.6. AUTOMATIC GOLD TARGET CONTROL

The automatic gold target control permits changing from electron irradiation to X-irradiation in less than a minute, without shutting down the machine. The original gold target control was mechanized with a motorized chainlink drive that

† High Voltage Engineering Corporation, Burlington, Massachusetts, U.S.A.

with a beam stabilizing pentode circuit† in the high voltage terminal, makes this a very practical method of operation.

3. Compatibility of Voltage, Current, and Power Measurements

With the instrumentation described above each of the factors in the equation $\int_0^\tau P\,dt = V\int_0^\tau I\,dt$ was independently measured. The integrated beam power $\int_0^\tau P\,dt$ was determined by the calorimeter the integrated beam current $\int_0^\tau I\,dt$ by the beam current integrator, and the accelerator terminal voltage (V) by the condenser divider voltmeter.

These three measurements must be consistent, that is V as measured by the voltmeter must be equal to $\int_0^\tau P\,dt / \int_0^\tau I\,dt$. This comparison is made in table 1. The accelerator voltage was held constant at 1.025 MeV with the condenser divider voltmeter. These data show the excellent agreement between the accelerator voltage as measured by the ratio

TABLE 1

Measurement of accelerator voltage with the beam current integrator and the calorimeter

$\int_0^\tau P\,dt$ (Joules)	$\int_0^\tau I\,dt$ (Microcoulombs)	$\frac{\int_0^\tau P\,dt}{\int_0^\tau I\,dt}$ (MeV)
5650.6	5500.4	1.0273
5620.9	5501.0	1.0218
5635.6	5500.3	1.0246
5647.5	5500.6	1.0267

Average: 1.0251 $\pm$ 0.0012 MeV.

$\int_0^\tau P\,dt / \int_0^\tau I\,dt$ and as measured by the condenser divider voltmeter. This agreement demonstrates that no serious errors exist because of faulty Faraday cup operation or improper corrections for radiation losses.

Acknowledgements

A laboratory such as the one discussed in this paper could not function properly without the aid of many supporting people. We wish to especially thank the accelerator staff for their capable assistance. We also wish to thank G. T. Orton, T. F. Crum, and C. O. Finney for assistance with the design and assembly of the beam current integrator. E. M. Sheen, W. G. Spear, and G. E. Driver were responsible for the design work and the construction of the beam sweep equipment. W. C. Roesch and E. E. Donaldson developed the extrapolation chamber and ionization chamber for electron and X-ray dosimetry and T. Larson developed the gold target control.

NUCLEAR INSTRUMENTS AND METHODS **10** (1961) 289–294; NORTH-HOLLAND PUBLISHING CO.

PARASITIC REFLECTIONS OF NEUTRONS IN CRYSTAL MONOCHROMATORS

K. BLINOWSKI and J. SOSNOWSKI

Institute for Nuclear Research, Warsaw

Received 19 November 1960

The intensity of a monoenergetic neutron beam obtained by reflection from a crystal monochromator is very often decreased due to the additional so called parasitic scattering. Since this effect gives several percent fluctuations of the intensity, it has to be taken into account in precise measurements. In particular it is important in neutron spectrum studies by Bragg reflection.

For a given reflecting plane two parameters are responsible for multiple scattering: Bragg angle and spatial orientation of the monochromator. Suitable choice of the second parameter permits the elimination of parasitic reflection.

The Cu monochromator has been rotated about an axis perpendicular to the (111) reflecting plane. The intensity of reflected thermal neutrons has been measured versus angle of rotation. Results showing the influence of multiple reflections are found to agree with calculated angular positions for chosen Bragg angles.

1. Introduction

In a recent paper O'Connor and Sosnowski have pointed out that intensity fluctuations observed in the thermal neutron spectrum measured with a crystal monochromator are due to parasitic Bragg reflections[1]). A slow neutron spectrum containing these fluctuations as inverted peaks is shown in fig. 1. It is seen that the majority of inverted peaks are identified as the effects of parasitic reflections. The authors have concluded that the density of inverted peaks and their magnitude prohibit the use of the crystal monochromator for precise measurements of neutron spectra.

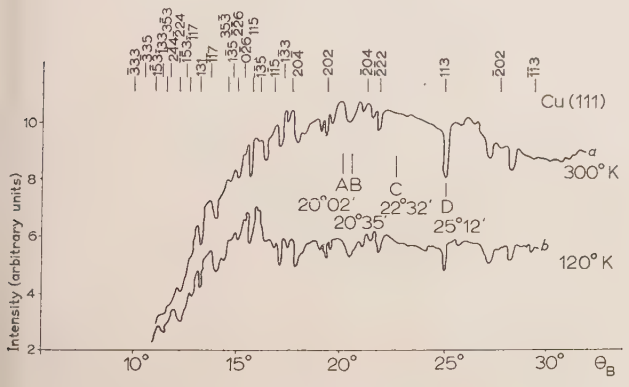

Fig. 1.
Slow neutron spectrum obtained with the Cu monochromator.

[1]) O'Connor D. A., J. Sosnowski, Report No. 134/I–B Institute for Nuclear Research, Świerk k/Otwocka, Acta Crystallographica (in press).

Their results have practical meaning for reactor neutron spectrometry but are limited to one spatial orientation of the monochromator. The Al and Cu monochromators were used in the measurements with the (111) reflecting plane and the $(\bar{1}10)$ plane of reflection oriented horizontally.

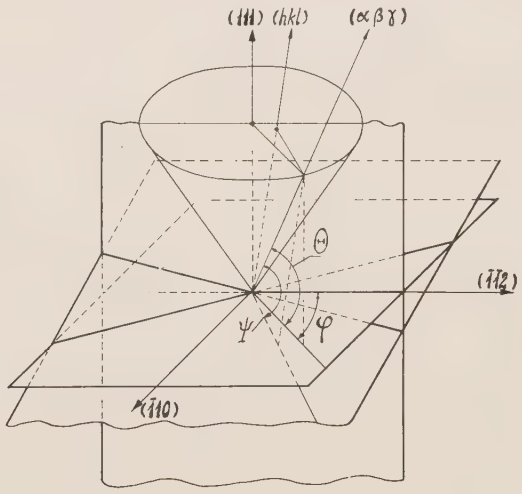

Fig. 2. Coordinate system for desdription of the parasitic reflection occuring with the main reflection from the (111) plane of a cubic structure.

The present paper reports an investigation of the parasitic reflections with the neutron monochromator changing continuously its orientation in space with the Bragg angle remaining constant. The principle of the experiment is made clear by fig. 2.

A suitable coordinate system connected with cubic structure has been chosen to describe the phenomenon.

The crystal with the (111) reflecting plane is rotated about an axis perpendicular to this plane. The $[\overline{\alpha}\ \overline{\beta}\ \overline{\gamma}]$ unit vector shows the direction of the incoming neutron beam, θ is the Bragg angle for the (111) plane. ψ is the Bragg angle for some (hkl) plane giving parasitic reflection. φ is an angle between the $[\overline{1}\overline{1}2]$ vector and the plane of main reflection given by the [111] and $[\alpha\,\beta\,\gamma]$ vectors.

2. Calculations

From the geometry of the system presented in fig. 2 the following relations are obtained:

$$\begin{aligned}
[\alpha\beta\gamma]\,[111] &= |\,111\,| \sin\theta \\
[\alpha\beta\gamma]\,[hkl] &= |\,hkl\,| \sin\psi \\
[\alpha\beta\gamma]\,[\overline{1}\overline{1}2] &= |\,\overline{1}\overline{1}2\,| \cos\theta\cos\varphi \\
[\alpha\beta\gamma]\,[\overline{1}10] &= |\,\overline{1}10\,| \cos\theta\sin\varphi\,.
\end{aligned} \tag{1}$$

$|\,\alpha\beta\gamma\,| = 1$ from the definition

We want to express the angle φ as a function of h, k, l and the Bragg angle θ, without parameters α, β, γ and ψ.

The solution of (1) gives:

$$2\sqrt{3}\,(h+k+l)\sin\theta + 3\sqrt{2}\,(-h+k)\cos\theta\sin\varphi + \\ + \sqrt{6}\,(-h-k+2l)\cos\theta\cos\varphi - 6\,|\,hkl\,|\sin\psi = 0. \tag{2}$$

From the Bragg equation we have

$$\sin\psi = \frac{d_{111}}{d_{hkl}}\sin\theta = \frac{|\,hkl\,|}{\sqrt{3}}\sin\theta\,. \tag{3}$$

Substituting for $\sin\psi$ in (2) and putting $\cos\varphi = (1-\sin^2\varphi)^{\frac{1}{2}}$ we find that:

$$\sin\varphi = \frac{1}{b^2+3c^2}\times \\ \times\,[\sqrt{6}\,ac\tan\theta \pm b(b^2+3c^2-2a^2\tan^2\theta)^{\frac{1}{2}}] \tag{4}$$

where

$$\begin{aligned}
a &= h+k+l-(h^2+k^2+l^2) \\
b &= h+k-2l \\
c &= h-k\,.
\end{aligned}$$

It follows that for a given Bragg angle θ only those crystallographic planes can participate in the parasitic reflection which have Miller indices fulfilling the relation:

$$\tan^2\theta \leqslant \frac{(h+k-2l)^2+3(h-k)^2}{2\,[h+k+l-|\,hkl\,|^2]^2}\,. \tag{5}$$

The values of $\theta_{\max}$ calculated from (5) are given in table 1. As seen from a comparison between the tabulated values and the slow neutron spectrum (fig. 1) all angular positions of inverted peaks are in agreement with the corresponding $\theta_{\max}$.

Four different Bragg angles $\theta_{\max}$ have been chosen in order to compare the experimental results with the calculations. They are denoted by A, B, C, D in fig. 1.

Table 2 contains the values of φ computed from (4).

3. Experimental

The measurements were performed on the crystal neutron spectrometer. The Cu monochromator with the (111) reflecting plane parallel to the crystal surface was used. The monochromator was covered with a 0.3 mm Cd foil and could reflect the neutron beam only from a circular area of 40 mm in diameter. The aluminium frame crystal holding was tightly connected to a selsyn axis as shown in fig. 3. A driving mechanism coupled to the other and of the selsyn axis was rotating the crystal at constant speed of about 90° per hour. The intensity

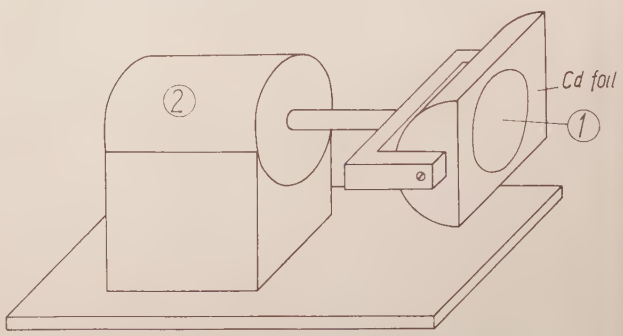

Fig. 3. Experimental arrangement. The Cu monochromator is 1, Selsyn is 2.

of reflected neutron beam was recorded continuously by a rate meter driving a pen recorder. The use of selsyns made it possible to control angular positions of the monochromator (the φ angle) and to put them on a tape with intensity diagram.

TABLE 1

The Bragg angles $\theta_{obs.}$ corresponding to parasitic reflections in the slow neutron spectrum (obtained by O'Connor and Sosnowski) compared with the values for θ_{max} calculated from (5).

hkl	θ_{max}	hkl	θ_{max}	hkl	θ_{max}
200	54°44′	400	25°14′	$\bar{4}20$	18°47′
020	54°44′	040	25°14′	$\bar{2}40$	18°47′
002	54°44′	004	25°14′	$20\bar{4}$	18°47′
$\bar{2}00$	25°14′	$\bar{4}00$	15°47′	$02\bar{4}$	18°47′
$0\bar{2}0$	25°14′	$0\bar{4}0$	15°47′	$0\bar{4}2$	18°47′
$00\bar{2}$	25°14′	$00\bar{4}$	15°47′	$\bar{4}02$	18°47′
				$4\bar{2}0$	18°54′
220	35°16′	331	13°16′	$\bar{2}40$	18°54′
202	35°16′	313	13°16′	$\bar{2}04$	22°34′
022	35°16′	133	13°16′	$0\bar{2}4$	22°34′
$\bar{2}20$	13°02′	$\bar{3}31$	22°34′	$04\bar{2}$	22°34′
$2\bar{2}0$	31°29′	$3\bar{3}1$	22°34′	$40\bar{2}$	22°34′
$20\bar{2}$	31°29′	$31\bar{3}$	22°34′	$\bar{4}2\bar{0}$	10°40′
$02\bar{2}$	31°29′	$13\bar{3}$	22°34′	$\bar{2}4\bar{0}$	10°40′
$0\bar{2}2$	31°29′	$1\bar{3}3$	22°34′	$\bar{2}0\bar{4}$	10°40′
$\bar{2}02$	31°29′	$\bar{3}13$	22°34′	$0\bar{2}\bar{4}$	10°40′
$\bar{2}\bar{2}0$	13°16′	$33\bar{1}$	11°39′	$0\bar{4}\bar{2}$	10°40′
$\bar{2}0\bar{2}$	13°16′	$3\bar{1}3$	22°00′	$\bar{4}0\bar{2}$	10°40′
$0\bar{2}\bar{2}$	13°16′	$\bar{1}33$	22°00′		
				422	10°02′
311	25°14′	$\bar{3}\bar{1}1$	13°16′	242	10°02′
131	25°14′	$\bar{3}1\bar{3}$	17°19′	224	10°02′
113	25°14′	$1\bar{3}\bar{3}$	13°16′	$\bar{4}22$	19°28′
$\bar{3}11$	22°12′	$\bar{3}31$	20°31′	$2\bar{4}2$	19°28′
$1\bar{3}1$	22°12′	$3\bar{3}\bar{1}$	20°31′	$22\bar{4}$	19°28′
$11\bar{3}$	25°14′	$3\bar{1}\bar{3}$	20°31′	$4\bar{2}2$	20°31′
$3\bar{1}1$	31°29′	$\bar{1}3\bar{3}$	20°31′	$\bar{2}42$	20°31′
$\bar{1}31$	31°29′	$\bar{1}\bar{3}3$	20°31′	$\bar{2}23$	20°31′
$\bar{1}13$	30°21′	$\bar{3}\bar{1}3$	20°31′	$2\bar{2}4$	20°31′
$1\bar{1}3$	31°29′			$24\bar{2}$	20°31′
$13\bar{1}$	31°29′	$\bar{3}\bar{3}\bar{1}$	6°13′	$42\bar{2}$	20°31′
$31\bar{1}$	31°29′	$\bar{3}\bar{1}\bar{3}$	6°13′	$\bar{4}\bar{2}2$	14°58′
$\bar{3}\bar{1}1$	19°17′	$\bar{1}\bar{3}\bar{3}$	6°13′	$\bar{2}4\bar{2}$	14′58°
$\bar{1}3\bar{1}$	19°17′			$\bar{2}\bar{2}4$	14°58′
$\bar{1}1\bar{3}$	19°17′	420	19°17′	$2\bar{2}\bar{4}$	14°58′
$1\bar{1}\bar{3}$	19°17′	240	19°17′	$\bar{2}4\bar{2}$	14°58′
$1\bar{3}\bar{1}$	19°17′	204	19°17′	$\bar{4}\bar{2}\bar{2}$	14°58′
$\bar{3}1\bar{1}$	19°17′	024	19°17′	$\bar{4}\bar{2}\bar{2}$	5°03′
		042	19°17′	$\bar{2}4\bar{2}$	2°02′
$3\bar{1}\bar{1}$	29°30′	402	19°17′	$\bar{2}\bar{2}4$	6°40′
$\bar{1}3\bar{1}$	29°30′				
$\bar{1}\bar{1}3$	29°30′				
$\bar{3}1\bar{1}$	10°02′				
$\bar{1}3\bar{1}$	10°02′				
$\bar{1}1\bar{3}$	10°02′				

TABLE 2
The azymuthal positions of monochromator at which additional reflections are expected

hkl	$\theta = 20°02'$	$\theta = 20°35'$	$\theta = 22°32'$	$\theta = 25°12'$
200	15°04′	14°36′	12°56′	10°34′
020	44°56′	45°24′	47°04′	49°26′
002	75°03′	74°36′	72°56′	70°34′
$\bar{2}00$	20°40′ (+ 60°)	22°49′ (+ 60°)	31°39′	56°35′
$0\bar{2}0$	200°40′ (+ 60°)	202°49′ (+ 60°)	211°39′	236°34′
$00\bar{2}$	39°20′	37°11′	28°21′	3°25′
220	58°58′	57°55′	54°04	48°17′
202	181°02′	182°05′	185°56′	191°43′
022	1°02′ (+ 60°)	2°05′	5°56′ (+ 60°)	11°43′ (+ 60°)
$2\bar{2}0$	216°33′	217°50′	222°49′	230°13′
$20\bar{2}$	23°27′	22°10′	17°21′	9°47′
$0\bar{2}\bar{2}$	23°27′	22°10′	17°21′	9°47′
$02\bar{2}$	83°27′	82°10′	77°21′	69°47′
$\bar{2}02$	83°27′	82°10′	77°21′	69°47′
311	200°40′	202°49′	211°39′	236°35′
131	20°40′ (+ 60°)	22°49′ (+ 60°)	31°39′	56°35′
113	39°20′	31°11′	28°21′	3°25′
$\bar{3}11$	20°40′ (+ 60°)	22°49′ (+ 60°)		
$1\bar{3}1$	200°40′ (+ 60°)	202°49′ (+ 60°)		
$11\bar{3}$	39°20′	37°11′	28°21′	3°26′
$3\bar{1}1$	216°33′	217°50′	222°39′	230°13′
$\bar{1}31$	36°33′	37°50′	42°39′	50°13′
$\bar{1}13$	83°27′	82°10′	77°21′	69°47′
$3\bar{1}\bar{1}$	190°08′	191°36′	197°10′	206°17′
$\bar{1}3\bar{1}$	10°08′ (+ 60°)	11°36′ (+ 60°)	17°10′ (+ 60°)	26°17′ (+ 60°)
$\bar{1}\bar{1}3$	49°52′	48°24′	42°49′	33°43′
$\bar{3}31$	50°24′/72°11′	53°42′	75°27′	
$3\bar{3}1$	230°24′	233°42′	255°27′	
$31\bar{3}$	9°36′	6°18′	195°27′	
$3\bar{1}\bar{3}$	214°29′	218°21′		
$\bar{1}33$	34°29′/85°31′	38°21′		
$\bar{3}3\bar{1}$	66°09′			
$3\bar{3}\bar{1}$	246°09′/267°56′			
$3\bar{1}\bar{3}$	207°56′			
$\bar{1}3\bar{3}$	27°56′/53°51′			
$\bar{1}\bar{3}3$	186°08′			
$\bar{3}\bar{1}3$	6°08′/32°04′			

4. Results and Comparison with Theoretical Data

As indicated in fig. 4 the intensity of the reflected beam was sufficiently high and the statisfical error could be neglected. Nevertheless some measurements were repeated in order to eliminate the accidental fluctuations. The background counting rate was constant and less than 2% of the intensity of the reflected beam. The intensity changes due to parasitic reflections are of the order of 10%. Diagrams B and D were expected to have the deep inverted peaks at $\varphi = 0°$ according to fig. 1. Indeed, a very broad inverted peak seen in diagram D

corresponds to the (113) peak at $\theta_B = 25°12'$. The agreement in both cases will be still better if we suppose that O'Connor and Sosnowski had their monochromators misoriented about the (111) vector on $\varphi = 2°$ i.e. the $(\bar{1}10)$ plane was deviated by 2° from the plane of reflection. Then the B peak not identified in fig. 1 would correspond to the (022) parasitic reflection, which occurs at $\varphi = 2°05'$ for $\theta_B = 20°35'$.

All angular positions of the monochromator within a full angle giving additional reflections and calculated from eq. (4) are in good agreement with the measured values. The superposition and overlapping of simultaneous parasitic reflections makes peaks broader and deeper. It is also interesting to notice that for certain λ's (see diagram D) as much as one third of all possible monochromator

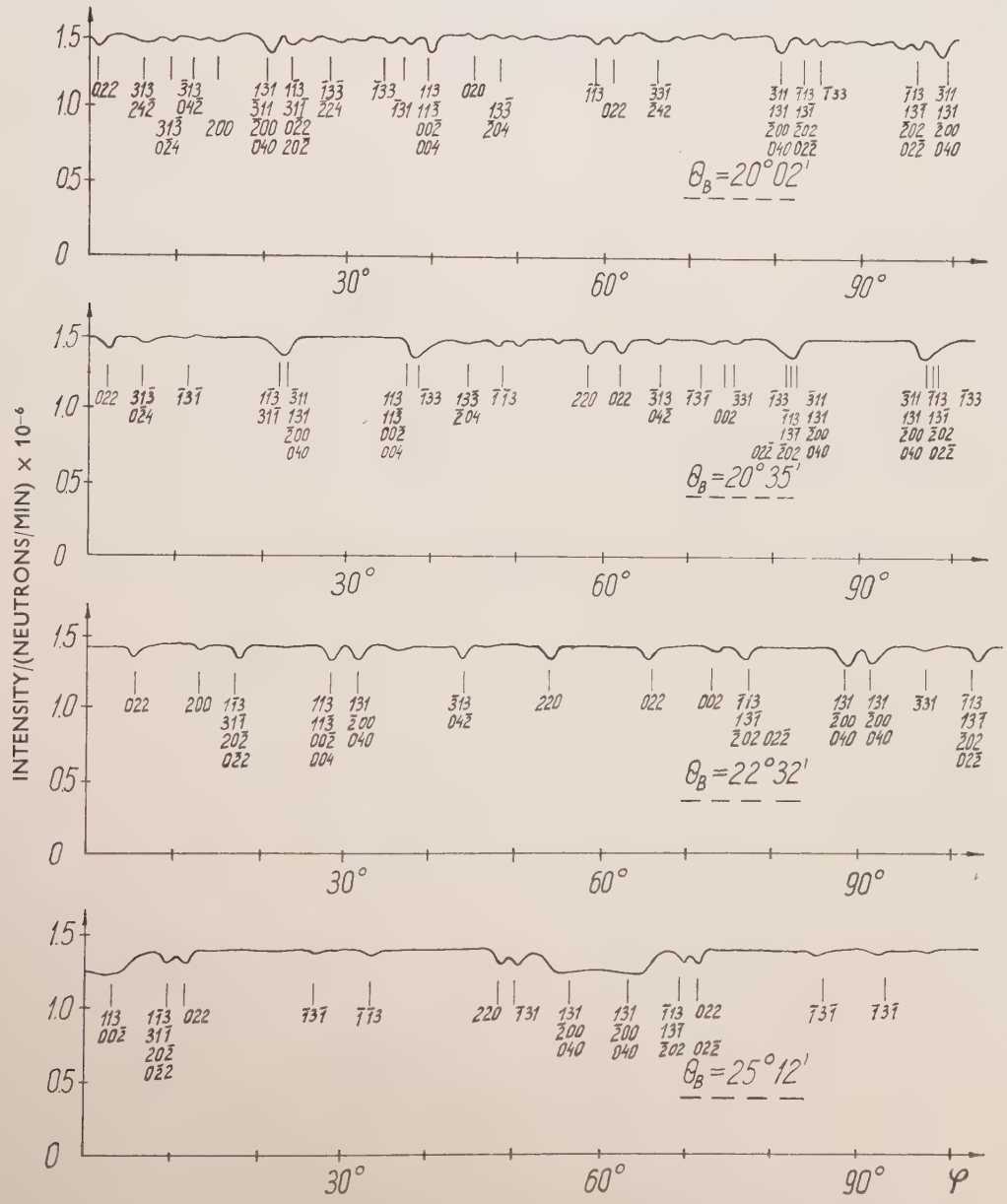

Fig. 4. The intensity dependance versus the angular orientation φ of a monochromator. Curves correspond to the Bragg positions A, B, C, D in fig. 1.

orientations give reflection disturbed and decreased by parasitic scattering.

5. Concluding Remarks

The use of a monocrystal as a monochromator for slow neutron spectrum measurements can be improved if there is a necessity for precise measurements.

Rotating the monochromator about an axis perpendicular to reflecting plane and choosing suitable φ one can eliminate multiple reflection. By doing that however the special attention has to be drawn to keep Bragg angle θ constant.

Acknowledgments

The authors are most indebted to dr. D. O'Connor for his suggestions in this experiment. We wish to thank Mrs. Stanisława Bogumił from the Applied Mathematics Department for the numerical calculations. We would also like to thank Ryszard Kula for his technical assistance in the work.

NUCLEAR INSTRUMENTS AND METHODS **10** (1961) 295–300; NORTH-HOLLAND PUBLISHING CO.

EIN MAGNETISCHES COMPTON-SPEKTROMETER ZUR UNTERSUCHUNG HOCHENERGETISCHER RÖNTGEN-BREMSSTRAHLUNG

K. FELBINGER, H. KULENKAMPFF, M. SCHEER und E. SCHRÜFER

Physikalisches Institut der Universität Würzburg

Eingegangen am 23. Dezember 1960

Construction and operation of a magnetic Compton-spectrometer are described. Application of the analysis of data measured with this spectrometer in order to obtain the Bremsstrahlung-spectrum is illustrated. As an example the intensity distribution of the Würzburg 30 MeV-Betatron is determined for a special case.

1. Einleitung

Das Grundprinzip des Compton-Spektrometers besteht darin, daß die zu untersuchende Quantenstrahlung in einer Konverterfolie Comptonelektronen auslöst, deren Energieverteilung in einem Magnetfeld analysiert wird. Gegenüber anderen Wechselwirkungen der Strahlung mit Materie zeichnet sich der Comptoneffekt dadurch aus, daß seine theoretische Behandlung als abgeschlossen und gesichert gelten kann. Für Elemente niedriger Ordnungszahl und bis zu Quantenenergien von etwa 50 MeV ist außerdem der Wirkungsquerschnitt für den Comptoneffekt hinreichend groß gegenüber dem für Paarbildung, sodaß die Zahl der Comptonelektronen zuverlässig ermittelt werden kann. Aus der gemessenen Energieverteilung der Elektronen kann die interessierende Energieverteilung im Spektrum der Röntgen-Bremsstrahlung berechnet werden, wenn für das benutzte Spektrometer Lichtstärke und Auflösung in Abhängigkeit von der Energie bekannt sind.

Derartige Spektrometer sind schon von mehreren Autoren beschrieben worden[1,2,3]). Für Untersuchungen an dem Würzburger 30 MeV-Betatron haben wir ein magnetisches Compton-Spektrometer konstruiert, das sich bereits bei vielen Messungen sehr gut bewährt hat. Es erscheint uns deshalb angebracht, im folgenden die besondere Konstruktion unseres Magneten, die zusätzlichen Meßanordnungen sowie als Anwendungsbeispiel die Untersuchung eines Bremsstrahlungsspektrums zu beschreiben.

[1]) J. W. Motz, William Miller, H. O. Wyckoff, H. F. Gibson und F. S. Kirn, Rev. Sci. Instr. **24** (1953) 929.

[2]) K. Ulmer und B. Ziegler, Z. ang. Phys. **8** (1956) 49.

[3]) J. W. Robson und E. C. Cregg, Phys. Rev. **105** (1957) 619.

2. Der Magnet

2.1. ALLGEMEINER AUFBAU

Für die Form erscheint ein zylindrischer Topfmagnet besonders günstig: Die Rotationssymmetrie erleichtert die Bearbeitung der Eisenteile, das Streufeld des Magneten ist nach außen scharf begrenzt und schließlich ergab sich die Möglichkeit einer sehr einfachen Konstruktion der Vakuumkammer. Als Material konnte ein speziell hierfür erschmolzenes, besonderes kohlenstoffarmes Eisen verwendet werden†.

Der Magnet ist in Fig. 1 in einem Vertikalschnitt, in fig. 2 in einem Horizontalschnitt dargestellt; seine äußeren Abmessungen betragen 83 cm in der Höhe und 55 cm im Durchmesser. Am Boden und Deckel des zylindrischen Joches sind die beiden Innenkerne (Durchmesser 26 cm) in der aus fig. 1 ersichtlichen Weise befestigt. Der mittlere Ring des zylindrischen Mantels bildet die äußere Wandung für die Vakuumkammer. Gegen den unteren und oberen Spulenraum ist die Vakuumkammer durch je einen Messingring abgeschlossen. Die

† Die Herstellung des Materials und die Bearbeitung wurde in grosszügiger Weise von der Dortmund-Hörder Hüttenunion übernommen. Wir sind dafür der Leitung dieses Werkes, insbesondere den Herren Direktor Dr. Harders und Dr. Knüppel zu sehr großem Dank verpflichtet.

Abdichtung gegen die Innenwand des Joches bzw. die beiden Innenkerne erfolgt durch Gummirundschnurringe. Diese werden durch zusätzliche Messingringe gegen die zu dichtenden Berührungsflächen gepreßt. Die auftretenden mechanischen Kräfte nehmen von außen eingeschobene Bolzen auf. Die beschriebene Art der Dichtung hat sich auch in langem Betrieb vollkommen bewährt.

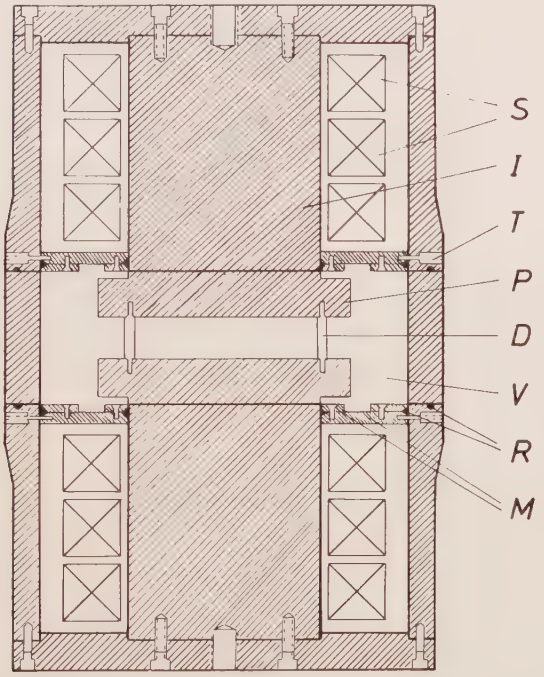

Fig. 1. Horizontalschnitt des Compton-Spektrometers

S. Spulen; I. Innenkern; T. Tragbolzen; P. Polschuh; D. Distanzstück; V. Vakuumkammer; R. Rundschurringe aus Gummi; M. Messingringe.

braucht man in der Wandung der Vakuumkammer drei Öffnungen (vgl. fig. 2). Die entsprechenden Ansatzrohre (Innendurchmesser 6 cm) sind mit Flanschen und Gummiringen am Mittelring des Spektrometers vakuumdicht befestigt; 10 μ dicke

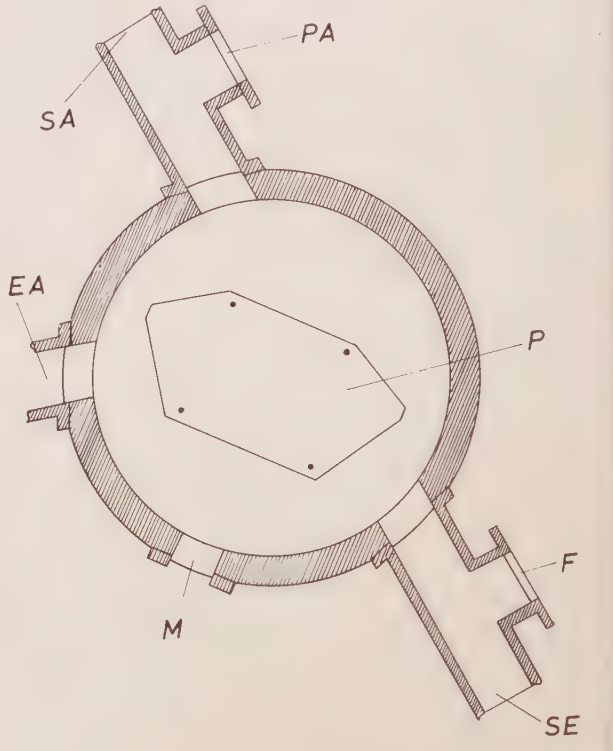

Fig. 2. Vertikalschnitt des Compton-Spektrometers

SE. Strahleintrittsrohr; SA. Strahlaustrittsrohr; EA. Elektronenaustrittsrohr; PA. Pumpanschluss; M. Öffnung für Magnetfeldmesser; F. Öffnung für die verschiebbare Konverterfolie; P. Polschuh.

Bei der Verwendung des Magneten als Compton-Spektrometer benutzen wir Polschuhe, die einen Ablenkwinkel von 72° ergeben. und die innerhalb der Vakuumkammer an den Innenkernen anliegen. Ein Umbau des Topfmagneten für andere Zwecke ist außerordentlich einfach, da Ober- und Unterteil mit den Spulen unverändert bleiben können und zu einer Änderung des Ablenkwinkels nur der Mittelring und die Polschuhe ausgewechselt werden müssen.

2.2. BESONDERE EINRICHTUNGEN

Für den Ein- und Austritt des Röntgenstrahles und für die im Magnetfeld abgelenkten Elektronen Hostaphanfolien sorgen dafür, daß der eintretende Röntgenstrahl und die austretenden Elektronen nur möglichst dünne Materieschichten durchsetzen.

Der ganze Topfmagnet ist auf einem Kugellagerring leicht drehbar angeordnet; seine Mittelebene kann mittels Gewindebolzen an drei Füßen genau der Höhe nach eingestellt werden. Damit hat man die zur exakten Justierung benötigten Freiheitsgrade.

Die Stromversorgung der Magnetspulen erfolgte bisher aus der Akkumulatorenbatterie des Instituts. Um diese nicht mit zu großen Strömen zu belasten, sind die sechs hintereinandergeschalteten Spulen

für eine Spannung von 120 Volt ausgelegt. Jede der Spulen hat 1050 Windungen; der Gesamtwiderstand der Spulen beträgt 56 Ohm.

Da bei Messungen an unserem Betatron maximale Elektronenimpulse von 1.2×10^5 Gauß cm auftreten können, benötigt man bei einem Krümmungsradius von 25 cm eine maximale Induktion von 4800 Gauß. Bei dem gewählten Polschuhabstand von 35 mm braucht man dazu eine Erregung von etwa 15000 Amperewindungen. Die maximale Verlustleistung beträgt im Dauerbetrieb 250 Watt; sie führt auch ohne besondere Kühlmaßnahmen zu keiner störenden Erwärmung der Spulen. Eine Kühlung der beiden Spulenräume mittels Preßluft war zwar vorgesehen, erwies sich jedoch bei allen bisherigen Versuchen als nicht nötig.

2.3. ENERGIE- UND RICHTUNGSBLENDE

Die zu untersuchende Röntgenstrahlung löst in der Konverterfolie F (vgl. fig. 3) Elektronen aus, die nach Ablenkung im Magnetfeld auf den Detektor D treffen. Zwischen der Quantenenergie k und der kinetischen Energie E eines unter dem Winkel ψ gegen die Richtung des Quants ausgelösten Comptonelektrons besteht dabei die allgemeine Beziehung

$$E = mc^2 \frac{2k^2 \cos^2 \psi}{(k + mc^2)^2 - k^2 \cos^2 \psi} . \qquad (1)$$

Es ist bei magnetischen Compton-Spektrometern zweckmäßig, den (mittleren) Austrittswinkel $\psi = 0$ zu wählen. In diesem Falle hat nämlich der im Winkel differentielle Wirkungsquerschnitt für die Bildung von Comptonelektronen ein Maximum. Außerdem folgt aus Gl.(1), daß der Winkel $\psi = 0$ dadurch ausgezeichnet ist, daß hier ein (für die Messung notwendiger) endlicher Raumwinkel $\Delta\Omega\psi$ den geringsten Einfluß auf die Energiezuordnung hat.

Konverterfolie und Detektor sind symmetrisch zum Magnetfeld aufgestellt, und zwar so, daß die Konverterfolie an den Ort des Eintritts in den Detektor abgebildet wird. An dieser Stelle befindet sich eine senkrecht (parallel zum Magnetfeld) stehende Blende von 5 mm Breite (Energieblende B_E in Fig. 3). Zusammen mit der Breite der Konverterfolie von gleichfalls 5 mm wird damit der maximale Energiefehler der durchgelassenen Elektronen zu $\pm$ 1% festgelegt.

Der Raumwinkel $\Delta\Omega\psi$ (Winkelapertur) wird durch eine kreisförmige Blende von 25 mm Durchmesser bestimmt; diese Blende B_A befindet sich 31 cm vor

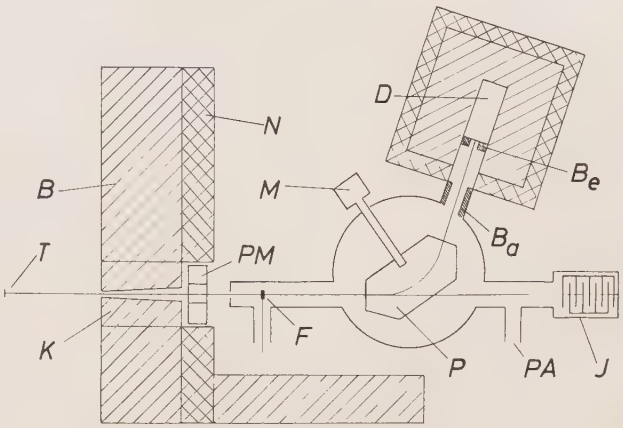

Fig. 3. Messanordnung (Gesamtaufbau schematisch)

T. Target; K. Kollimator; B. Bleiabschirmung; N. Neutronenabschirmung (Paraffin und Borsäure); F. Konverterfolie; M. Magnetfeldmesser; P. Polschuh; PA. Pumpanschluss I. Monitor (Ionisationskammer); B_a. Aperturblende; B_e. Energieblende; PM. Permanentmagnet; D. Detektor.

der Energieblende B_E. Der Raum zwischen den Blenden ist außerhalb der möglichen Bahnen nachzuweisender Elektronen mit Blei ausgefüllt. Dadurch wird weitgehend verhindert, daß Röntgenstrahlung den Detektor trifft, die von ausgeblendeten Elektronen an den Blenden erzeugt wird.

Die erforderliche endliche Dicke der Konverterfolie bewirkt, daß auch Elektronen mit falschem Winkel und damit falscher Energie in den Winkelbereich der Beobachtung hineingestreut werden; außerdem erleiden die Elektronen in der Folie einen geringen Energieverlust. Diese Einflüsse werden im Zusammenhang mit der theoretischen Behandlung der Auflösung und der Lichtstärke eines Compton-Spektrometers von Keil und Zeitler näher betrachtet (vgl. die nachfolgende Arbeit).

3. Messanordnungen

3.1. ZÄHLUNG DER AUSGELÖSTEN ELEKTRONEN

Bei den hier zu besprechenden Messungen diente als Konverterfolie eine 0.5 mm starke Berylliumscheibe mit einer Fläche von 5×7 mm^2. Sie wird an dünnen Fäden frei im primären Strahl gehalten,

dessen Querschnittsfläche an dieser Stelle größer als die Fläche der Berylliumscheibe ist. Die Folie kann durch Fernbedienung aus dem Strahlengang herausbewegt werden; beim Zurückschieben ist ihre Lage im Strahl durch einen Anschlag sicher festgelegt. Der Detektor besteht aus einem plastischen Szintillator (Pamelon, Durchmesser 50 mm, Dicke 38 mm) in Verbindung mit einem RCA-Multiplier 6342, der gegen magnetische Störungen durch einen Zylinder aus Mumetall abgeschirmt ist.

Die Impulse des Multipliers werden über eine Kathodenfolgestufe und einen Kettenverstärker einem Diskriminator zugeführt, Impulse hinreichender Höhe sodann von einem Zählgerät registriert. Das zeitliche Auflösungsvermögen von Diskriminator und Zählgerät beträgt 10^{-7} sec. Um den insbesondere von verzögerten Neutronen herrührenden Anteil des Nulleffektes möglichst weitgehend zu unterdrücken, wird das Zählgerät durch einen Freigabeimpuls nur für die Dauer der Strahlungsimpulse des Betatrons geöffnet.

Um von Schwankungen der Dosisleistung des Betatrons frei zu sein, müssen alle gemessenen Elektronenzahlen auf die gleiche Röntgenstrahldosis bezogen werden. Hierfür dient der Monitor I (vgl. fig. 3), eine Parallelplatten-Ionisationskammer deren Strom einen Kondensator von sehr großer Zeitkonstante (mehrere Tage) auflädt. Die Spannung an diesem Kondensator wird mit einem Elektrometerverstärker gemessen. Sobald sie einen vorgegebenen Wert erreicht, wird das Betatron automatisch abgeschaltet und gleichzeitig die Zählrate ausgedruckt.

3.2. MAGNETFELDMESSUNG

Da alle geometrischen Daten durch die Konstruktion des Compton-Spektrometers festgelegt sind, muß für die Aufnahme des Energiespektrums der nachzuweisenden Elektronen das Magnetfeld variiert und entsprechend genau gemessen werden. Hierzu diente eine Protonen-Resonanzapparatur, mit deren Hilfe die magnetische Feldstärke leicht mit der nötigen Genauigkeit ($\pm$ 0.1%) gemessen und konstant gehalten werden konnte. Die Meßsonde läßt sich durch eine vierte kleinere Öffnung im Mittelring des Topfmagneten zwischen die Polschuhe einführen.

4. Ausmessung eines Spektrums der Röntgen-Bremsstrahlung

4.1. AUFSTELLUNG UND JUSTIERUNG DER GESAMTAPPARATUR

Bei dem hier zu beschreibenden Versuch diente als Strahlungsquelle eine Innenantikathode unseres Betatrons, womit Röntgen-Bremsstrahlung mit einer Grenzenergie von 29 MeV erzeugt werden kann. Die Strahlung tritt durch ein planparalleles Glasfenster von 3 mm Dicke aus dem Beschleunigungsgefäß aus; aus ihr wird dann durch einen 35 cm langen Bleikollimator ein Kegel mit einem Öffnungswinkel von $\pm$ 0.325° ausgeblendet. Dicht hinter dem Kollimator befindet sich ein Permanentmagnet (Polschuhfläche 6×12 cm², Feldstärke 3500 Gauß), der die Aufgabe hat, den ausgeblendeten Röntgenstrahl von Elektronen und Positronen zu säubern, die an den Rändern des Kollimators erzeugt werden. In einer Entfernung von 132 cm von der Antikathode trifft dieser Strahl dann auf die Konverterfolie.

Besondere Sorgfalt mußte auf die Justierung der Apparatur verwendet werden. Es wird gefordert, daß sich die Antikathode, die Achse des Bleikollimators, die Mitten des Eintritts- und Austrittsfensters des Compton-Spektrometers und schließlich die Mitte der Konverterfolie exakt auf einer Achse befinden. Diese Justierung kann mit Hilfe eines Fernrohres, das auf die Strahlungsquelle eingerichtet ist, hinreichend genau durchgeführt werden. Zur wiederholten Kontrolle der Justierung während der Dauer der Messungen wurden ein Film am Austritt des Compton-Spektrometers (am Ort des Monitors) mit der ausgeblendeten Strahlung belichtet. Bei richtiger Justierung ergibt sich das Bild eines kreisrunden Strahles in der Mitte des Austrittsrohres.

Der Detektor muß vor falscher Röntgenstrahlung und vor Neutronen durch eine umfangreiche Abschirmung aus Blei und Paraffin geschützt werden.

4.2. BESTIMMUNG DER ZAHL DER COMPTON-ELEKTRONEN

In der Konverterfolie werden außer Comptonelektronen auch Elektronen ausgelöst, die durch Paarbildung erzeugt werden; diese Zahl muß gesondert bestimmt und in Abzug gebracht werden.

Wegen der symmetrischen Energieaufteilung auf Elektronen und Positronen bei der Paarbildung erhält man diese Zahl, indem man das Magnetfeld umpolt und die Zahl der Positronen mißt. In beiden Fällen ist der Nulleffekt zu berüchsichtigen, d.h. es sind die gleichen Messungen ohne Konverterfolie durchzuführen.

Bei Polung für Elektronen seien die Zählraten mit bzw. ohne Konverterfolie N_e bzw. N^0_e, bei Polung für Positronen entsprechend N_p bzw. N^0_p. Zur Ermittlung der Zahl M von Comptonelektronen einer bestimmten Energie sind demnach vier Messungen erforderlich; hieraus erhält man dann

$$M = M_e - M_p = (N_e - N_e^0) - (N_p - N_p^0) . \qquad (2)$$

Für ein Spektrum der Röntgen-Bremsstrahlung mit einer Grenzenergie von 29 MeV sind die Zahlen M_e und M_p der Elektronen bzw. Positronen in Abhängigkeit von der Energie in Fig. 4 dargestellt, ferner als Differenz die Zahl M der Comptonelektronen allein. Die Meßzeit für jede der vier Messungen bei der jeweiligen Magnetfeldstärke betrug etwa sechs Minuten.

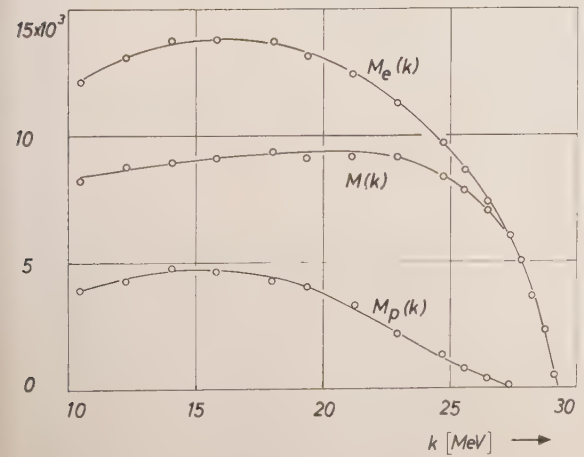

Fig. 4. Energieverteilung der Elektronen und Positronen. $M_e(k)$. Gesamtzahl der Elektronen; $M_p(k)$. Anzahl der Positronen; $M(k)$. Anzahl der Comptonelektronen. (Die statistischen Fehler ergeben sich aus den als Ordinaten eingezeichneten Zahlen der gezählten Elektronen bzw. Positronen.)

4.3. BESTIMMUNG DER FORM DES SPEKTRUMS DER BREMSSTRAHLUNG

Der Zusammenhang zwischen Elektronenenergie und Quantenenergie ist allgemein durch Gl. (1) gegeben; für den speziellen Fall $\psi = 0$ vereinfacht sich die Beziehung zu

$$E = \frac{k}{1 + \frac{1}{2}\frac{mc^2}{k}} \approx k - \tfrac{1}{2} mc^2 \qquad (1a)$$

d.h. die Maximalenergie der Comptonelektronen ist in unserem Energiebereich in sehr guter Näherung um 0.25 MeV kleiner als die Energie des auslösenden Quants. Weiter ist für die Zuordnung noch folgendes zu beachten:

a. Die dem Schwerpunkt der Elektronenlinie entsprechende Elektronenenergie ist um etwa $\frac{1}{2}\Delta k$ kleiner als die maximal mögliche Energie; dabei ist Δk die energetische Auflösung des Compton-Spektrometers (vgl. Keil und Zeitler, Fig. 5);

b. Im Mittel muß ein Comptonelektron die halbe Dicke der 0.5 mm starken Berylliumfolie durchsetzen. Für relativistische Elektronen ist der dadurch bewirkte Energieverlust praktisch unabhängig von der Elektronenenergie; er beträgt für 0.25 mm Beryllium rund 50 keV.

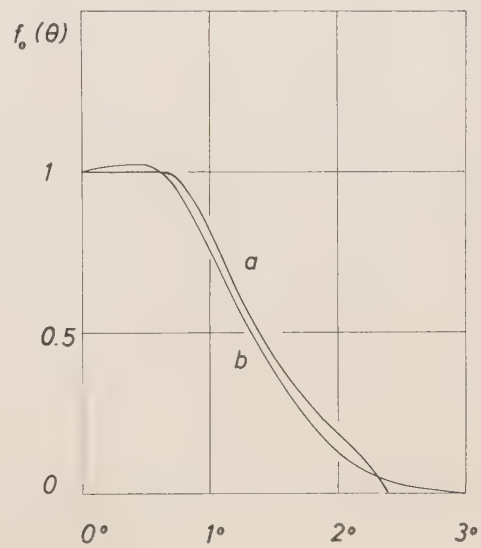

Fig. 5. Verlauf der Winkelapertur $f_0(\theta)$ des Würzburger Compton-Spektrometers: a. Gemessene Kurve; b. Approximation des gemessenen Verlaufs durch Gl. (4).

Zu einer gemessenen Elektronenenergie E_0 gehört also eine Quantenenergie

$$k = E_0 + \tfrac{1}{2}\Delta k + 0.3\ \text{MeV} . \qquad (3)$$

Zur Ermittlung der wahren Form des Spektrums der Röntgen-Bremsstrahlung muß die Lichtstärke

$L(k)$ des Compton-Spektrometers bekannt sein, die angibt, mit welcher Wahrscheinlichkeit ein Quant der Energie k ein registriertes Elektron ergibt. Man kann $L(k)$ anhand der Arbeit von Keil und Zeitler berechnen, wenn die dort definierte Winkelapertur $f_0(\theta)$ des Compton-Spektrometers durch eine Summe von Gaußfunktionen approximiert wird.

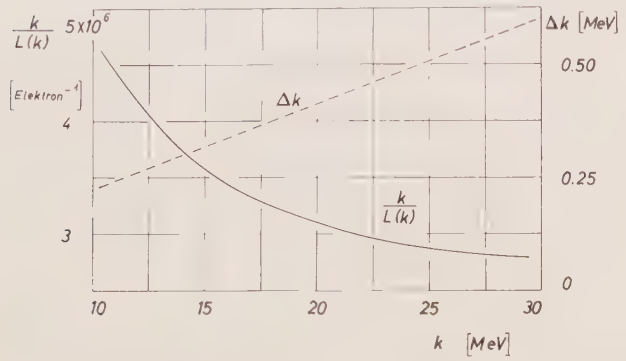

Fig. 6. Energieabhängige Grössen des Compton-Spektrometers, die zur Bestimmung des Spektrums aus der gemessenen Zahl und Energie der Comptonelektronen benötigt werden (vgl. Text).

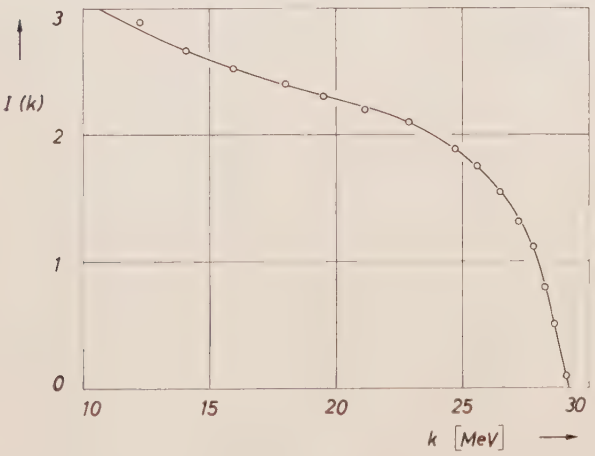

Fig. 7. Intensitätsverteilung des Spektrums der Röntgen-Bremsstrahlung für das im Text angegebene Meßbeispiel.

Der in fig. 5 dargestellte tatsächliche Verlauf der Winkelapertur wurde für unser Compton-Spektrometer unter Nachbildung der geometrischen Verhältnisse in einem optischen Analogieversuch sorgfältig bestimmt. Als sehr gute Näherung der gemessenen Winkelapertur erwies sich die Darstellung (vgl. fig. 5)

$$f_0(\theta) = 1.63 \times e^{-\frac{\theta^2}{1.56}} - 0.63 \times e^{-\frac{\theta^2}{0.50}} . \qquad (4)$$

Mit diesem Verlauf der Lichtstärke errechnet sich dann die Intensitätsverteilung $I(k)$ im Bremsstrahlungsspektrum folgendermaßen

$$I(k)\,\mathrm{d}k = \frac{M(E_0)}{L(k)}\,k\,\mathrm{d}k . \qquad (5)$$

Die Abhängigkeit der Funktionen $k/L(k)$ und Δk von der Quantenenergie k zeigt die fig. 6.

Fig. 7 zeigt schließlich das aus fig. 4 abgeleitete Spektrum der Bremsstrahlung bei 29 MeV. Die Strahlung wurde erzeugt in einer Platin-Antikathode von 0.184 mm Dicke, wobei durch eine besondere Anordnung[4]) dafür gesorgt war, daß die Elektronen die Antikathode nicht streifend in dünner Schicht, sondern "massiv" treffen. Die Beobachtungsrichtung war 0° gegen den Elektronenstrahl beim Auftreffen auf die Antikathode.

Die Ergebnisse weiterer Spektraluntersuchungen und Folgerungen daraus sollen demnächst an anderer Stelle mitgeteilt werden.

Der Deutschen Forschungsgemeinschaft und dem Bundesministerium für Atomkernenergie und Wasserwirtschaft danken wir für die Bereitstellung von Sach- und Personalhilfen, Herrn Physik-Ingenieur H. Häufglöckner für die Bedienung des Betatrons.

[4]) K. Felbinger, H. Häufglöckner, J. Niemann und M. Scheer, Naturw. **47**(1960) 55.

NUCLEAR INSTRUMENTS AND METHODS **10** (1961) 301–307; NORTH-HOLLAND PUBLISHING CO.

EINE THEORIE MAGNETISCHER COMPTON-SPEKTROMETER

E. KEIL und E. ZEITLER

Physikalisches Institut der Universität Würzburg

Eingegangen am 23. Dezember 1960

A theory is formulated to calculate luminosity and resolution of Compton-spectrometers in the energy range of 10 to 30 MeV. The formulae are evaluated approximately. The influence of quantum energy and geometry of the Compton-spectrometer on luminosity and resolution is discussed. Scattering of Compton-electrons is regarded.

1. Einleitung

Bei magnetischen Compton-Spektrometern wird der Compton-Effekt in einer Konverterfolie zur Messung von γ-Spektren benutzt. Die entstehenden Compton-Elektronen werden magnetisch analysiert. Fällt ein kontinuierliches Spektrum mit der Quantenzahl $Q(k)\,\mathrm{d}k$ im Energieintervall von k bis $k + \mathrm{d}k$ auf die Konverterfolie, werden im Detektor des auf die Energie E eingestellten Spektrometers $M(E_0)$ Elektronen angezeigt:

$$M(E_0) = \int N(E_0, k)\, Q(k)\, \mathrm{d}k\,. \tag{1}$$

Die Berechnung des Quantenspektrums $Q(k)\,\mathrm{d}k$ aus einer Anzahl von Meßwerten $M(E_0)$ erfordert die Lösung der Gleichung (1). Sie ist nur möglich, wenn die Übertragungsfunktion des Compton-Spektrometers $N(E_0, k)$ (Kern der Integralgleichung) bekannt ist.

In dem interessierenden Energiegebiet oberhalb 10 MeV läßt sich eine experimentelle Bestimmung der Übertragungsfunktion kaum durchführen, da monochromatische γ-Strahlung hinreichender Intensität schwer zu erzeugen ist. Deshalb ist man auf eine theoretische Behandlung angewiesen.

Für eine praktische Anwendung des Compton-Spektrometers ist es im allgemeinen zu aufwendig, die Auswertung nach (1) durchzuführen. Durch entsprechende Konstruktion des Spektrometers versucht man zu erreichen, daß die Übertragungsfunktion für jede eingestellte Energie E_0 nur in einem kleinen Bereich von Quantenenergien k nicht verschwindet. Betrachtet man das Spektrum in diesem Bereich als konstant, so erhält man:

$$M(E_0) = Q(k) \int N(E_0, k)\, \mathrm{d}k = Q(k) \cdot L(E_0)\,. \tag{2}$$

Das noch verbleibende Integral ist offensichtlich die Lichtstärke des Compton-Spektrometers, da es den Quotienten von Meßeffekt und Spektrum angibt.

Wegen (2) erhält man folgende Vorschrift zur Bestimmung von Quantenspektren aus Compton-Spektrometer-Messungen:

$$Q(k) = \frac{M(E_0)}{L(E_0)}\,. \tag{3}$$

Sie wurde bereits von Motz *et al.*[1]), Ulmer und Ziegler[2]) und Robson und Cregg[3]) benutzt. Da dieses Verfahren darauf beruht, daß die Auflösung R eines Compton-Spektrometers relativ gut ist, muß auch noch die Auflösung angegeben werden. Sie wird als das Verhältnis von Lichtstärke zur maximalen Höhe der Übertragungsfunktion N_m definiert:

$$R = \frac{L}{N_\mathrm{m}}\,. \tag{4}$$

Man ersetzt also bei der Definition der Auflösung die Übertragungsfunktion durch eine Balkenfunktion gleicher Fläche und gleicher maximaler Höhe. Diese Definition hat gegenüber der oft benutzten Definition durch die Halbwertsbreite den Vorteil, daß sie einer Asymmetrie der Übertragungsfunktion Rechnung trägt.

Das Ziel der vorliegenden Arbeit ist es, eine

[1]) J. W. Motz *et al.*, Rev. Sci. Instr. **24** (1958) 929.
[2]) K. Ulmer und B. Ziegler, Z. ang. Phys. **8** (1956) 49.
[3]) J. W. Robson und E. C. Cregg, Phys. Rev. **105** (1957) 619.

Theorie zu formulieren, mit deren Hilfe man Lichtstärke und Auflösung im Energiegebiet oberhalb 10 MeV berechnen kann. Die entstehenden Ausdrücke werden näherungsweise ausgewertet und der Einfluß der Quantenenergie und der Geometrie des Spektrometers auf Lichtstärke und Auflösung diskutiert. Damit werden gleichzeitig die Grenzen des in (3) angegebenen vereinfachten Auswerteverfahrens gezeigt.

2. Die Übertragungsfunktion

In einer Konverterfolie (Dicke $\mathrm{d}t$, Fläche F und Elektronendichte ρ) entstehen durch Compton-Effekt mit Quanten der Energie k Elektronen im Energieintervall E bis $E + \mathrm{d}E$ mit der Wahrscheinlichkeit:

$$\frac{\partial\sigma}{\partial E}(E, k)\, F\rho\, \mathrm{d}t\, \mathrm{d}E\,. \tag{5}$$

Dabei ist $\partial\sigma/\partial E\ (E,k)$ der in der Elektronenenergie differentielle Wirkungsquerschnitt für den Compton-Effekt. Bei fester Quantenenergie gehört zu jeder Elektronenenergie ein bestimmter Startwinkel ψ des Compton-Elektrons:

$$E = mc^2 \frac{2k^2 \cos^2\psi}{(k + mc^2)^2 - k^2\cos^2\psi}\,. \tag{6}$$

Diese Energie-Winkel-Beziehung läßt die zu messende Energie des Quants aus der Energie und dem Startwinkel des Compton-Elektrons berechnen. Die sich daraus ergebende Forderung einer gleichzeitigen Energie- und Winkelbestimmung erfüllt man, indem man die Konverterfolie als Elektronenquelle in einem Betaspektrometer benutzt, bei dem der Startwinkel durch ein Blendensystem festgelegt ist. Die in der Konverterfolie entstehenden Compton-Elektronen werden im Betaspektrometer energetisch analysiert und gelangen mit der Wahrscheinlichkeit $A_0\ (E, E_0, \psi)$ in den Detektor. E_0 ist dabei die eingestellte Energie des Betaspektrometers.

Geht man zu einer Konverterfolie der endlichen Dicke T über, kann der Einfluß der Streuung nicht mehr vernachlässigt werden. Nach ihrer Entstehung in der Tiefe t müssen die Compton-Elektronen noch die restliche Tiefe der Konverterfolie durchlaufen. Dabei werden sie durch Vielfachstreuung abgelenkt und treten unter einem anderen Winkel als dem Startwinkel aus der Konverterfolie aus. Da das Ansprechvermögen einerseits auf den Startwinkel bezogen sein soll, andererseits aber die Winkelausblendung nach dem Austrittswinkel erfolgt, muß die Vielfachstreuung durch eine Modifikation des Ansprechvermögens berücksichtigt werden. Das geschieht durch folgende Überlegung:

Wenn ein unter dem Winkel ψ in der Tiefe t startendes Elektron mit dem Winkel θ aus der Konverterfolie austreten soll, muß es um den Winkel φ abgelenkt werden. Es gilt:

$$\psi + \varphi = \theta\,. \tag{7}$$

Die Wahrscheinlichkeit für ein solches Streuereignis ist $s(\varphi, t)$. Ein unter dem Winkel θ aus der Konverterfolie austretendes Elektron erreicht aber mit der Wahrscheinlichkeit $A_0\ (E, E_0, \theta)$ den Detektor. Fragt man nach dem Ansprechvermögen für ein Elektron, das unter dem Winkel ψ startet, so sind alle Möglichkeiten zu berücksichtigen, bei denen nach (7) durch Streuung um den Winkel φ der Startwinkel ψ in irgendeinen Austrittswinkel θ überführt wird, wobei die drei Winkel durch (7) verknüpft sind:

$$A(\psi, E, E_0, t) = \int A_0(E, E_0, \theta)\, s(\varphi, t)\, \mathrm{d}\Omega_\varphi\,. \tag{8}$$

Da die Compton-Elektronen in jedem Schichtelement $\mathrm{d}t$ mit gleicher Wahrscheinlichkeit entstehen, ist das schichtdickenabhängige Ansprechvermögen noch über die Schichtdicke zu mitteln:

$$\bar{A}(\psi, E, E_0, T) = \frac{1}{T}\int_0^T A(\psi, E, E_0, t)\, \mathrm{d}t\,. \tag{9}$$

Nach der Gleichung (1) kann man die Übertragungsfunktion auch als die Anzahl der Elektronen betrachten, die bei der Energie E_0 gemessen werden, wenn genau ein Quant der Energie k die Konverterfolie trifft. Man erhält sie, indem man die Wahrscheinlichkeit, daß ein Elektron der Energie E in der Konverterfolie entsteht und im Detektor angezeigt wird, über alle Elektronenenergien integriert:

$$N(E_0, k) = F\rho\, T \int \frac{\partial\sigma}{\partial E}(E, k)\, \bar{A}(E, E_0, k, T)\, \mathrm{d}E\,. \tag{10}$$

Die Integration erstreckt sich dabei bis zur maximalen Energie E_m, die ein Elektron von Quanten der Energie k übernehmen kann:

$$E_\mathrm{m} = \frac{2k^2}{m_0c^2 + 2k}\,. \tag{11}$$

Bei der Beziehung (10) wurde benutzt, daß das Ansprechvermögen $A(\psi, E, E_0, T)$ mit Hilfe der Gleichung (6) in eine Funktion von E, E_0, k, T umgeschrieben werden kann.

Zur Bestimmung des Ansprechvermögens muß man berechnen, welchen Einfluß die Größe von Konverterfolie, Richtungsblende und Detektorspalt auf die Wahrscheinlichkeit haben, mit der ein unter dem Winkel θ aus der Konverterfolie austretendes Elektron der Energie E den Detektor erreicht, wenn das Betaspektrometer auf die Energie E_0 eingestellt

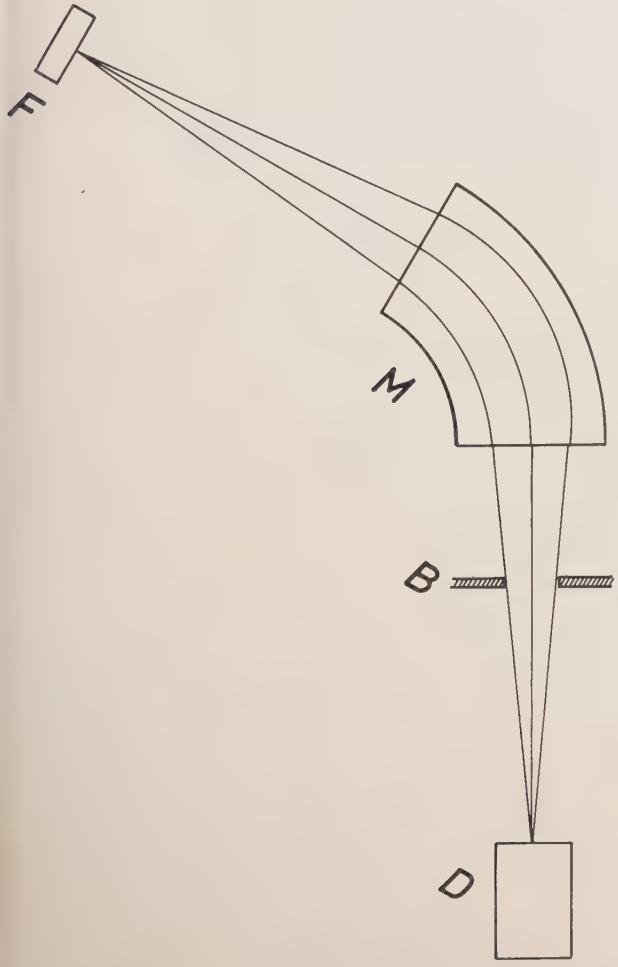

Abb. 1. Strahlengang im Würzburger Compton-Spektrometer. F Konverterfolie, M Sektormagnet, B Richtungsblende, D Detektor.

ist Zu diesem Zweck benutzt man die bekannten Abbildungsgleichungen in magnetischen Sektorfeldern und berechnet, welche Bedingungen die in der Konverterfolie startenden Elektronen erfüllen müssen, damit sie in den Detektor gelangen. Die einzelnen Strahlbegrenzungen werden also in die Ebene der Konverterfolie transformiert. Die Diskussion dieser gleichzeitigen Bedingungsgleichungen ist ziemlich umständlich. Man benutzt deshalb zweckmäßig ein optisches Analogiemodell, bei dem die transformierten Strahlbegrenzungen durch Blenden simuliert werden. Die passend geformten Blenden werden den Anfangsbedingungen entsprechend verschoben. Als Ansprechvermögen jeder Anfangsbedingung definiert man sinnvoll den

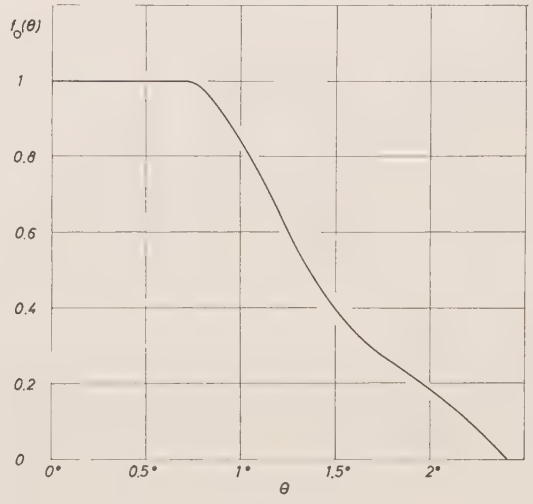

Abb. 2.
Winkelapertur des Würzburger Compton-Spektrometers.

Bruchteil der Konverterfolie, der dann in den Detektor abgebildet wird. Überträgt man diese Definition auf das Analogiemodell, so ist das Ansprechvermögen das Verhältnis der freigelassenen zur ganzen Fläche der "Konverterfolie". Leuchtet man diese Blende gleichmäßig aus, so ist der hindurchgehende Lichtstrom dem Ansprechvermögen proportional. Er läßt sich bequem mit einer Photozelle messen.

In dieser Arbeit wird das Würzburger Compton-Spektrometer†, dessen Strahlengang in Abb. 1 schematisch dargestellt ist, als Beispiel benutzt. Sein Ansprechvermögen wurde auf die oben geschilderte Weise bestimmt. Das wesentliche Ergebnis dieses Experiments ist die praktisch mögliche Separierbarkeit des Ansprechvermögens in zwei Faktoren, von denen der eine nur vom

† Vgl. die vorangehende Arbeit, S. 291.

Austrittswinkel θ, der andere nur vom relativen Energiefehler $\delta = (E - E_0)/E_0$ abhängt:

$$A_0(\theta, E, E_0) = f_0(\theta)\, g(\delta)\,. \tag{12}$$

Die Voraussetzung dieser Approximation – schmale Winkel- und schmale Energieapertur –

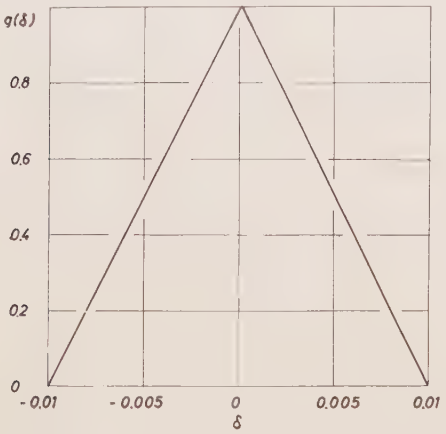

Abb. 3.
Energieapertur des Würzburger Compton-trSpekometers.

dürfte bei allen Compton-Spektrometern erfüllt sein. f_0 wird nämlich erst für große Energiefehler δ merklich von δ abhängig. Diese Abhängigkeit kann jedoch unberücksichtigt bleiben, da in diesem Bereich die Energieapertur nahezu verschwindet. Die Winkelapertur $f_0(\theta)$ des Würzburger Compton-Spektrometers ist in Abb. 2, seine Energieapertur $g(\delta)$ in Abb. 3 dargestellt. Die Energieapertur ist ein gleichseitiges Dreieck mit der Basislänge $2\delta_m$.

Bei der Berechnung des Ansprechvermögens wurde davon Gebrauch gemacht, daß die Verteilung der Compton-Elektronen rotationssymmetrisch ist. Die hier benutzte Bestimmung des Ansprechvermögens gilt daher nur, wenn die auf die Konverterfolie fallende γ-Strahlung nicht linear polarisiert ist.

Wegen der praktischen Separierbarkeit des Ansprechvermögens kann man jetzt auch die Gleichungen (8), (9) und (10) separieren und erhält:

$$f(\psi, t) = \int f_0(\theta)\, s(\varphi, t)\, \mathrm{d}\Omega_\varphi \tag{8a}$$

$$\bar{f}(\psi, T) = \frac{1}{T}\int_0^T f(\psi, t)\, \mathrm{d}t \tag{9a}$$

$$N(E_0, k) = F\rho\, T \int \frac{\partial\sigma}{\partial E}(E, k)\, g(\delta)\, \bar{f}(\psi, T)\, \mathrm{d}E\,. \tag{10a}$$

3. Auswertung der Theorie

3.1. BERECHNUNG VON $\bar{f}(\psi_1 T)$

Für eine analytische Auswertung wird die Winkelapertur durch eine Gaußsche Fehlerfunktion dargestellt:

$$f_0(\theta) = \exp(-\theta^2/a^2)\,.$$

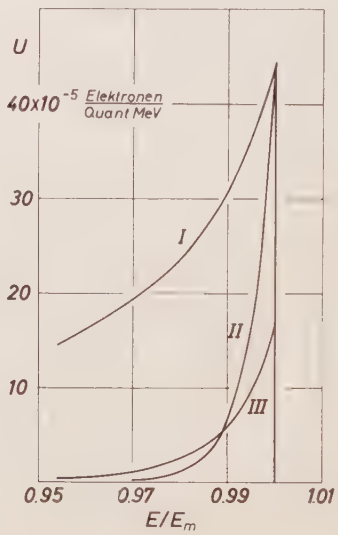

Abb. 4.
Differentielle Energiespektren der Compton-Elektronen.
$T = 0.0925\,\mathrm{g\,cm^{-2}}$ ($d = 0.5$ mm Be); $k = 10$ MeV; $E_m = 9.75$ MeV;
I: $a = \infty$; II: $a = \sqrt{2}$, $\varphi_0 = 0°$; III: $a = \sqrt{2}$, $\varphi_0 = 1°$.

Die Beschreibung der Winkelapertur spezieller Compton-Spektrometer durch eine Summe von Gaußschen Fehlerfunktionen (13) ist immer möglich. Im folgenden kann daher ohne Beschränkung der Allgemeinheit mit einer Gaußschen Fehlerfunktion weitergerechnet werden.

Die Streuwinkelverteilung wird entsprechend dem Vorgehen von Lanzl und Hanson[4]) ebenfalls durch eine Gaußsche Fehlerfunktion approximiert:

$$s(\varphi, t) = \frac{1}{\pi\varphi_0^2}\, \mathrm{e}^{-\varphi^2/\varphi_0^2} \tag{14}$$

mit

$$\varphi_0^2 = \frac{ct}{E^2}\,, \tag{15}$$

c kann in guter Näherung für ein Konverterfolienmaterial als konstant betrachtet werden.

[4]) L. H. Lanzl und A. O. Hanson, Phys. Rev. **83** (1951) 959.

Mit diesen Approximationen erhält man nach (8a):

$$f(\psi, t) = \frac{a^2}{a^2 + \varphi_0^2(t)} \exp\left(-\frac{\psi^2}{a^2 + \varphi_0^2(t)}\right). \quad (16)$$

Die nach (9a) durchzuführende Mittelung über die Schichtdicke ergibt:

$$\bar{f}(\psi, T) = \frac{a^2}{\varphi_0^2(T)} \left[Ei\left(-\frac{\psi^2}{a^2}\right) - Ei\left(-\frac{\psi^2}{a^2 + \varphi_0^2(T)}\right)\right]. \quad (17)$$

Wegen der Energie-Winkel-Beziehung wirkt sich die Ausblendung der Austrittswinkel als Energieblende aus; ψ kann als Energievariable aufgefaßt werden. Den Einfluß der Winkelapertur zeigt man am besten, indem man die differentiellen Energiespektren

$$U(E, k) = F\rho\, T \frac{\partial\sigma}{\partial E}(E, k) \cdot \bar{f}(\psi, t)$$

der Compton-Elektronen für verschiedene Winkelaperturen aufträgt (Abb. 4).

Kurve I ist das Spektrum der Elektronen beim Verlassen der Konverterfolie, wo sich die Richtungsblende noch nicht bemerkbar macht. ($\bar{f}(\psi,T) \equiv 1$). Durch den Einbau einer Richtungsblende erreicht man das schmälere Elektronenspektrum in Kurve II ($\varphi_0 = 0$). Leider verschlechtert die Vielfachstreuung dieses Ergebnis wieder (Kurve III); sie verbreitert die Winkelverteilung der Compton-Elektronen beim Verlassen der Konverterfolie, ohne daß sich deren Energieverteilung ändert. Daher werden sie durch die feststehenden Richtungsblende anders ausgeblendet als ohne Vielfachstreuung.

3.2. BERECHNUNG DER ÜBERTRAGUNGSFUNKTION

Zur Berechnung der Übertragungsfunktion ist noch die in (10a) geforderte Integration der mit der Energieapertur $g(\delta)$ multiplizierten differentiellen Energiespektren $U(E,k)$ über die Elektronenenergie durchzuführen. Wegen des komplizierten Zusammengangs (6) zwischen dem Startwinkel ψ und der Elektronenenergie E ließ sich die Integration nur numerisch durchführen. Abb. 5 zeigt ein Beispiel. Die theoretische Form der Übertragungsfunktion stimmt gut mit experimentellen γ-Linien von Motz *et al.*[1]) überein.

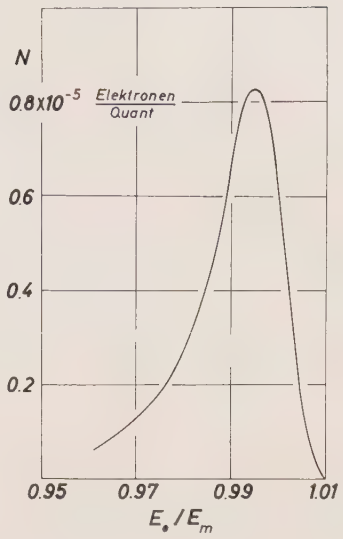

Abb. 5. Übertragungsfunktion $N(E_0,k)$ für $a = \sqrt{2}$ grad; $d = 0.5$ mm Be; $k = 10$ MeV; $E_m = 9.75$ MeV; $\delta_m = 1\,\%$.

3.3. BERECHNUNG DER LICHTSTÄRKE

Die Lichtstärke eines Compton-Spektrometers ist in der Einleitung als Integral der Übertragungsfunktion über die Quantenenergie k begründet und definiert. Die zunächst schwierige rechnerische Auswertung kann durch die Vertauschung von Parameter und Integrationsvariabler wesentlich vereinfacht werden.

Der Integrand trägt nur in einem kleinen Energiebereich, in dem die eingestellte Energie E_0 praktisch gleich der Quantenenergie k ist, zum Integral bei. Daher sind E_0 und k vertauschbar und die Lichtstärke wird:

$$L(k) = \int N(E_0, k)\, dE_0 . \quad (18)$$

Damit ist die Bestimmung der Lichtstärke auf ein Integral zurückgeführt, das sich z.B. durch graphische Integration der in Abb. 5 gezeigten Übertragungsfunktion lösen läßt. Für eine Diskussion der Lichtstärke ist es jedoch bequemer, einen geschlossenen Ausdruck zu haben. Daher schreibt man ausführlich:

$$L(k) = \int_0^\infty \left[\int_{E_0(1-\delta_m)}^{E_0(1+\delta_m)} U(E, k)\, g(\delta)\, dE\right] dE_0 . \quad (19)$$

Durch Anwendung des Mittelwertsatzes der Integralrechnung läßt sich die Lichtstärke als das

physikalisch leicht interpretierbare Produkt zweier Faktoren darstellen:

$$L = \Delta \cdot \lambda \,. \tag{20}$$

Dabei ist:

$$\Delta = E_0 \int_{-\delta_m}^{+\delta_m} g(x)\,\mathrm{d}x = E_0\,\delta_m \approx k\,\delta_m \,. \tag{21}$$

Δ gibt die Anzahl der Elektronen an, die in den Detektor gelangen, wenn ein Elektron pro MeV die Winkelapertur passiert, Δ kann als Lichtstärke des magnetischen Analysators aufgefaßt werden.

$$\lambda = \int_0^\infty U(E, k)\,\mathrm{d}E \tag{22}$$

λ gibt die Anzahl der Elektronen pro MeV an, die ein Quant pro MeV in der Konverterfolie erzeugt und in die Winkelapertur gelangen läßt. λ kann als Konversionsgrad der Konverterfolie angesehen werden. Die Berechnung von λ erfolgt zweckmäßiger im Winkelraum ψ:

$$\lambda = \int U(E, k)\,\mathrm{d}E = \int U(\psi, k)\,\mathrm{d}\Omega_\psi \,. \tag{23}$$

Sie läßt sich aber auch dann nicht mit dem exakten Wirkungsquerschnitt durchführen. Eine bessere Approximation als die von Motz *et al.*[1]) bei der Berechnung der Vielfachstreukorrektur benutzte Gaußsche Fehlerfunktion ist:

$$\frac{\partial\sigma}{\partial\Omega_\psi} = V\left(1 + \frac{\psi^2}{\psi_0{}^2}\right)^{-2} . \tag{24}$$

Hierbei ist V der Wirkungsquerschnitt in Vorwärtsrichtung $\psi = 0$ und ψ_0 ein charakteristischer Winkel, für den $\partial\sigma/\partial\Omega_\psi$ gerade $\frac{1}{4}V$ ist. V läßt sich exakt ausrechnen; für ψ_0 gilt:

$$\psi_0\, k = 45\ [\mathrm{MeV\ grad}] \,. \tag{25}$$

Mit der Approximation (24) wird die Lichtstärke:

$$L = PVF\,\Delta\,a^2 \cdot \left[\exp\left(+\psi_0{}^2/a^2\right) Ei\left(-\frac{\psi_0{}^2}{a^2}\right) - \mathrm{e}^{\psi_0{}^2/(a^2+\psi_0{}^2)}\, Ei\left(-\frac{\psi_0{}^2}{a^2+\psi_0{}^2}\right)\right] . \tag{26}$$

In der Konstanten P sind die vom Konverterfolienmaterial abhängigen Parameter zusammengefaßt:

$$P = \frac{\pi T \rho \psi_0{}^2}{\varphi_0{}^2} = \frac{\pi \rho 45^2}{c} \,. \tag{27}$$

Für Beryllium ist $P = 1.725 \times 10^{23}\ \mathrm{cm}^{-4}$.

3.4. BERECHNUNG DER AUFLÖSUNG

Die Berechnung der Auflösung erfolgt nach der Definition (4). Leider ist es nicht möglich, für die Auflösung eine geschlossene Formel anzugeben wie für die Lichtstärke. Zur Bestimmung der maximalen Höhe N_m der Übertragungsfunktion läßt sich eine numerische Berechnung ihres Verlaufs in der Nähe des Maximums nicht umgehen.

4. Diskussion der Ergebnisse

In den folgenden Abbildungen ist die Abhängigkeit der Lichtstärke und der Auflösung von den interessierenden Parametern dargestellt. Als apparative Parameter treten der Raumwinkel der Apertur a^2, die Dicke der Konverterfolie und die Auflösung des Betaspektrometers auf.

Experimenteller Parameter ist die Quantenenergie.

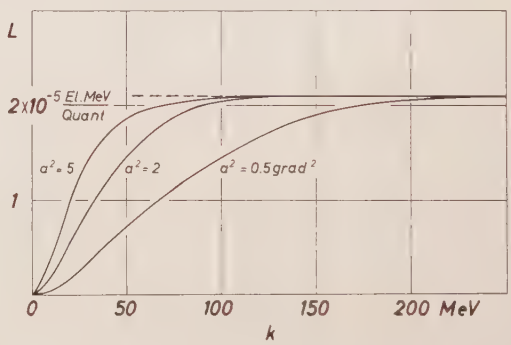

Abb. 6. Lichtstärke L als Funktion der Quantenenergie k $d = 0.5$ mm Be; $\delta_m = 1\,\%$.

Zum Vergleich eines Compton-Spektrometers mit anderen Spektrometertypen (z.B. Paarspektrometern) ist die Kenntnis der Abhängigkeit der Lichtstärke von der Quantenenergie wesentlich. Diese Abhängigkeit ist für verschiedene Aperturen in Abb. 6 widergegeben. Im Energiebereich von 30 bis 50 MeV ist die Lichtstärke von der Größenordnung 2×10^{-5} Elektronen MeV Quant^{-1}. Erwartungsgemäß liefern größere Apterturwinkel größere Lichtstärken. Bei höheren Energien jedoch ist die Verteilung der Compton-Elektronen so stark in Vorwärtsrichtung gebündelt, daß auch die kleinste Apertur den Elektronenstrahl nicht mehr beschneidet. Mit der hier verwendeten Näherung für den Wirkungsquerschnitt des Compton-Effekts wird

ein von der Winkelapertur unabhängiger Grenzwert von 2.2×10^{-5} Elektronen MeV Quant^{-1} erreicht. Dieser Grenzwert tritt wegen der Energieabhängigkeit des Compton-Effekts prinzipiell auf. Da die Lichtstärke das Produkt aus Konversions grad und Lichtstärke des Betaspektrometers ist, können beide

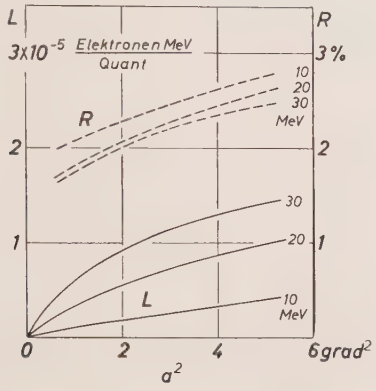

Abb. 7. Lichtstärke L und Auflösung R als Funktionen der Winkelapertur a. $d = 0.5$ mm Be; $\delta_m = 1\,\%$.

Faktoren einzeln diskutiert werden. Mit steigender Quantenenergie k treffen immer mehr der insgesamt entstehenden Compton-Elektronen in die Apertur, so daß der Konversionsgrad die gleiche Energieabhängigkeit annimmt wie der Gesamtwirkungsquerschnitt für den Compton-Effekt, nämlich k^{-1}; die Lichtstärke des Betaspektrometers kompensiert aber gerade diese Abnahme, da sie proportional zu k steigt.

Der Energieverlust der Compton-Elektronen in der Konverterfolie hat keinen Einfluß auf die Lichtstärke eines Compton-Spektrometers. Berücksichtigt man den Energieverlust näherungsweise, indem man die Konverterfolie in Schichten einteilt und jeder Schicht einen bestimmten Energieverlust zuteilt, dann zeigt sich, daß die Auflösung bei zunehmenden Konverterfoliendicken durch den Energieverlust kaum beeinflußt wird.

Die Lichtstärke L nimmt schwächer als linear mit dem Raumwinkel der Apertur zu (Abb. 7). Die schon erwähnte Bündelung der Compton-Elektronen erklärt auch die steigende Krümmung der Lichtstärkekurven mit wachsender Energie.

Die geringe Energieabhängigkeit der Auflösung ist eine Folge der Bündelung und der mit der Quantenenergie zunehmenden Winkelabhängigkeit der Energie der Compton-Elektronen (vgl. (6)).

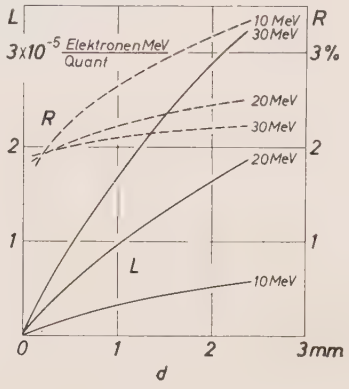

Abb. 8. Lichtstärke L und Auflösung R als Funktionen der Dicke der Konverterfolie d. $a = \sqrt{2}°$; $\delta_m = 1\,\%$.

Die Lichtstärke nimmt ferner praktisch linear mit der Dicke der Konverterfolie zu, Streuabsorption macht sich bei allen betrachteten Quantenenergien nicht wesentlich bemerkbar (Abb. 8). Dagegen ist die Verschlechterung der Auflösung mit zunehmender Schichtdicke stark von der Quantenenergie abhängig. Bei 10 MeV verschlechtert sie sich zwischen 0.2 und 2 mm um 50%, bei 30 MeV nur noch um 10%. Bei kleinen Energien muß man also durch passende Wahl der Konverterfoliendicke einen Kompromiß zwischen Lichtstärke und Auflösung finden, mit wachsender Quantenenergie wird die Konverterfoliendicke immer weniger kritisch.

Wir danken Herrn Prof. Dr. H. Kulenkampff für die Möglichkeit, diese Arbeit durchzuführen. Herrn Dr. M. Scheer sind wir für viele klärende Diskussionen zu Dank verpflichtet. Dem Bundesministerium für Atomkernenergie und Wasserwirtschaft sei für finanzielle Unterstützung an dieser Stelle ebenfalls gedankt.

NUCLEAR INSTRUMENTS AND METHODS **10** (1961) 308–314; NORTH-HOLLAND PUBLISHING CO.

A FAST TRANSISTORIZED DISCRIMINATOR

H. VERWEIJ

Nuclear Physics Division, CERN, Geneva

Received 23 December 1960

A fast transistorized discriminator is described. The threshold can be varied from 100 mV to 2.1 V. Stable operation is obtained for rates up to at least 10 Mc/s. The unit gives a negative output pulse of 2.5–3 V and a positive of 9 V, both into 125 Ω.

1. Introduction

A pulse height discriminator has been developed with the following requirements in mind:

a. Response to low level fast pulses (≈ 0.5 V and 10–20 ns).

b. A stable threshold over a long period.

c. Insensitive to temperature.

d. Insensitive to overload.

e. Capable of working at high repetition rates, (⩽ 10 Mc/s).

For vacuum tube discriminators in this field, the requirement a. is normally met by a preceding amplifier[1,2,3]). The sensitivity of these discriminators can be increased by a factor 10–100 by using biased-off or hold-off diodes in the feedback loop[4–8]).

The sensitivity of the discriminator described in this paper is obtained by the inherent sensitivity of its trigger circuit.

The complete circuit diagram is given in fig. 1. The discriminator consists of a variable threshold amplifier (T_1), a trigger circuit with a constant threshold (T_2, T_3 and T_4) and an output amplifier (T_5 and T_6).

The discriminator uses commercially available transistors 2N 501 or 2N 1500.

2. Threshold Amplifier

The trigger circuit consisting of T_2, T_3 and T_4 has a fixed trigger threshold, being ≈ 0.4 V at the collector of T_2. A current pulse through T_1 driving the collector of T_2 positive by more than 0.4 V fires the trigger circuit.

T_1 is a biased-off amplifier. By varying the amount of cut-off, a linear variation of the threshold and so a linear variation of the discrimination level, is obtained.

The arrangement R_6, D_2 and D_3 limits the maximum current through T_1 and serves as an overload protection, preventing multiple triggering occurring. Overloads of 50 times in the 100 mV position, and 10 times in the 2.1 V position, are acceptable (see fig. 8).

The steady current through D_2 and D_3 is ≈ 3 mA. When T_1 starts conducting, current will be transferred from D_2 and D_3 into T_1, the emitter load being the dynamic impedance of D_1, D_2, much smaller than 2k2, so that only weak negative feedback occurs.

For a driving voltage at the input, forcing T_1 into a higher current than 3 mA, D_1, D_2 will be cut off and heavy negative feedback will take place, due to R_6 (2k2), so that a further voltage increase at the input results only in a relatively small collector current increase.

Tube discriminators

[1]) F. J. M. Farley, Rev. Sci. Instr. **29** (1958) 595.

[2]) J. Mey, Rev. Sci. Instr. **30** (1959) 282.

[3]) D. F. Swift and V. Perez-Mendez, Rev. Sci. Instr. **30** (1959) 1004.

[4]) Kenneth A. McCollom, Nucleonics **17**, No. 6 (1959) pp. 72–77.

[5]) K. Kandiah, Proc. Inst. Electr. Eng. (London) **2** (1954) 101, 239.

[6]) Davidon and Frank, Rev. Sci. Instr. **27** (1956) 1.

[7]) N. F. Moody *et al.*, Electronic. Eng. (May 1952) 218.

[8]) Circuits using this technique have been developed in CERN.

Instrument Type CERN SC 3–6001;

Instrument Type CERN SC 3–6005.

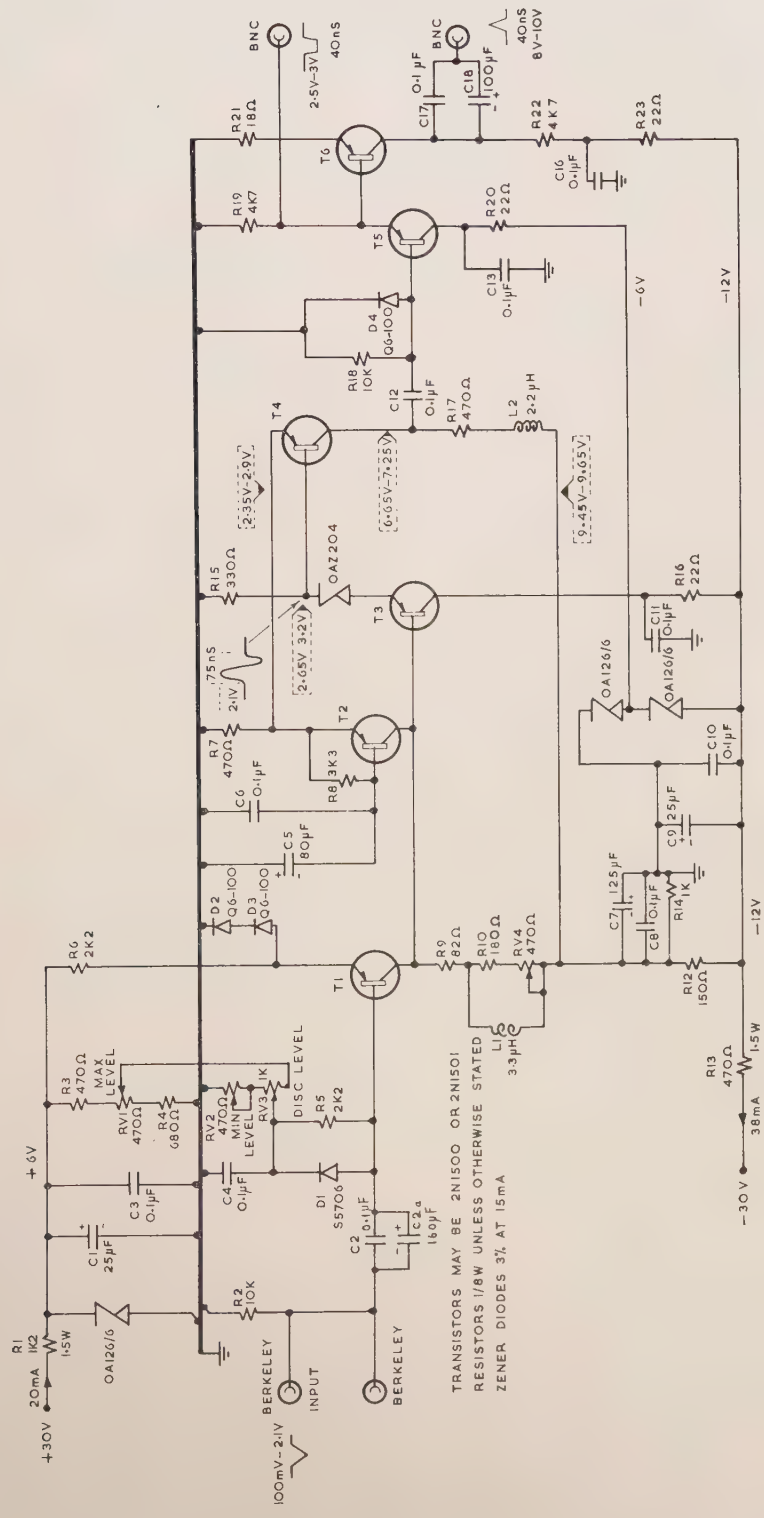

Fig. 1. Circuit diagram.

The discriminator range is adjusted with RV_1 and RV_2. The helipot RV_3 is mounted at the front plate, giving accurate adjustment of the discrimination level (see fig. 12).

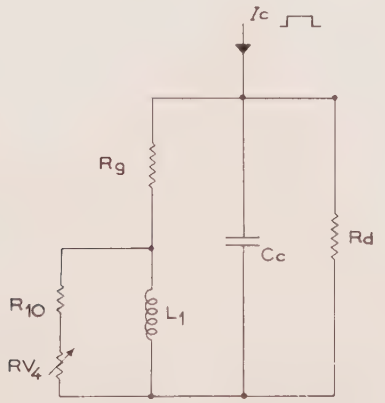

Fig. 2. Timing network in collector T_2.

D_1 is a protection for positive input voltages, and also a DC restoring diode.

3. Trigger Circuit

The trigger circuit is a monostable emitter coupled multivibrator, with a ringing circuit as the timing element.

In a steady state T_2 is off, T_3 and T_4 are on.

The current pulse in T_1 will drive the collector of T_2 positive. This is coupled to the emitter of T_2 via emitter followers T_3 and T_4. The base of T_2 is held at a constant potential, the common emitter DC level, by way of R_8, C_5, C_6 (neglecting I_{CBO}).

The positive signal on the common emitter brings T_2 into conduction, and so in a region of higher amplification, if sufficiently high (≈ 0.4 V at collector T_2), so that the loop gain becomes greater than unity, the circuit triggers.

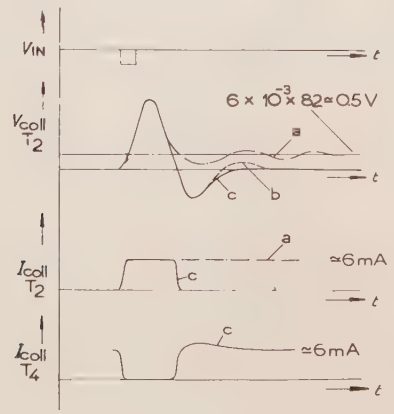

Behaviour for various settings of the damping potentiometer RV_4

a = Damping too high
b = " too low
c = " right

Fig 3. Behaviour for various settings of the damping potentiometer RV_4.

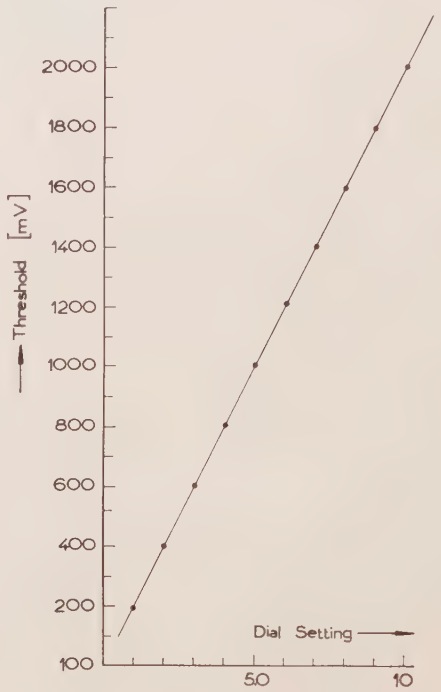

Fig. 4. Threshold versus dial setting.

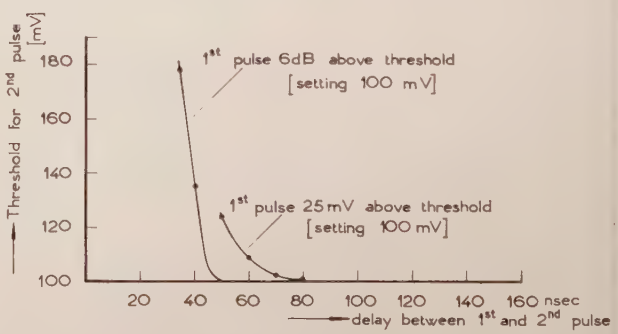

Fig. 5. Dead time.

The standing current in T_4 (≈ 6 mA) will be switched into T_2. After this, T_2 and T_3 are on, T_4 is off and the feedback loop is open again.

The collector network of T_2 consists of a ringing

network L_1, R_9, R_{10}, RV_4, the parasitic capacity C_c and R_d the input damping of T_3 (see fig. 2). The response of this network to a current step will be a

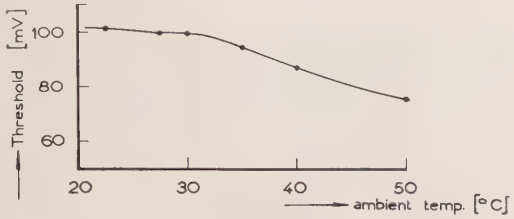

Fig. 6. Temperature stability.

damped sinusoidal oscillation, superimposed on a DC level (see fig. 3).

The collector of T_2 goes positive initially and wants to damp out around the indicated DC level. R_9 and the damping are so chosen that T_4 opens again when the collector goes negative. This makes the circuit retrigger and T_4 take the common emitter current. T_2 is off, T_3 and T_4 are on.

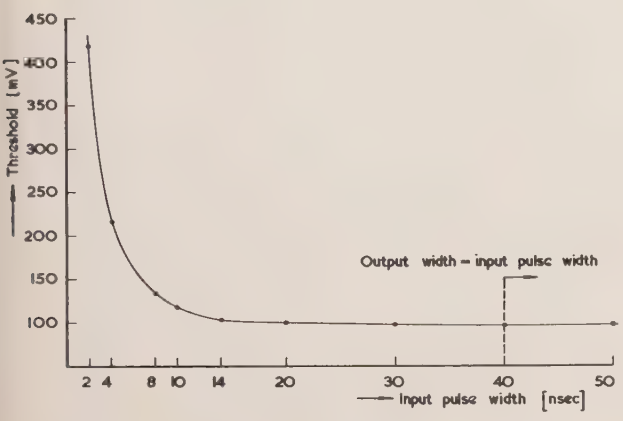

Fig. 7. Threshold versus input pulse width.

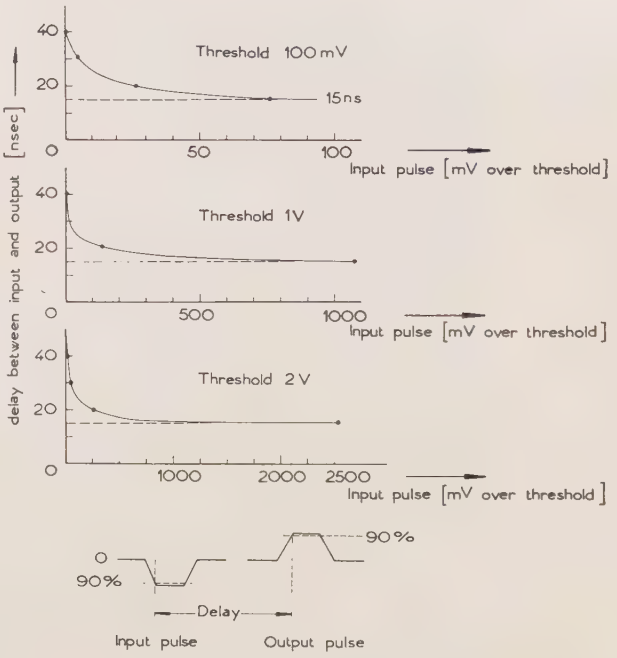

Fig. 9. Delay between input and output pulse.

The collector of T_2 goes negative and the damping is now equal or more than critical, so that the voltage will decay to the original DC level (see figs. 10a, 11a).

The damping is non-linear; this is an important

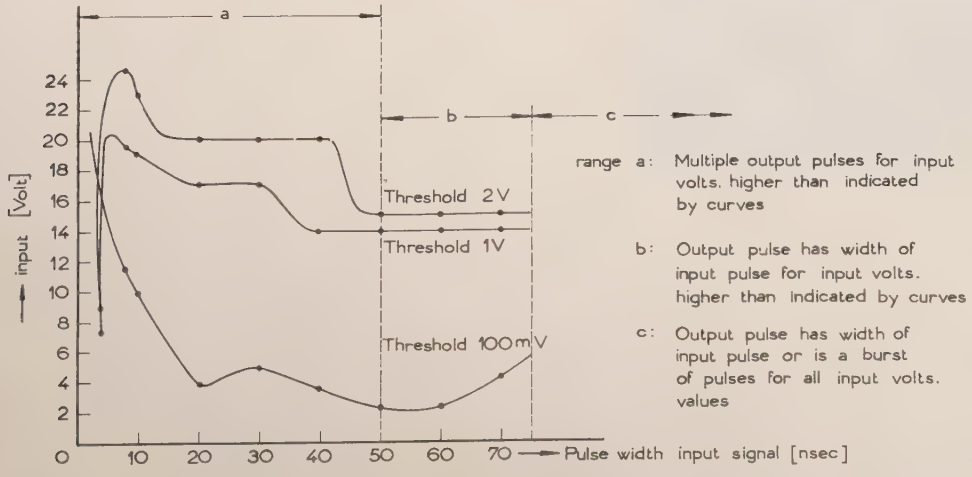
a
b
c
input [Volt]
Threshold 2V
Threshold 1V
Threshold 100mV
range a: Multiple output pulses for input volts. higher than indicated by curves
b: Output pulse has width of input pulse for input volts. higher than indicated by curves
c: Output pulse has width of input pulse or is a burst of pulses for all input volts. values
Pulse width input signal [nsec]

Fig. 8. Overload performance versus input pulse width.

part of the action. For the positive going part it sees an increasing input impedance of T_3, thus decreasing damping (underdamped period), while

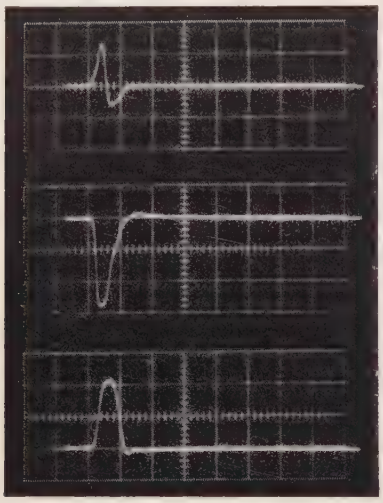

Fig. 10. Waveforms of a. Emitter T_3; b. Negative output; c. Positive output. Hor. sweep speed is 50 ns/div. Vert. sens 2V/div for a), 1V/div for b), 5V/div for c).

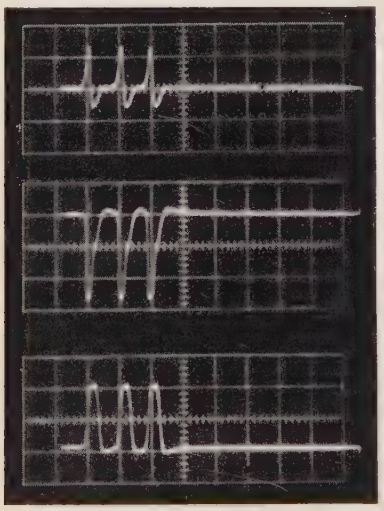

Fig. 11. Waveforms of a. Emitter T_3; b. Negative output c. Positive output. The input signal is three, 100 nsec spaced, pulses. Hor. sweep speed 100 ns/div. Vert. sens 2V/div for a), 1V/div for b), 5V/div for c).

for the negative going part, the damping will increase. The damping potentiometer RV_4 adjusts the damping to be equal or more than critical for the negative part, so that no overshoot occurs and T_2 remains off.

With the indicated values of L_1 and R_9 the circuit will be reset after ≈ 75 ns, this being the deadtime of the discriminator (see fig. 5).

No other storage elements are present besides the

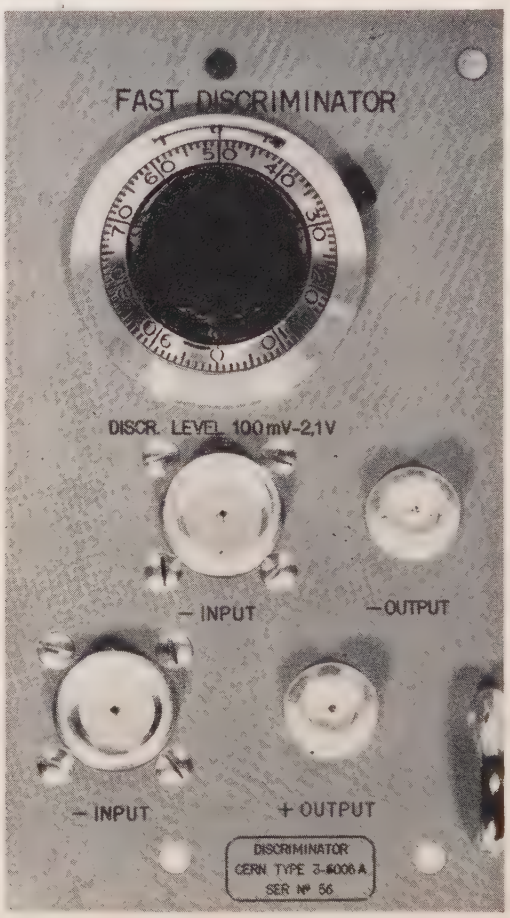

Fig. 12. Front view of discriminator.

L.C.R. circuit, as the feedback loop is DC coupled, resulting in a constant threshold for rates higher than 10 Mc/s (see § 5.2).

The voltage drop across R_{12}, which supplies the base-collector voltage of T_3, is rate independent as the passing current is constant, being switched from T_2 to T_4. All decoupling time constants are long compared to the burst lengths to be expected.

The trigger ratio, i.e. the output amplitude at collector T_4 just above the trigger threshold relative to the output just under the threshold, is about 4:1 and varies slightly with the β of the transistors.

The trigger circuit configuration of emitter coupling has been chosen because of its favourable

switching time (given by the transient response, gain and delay of the loop) compared to other arrangements.

T_3 is added to decrease the load of the base of T_4 on the collector network of T_2.

4. Output Amplifier

The output stage amplifies the signal from the trigger circuit to a level where it can be used for triggering other devices.

threshold, this effectively improving the trigger ratio.

The diode D_4 is a DC restoring diode, keeping the level constant for varying rates.

5. Performances

Many of these discriminators have been in use in Nuclear Physics experiments at CERN, and have proved to be reliable, and stable.

Despite the big spread in properties of the transistors 2N 501 and 2N 1500 (β may be from 20–200), it is not necessary to select them.

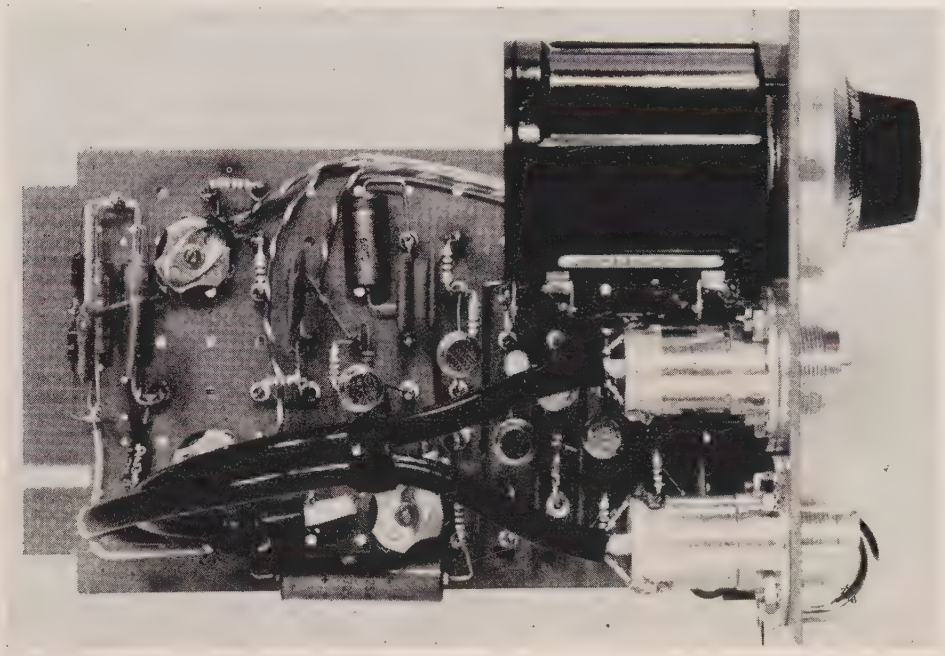

Fig. 13. Wiring of discriminator.

The negative signal from the collector of T_4 drives the emitter follower T_5.

T_5 gives a negative output of 2.5–3 V (fig. 10(b), 11(b)) and drives T_6, which delivers the positive output of 8–10 V (figs. 10(c), 11(c)), both measured across a 125 Ω load.

As both T_5 and T_6 are normally off, a suppression is achieved of the output signal from the trigger circuit, for input signals just below the threshold.

The various measurements were all made with square pulses from a mercury-wetted-contact pulse generator. The curves in figs. 4, 5, 6 and 9, were obtained with a 20 ns wide pulse.

5.1. THRESHOLD VERSUS DIAL SETTING

The relationship is shown in fig. 4 and is substantially linear. Multiplying the dial reading by two gives the threshold in mV.

The threshold is very sharp, the transition from 0 V to maximum output is attained by about 0.5 mV at 100 mV discrimination level, by 2 mV at 1 V and by 2.5 mV at 2 V level.

Transistorized discriminators

[9]) R. Gabriel, E. L. Garwin and C. M. York, Nucl. Instr. and Meth. 5 (1959) 247–253.

[10]) V. L. Fitch, International Conf. on High Energy Accelerators and Instrumentation, CERN 1959, 602.

5.2. DEAD TIME, RATE DEPENDENCY

The curve showing the dead time, the threshold variation as a function of the delay between two applied pulses, is given in fig. 5.

The dead time is also dependent on the amount by which the first pulse exceeds the threshold, this is obvious as the triggering delay for the first pulse decreases as its amplitude increases (see also fig. 9).

From fig. 5, we see that the dead time is 80 ns (12.5 Mc/s) in one case and 60 ns ($\approx$ 16.5 Mc/s) in the other, being safely within 100 ns (10 Mc/s).

When applying a 300 μs burst of 100 ns spaced pulses, at a rate of 50 c/s, simulating the conditions in a beam of the CERN synchro-cyclotron, no change of threshold or output, signal was observed.

No change in threshold was noticed when a 40 ms burst of 100 ns spaced pulses at a rate of $\frac{1}{3}$ c/s was applied; though the negative output was reduced from 2.5 V to 2V and the positive from 10 to 8 V, at the end of the burst. This latter test simulates the conditions in the beam of the CERN proton synchrotron.

5.3. TEMPERATURE STABILITY

Fig. 6 gives the dependency of the threshold on the temperature. Some compensation is obtained in the threshold amplifier by the application of two diodes D_2, D_3 in series.

5.4. INPUT PULSE WIDTH

The threshold as a function of the input pulse width is given in fig. 7. The response of the threshold amplifier and the trigger loop are the determining factors here.

The threshold is independent of the input pulse width from $\approx$ 15 ns upwards.

However, if the input pulse is wider than 40 ns, the output pulse will have the width of the input pulse. For input pulses wider than $\approx$ 80 ns, either one output pulse of this width occurs or a burst of pulses, having the lengths of the input pulse.

By a simple circuit modification, the output pulse will be a single pulse, having the width of the input pulse, for all input pulses wider than 40 ns. This is achieved if $R_9 = 82\ \Omega$ is changed into 56 Ω, R_{10} is short circuited and RV_4 is properly adjusted.

5.5. OVERLOAD

Certain combinations of very large pulse amplitudes and widths may cause multiple outputs. This is summarized in fig. 8.

5.6. DELAY BETWEEN INPUT AND OUTPUT PULSE

The delay between input and output pulse, as a function of the amount by which the input pulse exceeds the threshold, is given in fig. 9 for three discrimination levels.

It is seen that the delay is 40 ns just at the threshold and decreases to $\approx$ 15 ns when the input pulse is $\approx$ 50% over the threshold. This phenomena explains the difference in the curves of fig. 5.

The curves are independent of the input pulse width but determined by the input pulse risetime and discriminator response.

Acknowledgements

The author would like to thank Mr. E. Schüller for his assistance and contribution to the development. Mr. F. Iselin for useful suggestions in the early stage of the development, and Dr. I. Pizer, in charge of the Electronics Group, for his encouragement and stimulating discussions.

NUCLEAR INSTRUMENTS AND METHODS **10** (1961) 315–321; NORTH-HOLLAND PUBLISHING CO.

USE OF CATHODE RAY TUBES IN PULSE-HEIGHT SPECTROSCOPY

P. THIEBERGER† and I. BERGSTRÖM

Physics Department, The Royal Institute of Technology, Stockholm 70

Received 14 January 1961

The possibility of using cathode ray oscilloscopes for single channel pulse height analysis in gamma ray measurements has been studied. Two ways of generating signals obtained when the beam of a C.R.T. hits a certain part of its screen have been used for manual (one oscilloscope used) and automatic (two oscilloscopes used) analysis of pulse spectra from NaI-crystal detectors. The signals are obtained either by viewing the screen of a conventional C.R.T. by means of a photomultiplier tube or by making use of a specially designed C.R.T. provided with additional internal electrodes from which pulses are directly derived.

It is concluded that the equipment described in this paper is well suited for energy and intensity comparisons of gamma rays. It is shown that the energy linearity is good and that it is possible to record photo peaks corresponding to gamma-energies as low as about 5 keV. Compared to conventional set-ups this arrangement shows several advantages and not additional limitations are found.

1. Introduction

C.R.Ts. and oscilloscopes are designed and also generally used for visual observation and measurements of electrical signals. In cases where these visual measurements are inconvenient or impossible other more special instruments are usually utilized. This is for instance the case in nuclear pulse height and time spectroscopy, where the number of events of a certain type has to be counted rather than only the size and position of pulses investigated. It is evident that with the high counting rates present in most nuclear measurements, visual determination of the number of pulses in certain pulse height or time region is in most cases impossible. However, in several cases it has proved to be possible to replace with advantage this above mentioned specialized equipment with oscilloscopes, furnished with some arrangement for recording or registering the pulses appearing on a certain part of the C.R.T. Restricting ourselves to the field of nuclear spectroscopy, photographic recording has been used both for pulse height analysis[1]) ("gray wedge method") and half-life measurements[2]) (other references see[2])). The registering of events by means of a photomultiplier tube viewing the screen through a suitable slit arrangement has been used before, by others and by us, in the measurements of nuclear half-lives (see ref.[2])) but measurements of pulse height spectra along the same lines have been reported only in one case[3]) as far as we know. In this work we have investigated this last possibility and also measured pulse height spectra by making use of a specially designed C.R.T. from which an electrical signal may be derived each time the beam hits one of the ten additional electrodes with which it has been equipped. These electrodes which have the shape of small rectangular plates (cf. fig. 3) are located near the inner surface of the screen and are provided with connecting pins going through the frontal glass wall of the tube.

The two immediately apparent advantages of this kind of arrangements are:

1. The flexibility which is achieved by using an instrument which can be easily adapted for different types of measurements.

2. The possibility to observe and control visually the events to be recorded, for which purpose an oscilloscope in addition to the conventional instruments is often needed anyway.

† On leave of absence from the "Instituto de Fisica" San Carlos de Bariloche, Argentina.

[1]) W. Bernstein, R. L. Chase, and A. W. Schardt, Rev. Sci. Instr. **24** (1953) 437.

[2]) I. Bergström, E. C. O. Bonacalza, A. Jech, M. Perez and P. Thieberger, Nucl. Instr. and Meth. **8** (1960) 151. (In this paper a thorough survey is made of the previous applications of oscilloscopes to half-lives measurements.)

[3]) R. V. Gåsström, Physica **22** (1956) 619.

As will be shown and discussed below the method also has the following advantages:

3. The inherent linearity and good stability of the arrangement.

4. The accurate knowledge of the position of the origin on the energy scale.

5. The possibility of using the output pulses for fast coincidence work.

6. The simple way in which automatation of the measurements can be achieved.

and the sweep time is chosen in such a way that relatively "flat" pulses are obtained (fig. 2).

By changing the vertical amplification the channel width can be changed and adjusted. In the case of photomultiplier detection this can obviously also be done by changing the slit dimensions.

By superimposing a variable DC voltage to the pulse spectrum, via the second input of the type "D" Tektronix plug-in unit (see fig. 1), the pulses may be shifted in the vertical direction ("Slide back" technique). The spectrum is scanned by

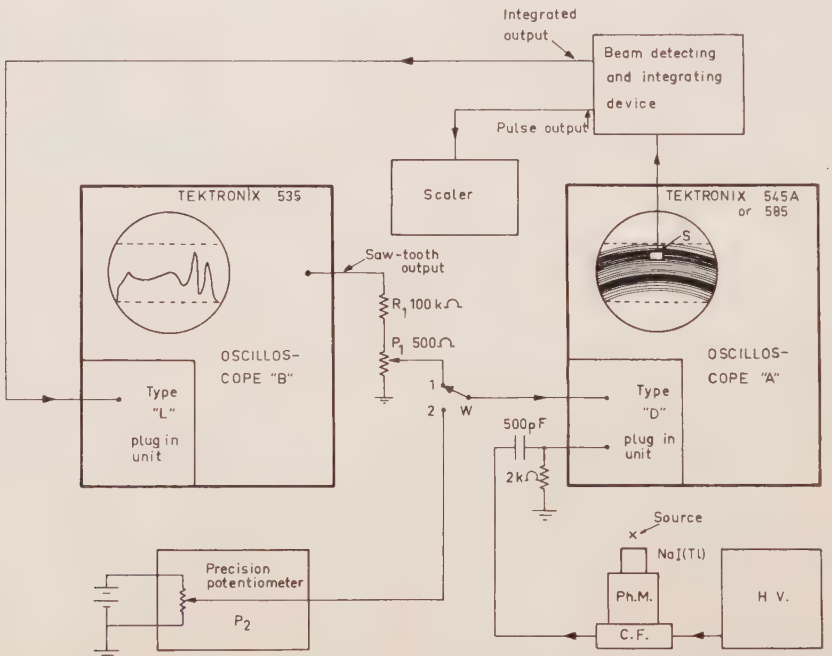

Fig. 1. Block scheme of the arrangement used for either manual or automatic recording of pulse height spectra from a gamma detector. When using the C.R.T. with additional electrodes the oscilloscope "A" was a Tektronix 545 A and the rectangle "S" represents in this case one of these electrodes, the "beam detecting and integrating device" being some kind of counting rate meter (see also fig. 3). In the case of photomultiplier detection, the oscilloscope "A" was a Tektronix 585 and the "beam detecting and integrating device" contains a photomultiplier tube viewing the oscilloscope screen from which pulses, and a voltage proportional to the pulse rate are derived (see also figs. 5 and 6). "S" is in this last case a slit in a black paper attached to the screen.

With the switch "W" in position "1" automatic recording of the spectrum is obtained by photographing the screen of oscilloscope "B" by means of a camera which stays open during the whole sweep time (slow single sweep operation). With switch "W" in position "2" use of the precision potentiometer P_2 is made and the spectrum is obtained point by point the pulses being counted with a scaler. (The diagram of the precision potentiometer is oversimplified.) The differentiating network at the input of oscilloscope "A" serves the purpose of eliminating long positive "tails" which would impair the resolution when strong samples are measured.

2. Equipment Used

In fig. 1 a block scheme of the arrangement used in all the measurements is given. The pulses from the gamma-detector are displayed on the screen of oscilloscope "A". Use of internal triggering is made

means of "S" (slit or additional electrode), which in both cases has a fixed position. The DC voltage, which is added to the pulse spectrum at the input stage of the preamplifier, can be changed manually by means of the precision potentiometer P_2 or

automatically by deriving a fraction of the sawtooth output voltage from oscilloscope "B" via the

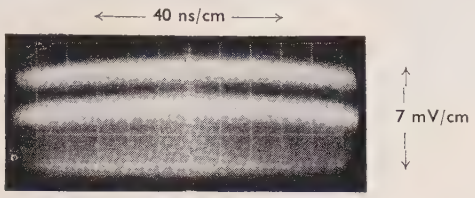

Fig. 2. Pulse distribution corresponding to the photopeaks of the two gamma-rays from a Co^{60} source as seen on the screen of oscilloscope "A" (fig. 1), under normal measuring conditions.

voltage divider R_1 P_1. In the first case the scaler is used to register the counts for each position of P_2 and respondingly the time constant in the integrating device. It is to be pointed out that oscilloscope "B" may as well be a slow oscilloscope provided an output voltage proportional to the horizontal deflection can be obtained and sufficient linear vertical amplification is available.

By disconnecting the detector from oscilloscope "A" and by letting its sweep free-run or by triggering it at a certain frequency the "base line" of the pulses is obtained and therefore an accurate determination of the zero energy position on the spectrum can be made by recording or registering the "peak" corresponding to this base line in the same way as the spectrum. An additional accurate

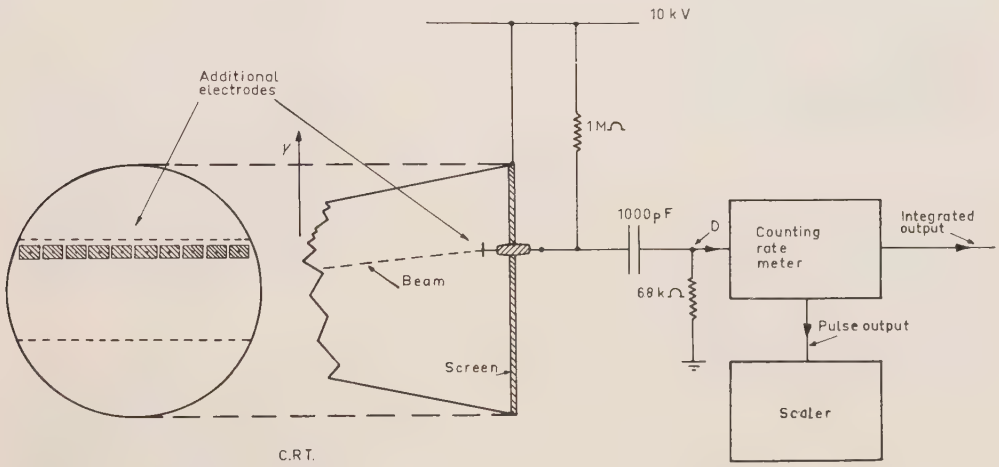

Fig. 3. Wiring diagram of the special C.R.T. as used for pulse height analysis. Only one of the 10 available additional electrodes is connected in this case. As no conventional counting rate meter was available the triggering circuit of an oscilloscope has been used, the gate pulses being fed directly to the scaler and through a R.C. integrating network to oscilloscope "B" (see fig. 1).

in the second a voltage proportional to the pulse rate at S is fed to the Y-amplifier of oscilloscope "B" so that the energy spectrum (intensity as a function of energy) is directly displayed on the screen of this oscilloscope and can be recorded photographically by means of a camera. This stays open during the whole sweep time, which in our case was generally about 2.75 minutes (slowest available sweep for the Tektronix 535 oscilloscope). A Polaroid camera was used and the developing time was 1 min. Thus the total time required for obtaining one spectrum was about 4 min. For the stronger sources this time could have been reduced considerably by choosing a higher sweep velocity and by reducing calibration point, which is generally not available when using conventional pulse height analyzers, is obtained in this way.

2.1. USE OF THE SPECIAL C.R.T.

The arrangement indicated in fig. 3 has been used with a Tektronix 545 oscilloscope (oscilloscope "A" in fig. 1). As indicated in fig. 3 only one of the 10 available additional electrodes was used. This C. R. T. has been designed for the construction of a multi channel time analyzer where use of all the 10 electrodes is going to be made.

As can be seen from fig. 4c the output pulses obtained for the fastest sweeps from one of the

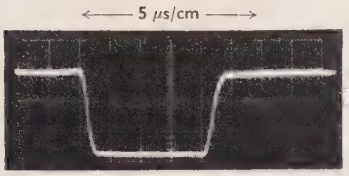

Fig. 4a

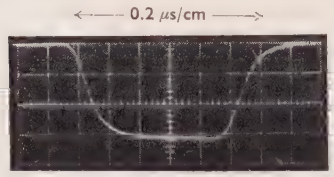

Fig. 4b

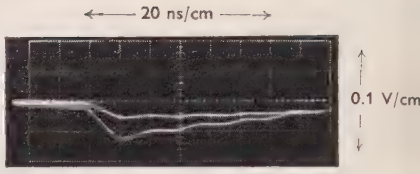

Fig. 4c

Fig. 4. Pulse shapes as measured at point D in fig. 3, by means of a Tektronix 585 oscilloscope. For the following sweep times in oscilloscope "A": a. 20 μs/cm; b. 1 μs/cm and c. 20 ns/cm. The smaller pulse in 4 c has been obtained by adding 25 pF in parallel with the oscilloscope probe the input capacitance of which is of about 10 pF. Therefore an approximate value of 13 pF is calculated for the stray capacitance of the plate plus wiring and a value of about 0.13 mA for the beam current is obtained.

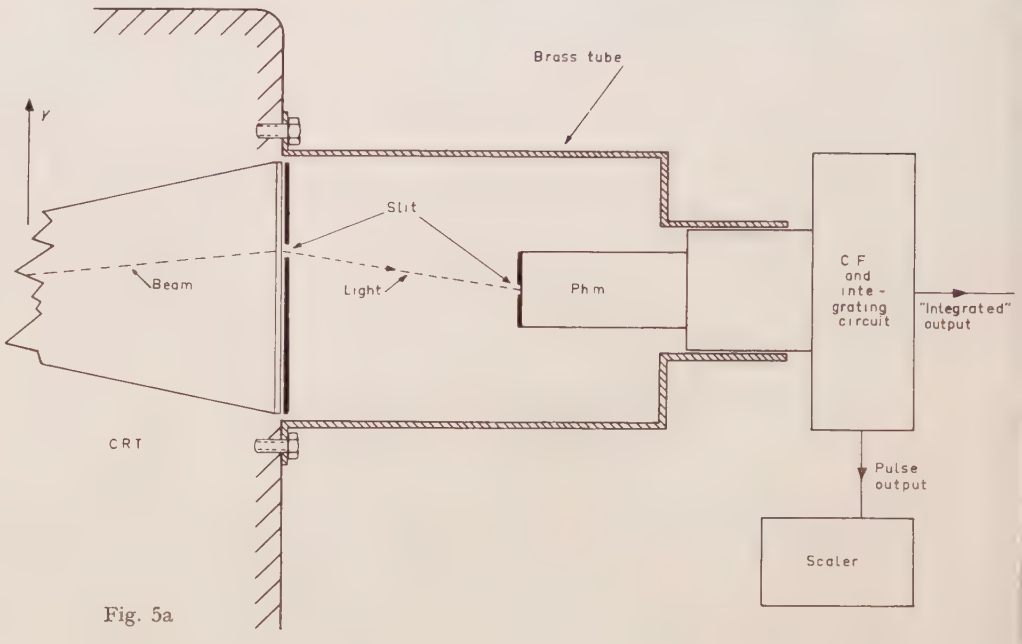

Fig. 5a

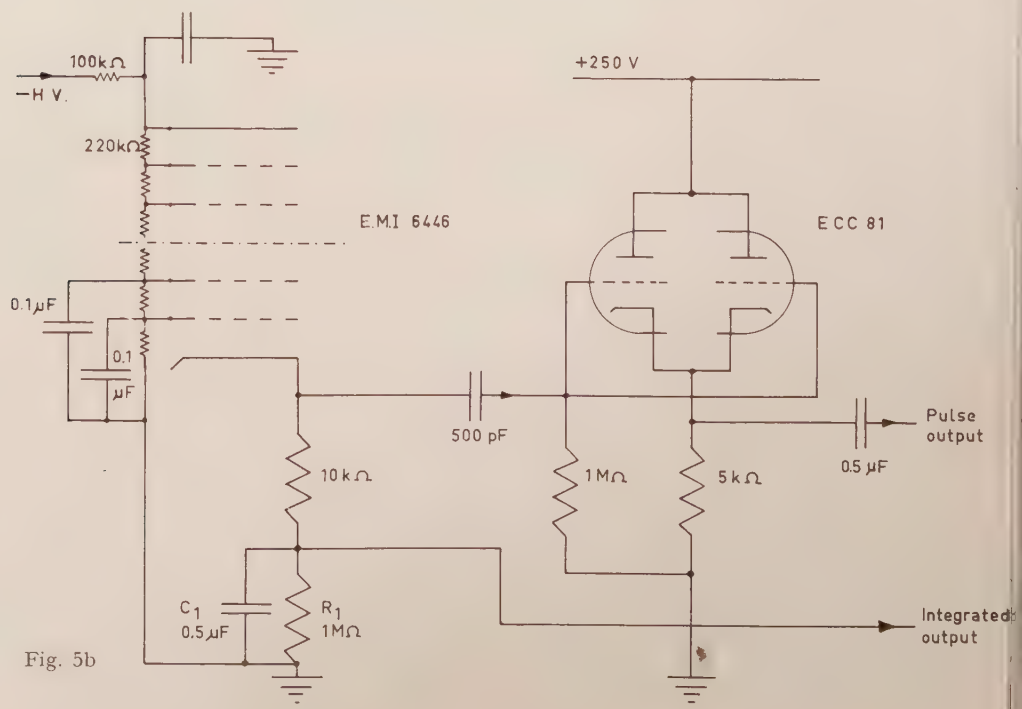

Fig. 5b

Fig. 5. Mechanical arrangement and circuit diagram of the device used for the photomultiplier detection of the beam. At the point marked "Integrated output" a voltage proportional to the mean value of the current from the photomultiplier collector and therefore proportional to the mean counting rate in the "channel" is obtained.

additional electrodes have *rise times* which correspond exactly to the time spent by the beam on the electrode which is about 1 cm long. For the slower sweeps, however, the *length of the pulses* correspond to this time, as may be expected. The possibility of using this fast rising pulses for fast coincidence work seems very attractive and is being investigated.

2.2. DETECTION BY MEANS OF A PHOTOMULTIPLIER TUBE

The arrangement indicated in fig. 5 has been used with a Tektronix 585 oscilloscope (oscilloscope "A" in fig. 1). The time constant of the integrating network was occasionally changed by changing resistor R_1.

In fig. 6 the pulse shape at the output of the

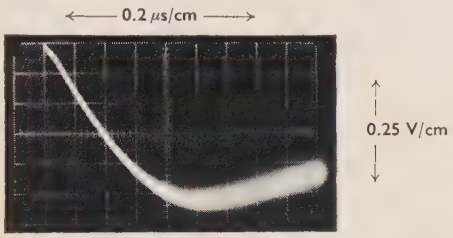

Fig. 6a

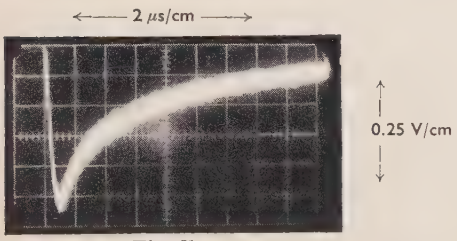

Fig. 6b

Fig. 6. Pulses at the output of the cathode follower (fig. 5) obtained with a sweep time of 10 ns/cm in the "A" oscilloscope and a slit length of about 1 mm.

cathode follower of fig. 5b has been photographed. Note the relatively slow rise time compared with the pulses of fig. 4c in spite of the fact that a C. R. T. with a relatively fast phosphor has been used.

3. Experimental Results

In figs. 7, 8 and 9 results obtained both with the special C. R. T. and with photomultiplier detection, and using manual and automatic recording of the

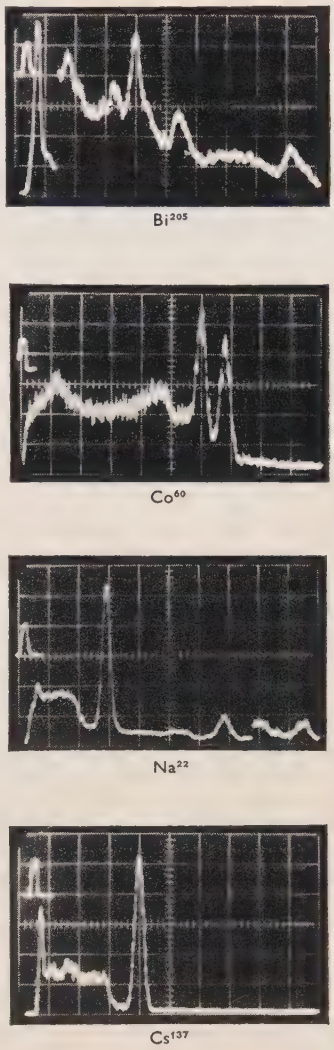

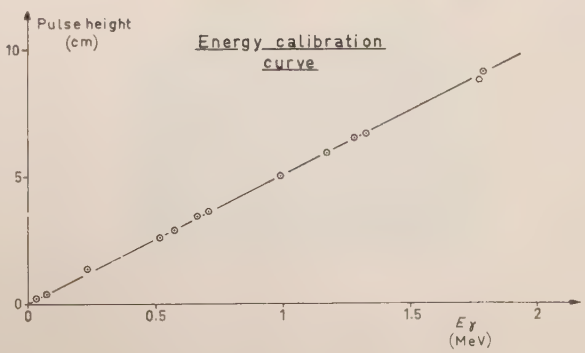

Fig. 7. Automatically recorded spectra obtained with the arrangement of fig. 1 making use of the spectral C.R.T. with additional electrodes (see fig. 3). The sweep time in oscilloscope "B" was of about 16.5 sec/cm. The "zero energy line" has been recorded for each of the spectra. The energy calibration curve shown has been obtained by visual estimate of the peak positions on the photographs.

spectra are shown. The reader is referred to the corresponding figure texts for information regarding these measurements.

As long as no fast pulses are required, the results obtained with the special C. R. T. and the ones obtained with photomultiplier detection do not show any marked difference. Nevertheless, for practical reasons the use of a C.R.T. as the one used by us or a similar tube (one additional electrode would of course be sufficient for this purpose), is to be preferred, if it is available. The use of a photomultiplier tube viewing the screen through a slit

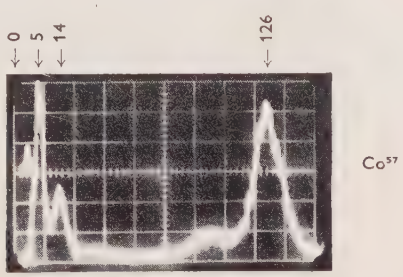

Fig. 8a

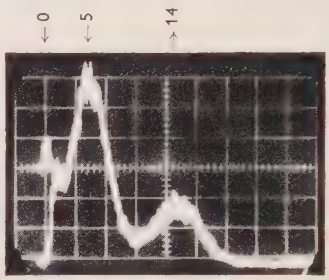

Fig. 8b

Fig. 8. Automatically recorded gamma spectra from the decay of Co^{57} as obtained with the arrangement of fig. 1 by making use of the photomultiplier detection technique (see also fig. 5). The zero energy peak is also in this case registered and in oscilloscope "B" the same sweep time as in the cases if fig. 7 has been used.

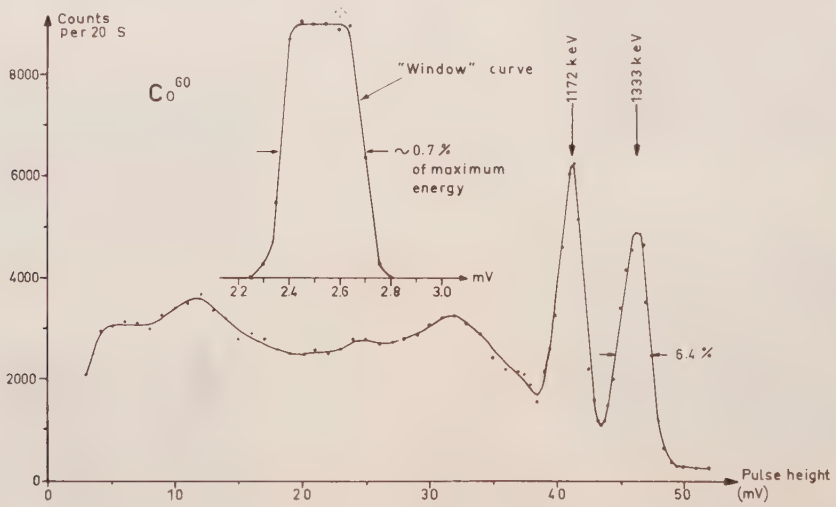

Fig. 9. Gamma spectra of Co^{60} obtained: a. with photomultiplier detection and manual operation.

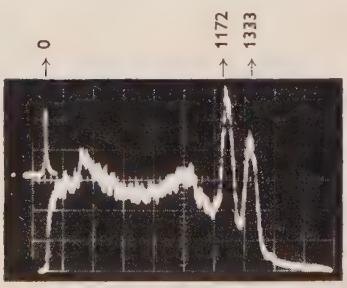

Fig. 9b

Fig. 9. Gamma spectra of Co^{60} obtained: b. with photomultiplier detection and automatic recording.

system requires a completely light tight arrangement (fig. 5a) and makes therefore the continuous visual observation of the pulses impossible. The very need of having an additional photomuliplier and a negative H.V. supply (see fig. 5b) are disadvantages which are nevertheless somewhat compensated by the more refined counting rate meter system needed when using the special C.R.T. In this last case the beam current could certainly be averaged by means of an integrating network, but the fact that the C.R.T. screen is operated at 10 kV above

ground makes the measurement of the resulting voltage drop somewhat complicated.

4. Final Remarks

The satisfactory results obtained regarding linearity and resolution are not surprising. So for example are modern oscilloscopes provided with fast D.C. coupled pulse amplifiers which make possible the application of the slide back technique used in this work. This technique is no doubt one of the most attractive alternatives for single channel pulse analysis, because accurate comparisons of pulse heights with D.C. voltages are independent of possible nonlinearities of the amplifiers. The comparison of the pulse height and the D.C. voltage is namely performed at the input stage and the response of this amplifiers to D.C. voltages and the pulse signals from the detectors used is the same. In addition it is possible to obtain with the same channel width a higher maximum resolution than in the more conventional method. The maximum resolution in the slide back method is namely given by the ratio of the dynamical range of the amplifier and the channel width rather than by the much smaller ratio of linear range and channel width in the other method. In our arrangement, especially in the case of an additional electrode, the "channel" is defined directly by the very sharp "characteristics" of what may be called a high performance two dimensional beam deflection tube, rather than by the triggering levels of the two conventionally used univibrators. It may be pointed out that such a "tube" is in fact able to carry out the functions for which two discriminators and an anticoincidence stage are usually required. The need of a horizontal, linear sweep is by no means essential and a suitable signal for the horizontal deflection can for instance be obtained by differentiating the analyzed pulse. In such a way one could certainly develop a pulse height analyzer along the lines of this work which could be considerably simpler than a complete oscilloscope. On the other hand, according to our experiences, the introduction of C.R.T. with one or more additional electrodes, while not limiting in any way the conventional use of the oscilloscopes, widens even more the field of applications in which these instruments are useful. In fact many possibilities in which C.R.T. oscilloscopes may be easily used as "active" controling or measuring devices rather than being only "passive" observation tools could be opened in this way.

Acknowledgements

The work with the cathode ray tube provided with internal electrodes was made possible by the kind cooperation of the Swedish Tektronix Representative, Ing. E. Ferner and by the Tektronix Company in the U.S., who on our request made and put at our disposal the tube in question.

One of us (P.T.) gratefully acknowledges a scholarship granted by the Argentine National Research Council (C.N.I.C.T.) and the hospitality and excellent working conditions offered to him in Sweden.

NUCLEAR INSTRUMENTS AND METHODS **10** (1961) 322–326; NORTH-HOLLAND PUBLISHING CO.

IMPROVED AUTOMATIC OPERATION OF A DOUBLE FOCUSING IRON-YOKE β-SPECTROMETER

E. ARBMAN and B. JUNG

The Gustaf Werner Institute for Nuclear Chemistry, University of Uppsala, Sweden

Received 19 December 1960

The construction and performance of an arrangement for the automatic operation of a double focusing β-spectrometer are described. Digital recording of the number of counts for a preset time and accurate advancement of the spectrometer current in 750 steps preserve high accuracy. The preset time is variable between 1 and 1090 seconds and the 750 steps can be spread over almost any part of the total momentum range of the spectrometer.

1. Introduction

In the original design of the β-spectrometer[1]) at this Institute, provision was made for an automatic operation in which the spectrometer current was continuously increased and the counting rate recorded by a rate-meter and a strip-chart recorder. This automatic operation, which has been frequently used, was found very convenient for surveying unknown conversion electron spectra and for studying nucleides with half-lives less than or about one hour. The analog display of the counting rate introduced, however, a reduction in the accuracy of line positioning and line intensity and more careful measurements were made manually. An automatic operation of the instrument without sacrifice in accuracy would be of great value, especially as the nuclear spectroscopy work at this Institute is mostly concerned with the decay properties of new or little investigated nucleides. This type of research, which we believe to be natural at an institute having both a 190 MeV proton synchrocyclotron and a mass separator for active substances, implies tedious measurements, as they cannot be confined to only special regions of the spectra.

2. Design Considerations

As the design of the automatic operation depends to a large extent on the spectrometer construction, we will start this section with a short description of the spectrometer features which have special bearing upon the automatic operation.

The double focusing magnetic field is formed by suitably shaped iron pole-pieces. The hysteresis effects inherent in a magnet containing iron necessitates a monotonous variation of the spectrometer current as otherwise both the correct field shape and the regular dependence of the focused electron momentum on the spectrometer current are destroyed. The best practical momentum resolution is about 0.2%, most of the conversion electron measurements being performed with a momentum resolution of about 0.4%. The precision in the conversion line positioning is thus of the order of a few parts in 10^4. The magnetic field strength is not measured directly but the focused momentum is calculated with a calibration procedure[2]) from measurements of the magnet current. The calibration is based on the current readings obtained for suitable well-known conversion lines. The current regulation system is briefly discussed in section 3 and here it should only be mentioned that it is well suited for automatic operation. In normal manual operation of the spectrometer, current readings are taken for each measured point on the spectrum and the number of counts for a preset time registered by a scaler and a timer. The spectrometer current is calculated from measurements with a precision potentiometer of the voltage drop over a resistor in series with the magnet coils (cf. fig. 1).

The basic principle in the design of the new

[1]) E. Arbman and N. Svartholm, Ark. Fys. **10** (1956) 1.
[2]) E. Arbman, Thesis, University of Uppsala, 1958.

automatic operation was to have a system as simple as possible, thereby securing a high reliability, but still with considerable flexibility regarding the time spent on recording a selected part of the spectrum.

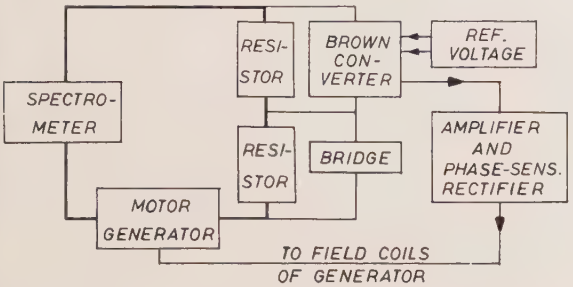

Fig. 1. Simplified block diagram of the spectrometer current regulation system. The "bridge" unit is a precision potentiometer utilized for taking current readings.

The manual as well as the old automatic operation should not be affected by the new arrangement.

Since a continuous variation of the spectrometer current necessarily introduces a line-broadening effect it was decided to have a step-wise regulation of the current. Although the absolute momentum resolution of the spectrometer is proportional to the momentum (i.e. approximately to the current), an advancement in equal steps was preferred as this allows a simpler and more flexible construction. In automatic operations normally only a restricted part of the spectrum can be studied at a time, because of the decay of the sample and the finite number of automatic steps available, and thus the change in absolute momentum resolution over that part is rather small.

An automatic process for measuring and recording the spectrometer current with sufficient accuracy would demand a highly elaborate equipment. However, with a sufficiently accurate current advance system, current readings are needed only at a few points on the spectrum and these can be made manually without appreciable reduction in the benefits of an automatic operation. As mentioned above the accuracy in the line positioning is normally limited by the line width to a few parts in 10^4. At least the same accuracy must be demanded of the current advance system.

Earlier designs[3]) for an automatic operation of β-spectrometers have utilized a counting rate registration either by a rate-meter and a strip-chart recorder or a numerical printer, recording the elapsed time for a preset number of counts. The drawbacks of the first system have already been pointed out. The second system has the merit of being numerical, but as the time registration is necessarily quantized, the accuracy will decrease when the counting rate increases. This is just the opposite of what is wanted when recording a line spectrum where the background is often uninteresting as compared to the peaks. Also the big differences in counting rates experienced in measurements of conversion electron spectra makes the choice of the preset number of counts very intricate. This difficulty is accentuated when studying short-lived nucleides because of the limited time available. Registration of the number of counts for a preset time does not have these disadvantages and is thus to be highly preferred. Also the ease in the subsequent handling of the data points in favour of this system. With the digital printers now commercially available this registration system offers no difficulties as might have been the case in earlier designs.

3. Design Description

A simplified block diagram of the spectrometer current regulation system is given in fig. 1. The current is supplied by a motor generator, the field-coil excitation of which is controlled by the amplified and phase-sensitively rectified error signal from a Brown converter, which compares the voltage over a series resistor through which the current flows, with a reference voltage (cf. the original description[1])). The reference voltage is supplied by the arrangement shown in fig. 2. The potentiometer P1 is manually operated and its position determines the starting point of the automatic run. (In the old automatic operation P1 is actuated by a motor through a reduction gear, which can also be used for the small current increments needed in the manual operation of the spectrometer.) The potentiometer P2 is operated by

[3]) W. C. Kelly and K. J. Metzger, Rev. Sci. Instr. **22** (1951) 665;
R. D. Birkhoff, A. W. Smith, H. H. Hubbell, Jr. and J. S. Cheka, Rev. Sci. Instr. **26** (1955) 959.

an electromagnetic device by pulses from the timing unit (cf. fig. 3). The pulses are fed to a solenoid actuating an escapement arm which advances a sawtooth gear on the shaft of P2 one step at a time.

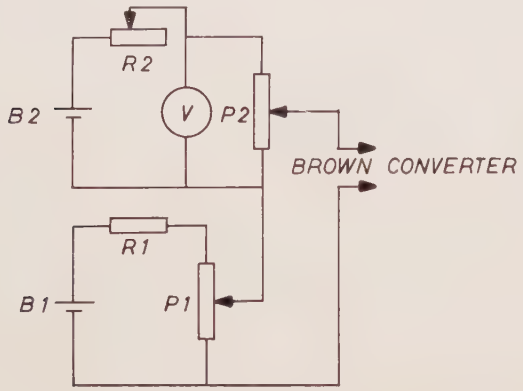

Fig. 2. Coupling scheme of the reference voltage supply. P1: 10 turn Spectrol, R = 1000 ohm, P2: 15 turn Helipot, R = 1000 ohm, rated linearity better than 0.05 %, R1: 675 ohm, R2: 20 000 ohm, B1 and B2: standard 1.5 V dry cells, V: voltmeter, 0–2 volt.

range. By the resistor R2 the current through the potentiometer P2, and thus the spectrometer current increments per step, can be varied within wide limits. The meter V shows the total voltage

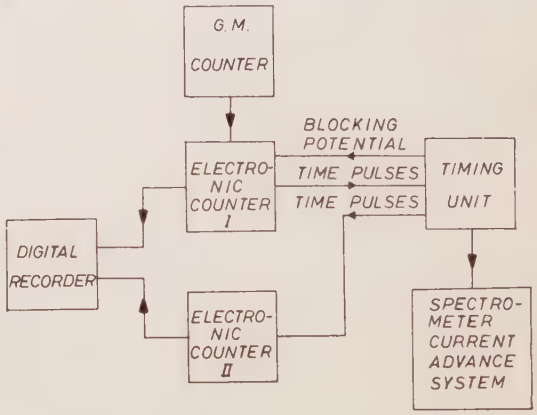

Fig. 3. Simplified block diagram of the timing, counting and recording equipment.
Electronic Counter I: Hewlett Packard Model 523B, Electronic Counter II: 6 Hewlett Packard Decade Counter Plug-In Units Model Ac-4, Digital Recorder: Hewlett Packard Model 560A.

A special spring action secures the proper step-wise advancement of the sawtooth gear. The gear has 50 teeth which in combination with a fifteen-turn potentiometer provides 750 steps. The potentiometer P2 has a rated linearity of better than 0.05 %. This means that the error in the current settings due to non-linearities should not exceed 0.4 steplengths, this being experienced at the end of the automatic drop over the potentiometer P2. The currents for the potentiometers P1 and P2, taken from the two dry cells B1 and B2, are purposely kept low, in order to secure high stability.

A simplified block diagram of the timing, counting and recording equipment is given in fig. 3. The central instruments are the Electronic Counter I and the Digital Recorder. The timing unit has

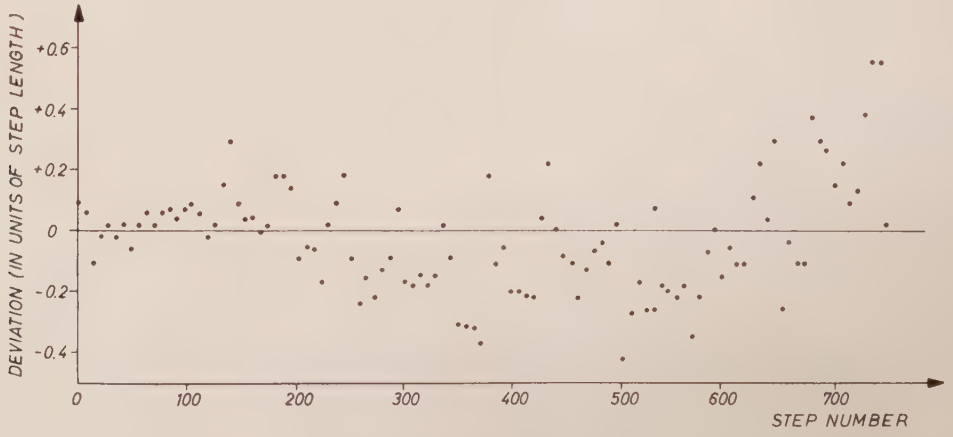

Fig. 4. Diagram illustrating the outcome of a test of the accuracy in the automatic current settings. The current was measured in every seventh of the 750 points. A least squares fit of a linear function of the step number to the measured values in every thirty fifth-point was used to calculate the expected value in every seventh point. The deviation (in units of steplength) of the calculated value from the measured one is given in the figure for every seventh point.

been incorporated to provide for longer counting times than the 0.001, 0.01, 0.1, 1 and 10 seconds available in the standard instrument. This is achieved by feeding a blocking potential to the "Control Gate Binary" of the Electronic Counter I. The blocking potential is applied from the start of a counting period for a time which is determined by a mechanical register counting a preset number of pulses obtained from the main instrument. The inherently high accuracy (2 parts in 10^6 according to the manufacturer) in the counting time is preserved as both the start and stop of the counting period is determined by the Electronic Counter itself, the blocking potential only preventing stopping pulses to arrive at the "Control Gate Binary" during the counting period. The timing unit admits counting periods of 1, 2, 3, . . . 109 seconds and 10, 20, 30, . . . 1090 seconds. This range has been found adequate in the present measurements with the spectrometer. Some minor modifications in the Electronic Counter circuitry were needed to provide means to apply the blocking potential and to obtain time pulses. The second scaler has been included to record the total time elapsed from the start of the automatic run, thus providing both a check on the proper functioning of the equipment and a means to identify different measuring points. At the end of a counting period, the timing unit feeds a pulse to the spectrometer current advance system, the start of the next counting period being delayed 1 or 10 seconds depending on the counting period used.

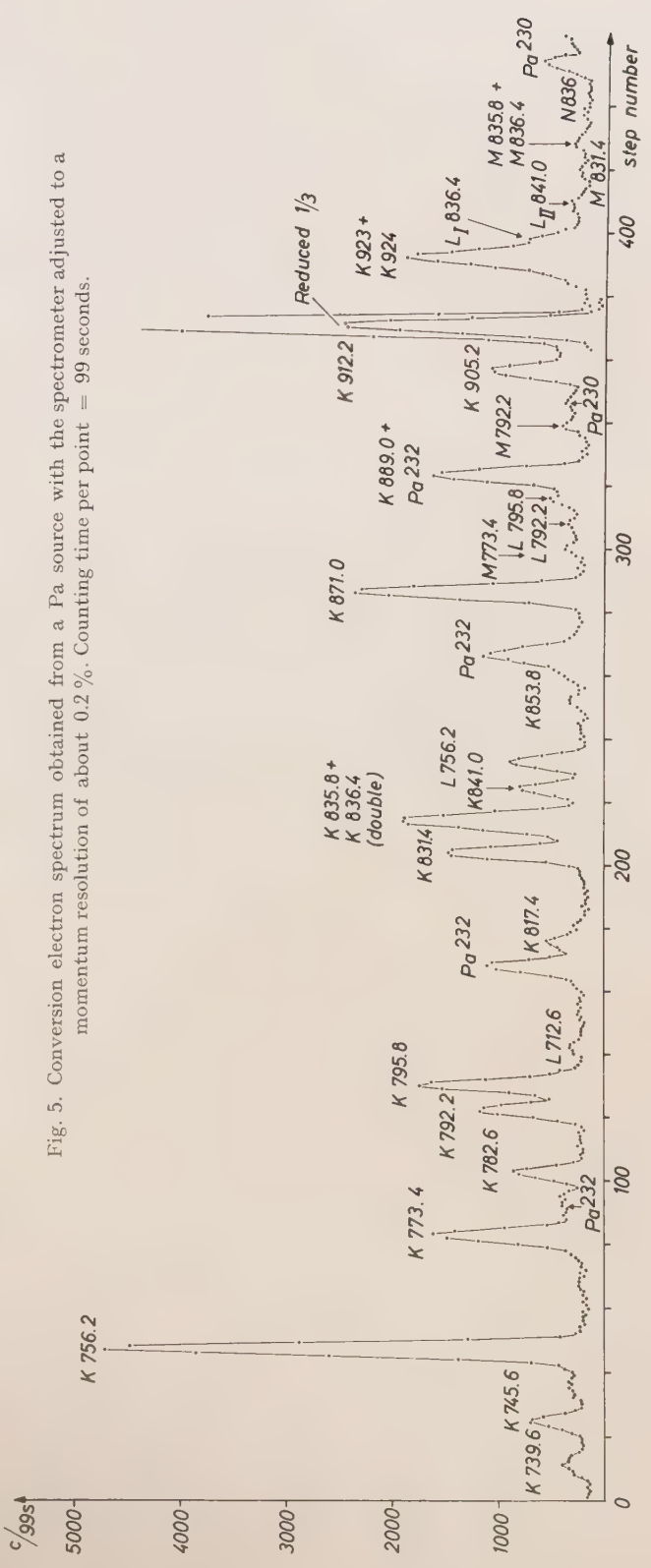

Fig. 5. Conversion electron spectrum obtained from a Pa source with the spectrometer adjusted to a momentum resolution of about 0.2 %. Counting time per point = 99 seconds.

4. Performance

The accuracy, which can be attained in the automatic operation of the spectrometer, is determined by several factors, the most important ones being the linearity of the potentiometer P2 and the precision in the step-wise rotation of its shaft, the constancy of the voltages from the two dry cells B1 and B2 and the performance of the current stabilization system. The overall accuracy in the automatic current settings can be tested by measuring the spectrometer current of several points in the automatic operation. In such a test the current was measured in every seventh of the 750 points. It was found that in 80 cases the measured value deviated

by less than 0.2 steplengths from the value calculated from a least squares fit of a linear function of the step number to the measured values of every thirty-fifth of the points. In 25 cases the deviation was between 0.2 and 0.4 steplengths and in 3 cases more than 0.4 steplengths. The distribution between negative and positive deviations was nearly identical as can be seen from fig. 4. (When recording a spectrum automatically, the spectrometer current is usually measured in several points and the current value in each point calculated from a least squares analysis, as described above.)

It is estimated that the current readings were accurate to about 0.1 steplengths, this figure including also possible fluctuations in the current stabilization system. The result of the test is thus in agreement with the calculations in section 2, where it was shown that non-linearities in the potentiometer P2 could be expected to introduce an error of 0.4 steplengths. Obviously the fractional uncertainty in the automatic current settings ($\Delta I/I$, where I is the spectrometer current) due to non-linearities in the current advance system depends on the fractional current increment per step. Assuming this to be 8 parts in 10^4 (which gives 5 points above half-height of lines recorded with a momentum resolution of 0.4%) one finds the fractional uncertainty from a 0.4 steplengths inaccuracy in the current settings to be 3 parts in 10^4, an acceptable figure according to the discussion in section 2. It should be remarked that the accuracy in the current readings is estimated to be 1 part in 10^4 under favourable conditions and somewhat lower when time restrictions are imposed on the measurements.

The new automatic operation of the spectrometer has been in use for more than one year and experience shows it to be very convenient and reliable. It has been extensively employed in several investigations, of which can be mentioned studies of the decays of Pa^{228} [4]), neutron deficient tellurium isotopes[5]), Tl^{199} [6]) and Tl^{197} [7]). (In these studies the potentiometer P2 was of a ten-turn type, allowing 500 automatic points. This number was recently increased by replacing the potentiometer with a fifteen-turn type.) One of the conversion electron spectra recorded in the study of the decay of Pa^{228} is given in fig. 5.

The automatic timing and count registration operation has also proved to be of great value in measurements of decay periods. A suitable conversion line is focused in the spectrometer and with the current kept constant the number of counts for a preset time is registered as a function of time. The constancy of the spectrometer current is sufficient to allow measurements extended over more than one day.

We are grateful to Professor The Svedberg for excellent working conditions. Ing. P. Isacsson has been responsible for the electronics connected with the equipment and his able collaboration is thankfully acknowledged. The work has been financially supported by the Swedish Atomic Research Council.

[4]) E. Arbman, S. Bjørnholm and O. B. Nielsen, Nucl. Phys. **21** (1960) 406.

[5]) R. W. Fink, G. Andersson and J. Kantele, Ark. Fys. (in press).

[6]) B. Jung and J. Svedberg, Nuclear Physics **20** (1960) 630.

[7]) B. Jung and J. Svedberg, Ark. Fys. (in press).

NUCLEAR INSTRUMENTS AND METHODS **10** (1961) 327–332; NORTH-HOLLAND PUBLISHING CO.

CHARGED PARTICLE DISCRIMINATION IN A CsI(Tl) DETECTOR†

J. A. BIGGERSTAFF, R. L. BECKER†† and M. T. McELLISTREM

University of Kentucky, Lexington, Kentucky

Received 12 December 1960

Two techniques requiring measurement of short time intervals are reported. A charged reaction product discrimination method has been developed which depends upon the fact that different types of charged particles of approximately the same energy yield significantly different fluorescent decay times in a CsI(Tl) scintillator. Tests have been conducted on the reaction products of the B_e^9 + d reactions and on the protons from the $C^{12}(d,p)C^{13}$ reaction. Using relative decay time measurements, alpha particles are clearly separated from protons or tritons. Protons and tritons are clearly separated from one another as long as the triton energy does not exceed the proton energy by as much as twenty percent.

1. Introduction

We wish to report a particle indentification scheme available with a CsI(Tl) scintillation detector which is convenient to use at low energies and which does not adversely affect any of the characteristics of the scintillation detector. In a paper on the fluorescent properties of CsI(Tl) Story, *et al.*[1]) showed that the particle identification may be performed by measuring the decay time of the fluorescence. The authors' conclusion was that the light output of CsI(Tl) following passage of a charged particle is characterized by a fast rise followed by a two component exponential decay. They found the light output of the phosphor was represented by:

$$L = A \exp(-t/T_1) + B \exp(-t/T_2)$$

with $0.4\ \mu\text{sec} \leqslant T_1 \leqslant 0.7\ \mu\text{sec}$ for particles other than electrons. The exact value of T_1 depended upon the type of particle or, more precisely, upon the average energy density deposited in the crystal by the particle. $T_2 \sim 7\ \mu$ sec for all particles. The slow amplitude B is approximately 3 percent of the fast amplitude A. Although the slow decay contains about 30 percent of the light, it has little effect on the time dependence of the fluorescence during the first microsecond or so of the decay.

A shape circuit has been designed and constructed to produce an output whose amplitude is proportional to the time of decay of L to one-half its orginal amplitude, a time interval of $\sim 0.5\ \mu$sec. This output is fed through a single channel analyzer to a gating circuit of the multi-channel analyzer. The single channel analyzer selects a decay time appropriate to a particular type of particle. In this manner, tritions, protons or alpha-particles may be separately studied. The separation is not complete for particles of all energies, because the shape circuit output has a weak dependence on input pulse amplitude. Alpha particles are clearly separated from protons and tritons if the alpha-particle energy does not exceed the proton energy by more than a factor of four. Tritons are separated from protons if the triton energy does not exceed the proton energy by more than twenty percent. Groups of particles not separated by the shape circuit will be separated in the energy spectrum, so that the limitations imposed by the amplitude dependence of the shape circuit are not serious. The operation of an earlier version of this circuit has been reported[2]), and a description of its application to aid the study of the $B^{10}(d, \alpha)Be^8$ reactions has been published[3]).

† This work was partially supported by the U.S. Atomic Energy Commission.

†† Now at Boston College, Chestnut Hill 67, Massachusetts.

[1]) R. S. Story, W. Jack and A. Ward, Proc. Phys. Soc. **72** (1958) 1.

[2]) R. L. Becker and J. A. Biggerstaff, Bull. Am. Phys. Soc. Ser. II, **4** (1959) 326.

[3]) R. L. Becker, Phys. Rev. **119** (1960) 1076.

2. Shape Circuit Design

Fig. 1 shows a block diagram of the electronics associated with the CsI(Tl) detector. The detector is operated inside an evacuated chamber designed to permit angular distribution measurements of charged reaction products[4]), The pulses from the anode of the Dumont 6467 photomultiplier are fed through an integrating circuit and cathode follower to the input of the 256-channel analyzer for energy analysis of the reaction products. Pulses from the last dynode of the photomultiplier are developed across a low resistance (10^3 ohms) and fed through a cathode follower to a wide band amplifier. The resistance is kept low so that the voltage at the dynode will faithfully reproduce the decay of the fluorescence. The decay time spectra of these pulses are analyzed in the shape circuit; its output is fed through the single channel analyzer to gate the selective storage of the 256 channel analyzer as indicated in fig. 1.

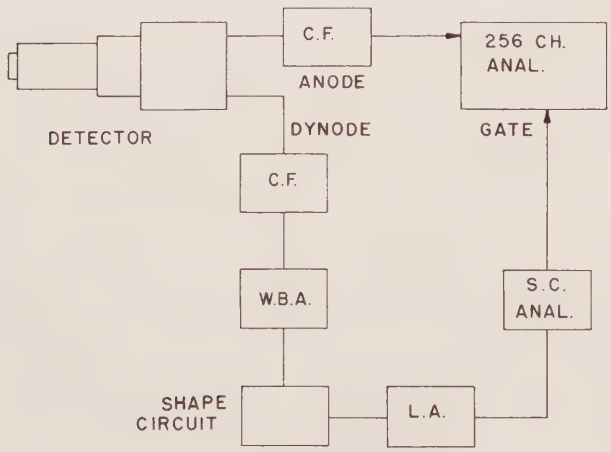

BLOCK DIAGRAM OF ELECTRONICS

Fig. 1. Block diagram of electronics. Anode pulses are integrated and fed to 256 channel analyzer for energy analysis. Dynode pulse is timed in shape circuit and is fed to gate of 256 channel analyzer through single channel analyzer. C.F. = cathode follower, W.B.A. = wide band amplifier, L.A. = linear amplifier, S. C. ANAL = single channel analyzer.

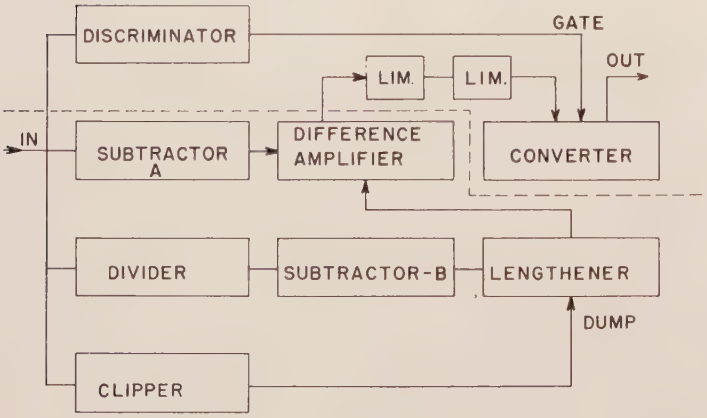

DECAY TIME ANALYZING (SHAPE) CIRCUIT

Fig. 2. Block diagram of shape circuit, showing functions of sections of the circuit. The pulse in path A is compared to a fraction of it from path B by the difference amplifier, and thus its decay time is measured. The limiters remove the amplitude dependence of this time measurement and the converter transforms time measurement to voltage.

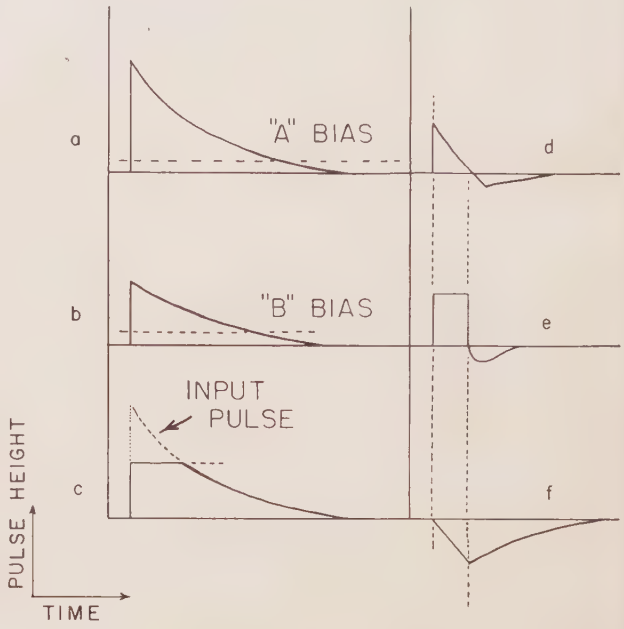

SHAPE CIRCUIT WAVEFORMS

Fig. 3. Pulses as they appear at various points of fig. 2. a.: A pulse, showing subtracted portion; b. B pulse (fraction of A pulse), showing level of subtraction; c. B pulse after lengthening and additional shaping; d. output of difference amplifier. The time the pulse is positive is a measure of decay time; e. output of limiters; f. output of converter. Decay of output is not properly represented.

A block diagram of the shape analyzing circuit is shown in fig. 2, and idealized wave forms at various points in the circuit are shown in fig. 3. Fig. 4 is a schematic of that part of the circuit shown below the dotted line of fig. 2 and fig. 5 is the part of the circuit above the dotted line. The

[4]) M. Seman, Masters' thesis, University of Kentucky (1958) (unpublished).

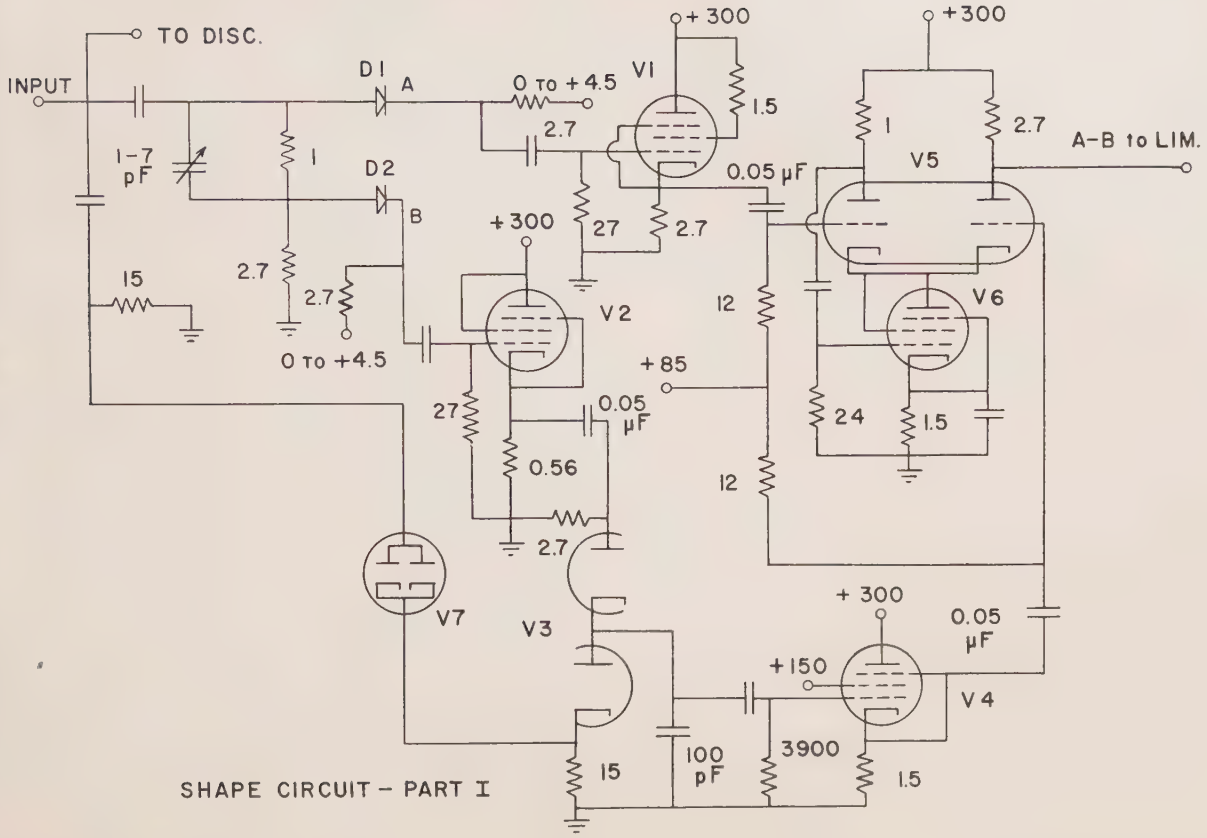

Fig. 4. Part I of shape circuit, including passive divider and subtraction networks, B pulse lengthener and difference amplifier. All unlabelled coupling capacitors are 0.01 μF; all unlabeled bypass capacitors are 0.1 μF. All resistance values are in units of 10^3 ohms.

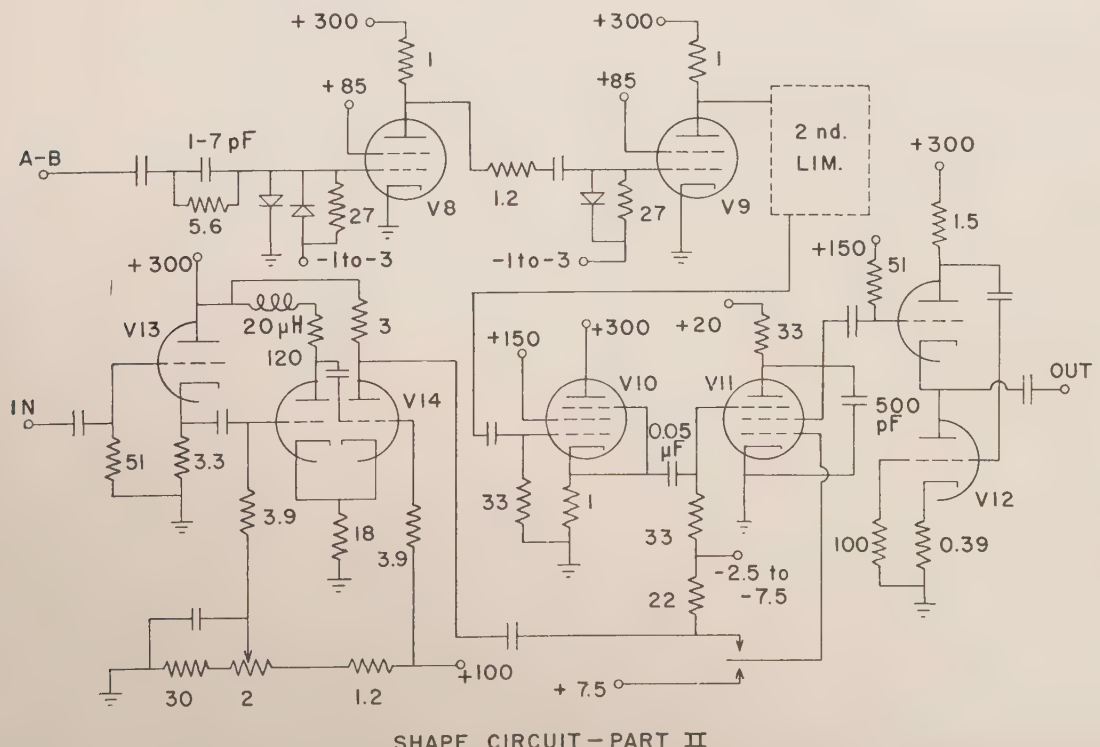

Fig. 5. Part II of shape circuit, including limiters, time-to-pulse-height converter and input pulse discriminator. All unlabeled coupling capacitors are 0.01 μF; all unlabeled bypass capacitors are 0.1 μF. All resistance values are in units of 10^3 ohms.

vacuum tubes indicated in figs. 4 and 5 are identified in table 1.

TABLE 1
Tube types used in shape circuit

6AK5	V6	6FV6	V8, V9
6AL5	V3, V7	6J6	V14
6AU6	V1, V4, V10	12AT7	V5, V13
6BN6	V11	5847	V2
6BZ7	V12		

Pulses at the input to the circuit enter three branches of it as indicated in fig. 4. One branch, proceeding through V7, fixes the length of a lengthened pulse to be just long enough for proper operation of the circuit. A branch goes to a discriminator, which prevents analysis of pulses unless they are large enough to saturate the limiters. The third and main branch of the circuit permits pulses to enter channels A and B through diodes D1 and D2, and these channels ultimately lead to opposite sides of the difference amplifier at V5. The positively biased diode D1 passes most of the input pulse, as indicated by the dotted subtraction level in fig. 3a; this pulse then proceeds through cathode follower V1 to the difference amplifier. Approximately sixty percent of the input pulse enters diode D2, and its subtraction level is shown in fig. 3b. This pulse proceeds through cathode follower V2 to a pulse lengthener at V3. The pulse is lengthened through the top half of V3 as long as the positive input pulse, which is fed to the cathode of the bottom half of V3, keeps the bottom half cut off. As the level of the input signal drops below the level of the lengthened signal, the bottom half of V3 conducts and "dumps" the lengthened B pulse, so that the shape of that pulse as it enters V4 is as given in fig. 3c. Cathode follower V1 isolates the input pulse from V5 grid current distortions, and V2 presents a low impedance charging path for the

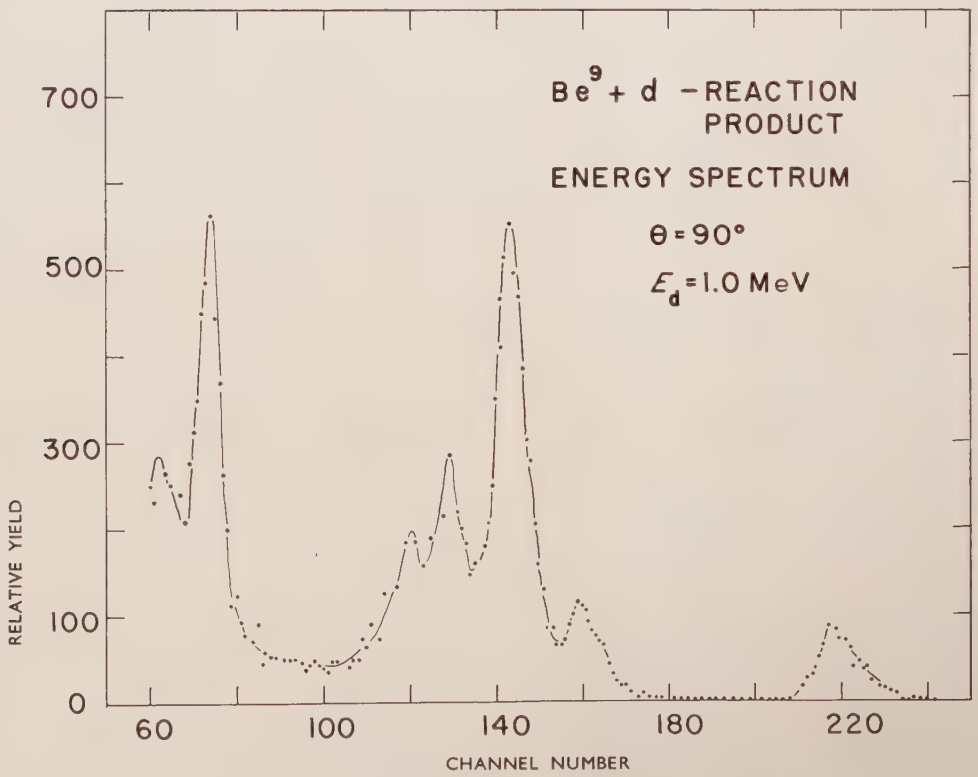

Fig. 6. Integrated pulse height spectrum of reaction products from a thin beryllium target at 90°. The group identifications from right to left are: $Be^9(d,p)Be^{10}$-ground state; $Be^9(d,t)Be^8$-ground state; $C^{12}(d,p)C^{13}$-ground state; $Be^9(d,\alpha)Li^7$-ground state; $Be^9(d,\alpha)Li^{7*}$-first excited state. Lower pulse height groups are deuterons scattered from target backing and from target. Energy resolution is 5 percent for 3.5 MeV protons.

100 picofarad capacitor of the pulse lengthener. As illustrated in fig. 5, the A-B output of the difference amplifier enters a two stage limiter composed of V8 and V9. A second, identical limiter follows, so that the pulse fed through cathode follower V10 to the grid of V11 appears as in fig. 3e. V11, a 6BN6 operated as a constant current source, converts the time duration of the pulse of fig. 3e into a pulse height. The output of the discriminator V14 may be applied to the control grid of V11 to prevent time-to-height conversion of small pulses. The output of the shape circuit is shown in fig. 3f.

3. Circuit Performance

The operation of this detection system has been tested with the products of the Be^9 + d reactions. The energy spectrum of these particles at 90 degrees from the incident beam is shown in fig. 6 for a deuteron energy of 1 MeV. The group in channel 218 contains the protons to the Be^{10} ground state; tritons to the ground state of Be^8 peak in channel 159; protons from the $C^{12}(d,p)C^{13}$ ground state reaction are the large group in channel 143. The carbon is a contaminant on our thin beryllium target. The two groups in channels 129 and 120 are the α-particles to the ground and first excited states of Li^7. The energy resolution of our CsI(Tl) scintillator is 5 percent for protons of 3.5 MeV. Fig. 7 shows the pulse height spectrum of the shape circuit output. The peaks are seen on top of a background which extends throughout the spectrum. The protons are expected to yield the longest decay time, and the protons to the ground states of C^{13} and Be^{10} were shown to correspond to the group of largest height in fig. 7. Similarly the α-particles were expected to have the shortest decay times in CsI(Tl), and the two groups of α-particles to the ground and first excited states of Li^7 were shown to correspond to the α-peak of fig. 7. Since the small group between the alphas and protons corresponds to a group in the energy spectrum of the correct pulse height to be tritons to the ground state of Be^8, they are identified as such. The background underlying the three particle peaks of fig. 7 arises from the presence of pulses in the shape circuit too small to properly saturate the limiters. These pulses could have been eliminated from the output with the discriminator, but instead the discriminator was set to just eliminate the intense elastically scattered deuterons from the output of the shape circuit. Since the background of fig. 7 corresponds to low energy particle groups,

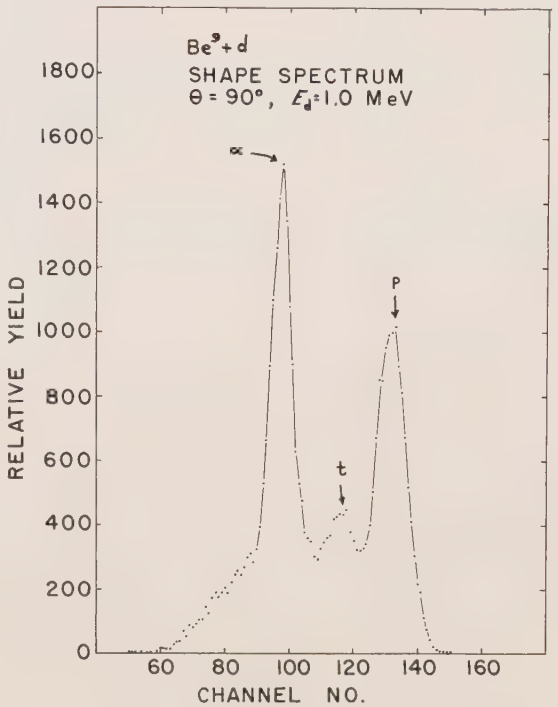

Fig. 7. Output of shape circuit. Experimental conditions are those of fig. 9. Identification of peaks in this output as α, triton and proton and groups was confirmed by noting that they gated the appropriate groups in the energy spectrum. A background, arising from pulses too small to properly operate the converter underlies most of the spectrum. Resolution of α or proton peak is 6.5 percent.

they will be separated from the higher energy groups of interest in the energy spectrum.

Fig. 8 shows a contour plot of the decay times and integrated heights of the CsI(Tl) pulses. The ordinate, relative decay times, represents the relative pulse sizes of the shape circuit output and the abscissa represents the integrated pulses from the detector. The ordinate scale is pulse height in volts at the input to the single channel analyzer. For the data of fig. 8, gating of the pulse amplitude spectrum was restricted to pulses in a 1 volt segment of the decay time spectrum. The data were obtained by scanning the entire decay time range with the 1 volt window of the single channel

analyzer. Each cluster of contours represents a group or adjacent groups of particles. A contour denotes a particular intensity level. The numbers assigned to the group centers are the relative peak intensities of those groups.

figures are not the same. In fig. 8 we see that the decay time resolution of both the α-particles and the protons is 6.5 percent. Protons and tritons are separated by 1.5 times the width of the protons; protons and alphas are separated by 5.5 times the

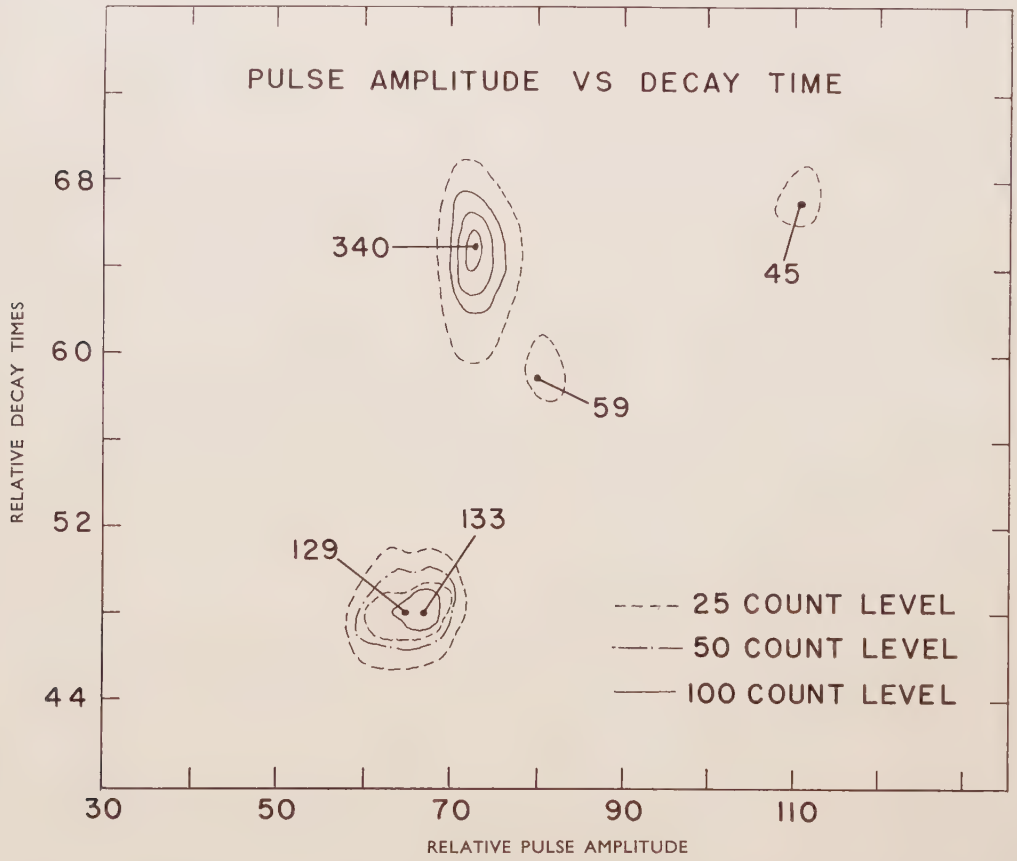

Fig. 8. Surface viewed from above. Coordinate out of the paper is relative yield. Numbers at arrows denote peak yields. Each set of contours represents a group except that at relative decay time = 48, which represents the two groups of fig. 6.

If we view the plot along the direction of constant ordinate, we see a shape spectrum similar to that of fig. 7, plotted against the voltage scale of the single channel analyzer. The 340 count and 45 count groups are the protons, the 59 count group is tritons and the remaining groups are α-particles. An energy spectrum, similar to that of fig. 6, is obtained by viewing the plot along the direction of constant abscissa. The scale of this spectrum is $\frac{1}{2}$ that of fig. 6. The data of figs. 6 and 8 were taken with different amounts of carbon contamination on the target, so that the relative yields of the two

α-width. Since the widths of these groups are a few volts and the noise level of the amplifier which feeds the single channel analyzer is 1 volt, the resolution of the shape circuit itself is somewhat better than 6.5 percent. That the shape output has a weak amplitude dependence is evident from a comparison of the two proton groups, whose ordinates differ by 3 percent. These two groups have energies of 3.5 MeV and 4.9 MeV. The circuit is presently in use to permit the study of the α-particles and tritons in the presence of the protons from the $C^{12}(d,p)C^{13}$ reaction.

NUCLEAR INSTRUMENTS AND METHODS 10 (1961) 333–338; NORTH-HOLLAND PUBLISHING CO.

ANALYTISCHES NAEHERUNGSVERFAHREN ZUR BERECHNUNG AZIMUTAL PERIODISCHER MAGNETFELDER IN KREISBESCHLEUNIGERN

H. NEU† und H. WERNER††

AEG-Forschungsinstitut, Frankfurt/M.

Eingegangen am 20. November 1960

This paper presents formulas for the approximate calculation of the average field and the flutter of the magnetic field arising from two-dimensional rectangular pole configurations. These formulas are useful for design and construction of isochronous cyclotrons and FFAG-synchrotrons. In deriving the formulas the actual field is replaced by a step function and the pole surface is supposed to have a constant magnetic potential.

1. Einleitung

In den letzten Jahren sind neue Typen von Kreisbeschleunigern interessant geworden, deren charakteristisches Merkmal ein in azimutaler Richtung periodisch schwankendes Magnetfeld ist. Zu dieser Gruppe von Beschleunigern gehören das FFAG (fixed field alternating gradient) – Synchrotron[1]) und das Isochron-Cyclotron[2]) (in der angelsächsischen Literatur auch AVF (azimutal varying field) – Cyclotron genannt. Azimutal periodische Felder lassen sich durch bestimmte Profilformen der Polschule der Magnete erzeugen. Eine praktische Aufgabenstellung bei der Planung solcher Maschinen ist die Berechnung der Profil-Dimensionen.

Die Theorie der Bahnbewegung fordert eine bestimmte Abhängigkeit des Magnetfeldes in der Bahnebene (Symmetrieebene des Magneten) von Radius und Azimut. Im Prinzip läßt sich ein dieses Feld erzeugendes Polschuhprofil finden, wenn man annimmt, daß die Oberfläche des Magneten ein konstantes magnetisches Potential (erste Annahme) besitzt[3,4]). Diese Annahme ist dann gerechtfertigt, wenn die Feldstärke nicht in die Nähe der Eisensättigung (etwa 20 kGauß) kommt, d.h. die Permeabilität des Eisens groß gegen eins ist. Praktisch ist aber die Auffindung einer dreidimensionalen Potentialfunktion für solche Profile nicht zu erhoffen.

Reduziert man das dreidimensionale Problem auf ein zweidimensionales (zweite Annahme), indem man geeignete Schnitte durch das Profil legt (beim "Thomas"-Zyklotron sind das z.B. Zylinderflächen, bei "Spiral"- Typen muß man die Schnitte senkrecht zu den Kanten legen) und die Krümmung der Profilkanten vernachlässigt, so lassen sich Näherungslösungen finden. Numerische Näherungslösungen der zweidimensionalen Potentialgleichung sind z.B. von der MURA (Midwest Universities Research Association) auf einer IBM 704 durchgeführt worden[5]).

Eine analytische Berechnung ist aber insbesonders bei der Planung von Beschleunigern sehr viel vorteilhafter. Sie wird möglich, wenn man zusätzlich sich auf "flache" rechteckförmige Profile (genaue Definition im nächsten Abschnitt) beschränkt (dritte Annahme). Man kann das Magnetfeld in der Symmetrieebene durch ein stückweise homogenes Feld mit Sprungstellen, mit anderen

† Jetzt Euratom, Gemeinsames Forschungszentrum Ispra (Italien).

†† Einige vergleichende numerische Ergebnisse entstammen Untersuchungen, die vom Office of Naval Research (Contract Nr. 228(09)) unterstützt wurden.

[1]) K. R. Symon, D. W. Kerst, u.a., Phys. Rev. **103** (1956) 1837.

[2]) Siehe z.B. R. S. Livingston und F. T. Howard, Nucl. Instr. and Meth. **6** (1959) 1.

[3]) F. Ollendorff, Berechnung magnetischer Felder (Springer, Wien, 1952).

[4]) H. Buchholz, Elektrische und magnetische Potentialfelder (Springer, Berlin, 1957).

[5]) L. J. Laslett, Analysis and Computations of magnetic fields arising from two-dimensional pole configurations of interest in spiral-sector accelerator, MURA-Rep. LJL-9.

Worten durch ein stufenförmiges Feld approximieren[6]). Wir wählen die Stufenfunktion so, daß man die Berechnungen explizit durchführen kann. Für das ursprüngliche Magnetfeld erhält man dadurch Näherungsformeln. Wir berichten über ein analytisches Verfahren zur Erlangung von Näherungsformeln für zwei bei der Berechnung der Isochron-Cyclotrons wichtige Kenngrößen des Feldes. 1. Das über die Teilchenbahn gemittelte Feld $<B>$, das die Umlaufzeit der Teilchen bestimmt. 2. Der sogenannte "Feldflutter" f, der ein Maß für die Feldschwankung in azimutaler Richtung ist und die Stabilität der Teilchenbahnen bestimmt. $<B>$ und f werden als Funktionen von Parametern angegeben, die das Profil charakterisieren. Der Parameterbereich entspricht den bei der praktischen Planung von Isochron-Cyclotrons interessierenden Profilen. Die Näherungsannahmen sind, wie oben erläutert: 1. Profiloberfläche ist Potentialfläche 2. zweidimensional 3. näherungsweise stufenförmiger Feldverlauf.

2. Der Mittelwert eines zweidimensionalen trapezförmig periodischen Magnetfeldes

In Fig. 1 ist ein rechteckförmiges zweidimensionales Profil skizziert mit einer Periodenlänge λ, den Polabständen g (gap) und h und der Rückenbreite a. In der Symmetrieebene $y = 0$ besitzt das magnetische Feld nur eine y-Komponente B_y; ihr qualitativer Verlauf ist ebenfalls in Fig. 1 skizziert. Als "flache" Profile sind solche Profile bezeichnet, deren Feldverlauf gekennzeichnet ist durch Abschnitte nahezu homogener Felder abwechselnder Stärke und dazwischenliegender Streufelder (trapezförmige Felder); die Streufelder sollen sich also nicht merklich überlappen.

Es soll der Mittelwert des Feldes in der Symmetrieebene gebildet werden. Der Grundgedanke unserer Näherungsmethode ist, den Feldverlauf $B_y(x)$ durch ein Rechteckfeld (gestrichelte Linie in Fig. 1) zu ersetzen, sodaß der Mittelwert erhalten bleibt. Der Abstand der so entstandenen fiktiven "magnetischen Kante" von der Profilkante ist im Falle, daß sich die Streufelder nicht merklich überlappen (homogene Feldabschnitte), nahezu unabhängig von a und λ, in erster Näherung also nur von g und h abhängig.

Es sei V_0 das magnetische Potential der Profiloberfläche, Null das Potential der Symmetrieebene. Da die Potentialgleichung gegen Ähnlichkeitstransformationen invariant ist, kann man die

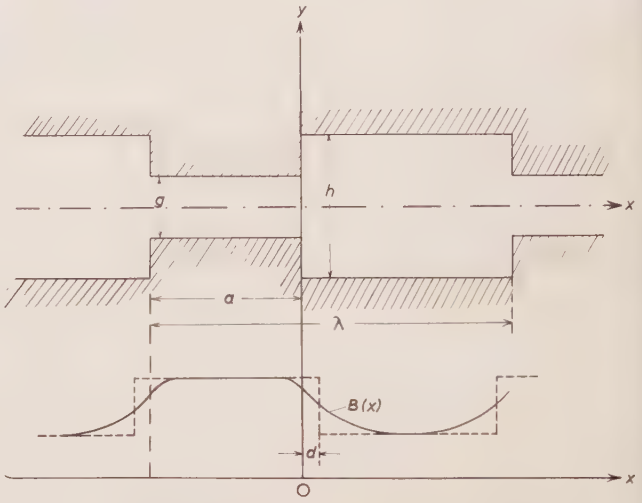

Fig. 1. Zweidimensionales Rechteckprofil mit Magnetfeld in der Symmetrieebene.
– – – – Ersatzfeld (Stufenfunktion)

Einheiten der geometrischen Größen beliebig wählen. Die charakteristischen Größen des durch das Potential erzeugten Feldes hängen nur von deren Verhältnissen ab. Zur Beschreibung der obigen Profilform (Fig. 1) kann man deshalb die Parameter

$$H = \frac{h}{g}; \quad \varkappa = \frac{a}{\lambda}; \quad s = \frac{g}{\lambda}; \quad D = \frac{d}{g} \tag{1}$$

einführen. Unter Benutzung des Ersatzfeldes berechnet sich der Mittelwert zu

$$<B>(x, 0) = B_{\max} \frac{a + 2d}{\lambda} + B_{\min} \frac{\lambda - a - 2d}{\lambda},$$

wobei d noch zu bestimmen ist. Wenn das Profil flach ist, so kann man mit ausreichender Genauigkeit setzen

$$B_{\max} = \frac{2V_0}{g}; \quad B_{\min} = \frac{2V_0}{h}.$$

Für den Mittelwert des Feldes erhält man dann

$$\overline{B(x, 0)} = <B> = \frac{2V_0}{gH} \left[1 + (H - 1)(\varkappa + 2Ds) \right]. \tag{2}$$

[6]) Eine andere Approximation ist angegeben bei B. L. Cohen u.a., Nucl. Instr. and Meth. 6 (1960) 105.

Für rechteckförmige flache Profile ist $D = d/g$ praktisch nur von $H = h/g$ abhängig. Man kann die beschriebene Näherungsmethode aber auch für andere Profilformen, z.B. Profil mit schrägen Flanken anwenden, solange Abschnitte nahezu homogenen Feldes vorhanden sind; D ist dann von zusätzlichen Parametern abhängig.

Für das Rechteckprofil soll D nun berechnet werden. Hierzu untersuchen wir zunächst das Feld einer einzelnen Kante als Grenzfall des Streufeldes eines Profils mit $\lambda \to \infty$, bzw. $s \to 0$.

3. Das Streufeld einer Kante

Das Magnetfeld einer in zwei Richtungen unendlich ausgedehnten Kante (Streufeld) mit der Symmetrieebene $y = 0$ (Fig. 2) erhält man durch

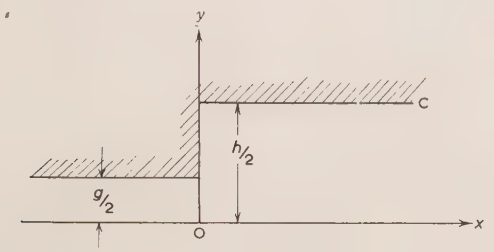

Fig. 2. Kante eines in positiver und negativer x-Richtung unendlich ausgedehnten Profils.

Gradientenbildung des Potentials. Gesucht ist eine Potentialfunktion $V(x,y)$, die für $y = 0$ den Wert 0 und auf der Kurve C einen konstanten Wert V_0 besitzt. Die Aufgabe läßt sich durch konforme Abbildung (siehe Math. Anhang) lösen.

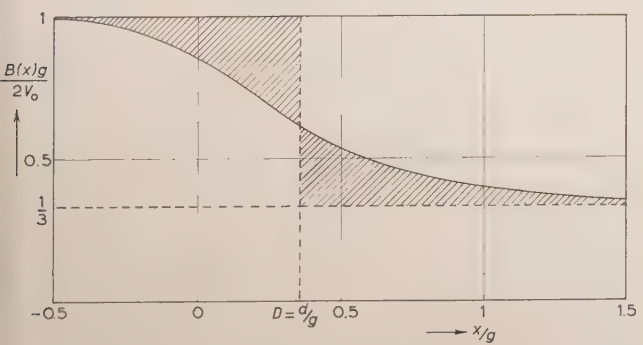

Fig. 3. Quantitativer Verlauf des Feldes einer Kante in der Symmetrieebene für $H = 3$. Profilkante bei $x = 0$, "magnetische" Kante bei $x = d$.

Das Magnetfeld besitzt in der Mittelebene $y = 0$ nur eine y-Komponente:

$$B_y(x, 0) = B(x) = \frac{2V_0}{gt},$$

$$x = \frac{g}{2\pi}\left[H \ln \frac{H+t}{H-t} - \ln \frac{t+1}{t-1}\right]. \qquad (3)$$

Der Parameter t kann die Werte 1 bis H annehmen.

In Fig. 3 ist der Feldverlauf $B(x)$ für $H = h/g = 3$ dargestellt; $2\,V_0/g$ und $2\,V_0/h$ sind die nach (3) asymptotisch erreichten Maximal- und Minimalwerte.

4. Eine Näherungsformel für das mittlere Magnetfeld eines zweidimensionalen periodischen Rechteckprofils

Die Kenntnis des Feldverlaufs (3) gestattet nun, den Abstand d der "magnetischen" Kante von der Profilkante zu berechnen. Wir wollen d so bestimmen, daß für den Grenzfall $s = 0$ der Mittelwert $<B>$ richtig ist. Dies ist dann der Fall, wenn die beiden in Fig. 3 schraffierten Flächen einander gleich sind, d.h. es soll gelten

$$\int_{2V_0/h}^{2V_0/g} [x(B) - d]\, dB = 0 .$$

Man erhält durch elementare Rechnung:

$$D = \frac{d}{g} = \frac{1}{2\pi(H-1)}\left[(H-1)^2 \ln\left(\frac{H+1}{H-1}\right) + 2H \ln\left(1 + \frac{(H-1)^2}{4H}\right)\right]. \qquad (4)$$

In der folgenden Tabelle 1 sind einige Werte von D und D_1 (vergleiche Abschnitt 5) für verschiedene H angegeben.

Tabelle 1

H	1.5	2	2.5	3	3.5	4
D	0.167	0.250	0.310	0.358	0.398	0.433
D_1	0.128	0.175	0.202	0.221	0.234	0.244

Im Bereich $1.5 \leqslant H \leqslant 4$, lässt sich D mit für viele Zwecke ausreichender Genauigkeit annähern durch

$$D(H) \approx 0.04 + 0.1\,H . \qquad (5)$$

Das in (2) eingesetzt ergibt eine einfache Näherungsformel für den Mittelwert eines Rechteckprofils in der Symmetrieebene, die nur noch die Parameter H, $\varkappa$ und s enthält.

$$<B> = \frac{2V_0}{gH}\left[1 + (H-1)(\varkappa + 0.08\,s + 0.2\,Hs)\right]. \quad (6)$$

Numerische Rechnungen, die unter Benutzung eines anderen Approximationsverfahren von einem der Verfasser[7]) auf einer IBM 709 durchgeführt wurden für $H = 2$, $H = 3$, $s \leqslant 0{,}2$ und verschiedene $\varkappa$-Werte, brachten eine Übereinstimmung mit Formel (2) (D-Werte nach (4)) innerhalb von $2^0/_{00}$.

5. Eine Näherungsformel für den Feldflutter eines zweidimensionalen periodischen Rechteckprofils

Der Feldverlauf in der Symmetrieebene eines periodischen Rechteckprofils nach Fig. 1 lässt sich darstellen durch

$$B_y(x, 0) = B(x) = <B>[1 + \phi(x)], \quad (7)$$

wobei ϕ eine mit λ periodische Funktion ist.

Der magnetische "Feldflutter" ist definiert durch

$$f = \left[2\left(\frac{<B^2>}{<B>^2} - 1\right)\right]^{\frac{1}{2}}. \quad (8)$$

Die anschauliche Bedeutung von f erkennt man sofort, wenn man ϕ als eine Fourier Reihe

$$\phi(x) = \sum f_\nu \sin(2\pi x\nu/\lambda)$$

schreibt. Dann folgt aus (8)

$$f = (\sum f_\nu^2)^{\frac{1}{2}}.$$

Der Feldflutter† f ist also im Falle einer sinusförmigen Schwankung identisch mit der relativen Amplitude der Feldschwankung, bei nicht sinusförmigen Feld ist f der Betrag der vektoriellen Summe der Fourier-Koeffizienten f_ν.

Um eine analystische Näherungsformel für f zu bekommen, gehen wir in ähnlicher Weise vor wie bei der Berechnung des mittleren Feldes $<B>$. Anstelle von $B(x)$ tritt jedoch in (8) das Quadrat $B^2(x)$ auf. Wir ersetzen daher das aus (3) gewonnene $B(x)$ durch eine andere Stufenfunktion, das Ersatzfeld B_{ers}, entsprechend der Definition

$$\begin{aligned} x < d_1 &: B_{\text{ers}} = 2V_0/g \\ x \geqslant d_1 &: B_{\text{ers}} = 2V_0/h \end{aligned} \quad (10)$$

und fordern, dass im Grenzfall $s = 0$ der Feldflutter exakt geliefert wird. Daraus folgt, dass d_1 sich mit Hilfe von (3) errechnet aus

$$\int_{2V_0/h}^{2V_0/g} [x(B) - d_1]\,\mathrm{d}(B^2) = 0.$$

Man erhält

$$D_1 = \frac{d_1}{g} = \frac{H-1}{2\pi}\ln\frac{H+1}{H-1}. \quad (11)$$

In Tabelle 1 ist D_1 für einige Werte von H angegeben.

Der Feldflutter errechnet sich aus der Definition (8) mit Hilfe des Ersatzfeldes (10)

$$f = \left[2\left(\frac{2}{<B>^2\lambda}\int_{-a/2}^{(\lambda-a)/2} B_{\text{ers}}^2(x)\,\mathrm{d}x - 1\right)\right]^{\frac{1}{2}}.$$

Man erhält unter Berücksichtigung der Formel (2) für den Mittelwert $<B>$ durch elementare Rechnung

$$f = \frac{H-1}{1 + (H-1)\xi}\left[2\xi(1-\xi) - 4\,\frac{H+1}{H-1}(D - D_1)s\right]^{\frac{1}{2}}. \quad (12)$$

Hierbei ist $\xi = \varkappa + 2\,Ds$; H, $\varkappa$ und s sind die nach (1) definierten Parameter des Profils; D und D_1 können den Näherungsformeln (4) bzw. (5) und (11) entnommen werden. Die Formel (12) ist nur sinnvoll für $\xi < 1$. Dies ist verständlich, da $\xi = \varkappa + 2Ds = (a + 2d)/\lambda$, und unsere Approximation ist sicher nur brauchbar, wenn $a + 2d$ kleiner als die Wellenlänge λ ist.

Trägt man f nach Formel (12) bei konstanten H und $\varkappa$ über s auf, so erhält man eine Kurve, die sich für wachsendes s nach unten krümmt und für ein gewisses endliches s sogar den Wert $f = 0$ liefert (Fig. 4, gestrichelte Kurve). Dies ist natürlich physikalisch unsinnig und weist uns darauf hin, dass nur der erste fast lineare Teil dieser Kurve eine gute Näherung darstellt.

Entwickelt man (12) nach Potenzen von s und berücksichtigt nur das lineare Glied in s, so folgt:

[7]) H. Werner, Schwarz's alternating method for boundary value problems of the third kind, Tech. rep. Univ. of South. Calif.

† In der amerikanischen Literatur wird manchmal die Grösse $F = \frac{1}{2}f^2 = \overline{\phi^2}$ als "Flutter" bezeichnet.

$$f = f_0 (1 - \alpha s), \quad \begin{cases} f_0 = \dfrac{[2\varkappa (1-\varkappa)]^{\frac{1}{2}}}{\varkappa + (H-1)^{-1}} \\ \alpha = \dfrac{(D - D_1)(H+1)(H-1)^{-1} + (2\varkappa - 1) D}{\varkappa (1-\varkappa)} + \dfrac{2D}{\varkappa + (H-1)^{-1}} \end{cases} \tag{13}$$

f_0 ist der exakte Wert für f im Grenzfall $\lambda \to \infty$.

Die Zahlenwerte von f_0 und α für einige Parameterwerte von H und $\varkappa$ gibt Tabelle 2.

TABELLE 2

$H =$		1.5	2	2.5	3	3.5	4
$\varkappa = 0.5$	$f_0 =$	0.283	0.471	0.606	0.707	0.786	0.849
	$\alpha =$	0.913	1.233	1.536	1.815	2.070	2.303
$\varkappa = 0.4$	$f_0 =$	0.289	0.495	0.650	0.770	0.866	0.945
	$\alpha =$	0.812	1.086	1.370	1.642	1.898	2.136
$\varkappa = 0.3$	$f_0 =$	0.282	0.499	0.670	0.810	0.926	1.023
	$\alpha =$	0.755	0.980	1.247	1.521	1.789	2.046

Die Werte für α in Tabelle 2 lassen sich mit einer Genauigkeit von einigen Prozent darstellen durch eine Funktion

$$\alpha (H, \varkappa) \approx (0.33 + 0.55\varkappa) H ,$$

so dass man zu einer vereinfachten Formel für f im Bereich $1.5 \leqslant H \leqslant 4$ und $0.3 \leqslant \varkappa \leqslant 0.55$ (dieser Parameter-Bereich interessiert beim Isochron-Cyclotron) kommen kann:

$$f(H, \varkappa, s) \approx \frac{[2\varkappa (1-\varkappa)]^{\frac{1}{2}}}{\varkappa + (H-1)^{-1}} \left[1 - (0.33 + 0.55\varkappa) Hs\right]. \tag{14}$$

Die den Formeln (13) bzw. (14) entsprechenden Geraden halten wir für eine bereits in einem grösseren s-Bereich gültige Annäherung (siehe Fig. (4)).

Die Geraden stossen schliesslich für gewisse grössere s zu negativen Werten von f vor (siehe Fig. 4), während die exakten $f(s)$ Kurven sich dem Wert $f = 0$ nur asymptotisch nähern. Sie ergeben für festes $\varkappa$ und H als Parameter eine Schar mit einer Enveloppe E. Es scheint, als stellt diese Enveloppe bereits eine Annäherung an die Einhüllende E' der exakten $f(s)$-Kurven für $\varkappa = \text{const.}$ und H als Parameter dar. Das Vorhandensein einer solchen Einhüllenden E' ist durchaus plausibel.

Für feste $\varkappa$ und s strebt f einem Grenzwert zu, wenn man H gegen unendlich gehen lässt. Das bedeutet nämlich, dass bei festen Werten für Wellenlänge λ,

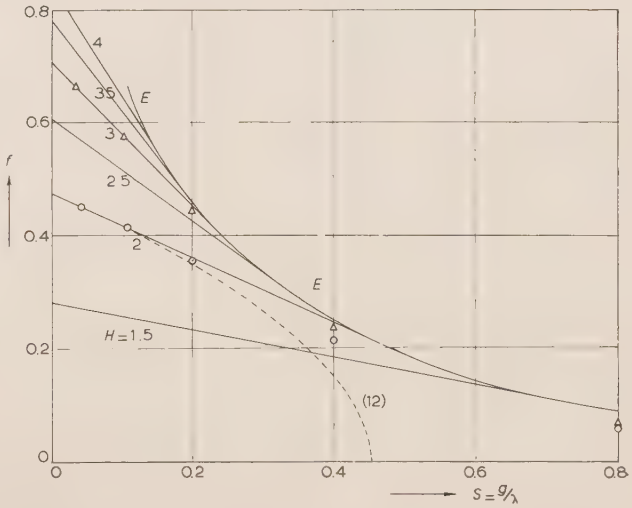

Fig. 4. Feldflutter f nach (14) für $\varkappa = 0.5$ und verschiedene $H = h/g$; – – – – berechnet nach (12) für $H = 2$; ⊙ Rechnung mit IBM 709 für $H = 2$: △ dgl. für $H = 3$.

gap g und Rückenbreite a durch Vergrösserung von h bzw. H der Flutterwert f nicht beliebig sondern nur bis zu einem gewissen Grenzwert erhöht werden

kann. Um den Grad der Annäherung von E an E' zu ermitteln, müssten allerdings noch weitere numerische Berechnungen durchgeführt werden.

Einige Vergleichsrechnungen, von denen einige Ergebnisse in Fig. 4 eingetragen sind, wurden im Western Data Processing Center (WDPC) an der University of California in Los Angeles durchgeführt, während einer der Autoren in Californien weilte. Wir möchten für die uns gebotene Möglichkeit, eine IBM 709 zu benutzen, und für die freundliche Unterstützung durch die Angehörigen des WDPC unseren Dank zum Ausdruck bringen.

Herrn Dr. K. Steimel, Leiter der AEG-Forschung danken wir für die Anregung und das rege Interesse an dieser Arbeit.

Mathematischer Anhang

Wir bilden den Raum zwischen der Kurve C der Fig. 2 und der x-Achse (komplexe z-Ebene) konform auf die obere Hälfte der komplexen Ebene $w = u + iv$ ab, etwa so, dass die x–Achse in die positive u-Achse, die Kurve C in die negative u-Achse übergeht. Man findet, dass die inverse Abbildung $z(w)$ geleistet wird durch†

$$\frac{2}{g} \cdot z(w) = i + \frac{1}{\pi}\left(H \ln \frac{H + t}{H - t} - \ln \frac{1 + t}{1 - t}\right),$$

$$t^2 = \frac{H^2 w + H^2}{w + H^2},$$

mit $t(0) = 1$ zur Festlegung des Wurzelvorzeichens und des Hauptwerts für den Logarithmus.

In der w-Ebene ist

$$V(u, v) = \mathscr{R}_e\left(\frac{V_0}{\pi i} \ln w\right)$$

eine Potentialfunktion, die in der z-Ebene, durch $z(w)$ übertragen, die geforderten Randbedingungen $V = 0$ für $y = 0$ und $V = V_0$ auf der Kurve C erfüllt.

† siehe[4]), S. 69–74.

NUCLEAR INSTRUMENTS AND METHODS 10 (1961) 339–342; NORTH-HOLLAND PUBLISHING CO.

FADING IN NUCLEAR EMULSIONS INDUCED BY ACID AGENTS

HANS ACKERMANN and HELMUT FAISSNER†

Physikalisches Institut der Universität Tübingen, Tübingen, Germany

Received 10 January 1961

β- and γ-ray induced background in nuclear emulsions of moderate and low sensitivity has been removed after the irradiation by treating with acid agents. The dependence of this background eradication on the pH of the solution, the duration of treatment and other parameters was studied in some detail. The eradication is uniform in depth and easily adjustable. For instance, it is possible to suppress β- and γ induced fog without destroying α-tracks. A stronger treatment removes the latent images of α-tracks too. The treatment causes no irreversible changes: after the removal of the acid medium the emulsions have their original sensitivity again. Under certain precautions, the acid can be brought into the emulsion before irradiation. This has the effect of an apparent desensitization. It has been ascertained, however, that also in this case the formation of the latent image is not impeded. Rather the active centres are removed within a few minutes after irradiation.

1. Introduction

The problem of fading in nuclear emulsions has attracted the attention of many authors[1–5]). It is known that oxidizing agents remove the latent image. This is also true for atmospheric oxygen, provided there is sufficient moisture present. All these facts are well accounted for by a fading theory of Albouy and Faraggi[6]). They assume that in the presence of moisture, silver atoms in the sensitivity centres are oxidized to silver ions:

$$4\,\mathrm{Ag} + \mathrm{O_2} + 2\,\mathrm{H_2O} \rightarrow 4\,\mathrm{Ag^+} + 4\,\mathrm{OH^-}\,. \qquad (1)$$

Generally, fading is an undesired process. However, it may be utilized for eradication of background in emulsions which have been stored. For this purpose, strongly oxidizing agents have been used, such as chromic acid[7,8]), $KMnO_4$[9,10]) and H_2O_2[11,12]). The danger with these methods is that the sensitivity of the emulsion may be reduced. It is also possible to eliminate the background, without loss of sensitivity, by warm water vapor[13–15]). But it is not easy to get an eradication uniform with depth for thicker emulsions.

According to eq. (1) there is a third possibility to induce fading[6]): instead of adding O_2 or H_2O on the left hand side, one can remove OH^- on the right hand side. This method should not impair the sensitivity of the emulsion. Moreover, as the pH is easily adjustable, it is especially suited for differential background eradication, for instance for suppressing γ-ray background without damaging tracks from low-energy protons or other heavily ionizing particles. This has been noted also by Benisz and Kierzkowski[16]).

Actually, our first observations have been made by accident: during a study of (γ,α) processes, performed at the Tübingen 16 MeV betatron, a drop of $Th(NO_3)_4$-solution (pH = 1.5) was brought onto the surface of an irradiated Ilford K.0 plate (200 μm thick), in order to compare the α-tracks expected from photo-reactions with those from radioactive decay. After development, the region soaked with $Th(NO_3)_4$-solution was almost completely free of γ-background, whereas the other parts of the plate were nearly opaque. On the other hand, the

† Now with CERN, Geneve 23, Switzerland.

[1]) K. B. Mather, Phys. Rev. **76** (1949) 486.
[2]) W. Hälg and L. Jenny, Helv. physica Acta **24** (1951) 508.
[3]) E. Schopper, S. Magun and W. Braun, Z. Naturforschg. 6a (1951) 338.
[4]) W. Lohmann, Z. Naturforschg. 11a (1956) 592.
[5]) S. Deutsch and E. Picciotto, Nuovo Cim. **6** (1957) 953.
[6]) G. Albouy and H. Faraggi, J. Phys. Radium **10** (1949) 105.
[7]) C. F. Powell et al., J. Sci. Instr. **23** (1946) 102.
[8]) P. Demers, Canad. J. Res. **25** (1947) 223.
[9]) L. N. Liebermann and H. H. Barschall, Rev. Sci. Instr. **14** (1943) 89.
[10]) J. De Felice, Phys. Rev. **74** (1948) 1244.
[11]) H. Yagoda and N. Kaplan, Phys. Rev. **73** (1948) 634.
[12]) A. Papkow, Z. Naturforschg. 11a (1956) 758.
[13]) M. Wiener and H. Yagoda, Rev. Sci. Instr. **21** (1950) 39.
[14]) G. Albouy, C. R. Acad. Sci. Paris **230** (1950) 1351.
[15]) B. Stiller, M. M. Shapiro and F. W. O'Dell, Rev. Sci. Instr. **25** (1954) 340.
[16]) J. Benisz and Z. Kierzkowski, Acta Phys. Polon. **18** (1959) 527.

Th-α-tracks did clearly show up. That even the formation of α-tracks can be impeded by the acid $Th(NO_3)_4$-solution was demonstrated by another observation: the number of α-tracks per unit area was found to be independent of the time between loading with $Th(NO_3)_4$-solution and development. This means that only during a short time α's are registered by the emulsion; as it was proved later, this occurs just during presoaking and development.

Initiated by these observations, a systematic study was undertaken using several Ilford emulsions irradiated with γ- and β-rays (Sec. 2). Later on the eradication of α-tracks was studied as well. It was ascertained that the accelerated fading results only from the low pH of the solutions (Sec. 3). The influence of other parameters, like duration of treatment, temperature, etc., was studied in some detail too.

The measurements show that fading can be induced in emulsions of low sensitivity by acid agents in a widely adjustable manner. A practical application is differential eradication with fairly arbitrarily selectable detection threshold (Sec. 4). Preliminary results of this work have been already communicated elsewhere[17]).

2. Experimental Procedure

2.1. EMULSION TYPES

For the systematic studies, Ilford emulsions of the types K.0, K minus 1 and K minus 2 were used. Some tests were performed with the highly sensitive K.5 emulsion. In this emulsion β- and γ-ray induced background could not be removed efficiently. However, natural fog accumulated in several month's storage could be reduced to a tolerable level.

The thickness was usually 200 μm. Only when the depth-dependence of the eradication was tested (Sec. 3.5), thickneses up to 600 μm were used.

2.2. IRRADIATION AND PROCESSING OF PLATES

The photoplates were irradiated with electrons or bremsstrahlung from the 16 MeV Tübingen betatron. Doses between 250 and 1000 roentgen (r) were used. α-tracks were provided by a source of natural radium. After treatment with the agent in question, the plates were washed in distilled water and developed with either Ilford ID.19 or amidol, using a standard temperature-cycle method of development[18,19]).

2.3. MEASUREMENTS

As a convenient measure of β- or γ-background, the number of blobs per unit volume was counted. The unit volume had 144 μm² area and 10 μm depth. For each plate the blob density was measured at 20 different places and over the entire depth, omitting only a few μm near each surface where fog was often induced by mechanical damage. The errors of measurements were negligible; the main uncertainty arose from the limited reproducibility of processing conditions.

The density of α-tracks was determined by blob-counting.

3. Results

3.1. INDEPENDENCE OF CHEMICAL STRUCTURE

A number of acid agents were tried, namely HCl, H_2SO_4, HNO_3, HCOOH, CH_3COOH and $Th(NO_3)_4$-solution. It was ascertained that the eradication depends only upon the pH. The chemical structure is irrelevant, provided only there are no secondary reactions with the components of the emulsion.

3.2. DEPENDENCE ON THE pH

The dependence of blob density on HNO_3-concentration is given in fig. 1. Already very low

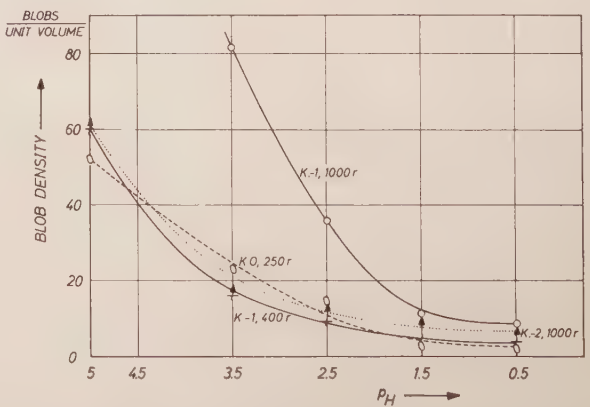

Fig. 1. Blob densities in γ-irradiated plates as a function of the pH of the eradication bath (HNO_3). The duration of treatment was 3 hours in all cases.

concentrations cause appreciable eradication. (Even our distilled water of pH = 5 had a definite effect,

[17]) H. Ackermann, Phys. Verh. **10** (1959) 15.
[18]) M. M. Shapiro, Handbuch d. Physik **45** (1958) 342.
[19]) M. Teucher, Ergebn. exakt. Naturwiss. **28** (1955) 407.

although this might in part be due to direct action of H_2O, according to eq. (1).) At higher concentrations there is saturation.

3.3. INFLUENCE OF THE DURATION OF TREATMENT

The duration of treatment was varied, using HNO_3 of 0.2% concentration (pH = 1.5) at 20°C. The results are given in fig. 2: after a rapid decrease

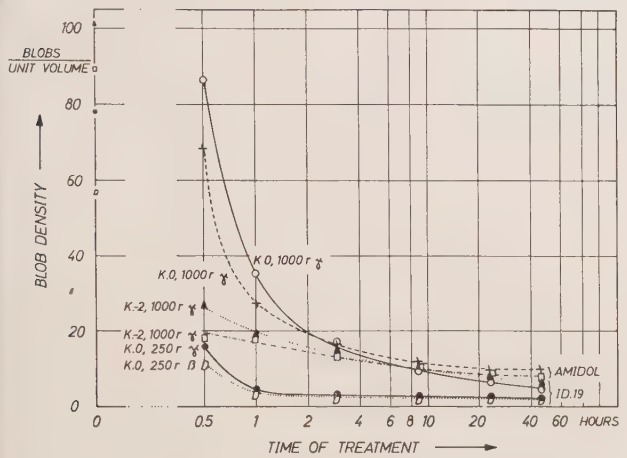

Fig. 2. Blob densities in γ- or β- irradiated plates as a function of duration of treatment in 0.2% HNO_3 (pH = 1.5).

within the first three hours, the blob density tends to a constant value which depends upon emulsion type and radiation dose. This is also true for the 1000r, K.0 plates which were completely black, when untreated, and which do not reach saturation in fig. 2: another set of measurements showed constant blob density between 26 and 212 hours.

3.4. INFLUENCE OF TEMPERATURE

The temperature influence is small; a slight increase in eradication between 5°C and 27°C was just noticeable.

3.5. UNIFORMITY OF ERADICATION

The blob density was independent of the depth when the treatment lasted longer than 30 minutes. Even emulsions as thick as 600 μm showed good uniformity.

3.6. PRESERVATION OF SENSITIVITY

The treatment by acid agents causes no loss of sensitivity. This was proved by subsequent exposure.

3.7. INFLUENCE OF RADIATION TYPE AND DEVELOPER

As it was anticipated, there is no significant difference between β- and γ-irradiated plates (see fig. 2). α-tracks in K.0 and K minus 2 emulsions are eradicated almost as easily as β- and γ-background: after one hour soaking in 0.2% HNO_3 they have completely disappeared.

Replacement of the Ilford ID.19 developer by amidol made no essential difference.

3.8. APPARENT DESENSITIZATION

β- and γ-background as well as α-tracks can be suppressed by soaking the plates prior to exposure. In this case one has to prevent the acid from evaporating again. This can be achieved by adding 25% glycerine to the solution. As it is demonstrated by fig. 3, the blob density in emulsions treated in this way and developed 12 hours after the exposure is nearly independent of radiation dose. The plates appear as if they were desensitized.

Actually, the formation of the latent image is not impeded. Rather, it was destroyed again during the time between exposure and development. By

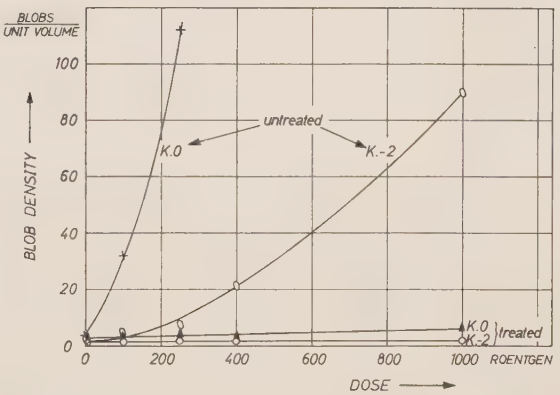

Fig. 3. Blob densities in K.0 and K minus 2 emulsions with and without soaking in (0.2% HNO_3 + 25% glycerine) before exposure as a function of γ-ray dose.

varying this time the following results were obtained for plates presoaked with HNO_3 (pH = 1.5) before exposure to α's:

a. Development in (alkaline) ID.19 immediately after exposure gives tracks of the same blob density as in untreated plates.

b. 3 minutes of waiting time is sufficient to

reduce the blob density to $\approx 10\%$ of this value.

c. After ≈ 7 minutes, the tracks are eradicated.

This proves that the apparent desensitization by low pH which has been noted also by other authors[20,21]) is in fact a result of the mechanism of induced fading discussed in the preceding paragraphs.

4. Conclusions

The present measurements bear out the expectations[6,18,19]) that fading can be induced by treatment with acid agents. Thus they may be considered as another confirmation of the fading mechanism as proposed by Albouy and Faraggi. Actually, the mechanism as given in eq. (1) is an oversimplification. More recent theories of the photographic process[22]) consider $2F^+$-centres as sensitivity centres. (A $2F^+$-centre is composed of a triplet of brominion vacancies and two electrons.) This complication is rather irrelevant in the present context, because in any case there is an oxidation of sensitivity centres.

The treatment with acid agents tends to suppress strongly the slightly activated centres in AgBr crystals. On the other hand, grains which had received more than a threshold value are developed with almost the same probability as if the treatment had not taken place. Consequently, the opacity-ionization curve for treated emulsions is much steeper than for untreated ones. Therefore, very different tracks may be produced for particles, which differ only slightly in ionization.

Up to now the main application of the reported effect was made in studies of fission of heavy nuclei, recently performed by our group. K minus 2 and L.0 emulsions loaded with U, Th, Pb, Tl and Bi were exposed to the external 600 MeV proton beam of the CERN synchrocyclotron[23]). Then they were treated for about one hour in HNO_3-solution of 0.2%. Although there were up to 200 fissions per microscope field for U, the background from protons was still negligible. Another series of measurements was concerned with the ionization behaviour of fission fragments near the origin[24]). Due to the steepness of the opacity-ionization curve, a fairly small change of the ionization produced a big effect in opacity. Thus it could be established that in about 50% of all cases, either the light fragement or the heavy one goes through an ionization maximum before it shows the familiar monotonic decrease with decreasing velocity.

Acknowledgements

We are indebted to Prof. H. Krüger for his constant interest and advice. The irradiations at the betatron have been made possible through the kindness of Dozent Dr. Breitling. We wish to thank our scanners Mrs. W. Andresen and Mrs. E. Martius for their reliable work. Finally it is a pleasure to acknowledge the co-operation of F. Gönnenwein and the other members of the Tübingen emulsion group. This work has been made possible by the financial support granted by the Bundesministerium für Atomkernenergie und Wasserwirtschaft.

[20]) J. Catala and J. Casanova, Anales real soc. espan. fisy quim. Ser. A **53** (1957) 169 (cited after Nucl. Sci. Abstr. **12** (1958) Nr. 3801).

[21]) M. Nicolae, Acad. rep. pop. Romine, Inst. fiz. atomică **9** (1958) 39 (cited after Nucl. Sci. Abstr. **13** (1959) Nr. 12600).

[22]) H. Pick, Naturwiss. **38** (1951) 323.

[23]) H. Faissner, H. Schneider and G. Wolf, Phys. Verh. **10** (1959) 133; Nucl. Phys. (in press).

[24]) H. Faissner, F. Gönnenwein, H. Schneider and G. Wolf, Z. f. Physik (in press).

NUCLEAR INSTRUMENTS AND METHODS **10** (1961) 343–347; NORTH-HOLLAND PUBLISHING CO.

A COUNTER TELESCOPE SYSTEM FOR FAST NEUTRON STUDIES

R. N. GLOVER, K. H. PURSER and E. WEIGOLD

Department of Nuclear Physics, Australian National University, Canberra

Received 31 January 1961

The design of a counter telescope to measure angular distributions in the range 0°–150° for neutron induced reactions is outlined. The operation and performance of the equipment which includes, in addition to the usual circuitry, fast coincidence equipment based on the detection of the associated α-particle from the d(t,n)α reaction and equipment to identify charged particles of different mass is described.

1. Introduction

The design of counter telescopes for use in neutron experiments and associated techniques have been reviewed earlier[1–3]). Telescopes of small solid angle have been used for angular distribution measurements but are mainly of the type in which forward angles are of particular interest.

The present telescope was specifically designed to allow measurements at backward angles. In addition to the usual circuitry, fast coincidence circuitry based on the detection of the recoil α-particle from the d(t,n)α reaction and equipment to separate particles of different mass were used. The result is a sensitive and versatile system for the study of neutron induced reactions leading to the emission of charged particles[4,5]).

2. Design

Figure 1 shows a cutaway view of the telescope which differs from previous designs in that the targets were mounted on a strip (A) which moved vertically, instead of a rotatable wheel, e.g.[1,2,6,7,8]). Thus the bulk of the telescope could be reduced and neutron scattering at all angles in the range 0°–150° made negligible (approximately 2%) by reducing the wall thickness over the area (B) surrounding the target. The important dimensions were:

distance from target to defining stop 15.1 cm;
diameter of target 2.5 cm;
diameter of defining stop 2.5 cm;
distance from neutron source to target (see fig. 2) 13.1 cm.

The angular resolution varied, since the target rotated with the telescope, from ± 7° at 30° to ± 4° at backward angles. The target strip held thick and thin polythene radiators, the target under study, a background blank and a small Po^{210} α-source used to check the gain of each proportional counter. Stable operation of these counters for periods of three weeks or more was realized by continuously circulating the counter gas (90% dry argon + 10% purified CO_2 at a total pressure of 11 cm Hg) through a 20 litre glass reservoir by means of a heated chimney.

The NaI crystal gave 5.5% resolution for 15 MeV recoil protons, no deterioration being observed over a period of several months.

3. Operation

Figure 2 is a simplified diagram of the target area, the electronic equipment and its operation. Detection of recoil α-particles from the t(d,n)α reaction in a solid angle of 0.057 sr defined in space

[1]) C. H. Johnson and C. C. Trail, Rev. Sci. Inst. **27** (1956) 468.
[2]) S. J. Bame, E. Haddad, J. E. Perry and R. K. Smith, Rev. Sci. Inst. **28** (1957) 997.
[3]) C. H. Johnson, Fast Neutron Physics, Part I (1960) pp. 247–295.
[4]) R. N. Glover and K. H. Purser, Nucl. Phys. **24** (1961) 431.
[5]) R. N. Glover and E. Weigold, Nucl. Phys. **24** (1961) 630.
[6]) F. L. Ribe and J. D. Seagrave, Phys. Rev. **94** (1954) 934.
[7]) J. R. Risser, J. E. Price and C. M. Class, Phys. Rev. **105** (1957) 1288.
[8]) G. Marcazzan, A. M. Sona and M. Pignanelli, Nuovo Cimento **10** (1958) 155.

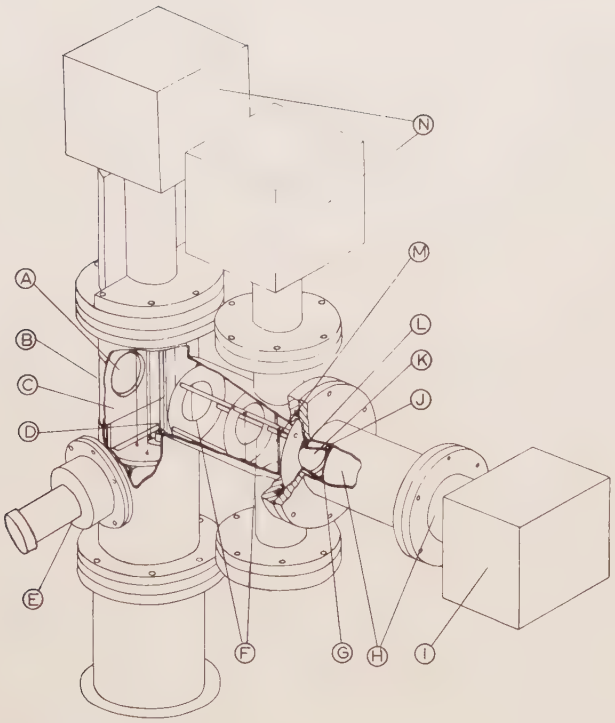

Fig. 1.

A Target strip pressed from 0.008″ thick tantalum and containing four $1\frac{1}{4}$″ holes for targets. The edges were perforated like 35 mm film.

B Steel front wall 0.015″ thick over the area surrounding the target, and lined with 0.010″ thick gold.

C Target strip box. The target strip was guided by two grooved steel bars which formed the sides of the box. To minimise neutron scattering at 90° the box was cut away and the guides milled to 0.020″ thick where the target was exposed.

D Front proportional counter; central wire 0.008″ thick tungsten with nickel sleeves to limit the sensitive length; electrical connection via a spring loaded brass plate and Kovar seal.

E External drive for sprocket fitting target strip perforations.

F Tantalum stops.

G NaI crystal held on photomultiplier face (H) by piano wires soldered into sides of reflecting cone (J).

H Dumont 6292 photomultiplier.

I Cathode follower.

J Light reflecting truncated cone coated with MgO[9]).

K Thin gold foil over mouth of cone.

L Tantalum stop defining telescope solid angle.

M Second proportional counter similar in design to first.

N Proportional counter head amplifiers.
Not shown: small plate glass window enabling accurate positioning of targets by visual alignment.
Lead gaskets used instead of 0-rings.

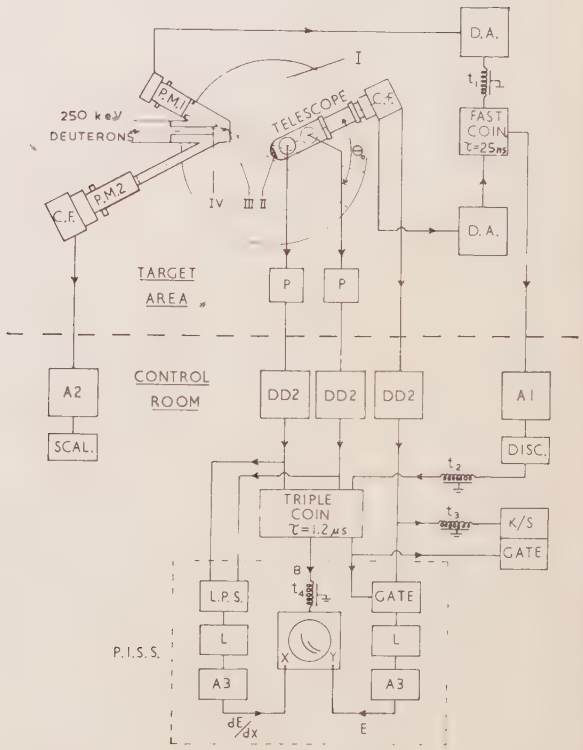

Fig. 2.

I Angular distribution table.

II Target under study.

III Tritium target.

IV Stop, diam 2 mm, at 2.5 cm from tritium target to prevent movement of defined neutron cone.

PM1 Recoil α-particle detector; plastic scintillator 0.05 mm thick on RCA 6655A photomultiplier.

PM2 α-particle flux monitor; CsI crystal 0.05 mm thick on Dumont 6292 photomultiplier.

CF Cathode follower.

P Preamplifier.

DA Distributed amplifiers Hewlett Packard Types 460A + B.

DD2 Fairstein double delay line amplifier.

A1, A2 Conventional high gain amplifiers.

P.I.S.S. Particle identification and selection system.

LPS Least pulse selector.

L Pulse lengthener.

A3 Long tailed pair amplifier.

B Brightening pulse to cathode ray tube grid.

a narrow neutron cone of angular width 13° within which the target under study had to be located. The addition of the fast coincidence requirement between the α-particle detector and the telescope scintillation counter prior to the usual triple coincidence provided a "clean" neutron beam and eliminated, except near 0°, substantial background due to protons (produced by neutron bombardment of the NaI crystal) travelling through the proportional counters towards the front of the telescope.

Rather special conditions were imposed on the fast coincidence circuitry. Firstly a fast resolving time was unnecessary since the flight time through the telescope of protons in the energy range 1–15 MeV varied from 4–16 ns. Secondly the coincidence/singles output pulse ratio had to be large for reliable operation with a time spread of pulses at one input. Thirdly one input had to handle a very high count rate from the recoil α-particle detector, and as a corollary photomultiplier noise had to be kept to a minimum. E180F limiters gave 2.2 V output pulses using 200 Ω shorted stubs and were shown to be capable of handling count rates as high as 3×10^6/sec. The 6BN6 fast coincidence circuit was operated as described by Green and Bell[10]). A coincidence/singles ratio of 15:1 was attained with a specially selected 6BN6. The resolving time was approximately 25 ns.

The provision of the fast coincidence circuitry alters the conventional setting up procedure[3]). The major differences are briefly as follows:

(a) The timing of the fast coincidence equipment was set for detection of the widest possible range of proton energies by displaying the gated output from the amplifier A1 on the kicksorter and adjusting the delay t_1 till the A1 pulse distribution, which depends on the overlap of the 15 MeV proton and α-particle pulses, lay just above the discriminator bias level required to reject singles.

(b) The target was set in the neutron cone by maximising, for each adjustment of the angular distribution table in turn, the count rate from the infinitely thick polythene radiator. To make the count rate particularly sensitive to position a mask was used to give an annular radiator of external diameter slightly greater than that of the target to be studied.

To prove that angular distributions were measured accurately, the distribution of recoil protons from the thin radiator and the shape of the energy spectrum at various angles on each side of the 0° position were recorded. Because of the finite resolution of the telescope, and $\cos^2\theta$ dependence of the recoil proton energy, the computer SILLIAC was used to calculate the spectrum shape and total counts therein relative to 0° for several angles. Good agreement was obtained between the experimental results and the computations. The minimum proton energy detected was determined by comparing the ratio of the observed counts at 65° and 0° with ratios predicted from the SILLIAC spectra, assuming different minimum energies. An energy of 1 MeV was found to be a reasonable lower limit if 15 MeV protons were also to be detected.

4. Fast Neutron Flux Measurement

Neutron flux can be measured absolutely to an accuracy of $\pm$ 2% by detection of the recoil α-particles in a small known solid angle[11]). The necessary calculations for the present geometry and tritium targets were carried out as described by Benveniste *et al.*[12]). Absolute measurements can also be made with a counter telescope to an accuracy of $\pm$ 2% by detection of recoil protons from a thin radiator[2]). In the present case these two independent methods consistently gave agreement within 3%. Thus it is felt that the flux was measured accurately and conversely that all protons recoiling within the solid angle of the telescope were detected.

It was noted that when instead the slow (energy) pulse from the telescope scintillation counter was used as the third input to the triple coincidence unit, the recoil proton count rate increased by approximately 10%. These additional proton counts were shown to have no associated α-particle. It was concluded that the effect was due to elastically scattered neutrons, probably scattered from the target assembly since the mass of material present

[9]) A. E. Souch and D. R. Sweetman, Rev. Sci. Inst. **29** (1958) 794.

[10]) R. E. Green and R. E. Bell, Nucl. Instr. **3** (1958) 127.

[11]) J. Benveniste, A. C. Mitchell, C. D. Schrader and J. H. Zenger, UCRL 5619 (1959), Nucl. Instr. and Meth. **7** (1960) 306.

[12]) J. Benveniste and J. H. Zenger, UCRL 4266 (1954).

was minimised only in the direction of the neutron cone. This point illustrates the advantage of a "clean" neutron beam.

5. Particle Identification

The smaller of two coincident ionisation loss (dE/dx) pulses from the proportional counters and the energy (E) pulse from the scintillation counter were applied to the X and Y plates of a cathode ray tube and a brightening pulse applied to the grid when a triple coincidence occurred (see dashed section of fig. 2). Since the mass of a charged particle is roughly proportional to the product $E(dE/dx)$, particles of different mass produce separate hyperbolae. In the energy range 1–10 MeV these hyperbolae were found to be of the approximate form $(E + 1.5)\,(dE/dx)$ (i.e. a constant 1.5 MeV added to the energy scale).

The equipment was set up for the identification of protons and deuterons by exposing thick polythene and deuterated polythene radiators simultaneously in the neutron cone and filming the resultant spot distribution on the cathode ray tube. The product $(E + 1.5)\,(dE/dx)$ was obtained for each reprojected spot from a set of calculated hyperbolae. Figure 3 shows typical separations. Hence an analysis chart was obtained delineating areas within which a spot had to lie to be identifiable unquestionably as a proton or deuteron. Particle identification was swift. Extraction of energy spectra by addition of the dots in each channel was relatively slow, but in the present case was limited by the rate of accumulation of experimental data. Figures 4 and 5 show typical frames of film.

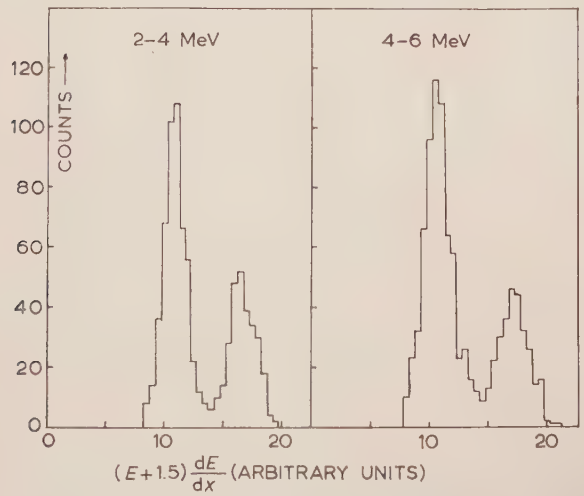

Fig. 3. Separation of protons from deuterons for the energy ranges 2–4 MeV and 4–6 MeV.

Fig. 4. Typical frame from the neutron bombardment of aluminium, showing the proton and deuteron hyperbolae and random events clustered near the origin.

Fig. 5. Typical frame illustrating background reduction achieved by rejection of random events.

6. Counter Telescope Background

Particle identification reduces background firstly by sharing the total background among the different particle types present and secondly by eliminating random events, since these generally consist of small E and small dE/dx pulses and therefore seldom satisfy the conditions for identification as a particle. Figure 5 illustrates the rejection

of random events and the large background reduction thus achieved. As a result it was possible to operate at high neutron flux (approximately 2.5×10^6 n/sec in the defined cone), thus decreasing considerably the time required to carry out an experiment, and yet to observe without difficulty protons of energy as low as 1 MeV.

Proton background may be due to:

(i) protons produced by neutron induced reactions in the NaI crystal traversing the telescope towards the front;

(ii) protons from the gold absorber lining the front wall (to remove protons from the thin steel wall);

(iii) protons from reactions in the gas of the front proportional counter.

Point (i) explains the background increase noted below 4 MeV in the 0° spectrum (fig. 6). The contrasting decrease at all other forward angles e.g. 40° spectrum, is due to the elimination of such protons by the fast coincidence requirement since there will be no associated recoil α-particle when the NaI crystal rotates out of the defined neutron cone. The decreasing background below 4 MeV suggested the effect of the Coulomb barrier of a heavy nucleus. Background spectra at all forward angles including 0° exhibited two maxima and a minimum around 7 MeV. Such a spectrum was predicted by Nemeth[13]) for protons evaporated from a heavy oscillating nucleus. The strong angular dependence of the total background suggested that the direct interaction mechanism predominated. The remaining background is therefore probably due to proton emission from the platinum target backing and gold absorber. Relatively unfavourable Q-values, and the background decrease below 4 MeV suggest that effect (iii) is not important. The increase at low energy at backward angles, e.g. 120° spectrum, was caused by a small contribution of random events at high flux because of much increased count rates in the scintillation and second proportional counters due to their proximity to the tritium target. The deuteron background was an order of magnitude smaller. The peak at forward angles may be due to the (n,d) pick-up reaction in platinum and/or gold.

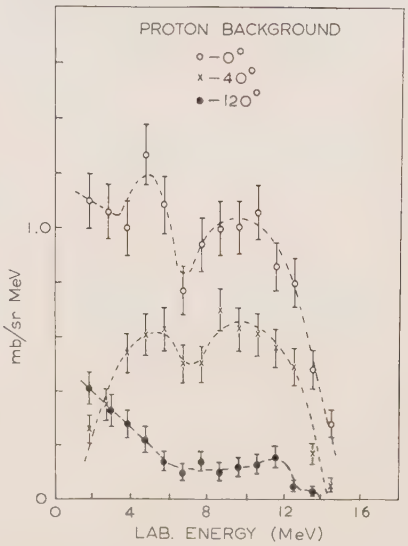

Fig. 6. Proton background spectra. The quoted cross sections are related to a 7 mg/cm² aluminium target of total mass 45.7 mg. 1.0 mb/sr·MeV is approximately equivalent to 0.01 counts/sec·MeV at a flux of 8×10^8 neutrons/sec into 4π.

Acknowledgment

The authors are indebted to Professor E. W. Titterton for his interest and encouragement. One of us (E.W.) would like to acknowledge the award of a scholarship from the Australian Institute of Nuclear Science and Engineering.

13) J. Nemeth, Nucl. Phys. 6 (1958) 686.

NUCLEAR INSTRUMENTS AND METHODS **10** (1961) 348–352; NORTH-HOLLAND PUBLISHING CO.

AN IMAGE INTENSIFIER-SCINTILLATOR DEVICE FOR DETERMINATION OF PROFILES AND IMAGES OF WEAK BEAMS OF IONIZING PARTICLES OR X-RAYS†

LAWRENCE W. JONES and MARTIN L. PERL

Harrison M. Randall Laboratory of Physics, The University of Michigan, Ann Arbor, Michigan

Received 17 January 1960

An instrument for determining the shape and intensity distribution of particle and X-ray beams has been developed using an image intensifier tube together with a bundle of filaments of scintillator. A description of the use of such a device in high energy, low intensity, secondary meson and proton beams is given. It is shown that the sensitivity of this instrument represents a significant improvement over alternative techniques.

1. Introduction

It is possible to construct a monitor for determining the intensity profiles of weak beams of high-energy charged particles or X-rays by combining filamentary scintillators with an image converter tube. Such a device, which we will refer to as a "Channeled Particle-Image Converter" or CPIC, has been constructed and used by the authors in meson beams from the Bevatron. A discussion of the problems of such monitoring and of existing methods in these fields follows. The CPIC as constructed is described along with calculations of conversion and detection efficiencies. Further extensions of this new instrument and other applications particularly to high energy X-radiology conclude the paper.

In high energy physics, beam transport systems consisting of quadrupoles, bending magnets, and electromagnetic separators are generally set in position according to calculations and measurements on the separate components[1]). The various operating currents are then adjusted about their predicted values to optimize the beam intensity and spatial distribution at the position of either a target of liquid hydrogen (or some other material) or the last slit of a beam separator. In order to monitor the beam profile in the target plane a small scintillation counter is frequently used, moving it back and forth and comparing its counting rate with a suitable monitor. Weigand[2]) has constructed a more elaborate profile monitor consisting of a row of scintillation counters connected to an oscilloscope in such a way that the oscilloscope trace gives beam intensity versus position in one dimension perpendicular to the beam axis. These methods are inconvenient and of limited resolution. The purpose of the monitor described here is to give a two-dimensional presentation of such a beam intensity distribution in weak particle beams.

A second area of usefulness of the same device is in the high-energy industrial X-radiography of thick castings or other objects, where it appears that considerable improvements over present technology are possible.

2. Principle of Operation

A large sheet of scintillator perpendicular to the beam axis viewed from a distance by eye or by a television or camera system has been used in several instances[3,4]) for viewing intense beams (e.g., 10^5 minimum ionizing particles per cm^2 per second or greater). However, the poor light collection efficiency and relatively poor efficiency of the detectors

† Supported by the U. S. Office of Naval Research.

[1]) H. K. Ticho, International Conference on High Energy Accelerators and Instrumentation – CERN 1959, Proceedings (Geneva, 1959) p. 387.

[2]) C. Weigand (private communication).

[3]) R. D. Sard, Proceedings of an International Conference on Instrumentation for High Energy Physics Berkeley, 1960 (Interscience publishers, New York, 1961).

[4]) J. S. Pruitt, Nucleonics **13** No. 8 (1955) 26.

used restricts this method to beams generally more intense than the secondary particle beams of accelerators such as the Bevatron and Cosmotron[5]).

By placing the scintillator very close to the large diameter photocathode of an image intensifier tube,

3. Experimental Device and Operation

Using this principle, a CPIC was assembled as indicated in figs. 1, 2, and 3. The image intensifier used was a Westinghouse WL7257 employing an S11 cathode and P11 phosphor; the cathode dia-

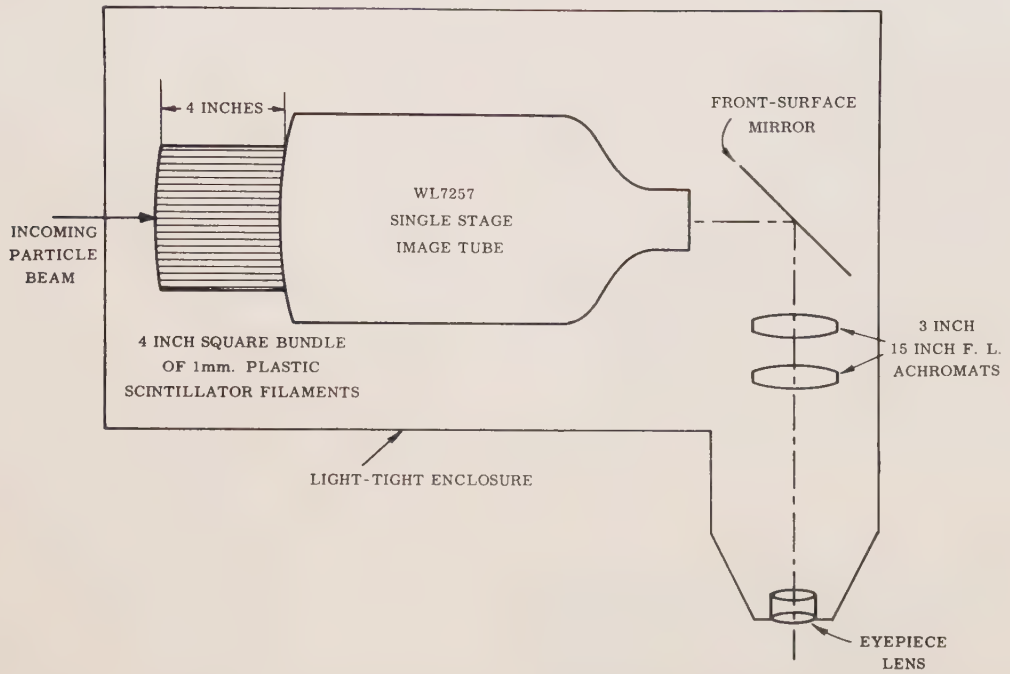
4 INCHES
FRONT-SURFACE MIRROR
WL7257 SINGLE STAGE IMAGE TUBE
INCOMING PARTICLE BEAM
3 INCH 15 INCH F. L. ACHROMATS
4 INCH SQUARE BUNDLE OF 1mm. PLASTIC SCINTILLATOR FILAMENTS
LIGHT-TIGHT ENCLOSURE
EYEPIECE LENS

Fig. 1. Schematic diagram of Beam Profile Monitor as assembled for early tests. The periscope optics allows the observer to be out of the beam.

the light collection and detection efficiency are both greatly improved, however the spatial resolution is poor, comparable to the thickness of the scintillator used. Briefly, an image intensifier (or image converter) tube consists of a photocathode, accelerating and focusing electrodes, and a phosphor-screen anode. Thus an image focused on the cathode is reproduced with increased brightness at the phosphor, where the brightness gain may be 10^2 to 10^4, depending on the image tube characteristics. The resolution can then be improved by constructing the scintillator of a bundle of filaments[6]) with its axis parallel to the beam. The filaments channel the light by total internal reflection, thus permitting use of a converter (scintillator) up to several centimeters thick. The resolution in this case is determined by the filament diameter and the thickness of the cathode envelope of the image tube.

meter is 5 inches, the phosphor diameter 1 inch, the cathode efficiency 8% (to blue quanta), and the quantum gain about 80 at 30 kilovolts operating voltage. The area demagnification from cathode to anode is 25:1 so that the above quantum gain corresponds to a brightness increase of 3000. The scintillator was in the form of 1 mm-diameter plastic filaments each 10 cm long arranged in a 10 cm square lucite frame. The tube was enclosed in a magnetic shield and a light-tight box. A viewing periscope allowed an observer to see the anode without undue radiation exposure in the beam proper.

A quantitative estimate of the performance of

[5]) In a modification of Sard's apparatus, Kerth has replaced the polaroid film by an image orthicon (Z 5294) viewing a sheet of sodium iodide through an $f/1.1$ lens and reports a sensitivity possibly as high as 10^4 particles per cm^2 per second.

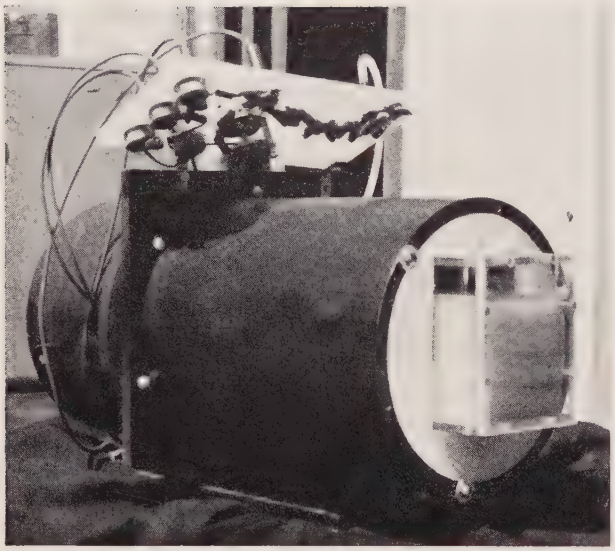

Fig. 2. Photograph of the image tube and scintillator assembly. The image tube is within the iron magnetic shield, the scintillator bundle is visible on the right. A resistor voltage divider network for supplying the focusing electrode voltages is mounted above the assembly.

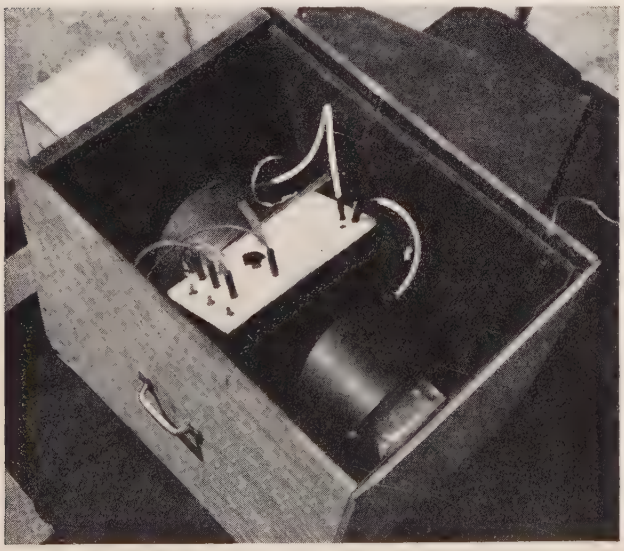

Fig. 3. Photograph of the image tube and scintillator assembly in place within its light-tight box (cover removed).

this system may be made as follows. A minimum-ionizing particle produces about 1.6×10^4 quanta per cm of path in plastic scintillator, and about 20% of these quanta are "piped" to each end by total internal reflection[6]) (assuming perfect surfaces on the filaments). Due to light losses from imperfect filaments, the light reaching one end of a 10 cm filament might be only 10^4 quanta. These traverse the $\frac{1}{8}$ inch cathode envelope and produce photoelectrons from the image tube cathode. From the measured image tube gain, about 8×10^5 quanta will be produced at the anode phosphor from each particle traversing the scintillator.

The WL7257 has an area demagnification of 25 from cathode to phosphor, so that an incident flux of N minimum-ionizing particles per cm^2 per second will produce about $2 \times 10^7 N$ photons per cm^2 per second at the anode. The resolution of this system is limited by the cathode envelope thickness to about 3 mm (at the cathode).

This system was used with a beam of 1.5 GeV/c negative particles (mesons) from the Bevatron. At a flux of 1000 particles per cm^2 per pulse the intensity distribution was readily visible, the beam center could be located, and the characteristic pattern of the beam due to the combined effects of bending magnet dispersion and chromatic aberration of the quadrupole was apparent. Measurements with scintillation counters were in agreement with the monitor observations.

4. Further Developments

The usefulness of this first device may be improved in several ways. First, the beam intensity pattern appeared to the observer on an otherwise dark background with no reference to space coordinates in the laboratory. It is planned to add fiducial lines to the image tube input on which the eye can focus between beam pulses and to which the beam intensity pattern may be referred.

The other factors which could be improved are the sensitivity of the system and a quantitative presentation of the beam intensity pattern to supplement the qualitative visual image. By

[6]) R. J. Potter and R. E. Hopkins, Proceedings of the Seventh Scintillation Counter Symposium, IRE Transactions NS–7, No. 2–3 (1960) p. 150;

G. T. Reynolds, p. 115, *ibid*; other relevant discussions of filament scintillators and image intensifier tubes are to be found in this volume; in session 7 in ref. [1]); in Advances in Electronics and Electron Physics **12** (Academic Press, New York, 1960); and in Proceedings of the Image Intensifier Symposium of the U.S. Army Engineers Research and Development Laboratory (1958) available through the Office of Technical Services, Washington, D.C.

replacing the filaments of plastic scintillator with filaments of thalium-activated sodium iodide or cesium iodide an increase of approximately a factor of ten in sensitivity would be realized, since the light produced per unit length of track in these materials is an order of magnitude greater than in plastic. However the fabrication of such filaments is more difficult than with plastic, and they are thus not readily available.

Coupling the image tube output to an image orthicon would allow remote viewing of the image as well as increased sensitivity. For example, a pair of $f/0.87$ Super Farron lenses would transmit about 15% of the light from the image tube anode to the cathode of an image orthicon, or about 10^5 quanta per incident particle in the scintillator in the example above. The image tube resolution is 10–15 line pairs per mm, so that the light from each filament is spread over an area determined by the thickness of the cathode envelope, the filament diameter, and the image tube demagnification. In the present case this is about 10^{-2} cm^2 or less. For N particles per cm^2 incident on the scintillator, there would be $3 \times 10^6 N$ photons per cm^2 on the orthicon cathode.

A conventional image orthicon (RCA 5820) requires at least 2×10^9 photons per cm^2 per second† to present to the eye a useful picture, thus such a system would have a threshold of 10^3 beam particles per cm^2 per seond. The photon density from a single beam particle would be about 10^7 per cm^2 at the orthicon cathode, thus at less than 1000 beam particles per cm^2 second the problem becomes one of detecting single beam particles. An intensifier image orthicon (RCA C–74036) should have sufficient sensitivity to record single beam particles[7]). A thin-target orthicon (G.E. type Z 5294) has a sensitivity intermediate between the conventional and intensifier orthicons, and a system employing such a G.E. orthicon together with the components described in section 3 is currently being assembled at the Lawrence Radiation Laboratory[8]).

The quantitative profile of the beam may be readily observed by disecting a single video scan line from the orthicon signal and displaying this video amplitude on an oscilloscope[9]).

As alternatives to the image tube-intensifier image orthicon system, one might have a two-stage image intensifier following the first tube with its output viewed by eye, an image orthicon, or even a vidicon. This system would also have ultimate sensitivity, in that it would permit detection of single beam particles.

Replacing the television tube by fast film (Kodak Royal-X Pan or Polaroid type 47) in the focal plane of the $f/0.87$ lenses would permit a photographic record of particle fluxes as an alternative to visual observation. The threshold sensitivity of such film corresponds to about 1000 beam particles per cm^2 incident.

The resolution of the system might be improved by using finer and shorter scintillator filaments and an image intensifier with either a very thin cathode envelope or a cathode window made of glass filaments. Both concepts have been incorporated into experimental tubes of the WL 7257 type. The advent of scintillating glass[10]) fabricated into filaments would permit finer filaments than possible with plastic.

It is also possible to use Čerenkov radiation in glass or plastic non-scintillating filaments, although in this case the system sensitivity is reduced an order of magnitude. In cases where a large neutron background exists, for example, this method of detection might be convenient.

Image tubes with cathodes 8 to 10 inches in diameter are being fabricated for medical radiology and will become available as light amplifiers for applications such as this.

† In addition to this rate threshold, there is also a total threshold because of the behavior of the eye and the properties of the television system. Not only must the rate be greater than 2×10^9 photons/cm^2 sec but also the total photons/cm^2 must be greater than 4×10^8. In these discussions it is important to distinguish between total integrated light (as relevant in photographic recording), light per second, light per pulse (of accelerators such as the Bevatron), and light per frame of television scan.

[7]) B. A. Bang, Proceedings of the 5th International Congress on High Speed Photography of the Society for Motion Picture and Television Engineers, Washington, D.C. (1960) (to be published).

[8]) Dale Dickinson (private communication).

[9]) L. T. Kerth, (private communication).

[10]) R. J. Ginther, Proceedings of the Seventh Scintillation Counter Symposium, p. 28.

5. X-ray Monitoring

This same combination of scintillation filaments and image intensifier should prove very useful in high-energy X-radiography. Currently, steel castings and other large objects are examined by directing the bremsstrahlung beam of a betatron directed through the object onto a sheet of X-ray film which in turn is usually mounted behind a thin sheet of lead as an intensifying screen. Exposures of 30 or 40 minutes are frequently necessary for sufficient detail on the film, primarily due to the poor efficiency of the film for high-energy electrons and X-rays. Pruitt[3]) has used a large sodium iodide crystal with a fast lens and film, however, the resolution and sensitivity of his method was not adequate for most purposes. For lower X-ray energies, a zinc sulfide-type phosphor screen is placed adjacent to the photocathode of an image intensifier tube, and it is indeed for this use that the WL 7257 type of image tube was developed[11]). However at energies well above the K absorption edge of zinc, the conversion efficiency of the thin phosphor is poor, and such devices are not generally useful above one MeV.

The CPIC as described above, using sodium iodide filaments, or using plastic scintillator filaments behind a thin lead sheet, would be capable of converting 10–20% of all incident X-rays in the energy range above one MeV. The resulting conversion electrons would produce light with the efficiencies computed above for minimum ionizing particles. Thus a single intensifier tube system would permit detection of X-ray fluxes of 10^3 to 10^4 quanta per cm^2 per second, and a system employing also an intensifier image orthicon or a second image tube should be capable of detecting every converted X-ray photon above one MeV.

Using glass scintillator filaments down to 10 microns diameter the technique might permit improvements in sensitivity and resolution also in the energy region below 100 keV. In fact such an X-ray converter screen of scintillator filaments might be generally useful aside from the image intensifier for visual observation (fluoroscopy) or photographic recording of X-ray images at higher intensities.

The limiting resolution of such X-ray intensifier systems is determined by the transverse range of the conversion electrons (from compton scattering, photoeffect, or pair production) in the scintillator filaments. At energies above one MeV this is of the order of a millimeter, roughly independent of energy. At energies less than 500 keV the resolution would improve. A corresponding limit to the resolution with high energy X-rays arises from compton-scattered X-rays from the object under study, and sets a limit to the resolution possible with any detection system.

A further use of the X-ray detector as a "pinhole camera" for extended sources of X-ray or gamma radiation has been considered. Here an image tube with a filamentary X-ray converter would be mounted in a lead or tungsten canister perhaps 1½ cm thick. A hole in the end of the canister opposite the converter would image the extended source on the filament array. All of the considerations discussed above apply. Such a device should find application in medicine, tracer techniques, and radiobiological safety.

6. Summary

A device for determining the intensity distribution of high energy particle beams consisting of scintillator filaments against the cathode envelope of an image intensifier tube has been built and successfully operated. Straight-forward extension of this technique will allow the sensitivity to be extended to the point where single particles of weak beams are resolved. The same technique carries over into X-ray detection, where corresponding advantages should be realized, particularly at X-ray energies above one MeV. Thus images consisting of radiation quanta should be detectable for quanta from 100 keV to arbitrarily high energies and at a level where at least every tenth quantum is seen.

Acknowledgement

It is a pleasure to acknowledge the hospitality of the Lawrence Radiation Laboratory during the testing of this monitor.

[11]) J. W. Coltman, Radiology 51 (1948) 359.

NUCLEAR INSTRUMENTS AND METHODS **10** (1961) 353–355; NORTH-HOLLAND PUBLISHING CO.

DETECTION EFFICIENCY OF A PLASTIC SCINTILLATOR FOR NEUTRONS IN THE ENERGY RANGE OF 1 TO 14 MeV

H. GRÄSSLER and K. TESCH

Physikalisches Institut der Technischen Hochschule Aachen, Germany

Received 20 January 1961

The detection efficiency of a plastic scintillator for neutrons in the energy range of 1 to 14 MeV is measured by scattering 14.1–MeV neutrons on polyethylene. The results are compared with theoretical calculations.

In measuring fast neutrons with hydrocarbon scintillators it is often necessary to know the change in detection efficiency with varying neutron energy. For energies below 5 MeV this efficiency has been measured producing neutrons by means of T(p,n)He^3 or D(d,n)He^3 reactions[1,2,3]). Using the T(d,n)He^4 reaction one gets the efficiency at 14 MeV whereas its energy dependence is usually determined by theoretical considerations. The calculation becomes particularly simple, if only single proton collisions of the neutrons in the scintillator are considered and if the presence of carbon is neglected (first approximation, see e.g.[4])). Hardy[2]) has carried out a more detailed computation including neutron energy loss by single and double collisions with protons and taking into account scattering effects by the carbon nuclei in the scintillator (second approximation). We considered it useful to check theoretical efficiencies by taking measurements for the whole range from 1 to 14 MeV varying neutron energy by scattering of 14-MeV neutrons on hydrogen. Comparing our experimental results as well as those of other authors with theoretical curves it can be shown that experiment and calculation are in agreement regarding both the energy dependence and the absolute values.

14.1-MeV neutrons from the T(d,n)He^4 reaction using 200-keV deuterons were scattered on polyethylene at different angles. The intensity and energy of scattered neutrons were measured by a time-of-flight spectrometer of conventional design (associated particle method) in order to discriminate hydrogen scattering against carbon scattering and to reduce background effects. To keep down the aperture of the scatterer with respect to the target and of the scintillator with respect to the scatterer the latter (4.5 cm long and 4.5 cm in diameter) was

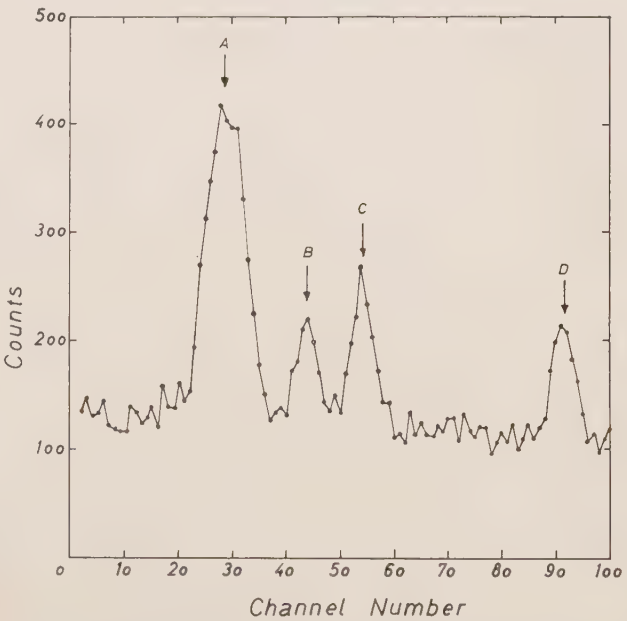

Fig. 1. Time-of-flight spectrum for 14–MeV neutrons scattered on polyethylene. E_b = 3.5 MeV, scattering angle 52°.

[1]) L. Cranberg and J. S. Levin, Phys. Rev. **103** (1956) 343.
[2]) J. E. Hardy, Rev. Sci. Instr. **29** (1958) 705.
[3]) N. A. Bostrom, I. L. Morgan, J. T. Prud'homme, P. L. Okhuysen and A. R. Sattar, WADC Techn. Report 58–88 (1958).
[4]) B. V. Rybakov and V. A. Sidorov, Fast-Neutron Spectroscopy (Consultants Bureau, Inc., New York).

placed at a distance of 42 cm from the neutron source, and the scintillator at 200 cm from the scatterer. The scintillator (Scintillator B, Pilot Chemicals) was 5 cm long and 5 cm in diameter, mounted on a RCA 7264 photomultiplier tube whose anode signal supplied the stop pulse for the time-of-flight system.

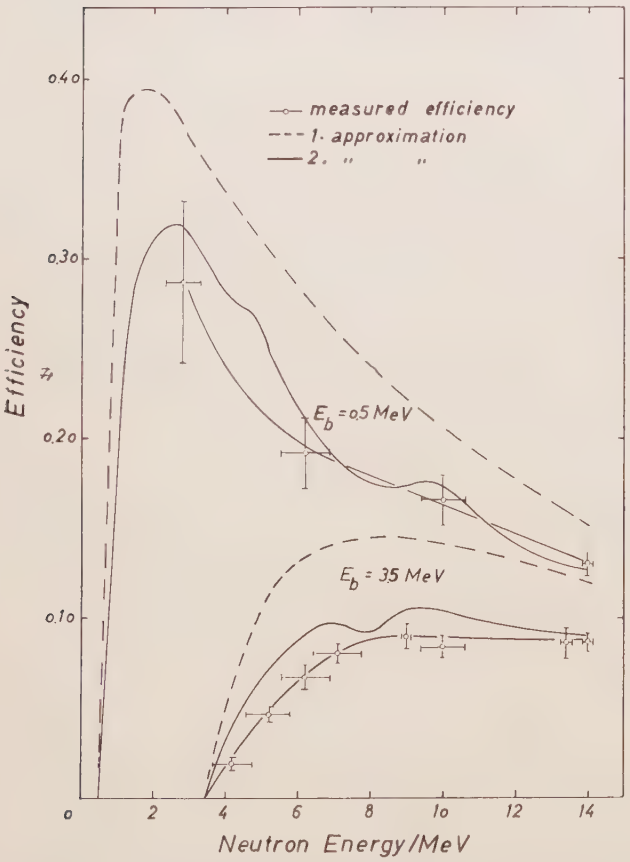

Fig. 2. Neutron detection efficiency of a plastic scintillator at the two thresholds $E_b = 0.5$ MeV and $E_b = 3.5$ MeV.

example fig. 1 shows the time-of-flight spectrum, including background, taken at the threshold $E_b = 3.5$ MeV and at a scattering angle of 52°. Following the curve, the peaks are due to neutron scattering from hydrogen (peak A, at 5.2 MeV), first-level inelastic scattering from carbon (peak B, at 8.8 MeV), elastic scattering from carbon (peak C, at 13.2 MeV), and the γ-rays from the inelastic scattering on carbon (peak D). Excitation of the second level of carbon has not been observed. The

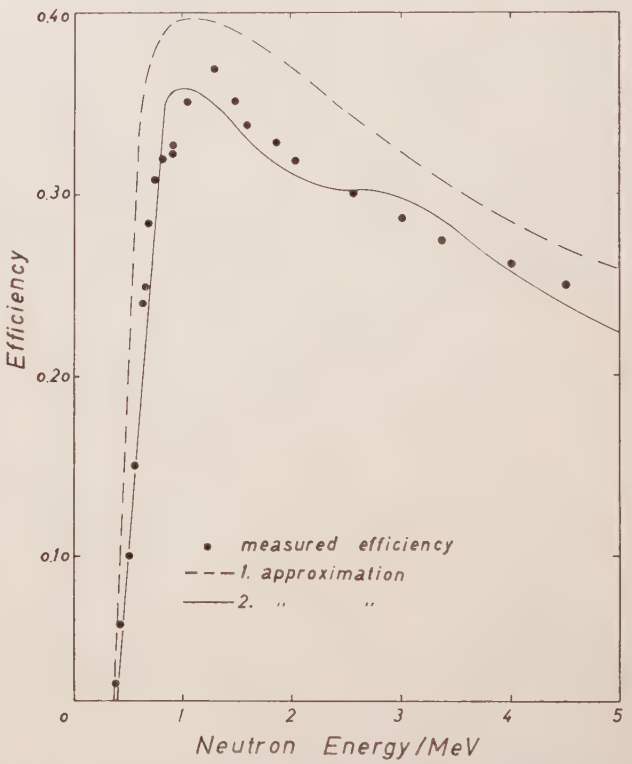

Fig. 3. Neutron detection efficiency measured by Cranberg and Levin and the corresponding calculated efficiency.

The smallest proton recoil energy accepted was conventionally determined by the pulse height at the last dynode. In contrast to experiments with the T(p,n)He^3 reaction this value cannot be fixed by direct measurements. Since however the ratio of the heights of proton to electron pulses in plastic scintillators is known[5,6]) the bias could be determined by means of γ-ray sources of known energy.

Measurements were taken for the two proton threshold energies of 0.5 MeV and 3.5 MeV. As an differential cross sections of elastic scattering and of inelastic scattering from the first excited level being known[7]) carbon peaks in addition to the hydrogen peak can be used to determine the efficiency of the scintillator. Therefore it was also possible to compute the contribution of inelastic scattering from carbon at small angles

[5]) M. Gettner and W. Selove, Rev. Sci. Instr. **31** (1960) 450.

[6]) H. C. Evans and E. H. Bellamy, Proc. Phys. Soc. **74** (1959) 483.

[7]) J. D. Anderson, C. C. Gardner, J. W. McClure, M. P. Nakada and C. Wong, Phys. Rev. **111** (1958) 572.

where the peaks A and B are no longer resolved.

At a bias energy of 0.5 MeV the background was so high that the individual peaks could not be resolved clearly. It was necessary to eliminate carbon effects by a subtraction method measuring neutron scattering on polyethylene and on a pure carbon scatterer under the same conditions.

The measured absolute neutron detection efficiency is given in fig. 2. The range of error indicated is due to the geometry of the arrangement, to background, to the uncertainty in the (n,p)-cross section, and to uncertainties in the neutron production rate. For 0.5 MeV threshold the error due to background increases for decreasing neutron energy. It may be noted that for 3.5 MeV bias the efficiency is nearly constant above 7 MeV. The other curves in fig. 2 represent calculations of the absolute efficiency resulting from the first and from the second approximation mentioned above. The irregular slope of the second approximation is due to resonances in the carbon cross section.

For further comparison we computed in the same way the efficiency for a plastic scintillator of 3.8 cm length and for a threshold energy of 0.3 MeV and compared it with data measured by Cranberg and Levin[1]) (see fig. 3). Similarly Hardy has compared his calculated efficiency with experiment in the energy interval of 2 MeV to 3.5 MeV. From all these comparisons it seems that the energy dependence as well as the absolute value of the efficiency can be predicted by calculation, if double collisions with protons and single scattering from carbon are taken into account. On the average the computations and the observed efficiencies differ by less than 10%. For many purposes this agreement will be quite satisfactory and the experimental determination of the efficiency may be saved. In some cases it may be sufficient to take the first approximation normalized by one absolute measurement.

The authors would like to thank Professor M. Deutschmann for his continuous interest and encouragement and Mr. R. Honecker for his help in running the experiment.

BOOK REVIEWS

DANIEL BLANC et GEORGES AMBROSINO: *Éléments de Physique Nucléaire*, Masson et Cie, Éditeurs, Paris-6e. 238 pages, 84 figures and tables; price NF 30.–.

In "Éléments de physique nucléaire", D. Blanc and G. Ambrosino present a short and clear introduction to the field of nuclear physics. To facilitate the presentation for readers, with no special education in mathematics, the authors avoid as far as possible theoretical developments. The book presents up-to-date information about all important parts of nuclear science, including e.g. the principles of thermonuclear reactions. Well chosen figures and numerous tables are included, and at the end of each chapter a short list of references is added. In the appendix, the authors present some tables and graphs which are very useful for practical applications of the results discussed in this book.

"Éléments de physique nucléaire" can be well recommended for nonspecialists as an introduction to the field of nuclear physics. In particular the book will be very useful for engineers dealing with problems involving some results of nuclear physics, for students of medicine interested in nuclear science etc.

The 9 chapters of the book deal with the following subjects:

1. Evolution of research in atomic structure, nuclear reactions and atomic energy; 2. Structure and stability of the atom; 3. The nuclei; 4. Radioactive disintegrations; 5. Nuclear reactions; 6. The neutron; 7. Fission, chain reactions; 8. Nuclear structure and nuclear cohesion; 9. Thermonuclear reactions; Appendix.

WERNER SCHNEIDER

LARS MELANDER: *Isotope effects on reaction rates* VI + 181 pages, price $ 6.00. (The Ronald Press Co., New York)

In this admirably written little book, kinetic isotope effects are discussed with special emphasis on principles. It starts with a very clear and consistent presentation of the theory for the prediction of rate-constant ratios from molecular data based on the theory of absolute reaction rates, followed by an illuminating discussion of the evaluation of such ratios from kinetic experiments. The main body of the book (about 100 pages) is then devoted to the isotope effects of hydrogen and carbon and, in the last chapter, a few cases with elements heavier than carbon are mentioned. Written by an expert, the book serves as an excellent introduction to this rapidly expanding field of research which is of great importance both to chemistry and physics. The systematic presentation, based on well integrated theories, also makes it a very interesting reading for advanced workers.

STIG CLAESSON

AUTHOR INDEX

Ackermann, Hans and Helmut Faissner, Fading in nuclear emulsions induced by acid agents 339
Alberigi Quaranta, Alessandro and Bruno Righini, Fast transistorized pulse height analyzer 25
Arbman, E. and B. Jung, Improved automatic operation of a double focusing iron-yoke β-spectrometer . . 322

Baldinger, E. and W. Czaja, On the energy expended per electron-hole-pair produced in p–n-junction-detectors (Letter to the Editor) 237
Becker, R. L., *see* Biggerstaff
Benaroya, R. and W. J. Ramler, Deflection coil for an external accelerator beam 113
Bergström, I, *see* Thieberger
Berkes, I., *see* Keszthelyi
Biggerstaff, J. A., R. L. Becker and M. T. McEllistrem, Charged particle discrimination in a CsI(Tl) detector 327
Binnie, D. M., Photons from positron beams in the GeV range 212
Blinowski, K. and J. Sosnowski, Parasitic reflections of neutrons in crystal monochromators 289
Boersma, H. J., *see* Rethmeier
Bougnot, G., *see* Sarazin

Cairns, D. J., T. C. Griffith, G. J. Lush, A. J. Metheringham and R. H. Thomas, The use of a counter controlled high pressure cloud chamber for experiments with charged particles 272
Caro, D. E. and J. L. Rouse, The Melbourne university variable energy cyclotron 249
Chapman, K. R. and S. Gowariker, A convenient method of constructing accelerator tubes (Letter to the Editor) 66
Cohen, A. V., J. A. Cookson and J. L. Wankling, A magnetic particle spectrometer for use with a 12 MeV tandem electrostatic generator 84
Cookson, J. A., *see* Cohen
Cranberg, L., Time-to-pulse-height converter as coincidence and anti-coincidence indicator (Letter to the Editor) 243
Csikai, J., E. Molnar and B. Schlenk, Investigations about the critical radius of the BF_3 counters 121
Czaja, W., *see* Baldinger,

Daniel, H., *see* Fehrentz
Daniel, H. and L. Jackson Laslett, Beta-ray spectrometer with curved exit slit 48
Demeter, I., *see* Keszthelyi
Dutt, P. K., Theory of "ion-bunching" in relation to the development of an electrostatic time-of-flight mass spectrometer 37

Elbek, Bent and Michiyuki Nakamura, Multichannel detector for use in particle spectrometers 164

Faissner, Helmut, *see* Ackermann
Fauska, H., J. W. Orth and F. H. Schmidt, Fixed frequency cyclotron operation with a regulator for dee voltage stabilization 73
Fehrentz, D. und H. Daniel, Einfluss der Quellendicke auf die gemessene Form eines Beta-Spektrums. . . 185
Felbinger, K., H. Kulenkampff, M. Scheer und E. Schrüfer, Ein magnetisches Compton-Spektrometer zur Untersuchung hochenergetischer Röntgen-Bremsstrahlung 295
Fodor, I., *see* Keszthelyi
Forsberg, H. G., *see* Westermark

Glover, R. N., K. H. Purser and E. Weigold, A counter telescope system for fast neutron studies 343
Goetze, G. and H. Kanter, A high gain image intensifier system with fast shutter action for application in high energy physics 224
Gowariker, S., *see* Chapman
Grässler, H. and K. Tesch, Detection efficiency of a plastic scintillator for neutrons in the energy range of 1 to 14 MeV 353
Griffith, T. C., *see* Cairns

Hazoni, Y., Circuit à plusieurs états stables utilisant des diodes tunnel 229
Hazoni, Y., A tunnel diode univibrator and pulse height discriminator 231
Högberg, L. and K. Vogel, Experiments with electrodeless generation and acceleration of plasma rings . 95
Hultberg, S., Computer service for calculation of the photoelectric *f* factor 24

Jackson Leslett, L., *see* Daniel
James, A. N. and C. M. P. Johnson, Wide band detection of small ion beam currents (Letter to the Editor) . . 68
Johnson, C. M. P., *see* James
Jones, Lawrence W. and Martin L. Perl, An image intensifier-scintillator device for determination of profiles and images of weak beams of ionizing particles or X-rays 348
Jonker, C. C., *see* Rethmeier
Jung, B., *see* Arbman

Kanter, H., *see* Goetze
Keil, E. und E. Zeitler, Eine Theorie magnetischer Compton-Spektrometer 301
Kelley, G. G., N. H. Lazar and O. B. Morgan, A source for the production of large DC ion currents 263
Kessler, Joachim, Doppelstreuexperiment mit Azimutwinkel integration (Letter to the Editor) . . . 245
Keszthelyi, L., I. Berkes, I. Demeter and I. Fodor, Detection of high energy γ-rays by plastic phosphors 193
Kulenkampff, H., *see* Felbinger

Kuo, L. G., M. Petravić and B. Turko, A $dE/dx - E$ counter telescope for charged particles produced in reactions with 14 MeV neutrons 53

Lacosta, F. and J. Leiss, A fast scaler for pulsed accelerators 189
Larson, H. V., *see* Myers
Lazar, N. H., *see* Kelley
Leiss, J., *see* Lacosta
Lush, G. J., *see* Cairns

McEllistrem, M. T., *see* Biggerstaff
Metheringham, A. J., *see* Cairns
Meijer, A. C., *see* Van Oostrum
Meyer, Ludwig, Die Bildungsgeschwindigkeit von Nebelspuren in der Nebelkammer 108
Mladjenović, Milorad, Gamma-ray measurements by the magnetic analysis of Compton and photo electrons 1
Molnár, E., *see* Csikai
Morgan, O. B., *see* Kelley
Myers, I. T. and H. V. Larson, Precision instrumentation for an electron accelerator 281

Nakamura, Michiyuki, *see* Elbek
Neu, H. und H. Werner, Analytisches Näherungsverfahren zur Berechnung azimutal periodischer Magnetfelder in Kreisbeschleunigern 333

Orth, J. W., *see* Fauska

Perl, Martin L., *see* Jones
Petravić, M., *see* Kuo
Purser, K. H., *see* Glover

Ramler, W. J., *see* Benaroya
Rethmeier, J., H. J. Boersma and C. C. Jonker, An improved circuit for pulse shape discrimination between neutrons and gamma rays (Letter to the Editor) 240
Righini, Bruno, *see* Alessandro Alberigi Quaranta
Rouse, J. L., *see* Caro

Samueli, J., *see* Sarazin
Sarazin, A., J. Samueli and G. Bougnot, Discriminateur d'amplitude rapide 202
Scheer, M., *see* Felbinger
Schlenk, B., *see* Csikai
Schmidt, F. H., *see* Fauska
Schrüfer, E., *see* Felbinger
Schuhl, C. et C. Tzara, Monochromateur de positrons en secteur d'orange 217
Seguinot, J., J. Teiger et L. van Rossum, Sélection de mésons K^+ dans un faisceau secondaire de "Saturne" 205
Sjöstrand, B., *see* Westermark
Sosnowski, J., *see* Blinowski
Svanheden, Åke, A cold cathode ion source for a synchrocyclotron 125

Teiger, J., *see* Seguinot
Tesch, K., *see* Grässler
Thieberger, P. and I. Bergström, Use of cathode ray tubes in pulse-height spectroscopy 315
Thomas, R. H., *see* Cairns
Turko, B., *see* Kuo
Tzara, C., *see* Schuhl

Valckx, F. P. G., Direct current stabilization of scintillation counters used with pulsed accelerators 234
Van Oostrum, K. J. and A. C. Meijer, Use of (p,γ) reactions in the efficiency calibration of a NaI crystal . . 31
Van Rossum, L., *see* Seguinot
Verweij, H., A fast transistorized discriminator 308
Vogel, K., *see* Högberg

Wankling, J. L., *see* Cohen
Weigold, E., *see* Glover
Werner, H., *see* Neu
Westermark, T., B. Sjöstrand and H. G. Forsberg, Some experiments on moisture determination with beta-ray transmission 45
Westermark, Torbjörn, A double-focusing magnetic spectrometer for studies of energy losses in matter of electrons from a 5 MeV betatron 129
Westermark, Torbjörn, Energy distribution and energy stability of the electron beam from a 5 MeV betatron 145
Westermark, Torbjörn, Measuring techniques for energy loss studies of 2.8 MeV betatron electrons in matter 169
Wilson, G. V. H., Phase changes near the cyclotron centre 259

Zeitler, E., *see* Keil

BOOK REVIEWS

Duquesne, M., R. Grégoire, M. Lefort et R. Devoret, Traveaux pratiques de physique nucléaire et de radiochimie (Gunnar Bäckström) 70
Bayet, M., Physique nucléaire (Gunnar Bäckström) 70
Liverhant, S. E., Elementary introduction to nuclear reactor physics (Evelyn Sokolowski) 70
Zucker, A., E. C. Halbert and F. T. Howard (Editors), Proceedings of the second conference on reactions between complex nuclei, held in Gatlinburg, Tennessee, May 2–4, 1960 (Ingvar Lindgren) 71
(Editors), Proceedings of the international conference on nuclear structure, Kingston, Canada, Aug. 29–Sept. 3, 1960 (Ingvar Lindgren) 71
Barnard, G. P., G. H. Aston and A. R. S. Marsh, Effects of variation in the ambient air on the calibration and use of ionization dosemeters (Ingrid Olsson) 71
Thring, M. W. (Editor), Nuclear propulsion (Lars Högberg) 247
Sector-focused cyclotrons. Proceedings of an informal conference, Sea Island, Georgia, February 2–4, 1959, (Mats Olsmats) 247
Uehling, E. A. (Editor), Penetration of charged particles in matter (Tor Ragnar Gerholm) 248
Stickland, A. C. (Editor) Reports on progress in physics (Tor Ragnar Gerholm) 248
Daniel Blanc et Georges Ambrosino, Eléments de Physique Nucléaire (Werner Schneider) 356
Lars Melander, Isotope effects on reaction rates (Stig Claesson) 356

SUBJECT INDEX

Accelerators and Reactors

Fixed frequency cyclotron operation with a regulator for dee voltage stabilization, H. Fauska, J. W. Orth and F. H. Schmidt . . . 73
Deflection coil for an external accelerator beam, R. Benaroya and W. J. Ramler . . . 113
A cold cathode ion source for a synchrocyclotron, Åke Svanheden . . . 125
Energy distribution and energy stability of the electron beam from a 5 MeV betatron, Torbjörn Westermark . . . 145
The Melbourne university variable energy cyclotron, D. E. Caro and J. L. Rouse . . . 249
Phase changes near the cyclotron centre, G. V. H. Wilson . . . 259
A source for the production of large DC ion currents, G. G. Kelley, N. H. Lazar and O. B. Morgan . . . 263
Precision instrumentation for an electron accelerator, I. T. Myers and H. V. Larson . . . 281
Analytisches Näherungsverfahren zur Berechnung azimuthal periodischer Magnetfelder in Kreisbeschleunigern, H. Neu und H. Werner . . . 333

Detectors

Use of (p,γ) reactions in the efficiency calibration of a NaI crystal, K. J. van Oostrum and A. C. Meijer . . . 31
Investigations about the critical radius of the BF_3 counters, J. Csikai, E. Molnár and B. Schlenk . . . 121
Multichannel detector for use in particle spectrometers, Bent Elbek and Michiyuki Nakamura . . . 164
Detection of high energy γ-rays by plastic phosphors, L. Keszthelyi, I. Berkes, I. Demeter and I. Fodor . . . 193
Charged particle discrimination in a CsI(Tl) detector, J. A. Biggerstaff, R. L. Becker and M. T. McEllistrem . . . 327
Fading in nuclear emulsions induced by acid agents, Hans Ackermann and Helmut Faissner . . . 339
Detection efficiency of a plastic scintillator for neutrons in the energy range of 1 to 14 MeV, H. Grässler and K. Tesch 353

Instruments and Methods for Nuclear Spectroscopy

Gamma-ray measurements by the magnetic analysis of Compton and photo electrons, Milorad Mladjanović . . . 1
Computer service for calculation of the photoelectric f factor, S. Hultberg . . . 24
Theory of "ion-bunching" in relation to the development of an electrostatic time-of-flight mass spectrometer, P. K. Dutt 37
Beta-ray spectrometer with curved exit slit, H. Daniel and L. Jackson Laslett . . . 48
A magnetic particle spectrometer for use with a 12 MeV tandem electrostatic generator, A. V. Cohen, J. A. Cookson and J. L. Wankling . . . 84
A double-focusing magnetic spectrometer for studies of energy losses in matter of electrons from a 5 MeV betatron, Torbjörn Westermark . . . 129
Einfluss der Quellendicke auf die gemessene Form eines Beta-Spektrums, D. Fehrentz und H. Daniel . . . 185
Parasitic reflections of neutrons in crystal monochromators, K. Blinowski and J. Sosnowski . . . 289
Ein magnetisches Compton-Spektrometer zur Untersuchung hochenergetischer Röntgen-Bremsstrahlung, K. Felbinger, H. Kulenkampff, M. Scheer und E. Schrüfer . . . 295
Eine Theorie magnetischer Compton-Spektrometer, E. Keil und E. Zeitler . . . 301
Use of cathode ray tubes in pulse-height spectroscopy, P. Thieberger and I. Bergström . . . 315
Improved automatic operation of a double focusing iron-yoke β-spectrometer, E. Arbman and B. Jung . . . 322
An image intensifier-scintillator device for determination of profiles and images of weak beams of ionizing particles or X-rays, Lawrence W. Jones and Martin L. Perl . . . 348

Instruments and Methods for High Energy Physics

A dE/dx–E counter telescope for charged particles produced in reactions with 14 MeV neutrons, L. G. Kuo, M. Petravić and B. Turko . . . 53
Die Bildungsgeschwindigkeit von Nebelspuren in der Nebelkammer, Ludwig Meyer . . . 108
Sélection de mésons K^+ dans un faisceau secondaire de "Saturne". J. Seguinot, J. Teiger et L. van Rossum . . . 205
Photons from positron beams in the GeV range, D. M. Binnie . . . 212
Monochromateur de positrons en secteur d'orange, C. Schuhl et C. Tzara . . . 217
The use of a counter controlled high pressure cloud chamber for experiments with charged particles, D. J. Cairns, T. C. Griffith, G. J. Lush, A. J. Metheringham and R. H. Thomas . . . 272
A counter telescope system for fast neutron studies, R. N. Glover, K. H. Purser and E. Weigold . . . 343

Letters to the Editor

A convenient method of constructing accelerator tubes, K. R. Chapman and S. Gowariker 66
Wide band detection of small ion beam currents, A. N. James and C. M. P. Johnson 68
On the energy expended per electron-hole-pair produced in p–n-junction-detectors, E. Baldinger and W. Czaja 237
An improved circuit for pulse shape discrimination between neutrons and gamma rays, J. Rethmeier, H. J. Boersma and C. C. Jonker 240
Time-to-pulse-height converter as coincidence and anti-coincidence indicator, L. Cranberg 243
Doppelstreuexperiment mit Azimutwinkel integration, Joachim Kessler 245

Miscellaneous

Some experiments on moisture determination with beta-ray transmission, T. Westermark, B. Sjöstrand and H. G. Forsberg 45
Measuring techniques for energy loss studies of 2.8 MeV betatron electrons in matter, Torbjörn Westermark 169

News Item

Imeko Conference, Budapest, June 26–July 1, 1961 72

Nuclear Electronics

Fast transistorized pulse height analyzer, Alessandro Alberigi Quaranta and Bruno Righini 25
A fast scaler for pulsed accelerators, F. Lacosta and J. Leiss 189
Discriminateur d'amplitude rapide, A. Sarazin, J. Samueli and G. Bougnot 202
A high gain image intensifier system with fast shutter action for application in high energy physics, G. Goetze and H. Kanter 224
Circuit à plusieurs états stables utilisant des diodes tunnel, Y. Hazoni 229
A tunnel diode univibrator and pulse height discriminator, Y. Hazoni 231
Direct current stabilization of scintillation counters used with pulsed accelerators, F. P. G. Valkcx 234
A fast transistorized discriminator, H. Verweij 308

Plasma Physics

Experiments with electrodeless generation and acceleration of plasma rings, L. Högberg and K. Vogel 95

Spotlight on Industry

This section appears each month and features various happenings of interest in the nuclear industrial world and objective information on products of the nuclear manufacturers. It is offered entirely as a service and all nuclear manufacturers are cordially invited to submit clearly objective and descriptive material on their endeavours and product developments for consideration for use in this section.

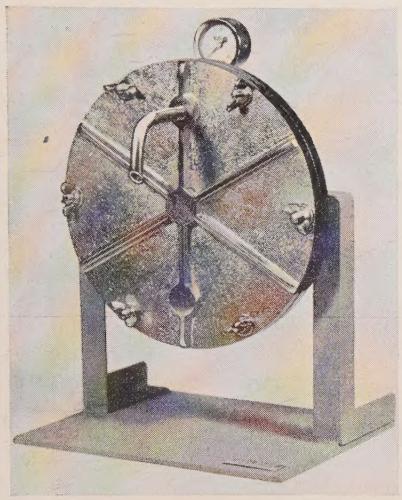

NEW PROCESS FILTER

Gelman Instrument Company, 106 North Main Street, Chelsea, Michigan, U.S.A.

The filter unit is based on the use of a porous plastic sheet with uniform submicron holes in it. The sponge-like cavity arrangement acts as a sieve to trap all particles of 0.1 micron and above in the filter. This "membrane filter" is housed in a metal container-support assembly and supported by a sintered stainless steel plate. The membrane filter portion is disposable. The filter holder is available in 3 different models for pressures of 50, 100 and 500 p.s.i. It is available in a choice of stainless steel or nickel plated bronze construction.

WIDE RANGE R-C OSCILLATOR

Solartron Laboratory Instruments Limited, Cox Lane, Chessington, Surrey, England

The new portable Solartron R-C Oscillator CO 1004 has been developed as a wide range general purpose laboratory instrument. It provides symmetrical low distortion sinewave outputs, of 0° and 180° phase relationship, over the wide frequency range of 10 c/s to 1 Mc/s. A "balance" control is incorporated to obtain perfect symmetry about earth, at low frequencies.

A five position range switch and the fine control of the clearly scaled dial gives a continuous and accurate coverage of the entire frequency range.

A balanced Wien network is used with variable capacity tuning giving a frequency accuracy within $\pm$ 2.5 %. The frequency stability is such that, over an eight hour period, the set frequency is held to within $\pm$ 0.2 %.

Total harmonic distortion is less than 1 % between 20 c/s—200 kc/s and less than 2 % outside these limits. The output level per phase is continuously variable up to 20 V r.m.s. into loads greater than 20 kΩ, 10 V r.m.s. into 600 Ω. Amplitude stability over the entire frequency range is better than $\pm$ 5 %.

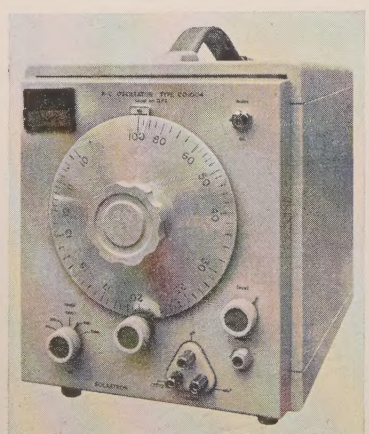

INTERTECHNIQUE

Announced the following new instruments

10 NANOSECOND SCALER

Resolving time is 10 nanosecond. Recurrent frequency is 20 Mc/s.

It can trigger a conventional scaler.

Display is achieved with two neon tubes and can be transmitted to another set of neon tubes or to a printer.

TRIPLE PULSE GENERATOR

The response of most radiation measuring circuits and pulse circuits in general, needs testing with three rather than two pulses.

Each pulse can be adjusted in amplitude (positive and negative) length and phase.

External and internal triggering can be used.

Output impedance of 100 Ω is of prime interest for transistorized circuit.

LOGARITHMIC DC AMPLIFIER

The instrument covers 6 decades with a drift lower than $\frac{1}{10}$ decade from — 40 + 70° C.

The connection with pressurized ionisation chamber (100 kg/cm^2) allows measuring radiation doses from 1 mR/h to 1000 R/h.

It is therefore a very stable, wide range instrument for measuring gamma doses in nuclear centers, around reactors, accelerators and for health monitoring in general.

A battery operated model is available for use in a car, plane or helicopter.

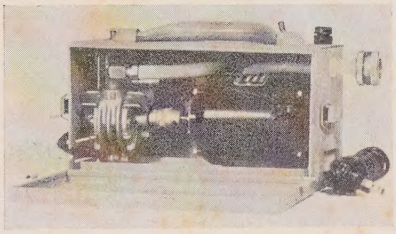

NEW AIR SAMPLER

Gelman Instrument Co., Chelsea, Michigan, Greenwood 2-4821, U.S.A.

A new air sampler for both continuous duty and survey air sampling has been developed. This sampler draws up to 16 liters/minute of air through a filter paper. The unit consists of vacuum pump, flowmeter and filter holder all built into a durable protective carrying case. Dimensions: 9″ × 5″ × 4.5″. Net weight is 8 lbs. The sampler operates on 110 volt 60 cycles with other voltages available. The motor is a split phase type and the pump is an oil-less carbon vane rotary positive displacement type. The air sampler is designed for 24 hours usage.

The filter holder is quickly connected or disconnected to the sampler by means of a new quick disconnect plastic fitting. This makes it possible to load filter holders in the laboratory and then make changes in the field in order to avoid contamination.

This air sampler can not only be used for air pollution studies but also for a variety of other dust sampling work. In the electronics industry it can be used to monitor "white" rooms to determine if areas are operating at design efficiency levels. In the chemical industry it can be used for checking air cleaning systems, for checking efficiency levels, and losses of valuable chemicals. Surgeons and medical researchers can use this unit for checking air borne pathogens. Atomic energy officials frequently use this type of device for checking emission of radioactive aerosols.

IONIZATION CHAMBERS

Plessey International Ltd., Ilford, Essex, England

A variety of neutron detectors are produced for the United Kingdom Atomic Energy Authority.

Among the types at present being supplied in quantity are PNI 1025 and PNI 1026 chambers.

Type PNI 1026 is a two electrode chamber and the PNI 1025 is a three electrode version incorporating gamma compensation. Although based on an original Harwell design, both types have a number of improved features. PNI 1026 chambers are to be installed with control equipment at the Berkeley nuclear power station.

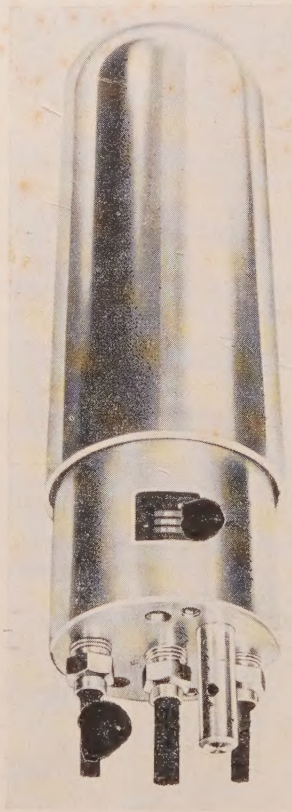

NEW PARTICLE DETECTORS

Single Crystal Division, Semi-Elements Inc., Saxonburg Boulevard, Saxonburg Pa., U.S.A.

A new Particle Detector has been developed that will detect alpha particles, protons, and heavier particles. These solid state radiation detectors utilize silicon in the resistivity ranges of above 10000 ohm cm material. The alpha particle energy detection is in the ranges of 0.5 to 10 MeV with a maximum operating voltages of 100 volts or more. The resolution of these detectors is below 4% and the signal-to-noise ratio is catalogued at 15 to 1, although many of the detectors on the final test bench show a 50 to 1 or more ratio.

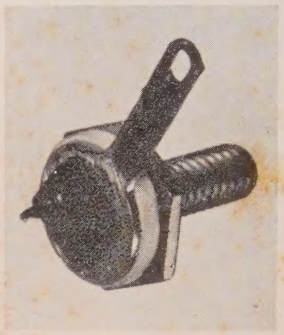

The detector is composed of single crystal high purity P-type silicon with a shallow N-type surface diffused layer Under a reverse bias of 10 to 100 volts, ion pairs produced in the diode by particles striking the upper surface of the crystal may be collected and amplified to give a signal proportional to the energy loss in the sensitive volume. The device is simple, rugged and mounted conveniently and is very unsensitive to gamma radiation because of the thin sensitive layer. The rise time of the pulse is suitable for use with all standard linear amplifier systems, although low noise charge sensitive preamplifiers are preferred for spectrometry applications.

The X-ray particle detector changes resistance by varying the amount of radiation present. Initial proto types on these solid state X-ray detectors show that the sensitivity of these X-ray detectors can be compared directly with the sensitivity of the crystal photomultiplier X-ray detector combinations that are currently being used. In many cases and instances, this development will replace photomultiplier tube crystal combination units, particularly in application where the response to X-ray pulses need not be fast as those that can be measured with the photomultiplier crystal combination. However, it is expected that the response will be able to be improved over the next few months.

Another advance of the solid state X-ray detector is that it does not show any fatigue effects, like that, that is observed by the photomultiplier X-ray detectors currently used, which do show effects of fatigue over prolonged periods of radiation.